A study of the ichnology, lithology and reservoir quality of the Palaeogene Grumantbyen Formation on Svalbard

Master thesis in Petroleum Geoscience

By

Ørjan Berge Øygard

11.11.2016

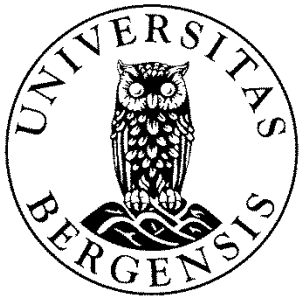

Department of Earth Science, The University of Bergen and

Department of Arctic Geology, The University Centre in Svalbard

Summary

The Palaeogene Grumantbyen Formation is one of the least understood formations in the geology of Svalbard. The objective of this thesis was to get a better understanding of the sedimentological development and depositional environment of the formation through detailed ichnological, lithological and petrographical studies. Finally, a detailed description of the reservoir quality of the formation will be presented.

The Grumantbyen Formation is highly bioturbated throughout the whole succession with only few signs of physical sedimentary structures. The ichnological study has led to an interpretation of seven different ichnofabrics occurring in the formation. There is a gradual transition between these ichnofabrics, and they are implying a change from a distal to a more proximal environment from the bottom to the top of the succession. 5 different lithofacies have been interpreted, and they show that the succession is gradually coarsening and shallowing upward from an offshore deposited sandy siltstone towards an upper shoreface deposited light silty sandstone. A gravel layer appearing erosional on top of the upper shoreface deposited lithofacies has been interpreted to represent a transgressive lag associated with the major flooding of the Grumantbyen Formation, and deposition of the superimposed Frysjaodden Formation.

The petrographical study shows a gradual increase in grain-size, better sorting, roundness, shape of the grains and decrease in matrix from the most distal towards the most proximal-lithofacies. This suggests that the energy conditions are getting stronger as a result of a gradual shallowing upward trend in the succession. The formation's appearance of glauconite in combination with high bioturbation intensity, lack of physical sedimentary structures and sandy input, has in this study been interpreted to represent a system with very little sediment input. A possible low, but continuous sediment input, which was greater than the available accommodation space is suggested, in order to have suitable conditions for glauconization and intense bioturbation. The buildup and progradation of the Grumantbyen Formation is therefore suggested to have been a slow process. A suggested shoreline-attached shallow-marine depositional environment is proposed. Possibly being a slightly prograding shoreface succession, that was provided with sediments from a source in the north-eastern parts of the system and prograded in a south-western direction.

The amount of matrix, cement and degree of compaction is suggested to have been the most important factors having a negative impact on the reservoir quality, leading to substantial loss of pore-space, due to significant burial. The reservoir quality of the Grumantbyen Formation was potentially good before significant burial, due to the grain-sorting behavior of organisms bioturbating the substrate, leading to well communication in the pore-network.

Acknowledgement

I would like to thank my main supervisor Dr. William Helland-Hansen (University of Bergen) and my co-supervisor Dr. Dirk Knaust (Statoil ASA, Stavanger) for the guidance, assistance, helpful discussions and most appreciated feedbacks during the work of this thesis. A special thanks to Dr. Dirk Knaust for being a good mentor and providing me with great assistance during the ichnological work of this thesis. Both wells and the outcrop section studied (Locality 1, Bolterdalen), were chosen in assistance with Dr. William Helland-Hansen and Dr. Dirk Knaust. I would like to thank both of them for assisting me during the fieldwork and logging of the wells. Sten-Andreas Grundvåg (University of Tromsø) also accompanied us during the fieldwork, and I would like to thank him as well for the assistance during the work carried out that day.

Statoil ASA has been very generous and helpful during the work of this thesis, by kindly giving me access to well BH-10-2008 (Sysselmannbreen core) and their core viewing storage. I would like to thank Sture Leiknes (Statoil ASA, Bergen) for having given me several weeks' access to Statoil's research Centre at Sandsli, Bergen in April/May 2016. A lot of the petrographical work of the thesis was carried out here, and I would especially like to thank Ruth Elin Midtbø (Statoil ASA, Bergen) for great assistance and guidance during the work of the petrography part. Two days of work was also carried out at Statoil's research Centre at Rotvoll, Trondheim. Lars Rennan (Statoil ASA, Trondheim) and Karen Melhuus (Statoil ASA, Trondheim) provided me with great assistance, by helping me analyze a selection of my samples in their Micro-CT scan during those days. I would like to express my greatest appreciation to both of them for sharing their time to help me during this work, also a thanks to Dr. Dirk Knaust for being a good traveling companion and mentor during the two trips to Rotvoll, Trondheim in November and December 2015.

I would also like to thank Store Norske Spitsbergen Kullkompani, who kindly gave me access to their core viewing storage in Endalen, Spitsbergen, where well BH-9-2006 was logged in August/September, 2015. Great thanks to Irina Maria Dumitru at the Department of Earth Science at The University of Bergen, for creating the thin sections which have been analyzed in this study.

I would like to thank my family and friends for the moral support during the work of this thesis. Last, but not least I would like to thank my girlfriend Jeanett for keeping up with my endless talk about this thesis, and always being supportive, encouraging and motivating.

Ørjan Berge Øygard Stavanger, 10.11.2016

Table of Contents

1 Introduction

1.1 Background

This thesis is based on well-data from well BH-10-2008 (Sysselmannbreen), BH-9-2006 and outcrop data from Bolterdalen, on Nordenskiöld Land, Svalbard. The Sysselmannbreen core was drilled on Nathorst Land, Svalbard for scientific purposes as collaboration between Statoil, Store Norske Kullkompani and NGU, to investigate the development of a prograding shelf. The core covers the Palaeogene Central Basin succession including the Grumantbyen Formation. Store Norske Spitsbergen Kullkompani has, in relation to coal prospects in the Todalen member of the Firkanten Formation, drilled multiple cores on Nordenskiöld Land which includes core material from the Grumantbyen Formation. Well BH-9-2006 is one of those wells drilled which have been investigated in this thesis.

Objective

Much work has been done on the deposits in the Palaeogene Central Basin. The Grumantbyen Formation however, being well exposed in the area around Longyearbyen, Adventdalen, lacks detailed studies and therefore it still remains as one of the least understood formations in the geology of Svalbard. Therefore the main objective of this thesis is to get a better understanding of the sedimentological development and depositional environment of the formation based on detailed lithological and ichnological studies of core and log material and through petrographical analysis assess the reservoir quality of the formation.

Previous work

In previous studies, this formation has been interpreted to be mainly deposited in a shelf setting, although detailed sedimentary processes and the sequence-stratigraphic development remains poorly understood. The “Green sandstone series” was the first name given to the formation by Nathorst (1910), and later it was renamed by Major and Nagy (1964) to the Sarkofagen Formation. A few years later it received its final and current name by Livsic (1967), which is based on the abandoned Russian mining society, Grumantbyen along the coast of Isfjorden, where the formation not surprisingly is well exposed. Previous work on the formation is in relation to general studies on the Palaeogene Central Basin which includes Kellogg (1975), Steel (1977), Steel et al. (1981), Steel et al. (1985) and Bruhn and Steel (2003). Nysæther (1966) performed a petrographical study on the Palaeogene succession on Nathorst Land, where the Grumantbyen Formation is referred to as the Sarkofagen Formation. Recent work by Simonstad (2011) and Vilberg (2011) have been particularly important for this study. The palaeogeographical work done in Espen Simonstads master thesis (2011) on the Grumantbyen Formation, acts as a fundament for the work done in this study.

1.2 Methods

Fieldwork and Core Analysis

Lithological study of wells and outcrop has been a fundamental part of the work done in this thesis. In order to examine core material and outcrop, lithostatigraphic logging was necessary (Figure 1.1). Lithostratigraphic logging includes measuring thickness of layers/successions, identifying discontinuity surfaces, observation of lithology, grain-size, sedimentary structures, trace fossils, bioturbation intensity and color. Equipment used during logging of wells and outcrop in the field includes; grain-size card, pencils, millimeter paper, binocular, benchmark, ruler, geological hammer, hand magnifier and digital camera. A satellite phone with GPS and altimeter was used to measure the thickness/height of the entire outcrop and parts of the succession. Wells and outcrop sections were logged in the scale of 1:50. The raw logs were later digitized by the use of two different computer softwares. Sedlog 3.1 was used to capture lithological changes based on variations in the silt- and sand content, which marks the outline of the logs. Adobe Illustrator CC was subsequently used to complete the logs with different sedimentary structures, trace fossils, bioturbation intensity, ichnofabrics, ichnofacies and color codes.

Figure 1.1: *Cores from well BH-9-2006, depth: 135.00 – 140.00. Top depth right side and bottom depth left side. Store Norske Spitsbergen Kullkompani.*

Trace fossil analysis

Most parts of the Grumantbyen Formation is totally bioturbated; therefore a detailed trace fossil-analysis became necessary for its characterization. The investigation includes the distinction of trace fossils, ichnofabrics and ichnofacies in order to obtain a better understanding of the development of the different lithofacies. Trace fossils are described as fossilized remains of the biogenic activity of organisms in sediments of different environmental settings. These mainly appear as burrows (dwelling or feeding traces). Different kinds of burrows reflect energy levels were the organisms lived and thrived, which act as indicators of different depositional environments. Trace fossils act as both

sedimentary and biogenic structures, and have an important impact on the sediments by destroying primary physical sedimentary structures.

Biogenic activity resulting in reorganization of sediments and soils by the activity of organisms and plants, are referred to as bioturbation (Richter, 1936). The bioturbation index (BI) proposed by Hans-Erich Reineck (1963) was based on boxcore material of modern sediments taken from the North Sea (Table 1.1). There is a question on whether or not this index can actually be used on lithified sedimentary rocks containing trace fossils, affected by compaction and burial over time. Still we decided to use the percentage bioturbation values of Reineck (1963), as a guide to distinguish the amount of bioturbation in the formation studied. The bioturbation index is divided into separate divisions of bioturbation ranging from 0 (none) to 6 (completely bioturbated) defining terms of burrow density, amount of burrow overlap and the clarity of the original sedimentary fabric (Taylor and Goldring, 1993).

Grade	Percent bioturabated	Classification
0	0	No bioturbation
1	1-4	Sparse bioturbation
2	5-30	Low bioturbation
3	31-60	Moderate bioturbation
4	61-90	High bioturbation
5	91-99	Intense bioturbation
6	100	Complete bioturbation

Table 1.1: *The bioturbation index (BI)* (modified from Reineck, 1963).

The different trace fossils observed in the formation have been described under Chapter 3.1 based on appearance, composition, shape, size, architecture and orientation. The abundance and reappearance of the same trace fossils have further been described in Chapter 3.2 by use of the ichnofabric concept by Taylor and Goldring (1993). An ichnofabric is described as the sediment's texture and internal structure as a result of bioerosion and bioturbation at every scale (Taylor and Goldring, 1993). An ichnofabric analysis studies both the biogenic and physical effects within the sediment (Taylor and Goldring, 1993). In this thesis ichnofabric constituent diagrams have been used in order to give a graphical representation of the different ichnofabrics present. The ichnofabric constituent diagrams record parameters such as a detailed analysis of the ichnotaxa present, ichnodiversity, size and order of emplacement (Taylor and Goldring, 1993). According to Taylor and Goldring (1993, p. 145) 'the order of emplacement of the ichnotaxa is determined by assessing the cross – cutting relationships, the sharpness of outlines, and the nature of infills'. The ichnofabric analysis is proven to be a useful method in the understanding and interpretation of depositional sequences and the associated

depositional environment, when physical sedimentary structures are nearly absent (Ekdale, 1992). In Chapter 6 a discussion regarding the depositional environment of the Grumantbyen Formation is undertaken where the concept of ichnofacies becomes relevant. The concept of ichnofacies describes the reoccurrence of biogenic traces which reflects certain combinations of organism behavior (ethology) in response to environmental conditions (Maceachern et al., 2007). Information regarding sedimentation rates, oxygenation and salinity are some of the properties described by the use of the ichnofacies concept (Maceachern et al., 2007).

Samples – Field and Well

In total 21 samples were taken from outcrop during fieldwork and during logging of well BH-9-2006, 10 from the outcrop and 11 from the well with the aim of examining the different lithological and ichnological variations at pore scale. The samples from well BH-9-2006 had a diameter of approx. 5.08 cm and a length of 8.5-21 cm. The samples were sealed in plastic folio and aluminum, and then marked with number and top/bottom – depth. For the field sampling, altitude and coordinates were noted.

Thin – section analysis

Optical Microscopy

In total 10 thin-sections from the outcrop locality and 11 thin-sections from well BH-9-2006 were made. The thin-sections from well BH-9-2006 were colored blue to highlight pore-space distribution. A Nikon E200 optical microscope was used to study and describe the thin-sections. Petrographic properties were analyzed both in plane-polarized-light (PPL) and cross-polarized-light (XPL). Properties include grain-size, sorting, roundness, fabric, alteration and composition. Grain-size calculation was based on counting points with a 10X10 magnification, meaning that the image being viewed is 100 times bigger than its actual size. A total of 20-30 grains counted per thin-section is sufficient in order to get an approximation of mean value. A more accurate grain-size calculation was also done at Statoil ASA, Bergen – Sandsli. By the use of a Nicon Digital Sight to take pictures of each thin-section, I was able to perform a length measurement of grains through the NIS – Elements BR software. The pictures were also taken with 10X10 magnification, and the software automatically gives you a calculated mean value based on all the grains measured in the sample.

Modal Analysis - Point Count

In order to get a more detailed description on mineral content and pore-space distribution in the thin-sections, a modal analysis was useful (Dickinson, 1970). In total 5 thin-sections from the outcrop locality and 7 thin-sections from well BH-9-2006 representing the different lithofacies and

ichnofabrics were studied. A Nikon Eclipse LV100POL optical microscope with a Nicon Digital Sight to use with the software NIS – Elements BR and a Swift Model F point counter were used at Statoil's research Centre at Sandsli, Bergen. The modal analysis is based on 300 points counted with a step length of 0.3 mm and 20X10 magnification. Each point counted is based on recognition of different framework and authigenic minerals and was divided into 11 groups based on a maximum of 12 different counting steps found on the point counting apparatus. When finished counting, the result was transferred into an Excel chart manually. Pre-set equations are able to classify the thin-section based on the observations and the results are plotted into a quartz, feldspar and lithic fragments (QFL) diagram (Dickinson, 1970).

SEM & XRD

In order to distinguish the composition of the matrix content in the different samples and supplement the thin-section analysis, both a Scanning Electron Microscope (SEM) and X-ray Diffraction (XRD)-analysis was necessary. From the thin-sections described in the optical microscope, a total of 5 samples from well BH-9-2006 were chosen to represent the main lithofacies and ichnofabrics reoccurring in the Grumantbyen Formation.

Both the SEM and XRD – analysis was done at Statoil's research Centre at Sandsli, Bergen. The main objective was to get a better understanding of the clay and matrix content in the samples, which had proven sometimes to be difficult to identify just by using the optical microscope. The SEM analysis acts as an effective method in identifying different minerals on a small scale, while the XRD analysis is more susceptible to identify different chemical compositions in the sample. The XRD analysis is therefore a good supplement to the mineral identification of the SEM analysis.

Computed Tomography (CT) - 3D visualization of Core Material

The 11 samples taken from well BH-9-2006 were brought to Statoil's research Centre at Rotvoll, Trondheim in November and December 2015. The ambition was here to use a Computed Tomography (CT) – Scan to detect 3D internal architecture and shape of different trace fossils in the samples. Micro-CT is becoming a more frequently used non-destructive 3D imaging and analysis technique within geoscience, with the ability of studying internal structures of a large variety of objects with resolution down to a few hundred nanometers (Cnudde and Boone, 2013). In micro-CT systems, the object which is under investigation rotates (Figure 1.2), while X-ray source and detector remain stationary (Cnudde and Boone, 2013). The setup found in micro-CT systems causes a higher accuracy which is necessary at high resolutions (Cnudde and Boone, 2013).

Two different North Star Imaging Computed Tomographs were used to scan the 11 samples. They both create a 3D visualization of the sample which is made up of a stack of 2D imaging slices in X/Y, X/Z and Y/Z – orientation (Figure 1.3). The scanning process is highly operator dependent and requires knowledge of the limitations in order to create the best possible image of the object. Specialized 3D rendering software such as Avizo is crucial for visual inspection of the 3D volume of the object (Cnudde and Boone, 2013). Volume segmentation is the most critical and complex operation when analyzing the scanning results in the Avizo software. 3D rendering and segmentation of the datasets in Avizo is quite time consuming, and the software also needs a powerful computer with lots of CPU-force. Most of the work done in Avizo took place in January 2016 at Statoil, Stavanger. A total of 5 of the originally 11 samples were volume segmented in Avizo, based on the quality of the volume output and limitations to different lithological compositions. The micro-CT scan reveal far better results with silt/mud abundant samples than clean sandstone samples in terms of final volume segmentation.

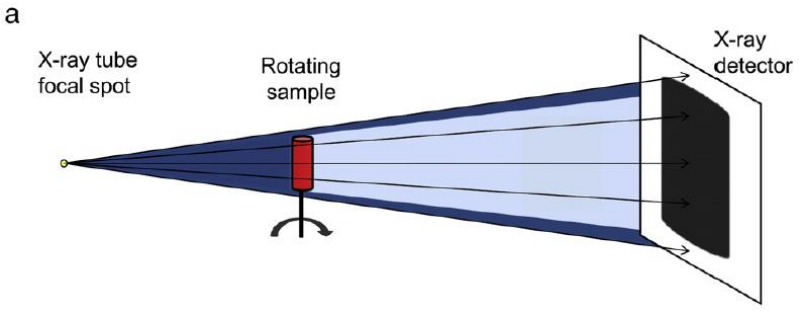

Figure 1.2: *Typical lab-based micro-CT setup with a conical X-ray beam, object in red rotates during scanning, from* Cnudde and Boone (2013).

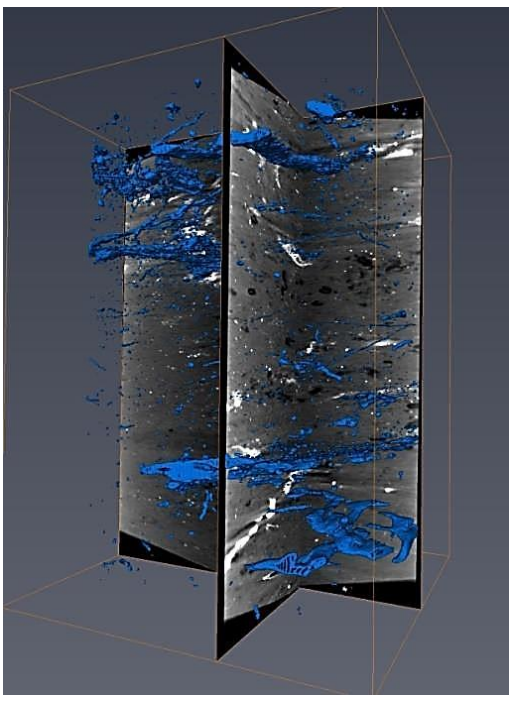

Figure 1.3: *Final result of sample 5 with 2D imaging slices in X/Z and Y/Z-orientation, which have been volume segmented in order to display internal trace fossils in the sample.*

2 Geological Framework

2.1 Tectonic setting

Opening of the Arctic Ocean and the North-Atlantic in late Cretaceous, led to uplift in north which maintained throughout the Cretaceous which was more extensive than the simultaneous sea level rise at the time. This resulted in the northern and western part of the continental shelf to be subaerial exposed and eroded, which created an unconformity in the lower part of the tertiary succession being developed in a southern direction (Dallmann, 1999). In central parts of Spitsbergen, the Cretaceous deposits are overlain by Palaeogene successions, with an angular unconformity separating them. In the Palaeogene a high-lateral transtension anlongside the De Geer-faultzone in Paleocene was followed by high-lateral transpression in Eocene, as a result of the movement of Greenland drifting by the western coast of Svalbard due to the opening of the North-Atlantic and Arctic Ocean (Talwani and Eldholm, 1977; Johnsen et al., 2001). The tectonic activity led to volcanism in the south-west and the north-west and also creation of the western Spitsbergen fold and Thrust belt with a resulting central basin in Spitsbergen (Steel et al., 1985; Worsley, 2008). The sediment transport direction was changed from east north-east to west, and the De Geer Line, the plate boundary between Greenland and Svalbard became the main sediment source to the central basin (Steel et al., 1985). The central basin is interpreted to represent a regional foreland basin with cyclic subsidence and infill of both continental and marine clastic sediments (Figure 2.1), with the deepest area located to west of the basin (Steel et al., 1985; Helland-Hansen, 1990). The central basin covers an area of nearly 12 000 km^2, and stretches from the Isfjorden in north to Sørkapp Land in the south (Schlegel et al., 2013).

2.2 Van Miljenfjorden Group

The Palaeogene deposits represented in the sedimentary succession of the central basin, Spitsbergen is known as the Van Miljenfjorden Group (Harland, 1969). The group consists of 7 formations and there is a general agreement that they represent deposits of Paleocene and Eocene age, although the lithological boundary between the Paleocene and Eocene strata remains unclear (Dallmann, 1999). The Van Miljenfjorden Group is made up of the following formations; Firkanten, Basilika, Grumantbyen, Frysjaodden, Hollenderdalen, Battfjellet and Aspelintoppen (Figure 2.2). The deposits in the Van Miljenfjorden Group represents three main depositional phases; a transgressive and two regressive phases (Steel et al., 1985).The two lowermost are intermediate scale transgressive-regressive cycles. The first one represents the Firkanten-to lower Basilika-Formation, and the next one from the Basilika-to the Grumantbyen-Formation (Bruhn and Steel, 2003). The third main depositional

cycle was a regressive mega-sequence deposited during the main formation phase of the west Spitsbergen orogeny, and includes the Frysjodden, Battfjellet and Aspelintoppen-Formations. The sedimentary record of the Palaeogene Central Basin is nearly 1.5 km thick in the north of Van Miljenfjorden and increasing to almost 2.5 km towards the south of the basin. During the Cretaceous the Svalbard archipelago was dominated by a worm and humid climate, which also extended into the Palaeogene despite the fact that the archipelago was situated in the northern temperature zone at the time (Worsley, 2008).

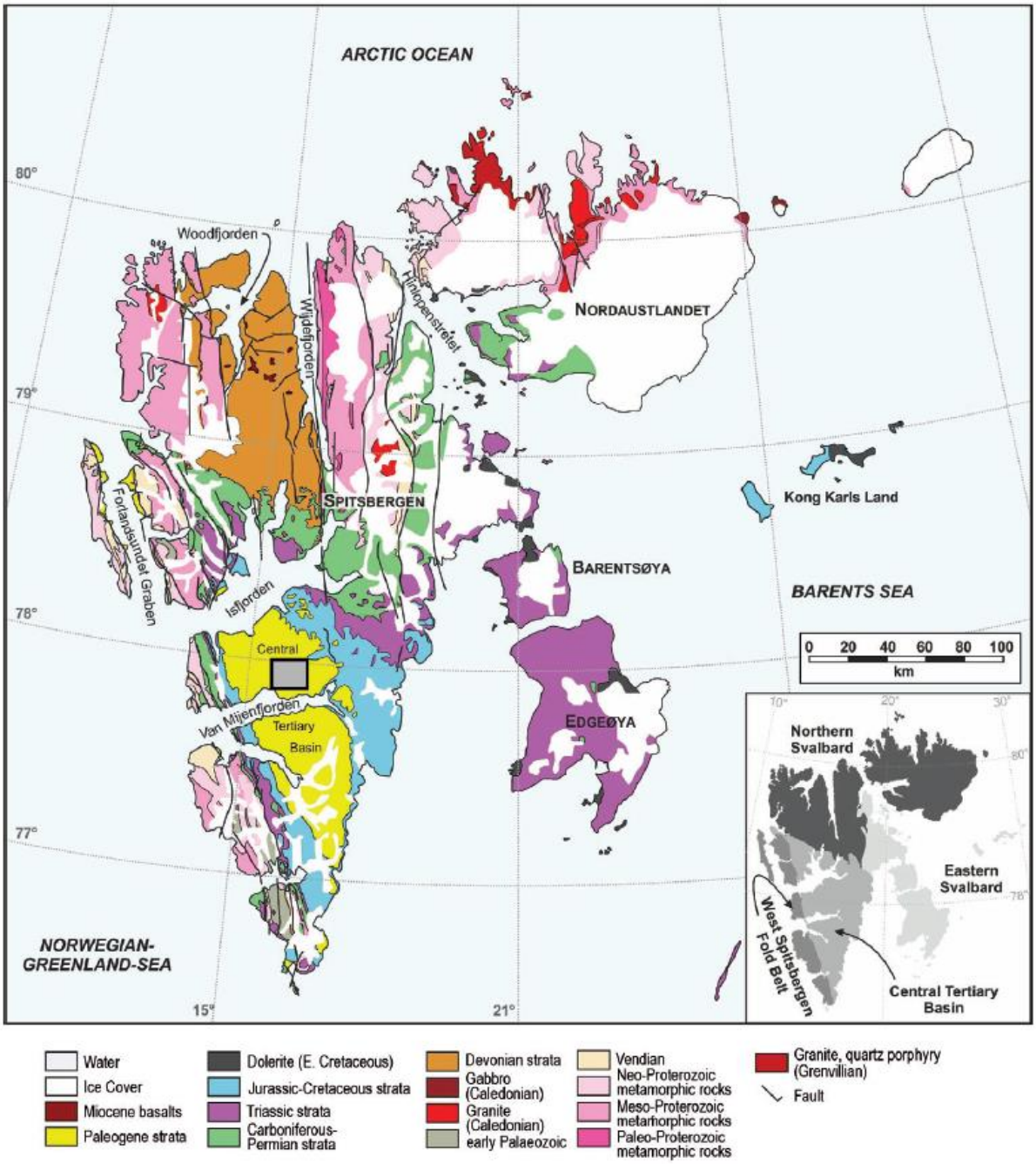

Figure 2.1: *A Simplified geological map of the Svalbard Archipelago. The Central Basin is filled with Palaeogene strata (marked in yellow color). After Dallmann et al. (2002).*

Early Paleocene

The Firkanten Formation is the lowermost formation in the Van Miljenfjorden Group and has a thickness around 200 m (Figure 2.2). The Firkanten Formation is divided into four members; the proximal Grønnfjorden, Todalen, Endalen and a distal finer-grained member, called the Kalthoffberget. The Grønnfjorden member represents the first deposits in the Van Miljenfjorden Group, and lies directly on top of the marine shales from lower Cretaceous (Bruhn and Steel, 2003). The member consists of sandy conglomerates and is interpreted to represent braided river systems coming from the eastern parts of the basin (Bruhn and Steel, 2003). The Todalen member consists of shales, sand and coal, and has been interpreted to represent a deltaplain deposit in a fluvial dominated delta system (Steel et al., 1981). The overlying Endalen member is interpreted to represent the forsets of a delta front, primarily consisting of quartz arenite (Steel et al., 1981). In the southern parts of the Palaeogene Central Basin, the Endalen member becomes finer-grained; this unit is referred to as the Kalthoffberget member, and consists of lower delta front and prodelta-deposits (Steel et al., 1981).

The Basilika Formation is superimposed the Firkanten Formation (Figure 2.2), and varies in thickness from 20 m in the north-eastern parts of the basin to more than 300 m in the south and south-western areas. The Basilika Formation is interpreted to represent a prodelta deposit, and consists primarily of dark offshore shales which appears slightly more silty and sandy towards the top of the succession in a north-eastern direction (Steel et al., 1981). Based on the general development upwards in the sequence from the Firkanten to Basilika-Formation, the complete succession is interpreted to represent a transgressive mega-sequence in the Van Miljenfjorden Group (Steel et al., 1981).

Middle and late Paleocene

The second depositional cycle of the Palaeogene Central Basin includes the uppermost part of the Basilika Formation, the overlying Grumantbyen Formation and the Hollenderdalen Formation (Figure 2.2). The Grumantbyen Formation is a highly bioturbated sandstone sequence, with a characteristic green color due to the high content of glauconite. The formation is measured to be at its thickest in the north and north-eastern parts of the basin and thins towards the south and south-west. In the southern parts of the basin the Grumantbyen Formation interfingers with the Basilika Formation (Dallmann, 1999). The formation is not well understood due to its homogeneous look, glauconitic content, intense bioturbation and lack of physical sedimentary structures. The high bioturbation intensity has indeed rearranged the sediments and as a result there are only a few physical sedimentary structures occurring throughout the entire succession. An overall coarsening upward trend, with several minor coarsening upwards successions, does however appear together with a noticeable increased appearance of physical sedimentary structures in the upper part of the formation (Bruhn and Steel, 2003). An

offshore origin has previously been suggested based on the glauconitic content and bioturbation intensity (Steel, 1977; Steel et al., 1981). Steel et al. (1981) interpreted the formation to be an offshore bar complex based on its characteristics. The age of the formation is suggested to be middle to upper Paleocene (Manum and Throndsen, 1986). Towards late Paleocene uplift in the fold and thrust belt in the west resulted in deposition of the Hollenderdalen Formation, which is thinning out in a easterly direction (Dalland, 1977; Steel et al., 1981). The formation is composed of shallow, tide-dominated, deltaic sandstone units with a gradual transition into shales (Dalland, 1977). The Hollenderdalen formation together with the upper part of the Basilika formation and the Grumantbyen Formation, is interpreted to represent the first of two regressive mega-sequences (Steel et al., 1981).

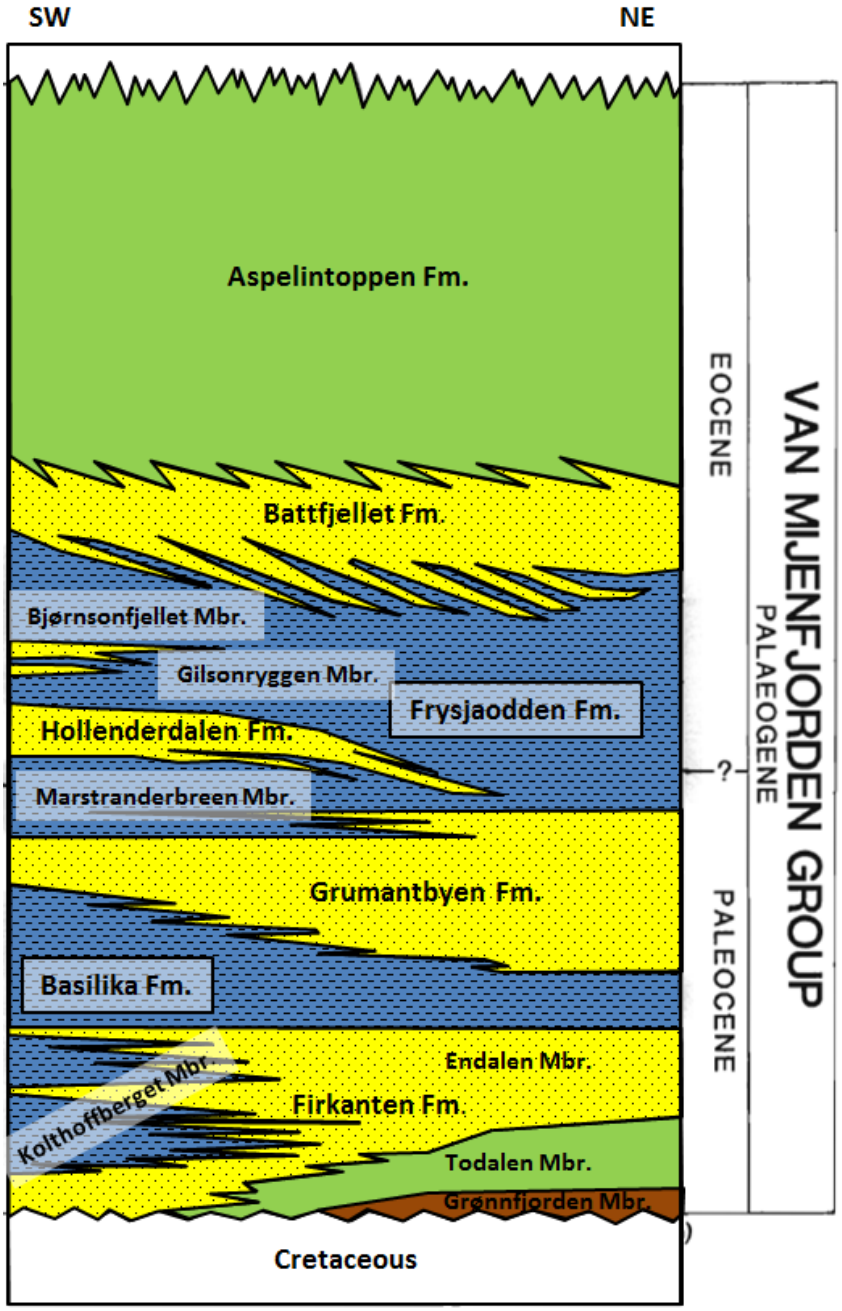

Figure 2.2: *A stratigraphic overview of the Palaeogene Central Basin* (modified from Steel et al., 1985).

Late Paleocene and early Eocene

The second and last regressive mega-sequence in the Palaeogene Central Basin started with the Frysjaodden Formation (Figure 2.2). The Frysjaodden Formation consists of thick deposits (200-400 m) of shale which is interfingered by sandstone wedges of the Hollenderdalen Formation and the Bjørnsonfjellet member in the west of the basin (Steel et al., 1981; Dallmann, 1999). The Bjørnsonfjellet member is interpreted to be deposits of basin-floor fans (Johannessen and Steel, 2005). The Frysjaodden Formation can further be divided into two subgroups; the Mastranderbreen and Gilsonryggen-members, which is separated from each other by the intermediate Hollenderdalen Formation (Figure 2.2). The deposition of the Frysjaodden Formation took place in the late Paleocene to early Eocene, at the same time as the thrusting of the western Spitsbergen fold belt, which resulted in uplift and a change in sediment input from north-east to instead west (Helland-Hansen, 1990). The formation is interpreted to represent a pro deltaic deposit with a deltaic source west of the basin margin, which have been incorporated in the east prograding western Spitsbergen fold and thrust belt (Harland et al., 1997).

The Battfjellet Formation is superimposed and interfingers the offshore shales of the Frysjaodden Formation (Figure 2.2) (Steel et al., 1981). The Battfjellet Formation is represented in nearly the whole Palaeogene Central Basin, and shows its greatest thickness south of the Van Miljenfjorden and pinches out towards the north-eastern parts of the basin. The formation is composed of planar-parallel-laminated and cross-stratified white sandstone with minor inputs of silt and shale (Dallmann, 1999). The formation is a marine sandstone sequence interpreted to represent a coastline delta front deposit of Eocene age (Steel et al., 1981). The formation shows an easterly progradation with input from the west (Helland-Hansen, 2010). Although the sedimentary facies shows a dominance of wave activity within the sediments, in the western parts of the basin evidence of fluvial processes and gravity flows exists which have had a significant impact on the distribution of the sand (Helland-Hansen, 1985).

The Aspelintoppen Formation is the last formation in the Palaeogene succession in the Central Basin and is the final ending of the second regressive mega-sequence (Figure 2.2) (Helland-Hansen, 1990). The formation shows a great thickness of more than 1000 m south of the Van Miljenfjorden, while in the northern areas the formation is only preserved as thin remains on the peaks (Steel et al., 1981). The formation consists of poorly sorted sandstones and conglomerate, with thin coal seams and characteristic plant fragments such as leafs, in both coarsening and fining upward sequences (Dallmann, 1999). The formation is interpreted to represent a terrestrial deltaplain deposit dominated by floodplain and lacustrine sediments of Eocene, possibly Oligocene age (Steel et al., 1981). The shoreline at the time of deposition is suggested to have been oriented north-south, with the sediments coming from the west and prograding in an easterly direction (Helland-Hansen, 1990).

2.3 Study area

The Palaeogene Central Basin is located in the southern parts of Spitsbergen, which is the largest island in the Svalbard Archipelago in the north-western Barents Sea (Figure 2.1). The study area is located on Nordenskiöld Land and Nathorst Land (Figure 2.3). Well BH-10-2008 (Sysselmannbreen core) is located 4.5 km to the southwest of Isnibba at Nathorst Land, and the well was studied in March 2015 and 2016 at Statoil's research Centre at Sandsli, Bergen. Fieldwork and the study of well BH-9-2006 were done in August/September 2015. Well BH-9-2006 was studied at Store Norske Spitsbergen Kullkompani's core view storage in Endalen, Spitsbergen. Two days of fieldwork was carried out in mid-August 2015 in Bolterdalen, Spitsbergen. In Bolterdalen the Grumantbyen Formation is well exposed and easy accessible. One location (Locality 1, Bolterdalen) was chosen and logged in assistance with my main supervisor Dr. William Helland-Hansen (University of Bergen), my co-supervisor Dr. Dirk Knaust (Statoil ASA, Stavanger) and Sten-Andreas Grundvåg (University of Tromsø). The logs from the two wells and the outcrop studied (Locality 1, Bolterdalen) are found in the appendix chapter.

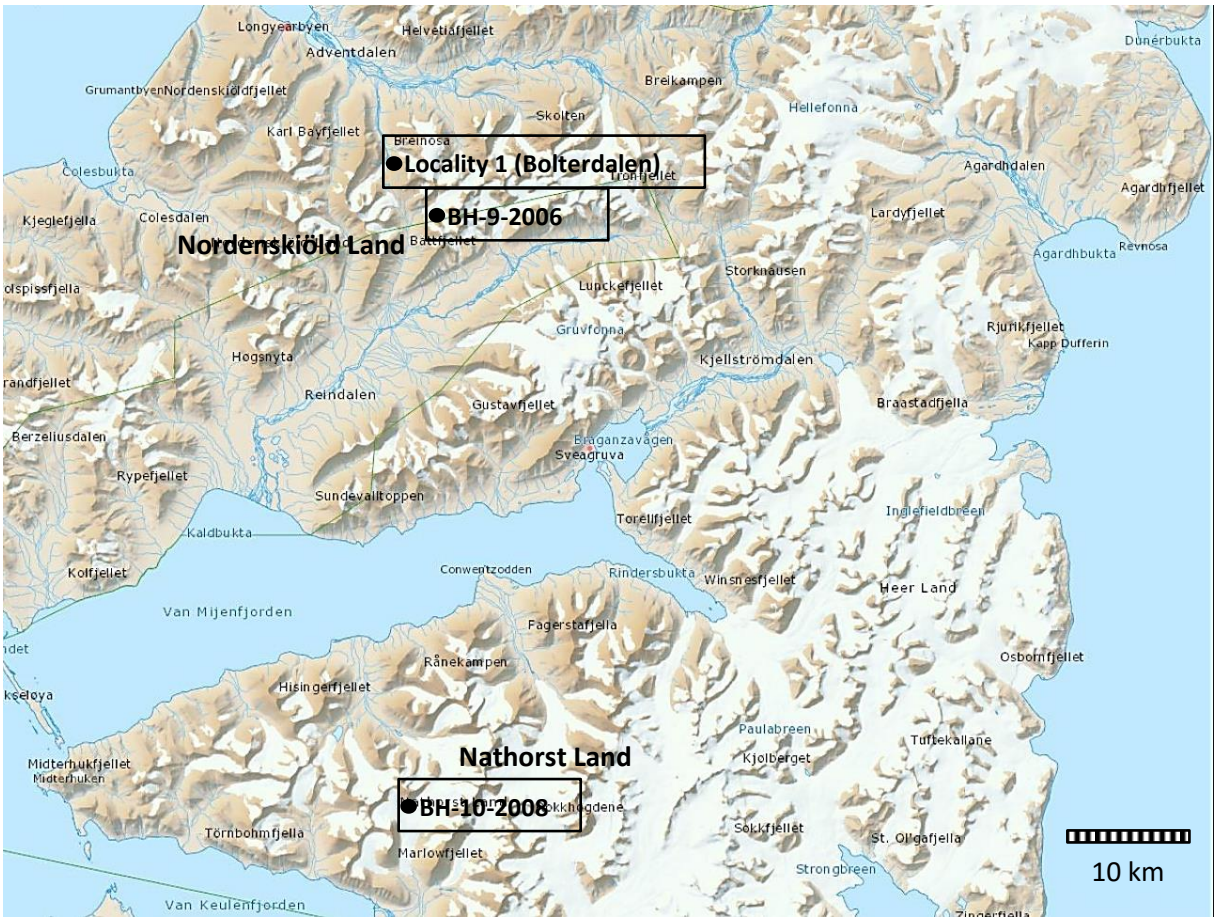

Figure 2.3: *Map showing the study area at Nordenskiöld Land and Nathorst Land, with the different wells and the outcrop studied as described above. Map modified from the Norwegian Polar Institute.*

3 Ichnology

The Grumantbyen Formation is characterized as being intense bioturbated throughout the whole succession, with exception of a few intervals containing physical sedimentary structures. Because of intense weathering, the trace fossils were harder to identify in the field compared to the core-sections in the wells. Based on the great abundance of different trace fossils occurring in the formation, a detailed description and their sedimentological importance and influence are given in this chapter. A total of 7 different trace fossils have been identified and are described in terms of appearance, composition, shape, size, architecture and orientation. The abundance and reappearance of the same trace fossils have further been described by use of the ichnofabric concept by Taylor and Goldring (1993) later in the chapter.

3.1 Trace fossils

Cylindrichnus (Cyl) – Howard (1966)

Description

Cylindrichnus occurs in both wells and is well represented in the lower part of well BH-9-2006 in association with *Teichichnus*. In well BH-10-2008 the trace fossil appears scattered in the middle and upper part where it is relatively abundant, whereas it was not recognized in the outcrop section studied (Locality 1, Bolterdalen). In core view the trace fossil is observed as vertical and perpendicular to the bedding plane with an architecture being slightly curved U- or bow-shaped (Figure 3.1 & Figure 3.2). The burrow is composed of a central tunnel with a sand filled core surrounded by mud lining. These are the characteristics of the ichnospecie *Cylindrichnus concentricus* (Howard, 1966). The bow shaped burrows typically measures a diameter > 4.0 mm and a maximum length of approx. 30-50 mm.

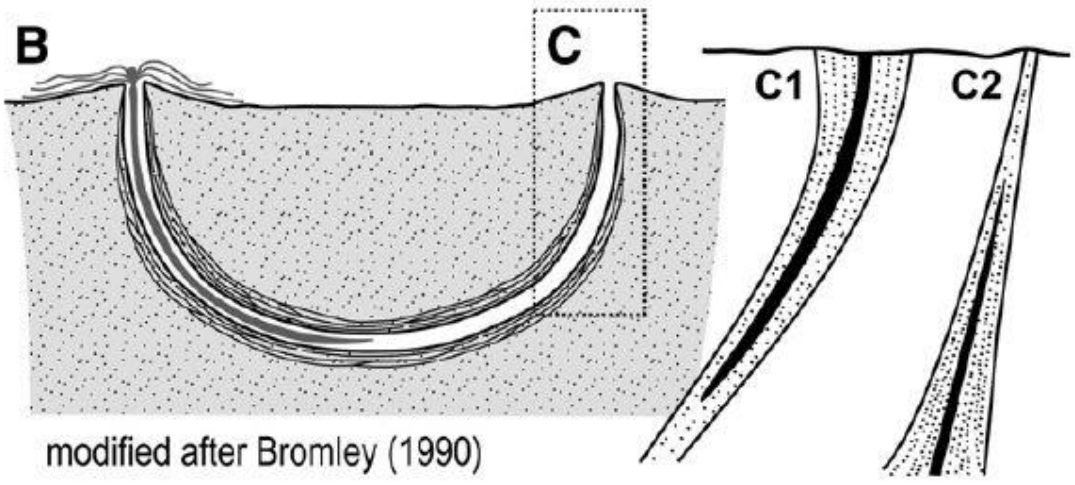

Figure 3.1: *Reconstruction of the architecture of Cylindrichnus concentricus, illustrating a bow-shaped burrow* (Drawing modified from Bromely, 1990).

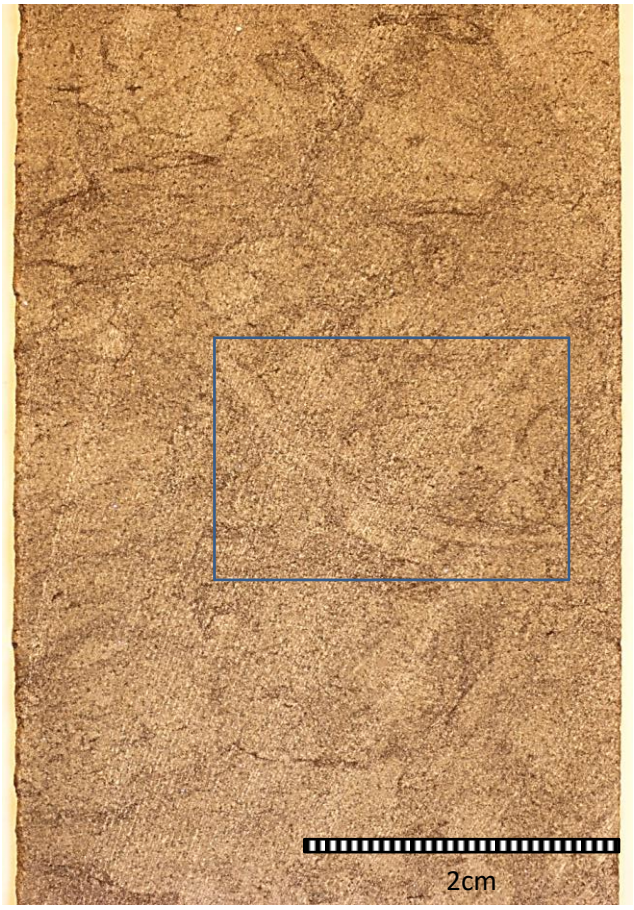

Figure 3.2: *Vertical-section with Cylindrichnus concentricus, in well BH-10-2008, depth 873.75 m.*

Interpretation

The bow-shaped architecture of *C. concentricus*, with the characteristic two openings at the sediment surface that can be seen in cross – section, suggests that the dwelling structure was formed by either a filter-feeding animal or a surface deposit feeder (Frey and Howard, 1990; Ekdale and Harding, 2015). The characteristic thick and concentrically laminated lining of *C. concentricus* display remarkable similarities to the linings found today in modern burrows produced by *Terebellid polychaetes* (Belaústegui and de Gibert, 2013). The trace fossils appearance with high-diverse ichnoassemblages including *Teichichnus* and *Palaeophycus* is not uncommon (Frey and Howard, 1990).

Ekdale and Harding (2015) discovered well developed *C. concentricus* in hummocky cross stratified beds produced above storm-wave base by oscillating currents associated with storms. The tracemaker is a suspension feeder and therefore it would rely on such currents in a high-energy hydrodynamic environment in order to feed. Today *C. concentricus* is known as a widespread trace fossil found in diverse shallow-marine to offshore transition zone sediments of Mesozoic and Cenozoic age around the world (Frey and Howard, 1985; Frey and Howard, 1990).

Macaronichnus (Mac) – Clifton and Thompson (1978)

Description

Macaronichnus was observed in both wells and the outcrop section studied (Locality 1, Bolterdalen). At the outcrop the trace fossil shows a cylindrical tube with a meandering form that runs parallel to the bedding plane (Figure 3.3). The trace fossil typically occurs in dense concentrations. In core view the tubes appear as crowds of straight to curving-horizontal cylindrical burrows with an elongate to oval or circular shape (Figure 3.4). These are the characteristics of the ichnospecies *Macaronichnus segregatis* (Clifton and Thompson, 1978). *Macaronichnus* is easily identified by its light colored tube core being sand filled with a diagnostic dark colored mantle. The burrow occurs in very fine to medium-grained sand. The diameter of the tubes ranges between 2.0-5.0 mm and on bedding planes as seen in the outcrop the length of the burrows measures several centimeters. In both, wells and outcrop, *Macaronichnus* is especially abundant in the uppermost section, where it can occur with wave-ripple-cross-lamination (WRCL). The burrows generally appear in less silty sandstone intervals, an exception is well BH-10-2008 where *Macaronichnus* also appears in the lower part of the well, which is dominated by a relatively high input of silt.

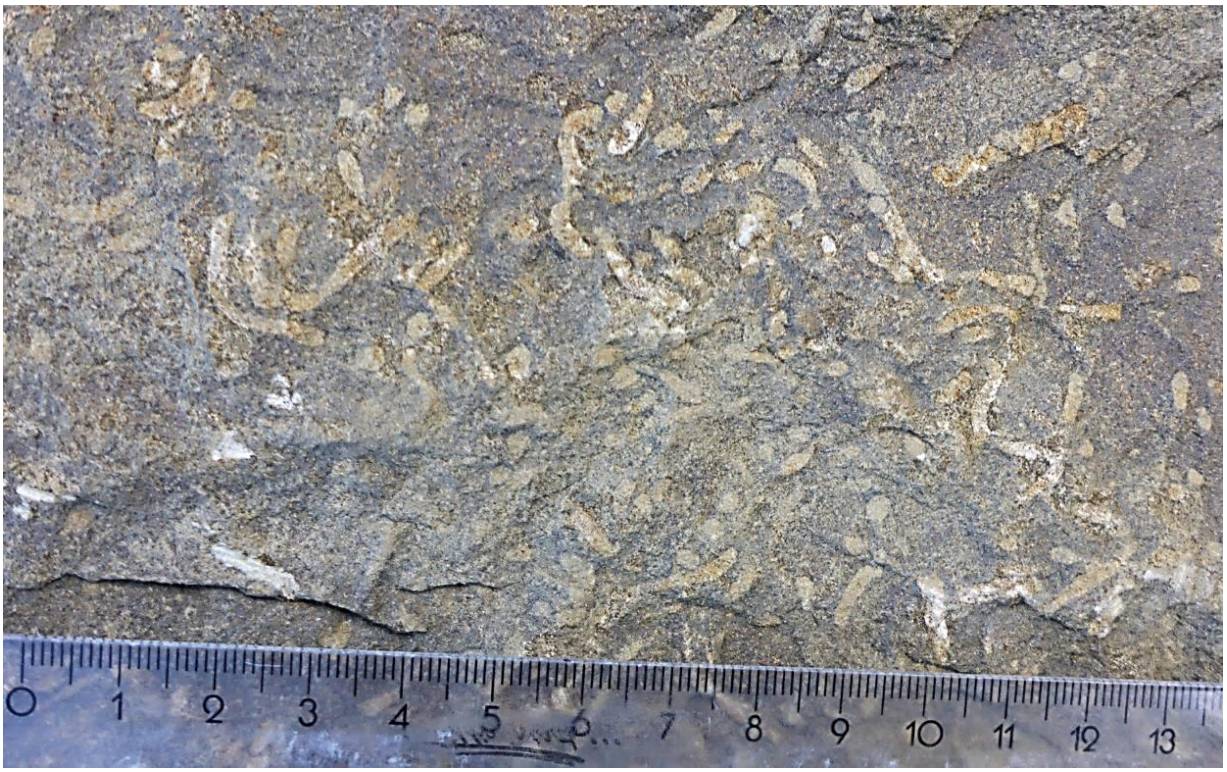

Figure 3.3: *Macaronichnus segregatis occurring with a near meandering form parallel to the bedding plane, Locality 1 (Bolterdalen). Scale in cm.*

Figure 3.4: *Vertical-section with Macaronichnus segregatis occurring in a calcite cemented interval in well BH-9-2006, depth 195.00 m.*

Interpretation

Modern studies of similar intrastratal trails reveal that *M. segregatis* is produced by marine opheliid polychaetes, such as *Ophelia limacina* (Clifton and Thompson, 1978), *Euzonus mucronata* (Seike, 2007) and *Travisia japonica* (Seike et al., 2011). These polychaetes are deposit feeders that sustain themselves on microbes at the surface of the quartz grains (felsic) through selective ingestion where dark-colored grains (mafic) are sorted around their bodies (Clifton and Thompson, 1978). Orientation of the trace fossil can be used as an indicator of beach morphodynamics, palaeo-shoreline orientation, ancient sea-level and environmental conditions (Seike, 2007; Bromley et al., 2009; Seike et al., 2011; Uchman et al., 2016). The polychaete worms tend to move in various directions during fair-weather conditions (summer) and are forced in a more straight landward direction during storm conditions (winter).

Macaronichnus is a characteristic shallow-marine trace fossil predominantly occurring in foreshore, shoreface, intertidal and shallow subtidal environments (Clifton and Thompson, 1978; Seike, 2007; Bromley et al., 2009). Pemberton et al. (2001, p. 128) indicated that *Macaronichnus* also occurs in tempestites created as a result of bigger storms. Longshore and upwelling currents could also provide suitable conditions for the trace maker to live in upper slope environments (Knaust, pers. comm. 2015). *M. segregatis* has frequently been reported from Mesozoic and Cenozoic deposits and is a common constituent of the *Skolithos* Ichnofacies (Pemberton et al., 2012).

Nereites (Ne) – Macleay (1839)

Description

In core view, *Nereites* appears as clusters of elongated horizontal to sub-horizontal-wavy dark ribbon structures bounded by lighter zones (Figure 3.5). *Nereites* is identified by its asymmetric shape mainly consisting of fine-grained material that is enveloped by a light "halo" of reworked slightly coarser grains. The ribbons width varies in size from 3.5-16 mm and 1.2-3.0 mm in height. The lighter halos measure a width of about 1.0-2.5 mm. The burrows have not been observed to cross-cut each other. *Nereites* is especially prominent in the lower section of well BH-10-2008 (Appendix 11) and in two separate intervals in the lower half of well BH-9-2006 (Appendix 13). In both wells, the trace fossil abundance gradually decreases upward in conjunction with a coarsening upward trend of the sediments. *Nereites* was not recognized in the outcrop section studied (Locality 1, Bolterdalen).

Figure 3.5: *Vertical-section with Nereites in well BH-9-2006, sample 2, depth 386.70 m.*

Interpretation

The ribbons seen as dark spots in core view are fecal strings created by *Nereites* producers (Pervesler et al., 2008). The enveloped lighter halo represents a reworking zone around the fecal string, implying active grain sorting by the burrowing animal (Wetzel, 2002; Pervesler et al., 2008). The *Nereites* burrows are found in muddy to fine sandy sediments just above the redox boundary (Wetzel, 2002). Sediment grain-size acts as a significant control on the occurrence and distribution of *Nereites* producers. The redox boundary marks a transition from oxic to anoxic conditions, were microbes

thrive and provide food for the *Nereites* producers; the burrows are hence completely absent in anoxic sediments (Wetzel, 2002). Based on its occurrence, Seilacher (1967) introduced the *Nereites* Ichnofacies as a common type of trace fossil community in turbidite sequences typically found in deep-marine environments (basin-floor deposits). Frey and Pemberton (1984, p. 193) suggested that *Nereites* Ichnofacies were related to environments such as; 'bathyal to abyssal, mostly quiet but oxygenated waters with very slow accreting substrates'. *Nereites* also occurs in slope and shelf deposits, where deposition of moderate energy dominates (e.g. *Zoophycos* and *Cruziana* Ichnofacies) (Knaust, pers. comm. 2016).

Palaeophycus (Pal) – Hall (1847)

Description

Palaeophycus was only observed in well BH-9-2006 and in the outcrop section studied (Locality 1, Bolterdalen). In the field the burrow was especially abundant in the lower part of the studied section, while it appeared scattered in the lower section of well BH-9-2006. At the outcrop the trace fossil is especially well developed along the bedding plane (Figure 3.6). Here the burrow shows a straight to sinuous-cylindrical architecture with a thin light wall surrounding the tube. In the vertical section at the outcrop the burrow is seen in cross-section displaying a collapsed oval to circular shape of the tube, this is also how the burrow occurs in well BH-9-2006 (Figure 3.7). These are the characteristics of the ichnospecie *Palaeophycus tubularis* (Hall, 1847). The burrow is generally composed of the same lithology as the host stratum. The tubes measure a diameter between 5.0-15.0 mm and a length of several centimeters on the bedding plane seen at the outcrop.

Figure 3.6: *Palaeophycus tubularis seen on bedding plane, Locality 1 (Bolterdalen). Scale in cm.*

Figure 3.7: *Palaeophycus tubularis seen in vertical-section, Locality 1 (Bolterdalen). The observed collapsed oval to circular tubes shows signs of oxidation due to weathering. Scale-finger=8 cm.*

Interpretation

Palaeophycus is interpreted as dwelling structures produced by predaceous worms that reflect a suspension and/or predatory feeding strategy (Pemberton and Frey, 1982; Frey and Howard, 1990; Pervesler et al., 2008). The burrow wall can be used to secure a dwelling/refuge structure or it might be the by-product of selective deposit-feeding. Collapsed burrow segments seen in core view are diagnostic features of *P. tubularis* (Frey and Howard, 1990). *Palaeophycus* has been recorded amongst *Planolites, Cylindrichnus, Teichnichnus* and other trace fossils in the lower shoreface to offshore transition zone sediments (Pemberton and MacEachern, 1992). *Palaeophycus* has also been recorded in thinly-bedded turbidite sandstones in mid to outer fan deposits and also in continental environments (Crimes et al., 1981).

Schaubcylindrichnus (Sch) – Frey and Howard (1981)

Description

Schaubcylindrichnus was observed in both wells and the outcrop section studied (Locality 1, Bolterdalen). Both in the field and in core view the trace fossil was mainly observed in a cross-section of the burrow (Figure 3.8). The trace fossil appear as a tube which is arranged either as totally isolated or in closely packed groupings, with a number of tubes ranging from 4-12. *Scaubcylindrichnus* has a characteristic white ring or wall lining around the tube. White minerals constitute the wall linings that surround the passive burrow fill (Frey and Howard, 1981; Kikuchi et al., 2016). The tubes observed have a diameter between 2.0 – and 3.0 mm, and the clear visible white wall is approx. 1.0 – to 2.0 mm thick. These are all characteristics of the ichnospecies *Schaubcylindrichnus coronus* (Frey and Howard, 1981), the only valid ichnospecies (Figure 3.9). The trace fossil appears in various grain-sizes from clay to fine sand, and is therefore observed throughout the entire succession both in the field and in the wells. An exception might be in the upper part of well BH-9-2006 and the uppermost interval of the logged outcrop section (Locality 1, Bolterdalen), were the trace fossil is nearly absent.

Figure 3.8: *Vertical-section with Schaubcylindrichnus coronus, Locality 1 (Bolterdalen). Scale in cm.*

Interpretation

Schaubcylindrichnus was early interpreted to be produced by either gregarious deposit feeders or filter feeders (Frey and Howard, 1981; Frey and Howard, 1990; Frey and Pemberton, 1991; Pemberton et al., 2001). These early interpretations, based on material from Upper Cretaceous Utah, were obtained from incomplete specimens, and an ongoing debate has risen on whether or not these interpretations should be reconsidered. Recent work done by Löwemark and Nara (2010) and Kikuchi et al. (2016) on Miocene and Pleistocene deposits of central Japan, suggest that these earlier interpretations should be ruled out in favor of a funnel-feeding behavior of a worm-like organism (e.g. a polychaete).

Schaubcylindrichnus is usually well preserved, it cross-cut other trace fossils which indicates that it was produced at a later stage in the burrow succession. According to Frey and Pemberton (1991) it is likely that bigger clusters of tubes may indicate a stable environment. *Schaubcylindrichnus* is known to be a good indicator of shoreface settings, especially under high-energy conditions, but a study done by Frey and Pemberton (1991) provide evidence that this trace fossil also occurs in proximal parts of the offshore zone. Studies done in central Japan reveal that *Schaubcylindrichnus* is found in totally bioturbated muddy sandstones and sandy mudstones on the continental slope in offshore-transition to offshore deposits (Nara, 2006; Löwemark and Nara, 2010).

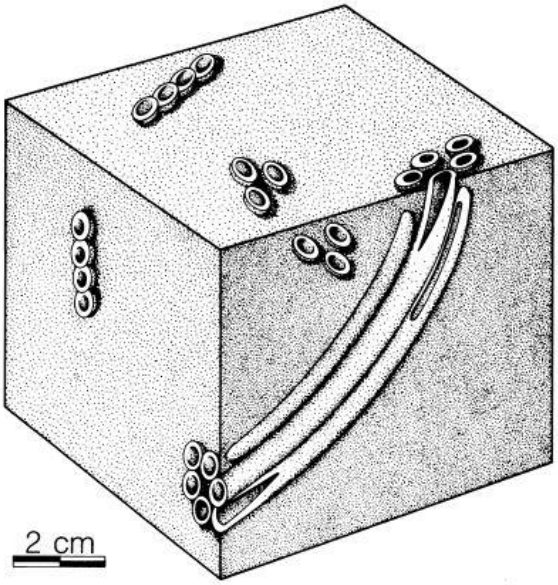

Figure 3.9: *Illustrative drawing of Schaubcylindrichnus coronus, after* Frey and Howard (1990).

Teichichnus (Tei) – Seilacher (1955)

Description

Teichichnus was observed in both wells and is especially abundant in the lower part of well BH-9-2006. In well BH-10-2008 the trace fossil occurs in scattered intervals throughout the section, whereas it was not observed in the outcrop section studied (Locality 1, Bolterdalen). In core view *Teichichnus* shows a vertical slightly curved architecture composed of several closely stacked, partially overlapping tubes (Figure 3.10). In cross-section the burrow appear as straight to sinuous and is oriented at various angles with respect to bedding, showing a diagnostic zigzag pattern. The trace fossil occurs as isolated and is not observed in dense groupings. *Teichichnus* appears in core-section as sand- and mud-filled burrows with a cylindrical sand core at the top of the burrow. *Teichichnus* reaches a maximum length of approx. 40-60 mm and a width of about 5-20 mm.

Interpretation

Teichichnus is interpreted as a feeding-dwelling burrow, produced by deposit-feeding, wormlike organism, probably an annelid, crustacean or holothurian, that migrated upward from a horizontal to subhorizontal tunnel (Frey and Bromley, 1985; Frey and Howard, 1990; Pemberton et al., 2001). *Teichichnus zigzag* (Frey and Bromley, 1985) is the name of the ichnospecie that is most prominent in the Grumantbyen Formation, which is recognized by a characteristic zigzag pattern (Figure 3.10). According to Pemberton et al. (2001) *Teichichnus* is associated with lower shoreface to offshore environments in the *Cruziana* Ichnofacies, this is also supported by Frey and Howard (1990, p. 804) who observed *Teichichnus*; 'primarly in the upper offshore deposits amongst *Cylindrichnus concentricus, Palaeophycus tubularis* and other trace fossils'. *Teichichnus* is also proven to be abundant in marginal-marine environments with brackish conditions (lagoons, estuaries, tidal flats, delta tops), where it is almost monoichnospecific (Wightman et al., 1987; Knaust, pers. comm. 2016).

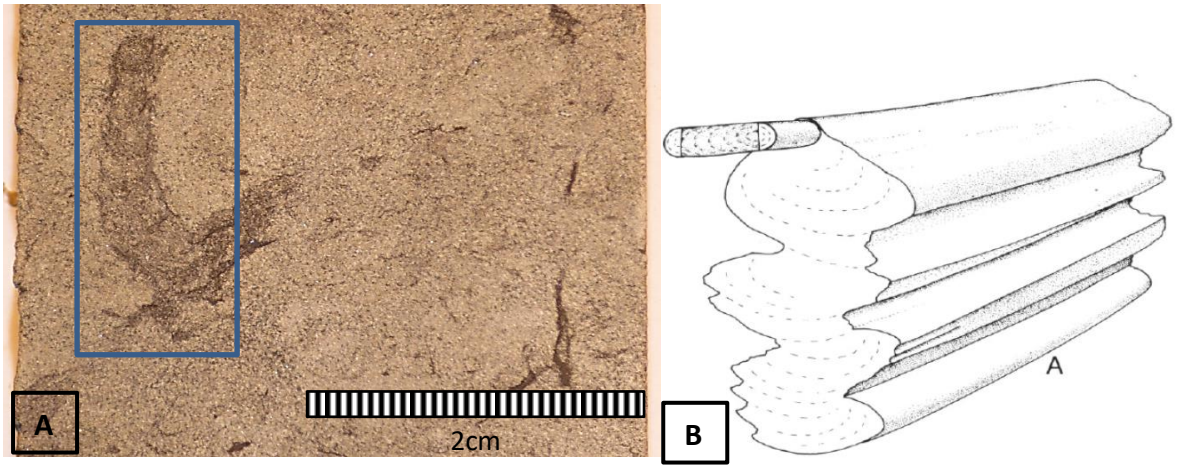

***Figure 3.10**: (A) Vertical-section with Teichichnus zigzag in well BH-10-2008, depth 853.30 m. (B) Illustrative drawing of Teichichnus zigzag, after* Frey and Bromley (1985).

Virgaichnus (Vir) – Knaust (2009)

Description

Virgaichnus is well represented in both wells and in the outcrop section studied (Locality 1, Bolterdalen). The trace fossil is observed to occur in dense concentrations in a diverse community of trace fossils. The trace fossil is common in silty to sandy substrates, and is observed nearly throughout the whole succession both in the field and in the wells. The average burrow diameter is about 0.5 mm, whereas burrow length and penetration depth can differentiate between a few millimeters to several centimeters. Because of its size, *Virgaichnus* was first described as tiny mud-filled burrows. More detailed investigation did however reveal certain characteristics associated with the recently discovered ichnospecies *Virgaichnus undulatus* (Knaust, 2009).

Virgaichnus is passively filled with mud and have a surrounding smooth wall (Knaust, pers. comm. 2016). The burrow has a complex three – dimensional architecture. Observations from the outcrop section, core view and Micro-CT show a burrow that is highly irregular with both horizontal and inclined elements (Figure 3.11). The sub-vertical elements show both Y-shaped and T-shaped branching. Outcrop sections show that *Virgaichnus* has a straight to meandering form and varying thickness in bedding-plane view (Figure 3.12). The Micro-CT results show inclined elements with pinch-and-swell features creating almost bulbous enlargements along the burrow (Knaust, pers. comm. 2016) (Figure 3.13). The inclined burrows also seem to be slightly spiral between these bulbous enlargements. The horizontal elements have a distinctive alternating blade-like contraction feature. The burrows are observed to cross-cut each other as well as other trace fossils.

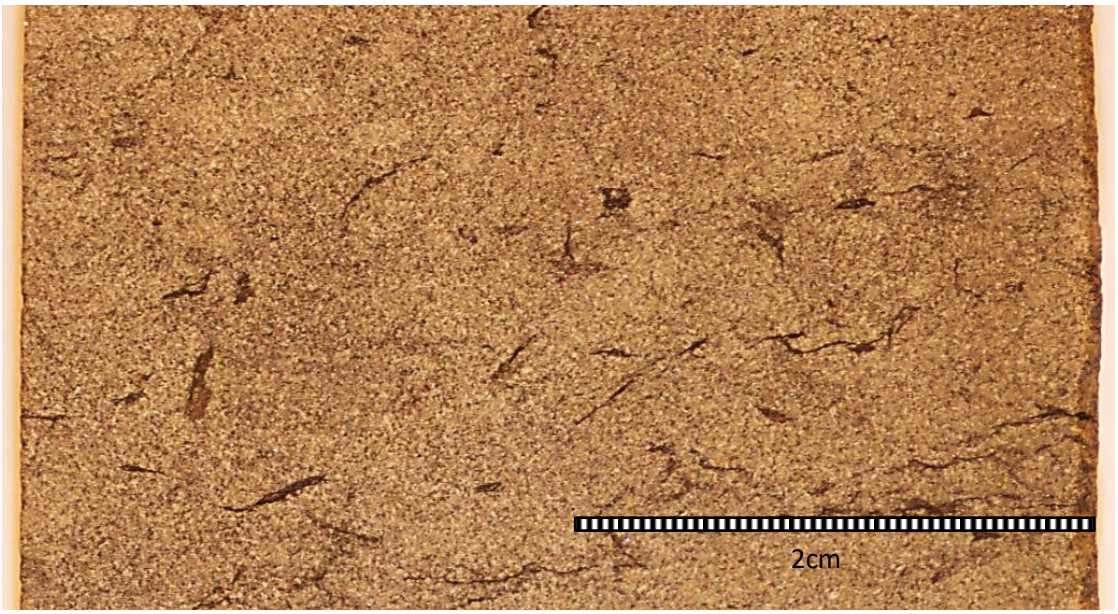

Figure 3.11: *Vertical-section with Virgaichnus undulatus in well BH-10-2008, depth 916.62 m.*

Figure 3.12: *Virgaichnus undulatus in bedding-plane view showing both straight and meandering form, Locality 1 (Bolterdalen). Photo: Dr. Dirk Knaust (2015). Scale bar = 1 cm.*

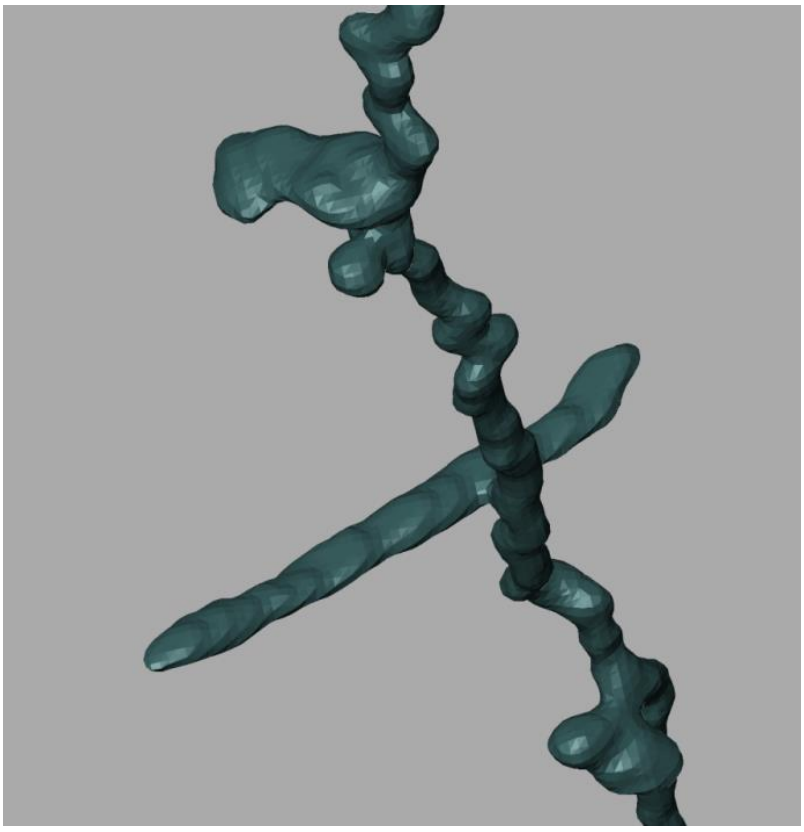

Figure 3.13: Micro CT-scan of sample 2, well BH-9-2006, depth: 386.70 m. The CT-scan displays mud-filled Virgaichnus undulatus as an inclined element with pinch-and-swell features creating almost bulbous enlargements along the burrow. A horizontal burrow element displays alternating blade-like contractions (Knaust, pers. comm. 2016). The average burrow diameter varies between 0.3 and 0.6 mm.

Interpretation

Meiobenthic trace fossils studied in Late Permian carbonates in Oman are suggested to have been produced by a highly deformable vermiform body known as nemerteans which could have created the *Virgaichnus* burrow systems (Knaust, 2009). *Virgaichnus undulatus* reflects an undulating burrow pattern with bulbous enlargements and alternating blade-like contractions that can be explained by a certain behavior of extremely flexible nemerteans (Knaust, 2009).

Meiobenthic trace fossils are highly important in the ichnological record, but their study is underrepresented and therefore still under debate (Knaust, 2007). Recent studies of modern environments reveal that meiobenthic trace fossils dominate in a number of ecosystems, and therefore they play an important role in the bioturbation of sediments of deposits ranging from continental to deep marine settings (Knaust, 2009). *Virgaichnus* occurs in environments with both low and high-energy conditions in the Grumantbyen Formation, together with a diverse community of trace fossils. This also points to well preservation potential based on occurrence in the succession. The only study on *Virgaichnus undulatus* has documented its occurrence in shelf deposits dominated by quiet sedimentation conditions in shallow-marine environments, such as in Late Permian Saiq Formation in Oman (stable inner shelf), Upper Jurassic Heather Formation in the Norwegian North sea (shelf turbidites) and Lower Cretaceous Åsgård Formation in the Norwegian North sea (shelf) (Knaust, pers. comm. 2016). Based on the observations done on the *Virgaichnus undulatus* burrow it has been suggested that it stands as a component of the *Cruziana* Ichnofacies (Knaust, pers. comm. 2016).

3.2 Ichnofabrics

In this chapter the abundance and reappearance of the same trace fossils occurring in the Grumantbyen Formation are being further described under the ichnofabric concept. An ichnofabric is described as the sediment's texture and internal structure as a result of bioerosion and bioturbation at every scale (Taylor and Goldring, 1993). An ichnofabric analysis studies both the biogenic and physical effects within the sediment (Taylor and Goldring, 1993). A total of seven ichnofabrics have been identified, and will be described in this chapter. A gradual transition between these ichnofabrics is not uncommon, and some of the ichnofabrics are more frequently related to each other throughout the succession.

Ichnofabric constituent diagrams have been used in this chapter in order to give a graphical representation of the different ichnofabrics present in terms of description and comparison, and also to understand the order in which they were emplaced (Figure 3.14). The bioturbation index and ichnofabric constituent diagram are complementary as each attempts to record a different aspect of bioturbation (Taylor and Goldring, 1993). In the intervals were the sediments are completely bioturbated (BI=6, 100 %), no sedimentary structures are present. The primary sedimentary fabric has gradually been destroyed by repeated reworking and multiple burrow overlaps. This repeated reworking could potentially create total "chaos" in the sediment's texture, making it completely homogeneous and difficult to identify the associated traces. This is referred to as *diffuse bioturbated texture*, and it can be observed in intervals in between the other characteristic trace fossils identified.

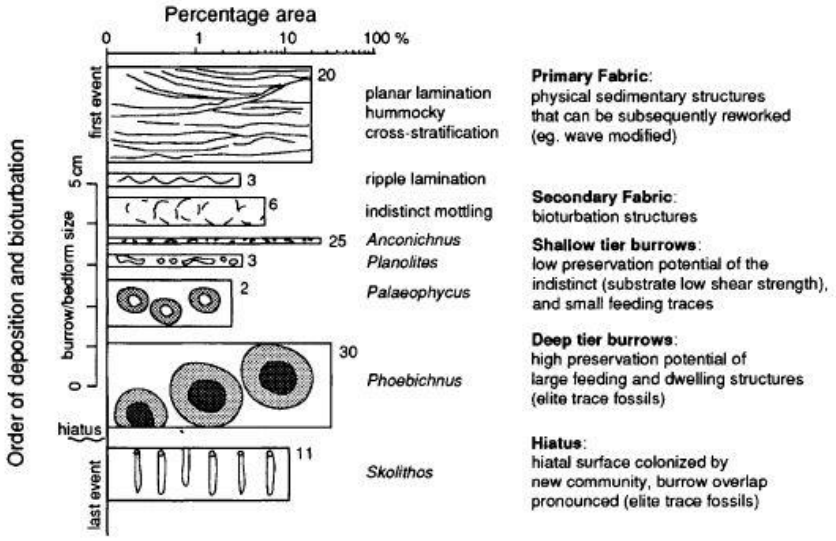

Figure 3.14: *The ichnofabric constituent diagram records on the horizontal axis the percentage area occupied by the primary and secondary sedimentary structures, plotted to a log-scale (Taylor and Goldring, 1993). The vertical axis records the primary sedimentary structures, ichnotaxa present, ichnodiversity, size and order of emplacement* (Taylor and Goldring, 1993).

Cylindrichnus – Ichnofabric

Cylindrichnus – Ichnofabric (Figure 3.2) occurs in lithofacies F.2-F.4 (Chapther 4.1), and is well represented in Lithofacies F.3. It accounts for 26.7 % of the total amount of ichnofabrics present in Lithofacies F.3 (Figure 3.28). A detailed description of the ichnofabric is given in (Table 3.1), and based on this description an ichnofabric constituent diagram is illustrated in (Figure 3.15).

Sample/Interval	Well BH-10-2008. Depth: 873.70-873.92 (22 cm)
Lithology	Very fine-grained, well-sorted, medium gray-color, moderately silty sandstone with a few moderate number of wave-ripple-cross-laminations (WRCL)
Bioturbation intensity	Intensely bioturbated (BI=5 – 95 %)
Ichnotaxa/Ichnodiversity	*Cylindrichnus concentricus* = 80 %, 3.0 mm (diameter), 2.7 cm (length) *Virgaichnus undulatus* = 16 %, 0.5 mm (diameter), 1.0 cm (length) *Macaronichnus segregatis* = 4 %, 2.0 mm (diameter)
First to last-event **Percentage of area**	1. Wave-ripple-cross-laminations (WRCL) = 25 % 2. *Macaronichnus segregatis* (Mac) = 3% 3. *Virgaichnus undulatus* (Virga) = 12 % 4. *Cylindrichnus concentricus* (Cyl) = 60 %
Palaeoenvironment	Lower shoreface

Table 3.1: *Ichnofabric analysis of a Cylindrichnus – Ichnofabric.*

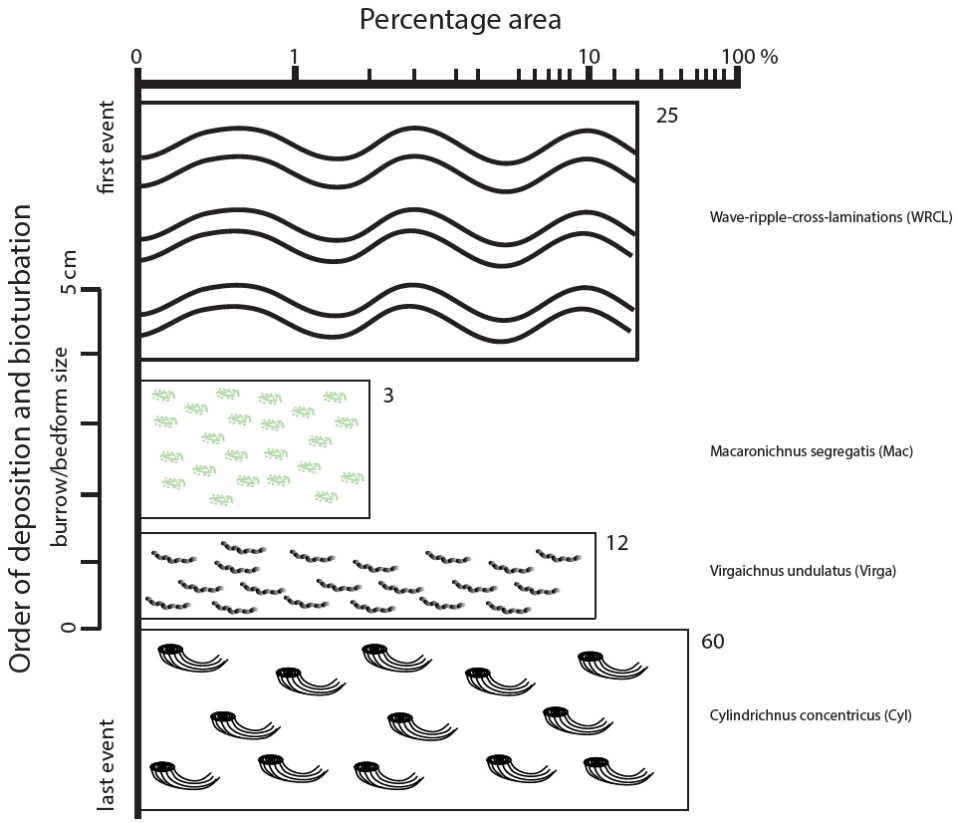

Figure 3.15: *An ichnofabric constituent diagram based on* (Table 3.1).

Macaronichnus – Ichnofabric

Macaronichnus – Ichnofabric (Figure 3.16) occurs in lithofacies F.3 & F.4 (Chapther 4.1), and is well represented in Lithofacies F.4. It accounts for 45.0 % of the total amount of ichnofabrics present in Lithofacies F.4 (Figure 3.28). A detailed description of the ichnofabric is given in (Table 3.2), and based on this description an ichnofabric constituent diagram is illustrated in (Figure 3.17).

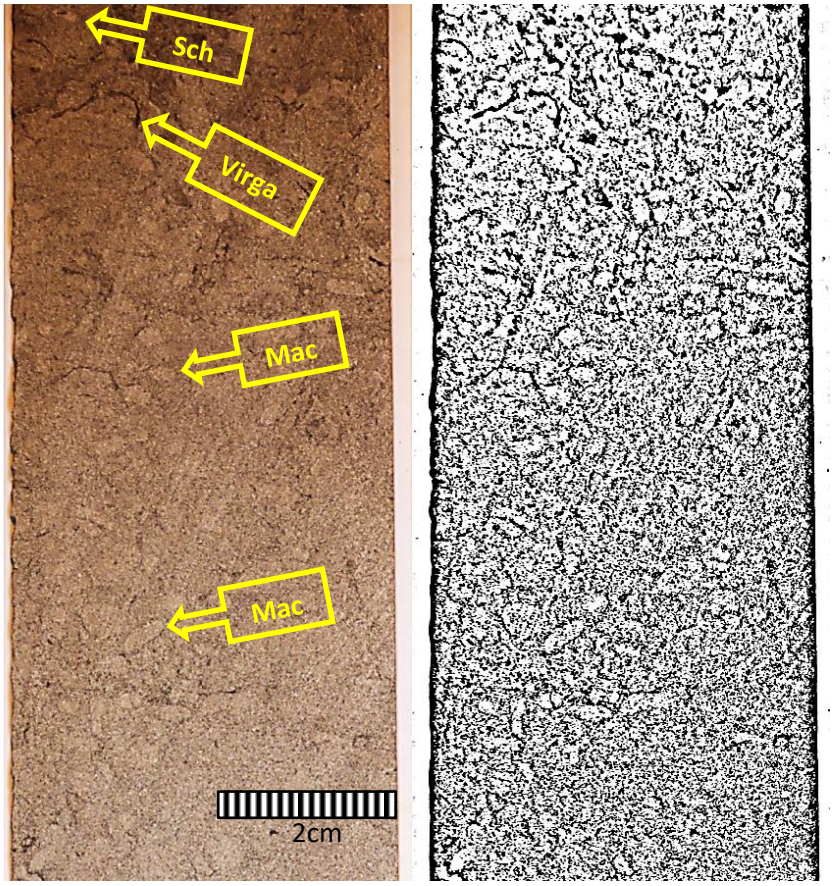

***Figure 3.16**: Vertical-section with Macaronichnus – Ichnofabric, well BH-10-2008, depth: 813.85 m. The right picture is a black&white filter applied to the original in order to better visualize the elongate to oval or circular shapes of the Macaronichnus burrow in the core.*

Sample/Interval	Well BH-10-2008. Depth: 813.63-814.00 (37 cm)
Lithology	Very fine to fine-grained, very well sorted, pale green-color, light silty sandstone
Bioturbation intensity	Completely bioturbated (BI=6 – 100 %)
Ichnotaxa/Ichnodiversity	*Macaronichnus segregatis* = 75 %, 2.0 mm (diameter), 5.0 mm (length) *Virgaichnus undulatus* = 20 %, 0.5 mm (diameter), 1.0 cm (length) *Schaubcylindrichnus coronus* = 5 %, 3.0 mm (diameter)
First to last-event **Percentage of area**	1. Diffuse bioturbated texture (chaotic bioturbated-sand) = 40 % 2. *Macaronichnus segregatis* (Mac) = 45 % 3. *Virgaichnus undulatus* (Virga) = 12 % 4. *Schaubcylindrichnus coronus* (Sch) = 3 %
Palaeoenvironment	Upper-shoreface

***Table 3.2:** Ichnofabric analysis of a Macaronichnus – Ichnofabric.*

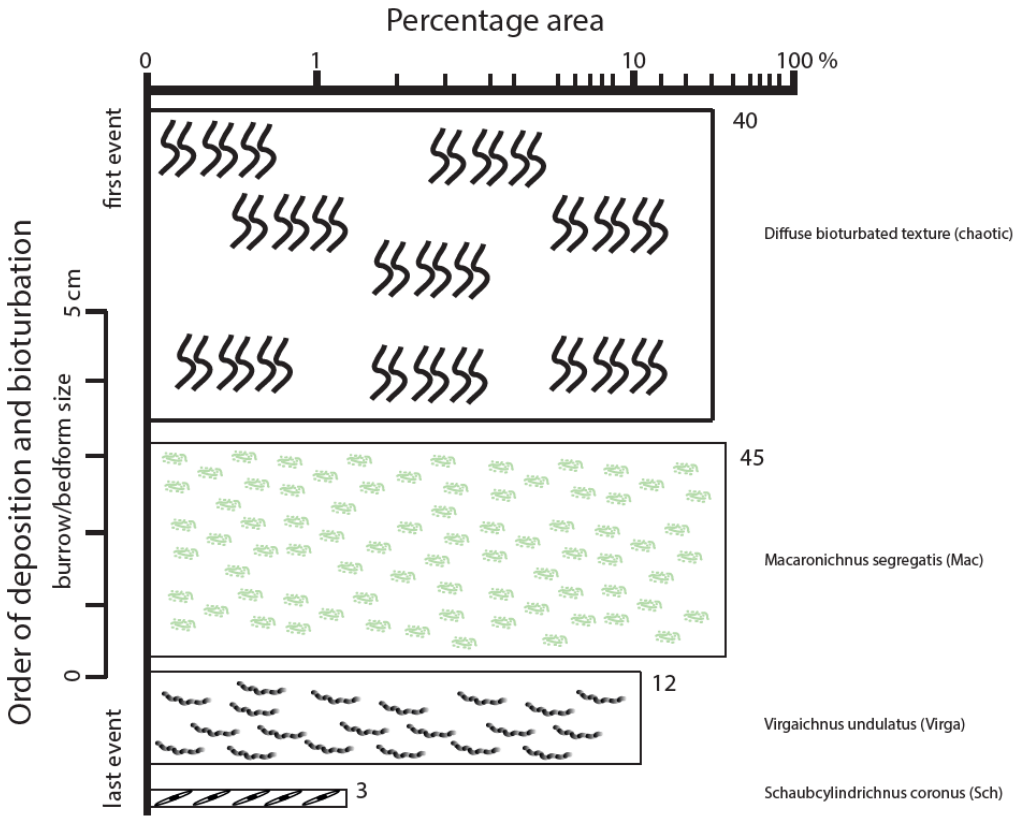

Figure 3.17: *An ichnofabric constituent diagram based on* (Table 3.2).

Nereites – Ichnofabric

Nereites – Ichnofabric (Figure 3.18) is very well represented in Lithofacies F.1 (Chapter 4.1), were it is quite abundant and account for 65.0 % of the total amount of ichnofabrics present in Lithofacies F.1 (Figure 3.28). A detailed description of the ichnofabric is given in (Table 3.3), and based on this description an ichnofabric constituent diagram is illustrated in (Figure 3.19).

Sample/Interval	Well BH-9-2006. Depth: 381.50-381.60 (10 cm)
Lithology	Clay to silt grain-size, very well-sorted, dark-color, sandy siltstone
Bioturbation intensity	Completely bioturbated (BI=6 – 100 %)
Ichnotaxa/Ichnodiversity	*Nereites* = 94.4 %, 0.2-0.5 mm (diameter), 1.0-2.0 mm (length) *Schaubcylindrichnus coronus* = 5.6 %, 1.5 mm (diameter)
First to last-event Percentage of area	1. Diffuse bioturbated texture (chaotic bioturbated-silty substrate) = 45 % 2. *Nereites* (Ne) = 52 % 3. *Schaubcylindrichnus coronus* (Sch) = 3 %
Palaeoenvironment	Offshore

Table 3.3: *Ichnofabric analysis of a Nereites – Ichnofabric.*

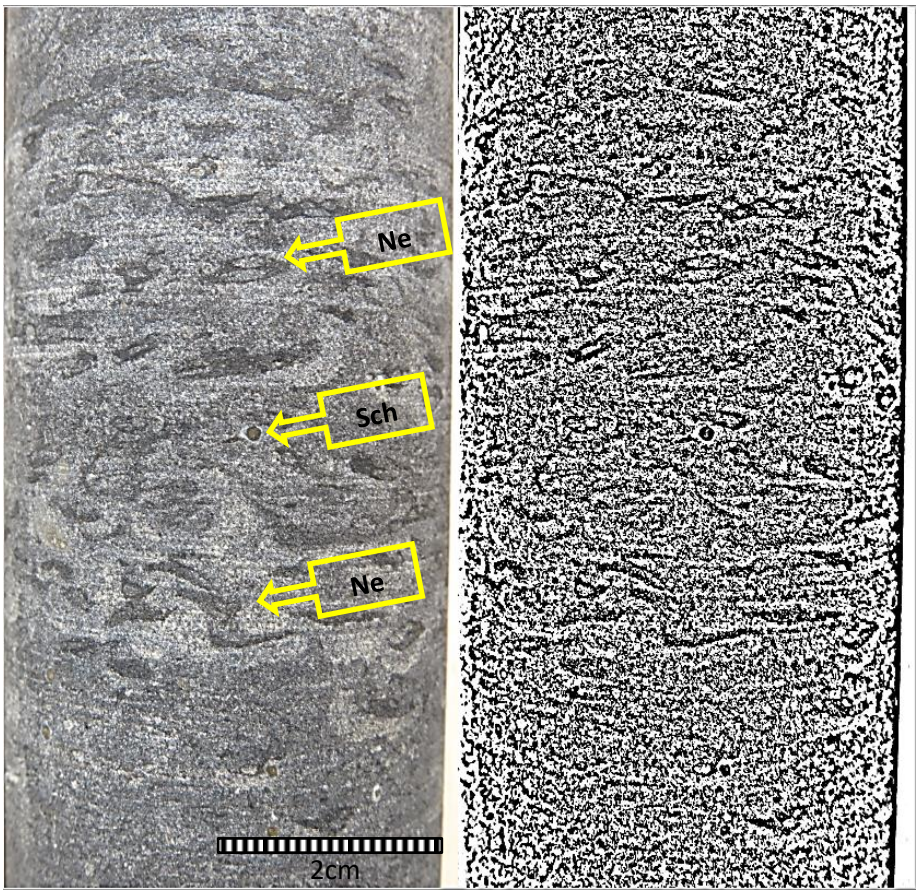

Figure 3.18: *Vertical-section with Nereites – Ichnofabric, well BH-9-2006, depth: 381.55 m. The right picture is a black&white filter applied to the original in order to better visualize Nereites which appears as clusters of elongated horizontal to subhorizontal-wavy dark ribbon structures bounded by lighter zones in the core.*

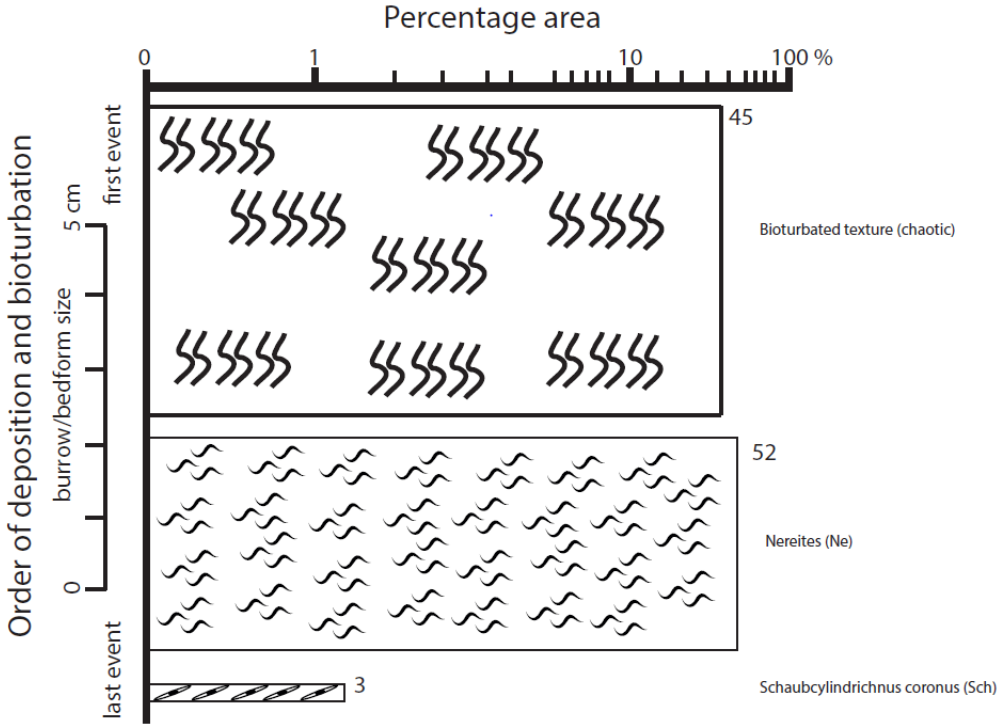

Figure 3.19: *An ichnofabric constituent diagram based on* (Table 3.3).

Teichichnus – Ichnofabric

Teichichnus – Ichnofabric (Figure 3.20) occurs in lithofacies F.2 & F.3 (Chapther 4.1), and is best represented in Lithofacies F.2. It accounts for 14.0 % of the total amount of ichnofabrics present in Lithofacies F.2 (Figure 3.28). A detailed description of the ichnofabric is given in (Table 3.4), and based on this description an ichnofabric constituent diagram is illustrated in (Figure 3.21).

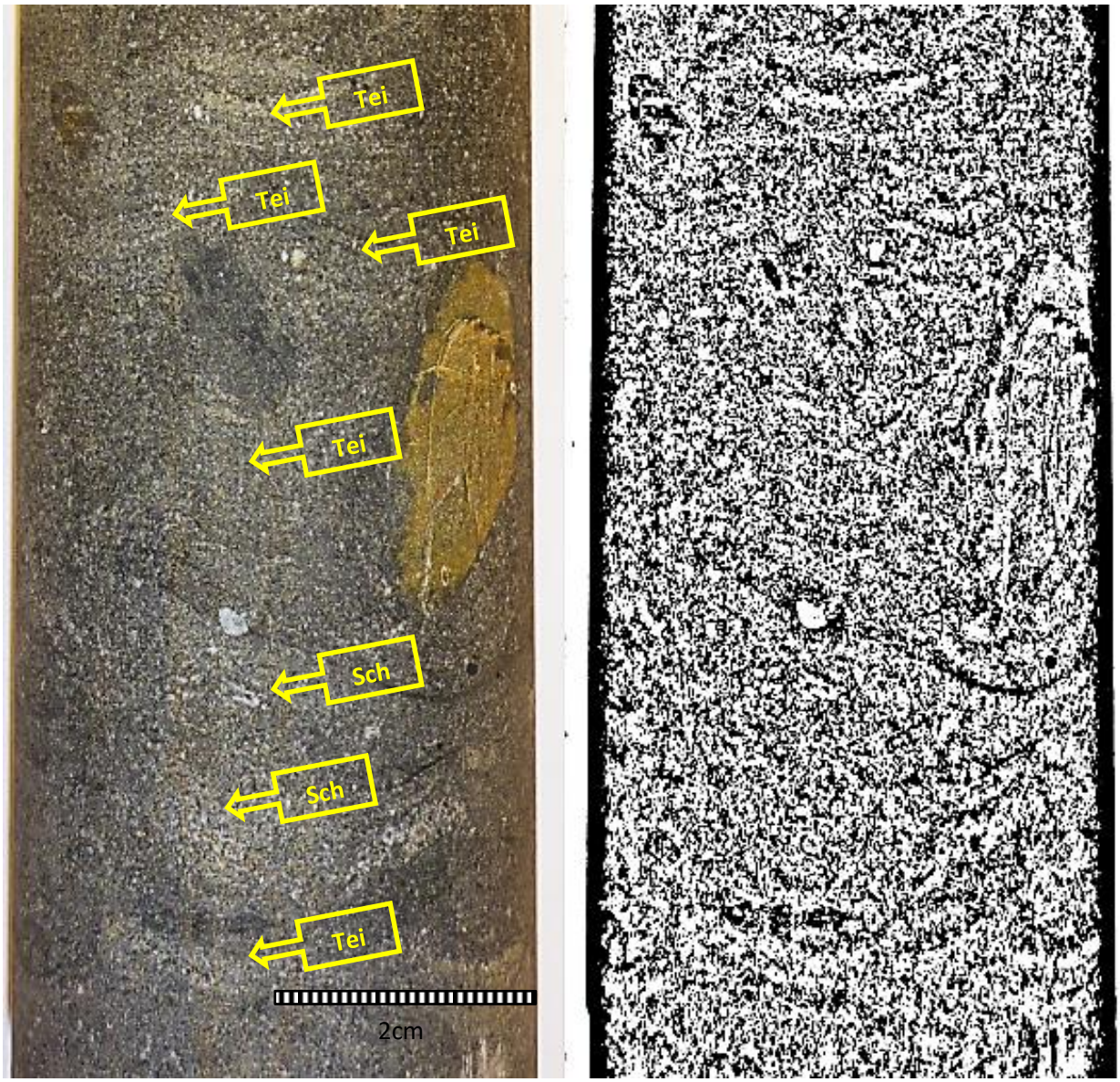

Figure 3.20: *Vertical-section with Teichichnus – Ichnofabric in well BH-9-2006, sample 4, depth: 317.50 m. The right picture is a black&white filter applied to the original in order to better visualize Teichichnus which appear with vertical slightly curved architecture being closely stacked with a diagnostic zigzag pattern.*

Sample/Interval	Well BH-9-2006. Sample 4. Depth: 317.45-317.65 (20 cm)
Lithology	Very fine-grained, very well-sorted, dark gray-color, silty sandstone
Bioturbation intensity	Completely bioturbated (BI=6 – 100 %)
Ichnotaxa/Ichnodiversity	*Teichichnus zigzag* = 70 %, 0.5-2.0 cm (width), 4.0-6.0 cm (length) *Schaubcylindrichnus coronus* = 30 %, 1.0 mm (diameter)
First to last-event **Percentage of area**	1. Diffuse bioturbated texture (chaotic bioturbated-sand) = 50 % 2. *Teichichnus zigzag* (Tei) = 35 % 3. *Schaubcylindrichnus coronus* (Sch) = 15 %
Palaeoenvironment	Offshore transition

Table 3.4: *Ichnofabric analysis of a Teichichnus – Ichnofabric.*

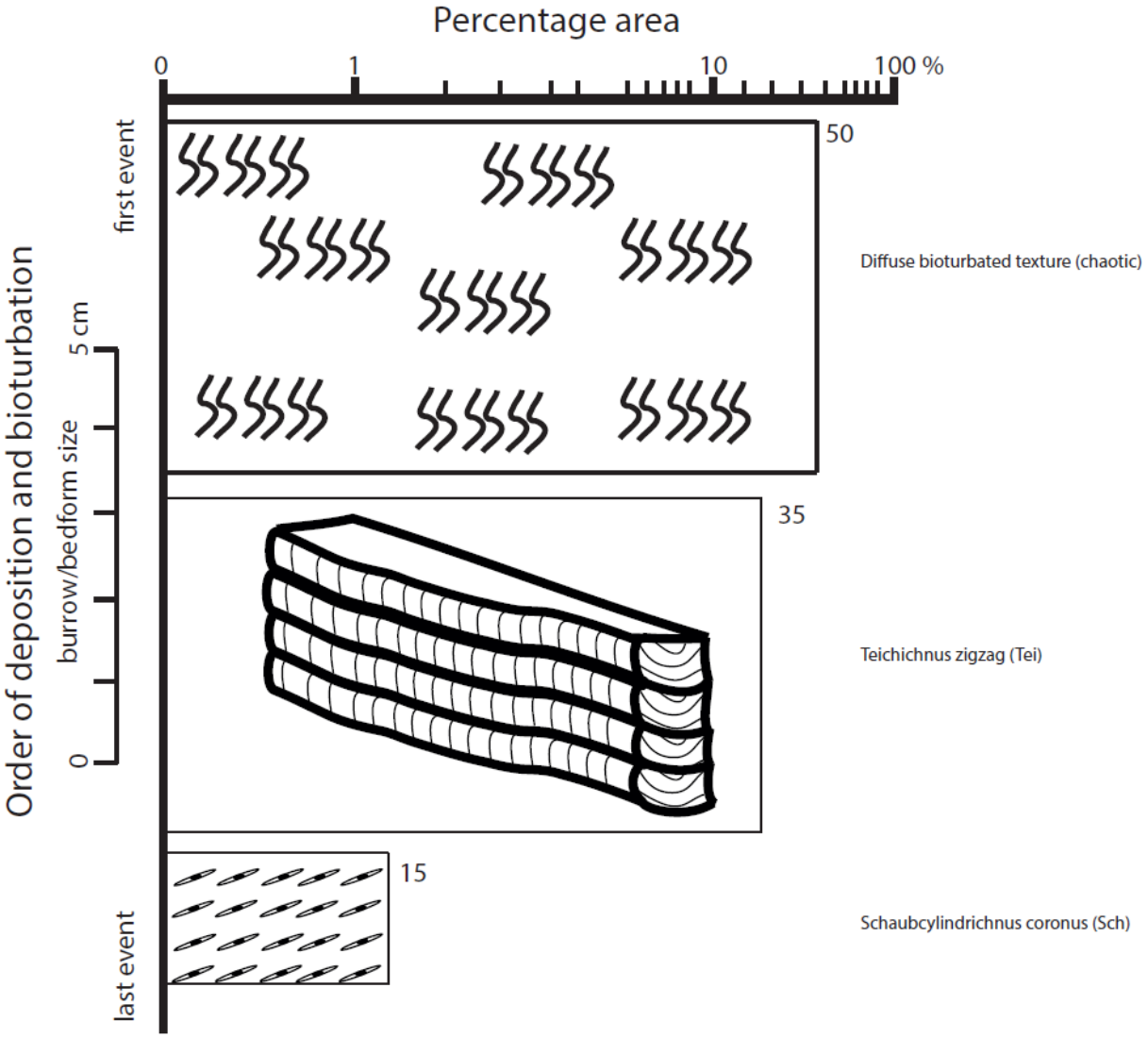

Figure 3.21*: An ichnofabric constituent diagram based on* (Table 3.4).

Virgaichnus – Ichnofabric

Virgaichnus – Ichnofabric (Figure 3.22) is well represented in all of the Lithofacies (Chapter 4.1), but clearly shows a great abundance in Lithofacies F.2. Here it accounts for 53.0 % of the total amount of ichnofabrics present (Figure 3.28). A detailed description of the ichnofabric is given in (Table 3.5), and based on this description an ichnofabric constituent diagram is illustrated in (Figure 3.23).

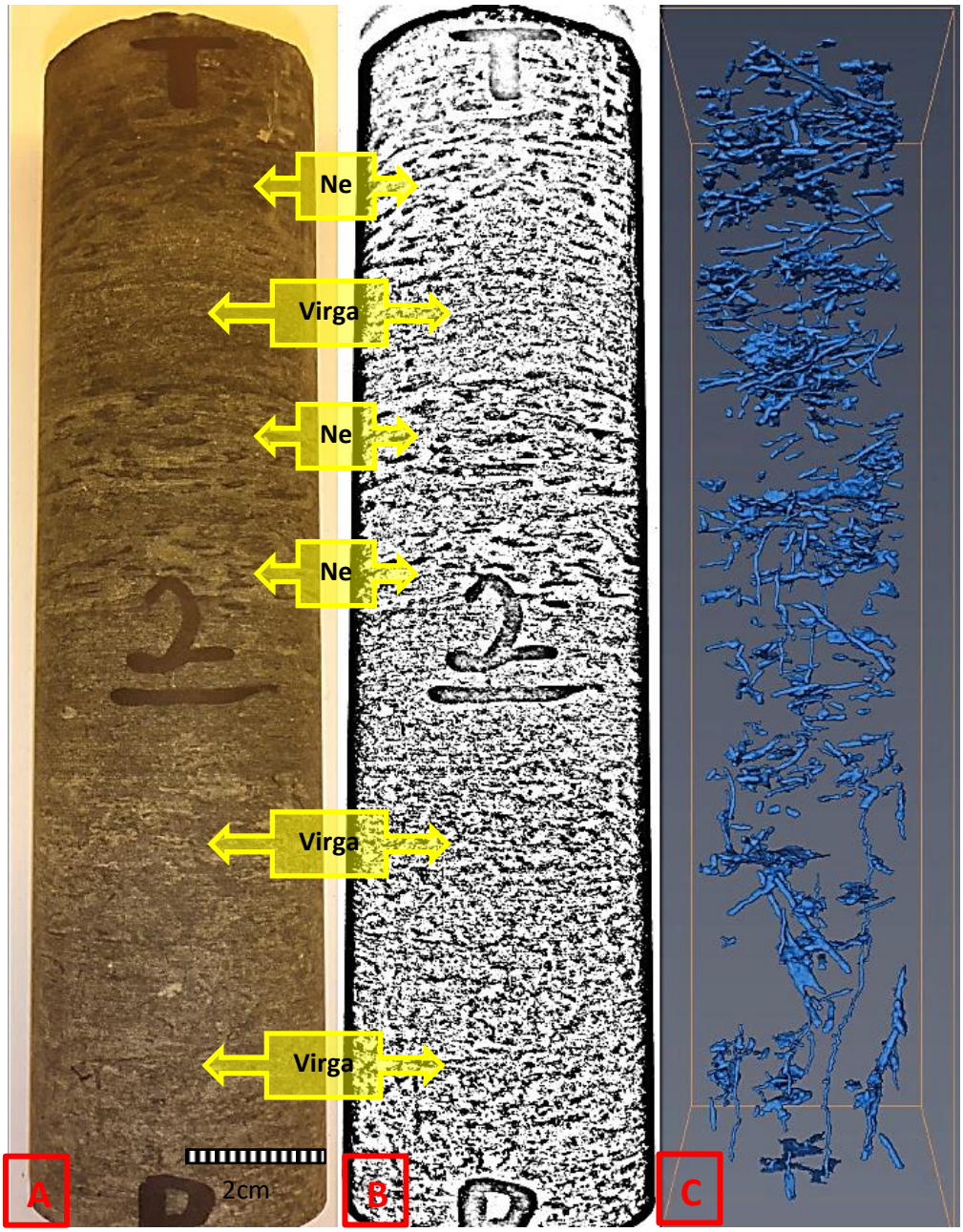

Figure 3.22: *(A) Vertical-section with Virgaichnus – Ichnofabric in well BH-9-2006, sample 2, depth: 386.62-386.82 m. (B) Black&white filter applied to the original in order to better visualize Virgaichnus as a burrow that is highly irregular with both horizontal and inclined elements. Nereites is also strongly represented in the sample, especialy in the 2D-view. (C) 3D-result of the sample from the micro-CT scan showing numerous Virgaichnus burrows branching in different directions. The average burrow diameter varies between 0.3 and 0.6 mm.*

Sample/Interval	Well BH-9-2006. Sample 2. Depth: 386.62-386.82 (20 cm)
Lithology	Very fine-grained, very well-sorted, dark-color, sandy siltstone
Bioturbation intensity	Completely bioturbated (BI=6 – 100 %)
Ichnotaxa/Ichnodiversity	*Virgaichnus undulatus* = 60 %, 0.5 mm (diameter), 1.0 cm (length) *Nereites* = 40 %, 0.2-1.0 mm (diameter), 1.0-5.0 mm (length)
First to last-event **Percentage of area**	1. Diffuse bioturbated texture (chaotic bioturbated-silty substrate) = 50 % 2. *Nereites* (Ne) = 20 % 3. *Virgaichnus undulatus* (Virga) = 30 %
Palaeoenvironment	Offshore

Table 3.5: *Ichnofabric analysis of a Virgaichnus – Ichnofabric.*

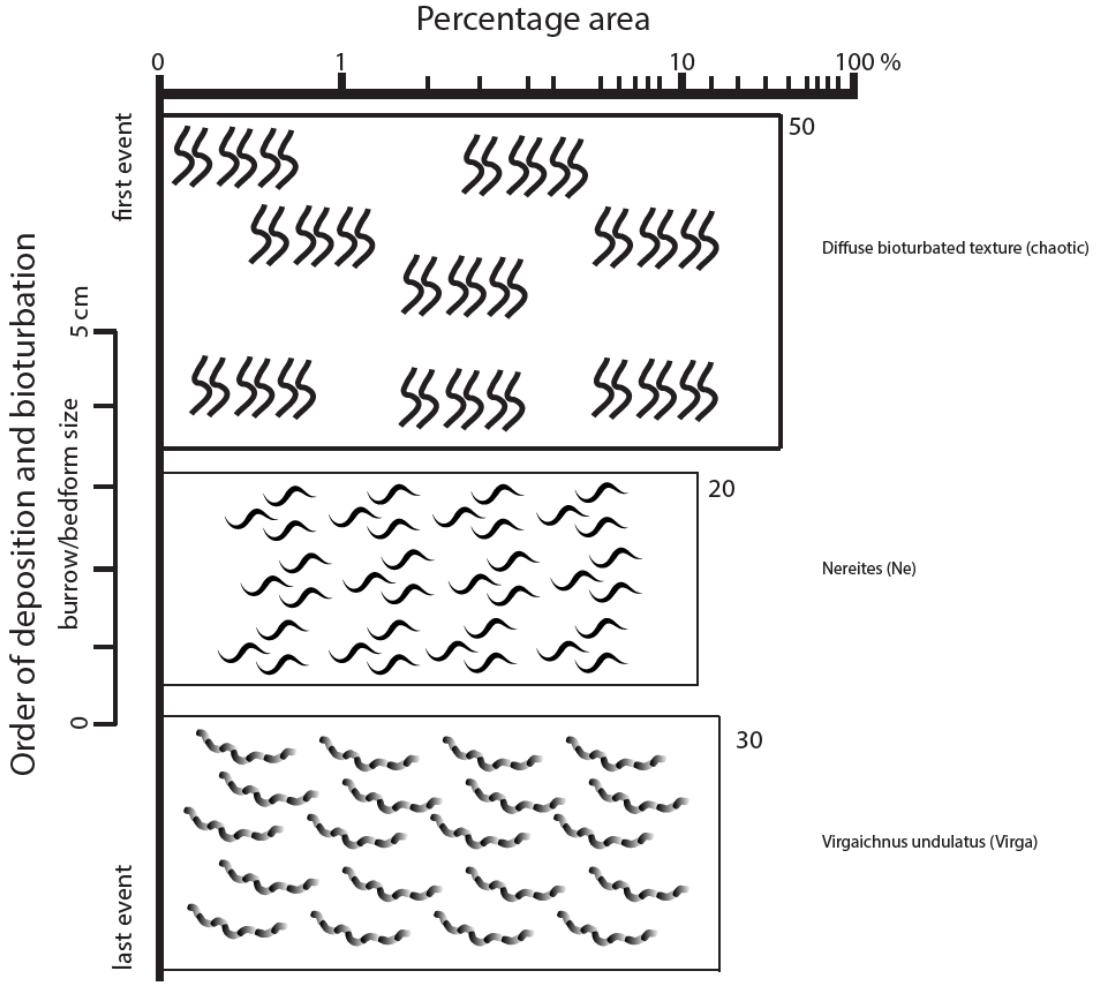

Figure 3.23*: An ichnofabric constituent diagram based on* (Table 3.5).

Palaeophycus – Ichnofabric

Palaeophycus – Ichnofabric (Figure 3.24) occurs in lithofacies F.2-F.4 (Chapther 4.1), and is well represented in Lithofacies F.3. It accounts for 20.0 % of the total amount of ichnofabrics present in Lithofacies F.3 (Figure 3.28). A detailed description of the ichnofabric is given in (Table 3.6), and based on this description an ichnofabric constituent diagram is illustrated in (Figure 3.25).

Figure 3.24: *Palaeophycus – Ichnofabric seen on bedding plane at Locality 1, Bolterdalen. Palaeophycus shows a characteristic straight-cylindrical architecture. The right picture is a black&white filter applied to the original in order to better visualize the burrow architecture marked in yellow. Scale in cm.*

Sample/Interval	Locality 1, Bolterdalen. 15.0 m-log.
Lithology	Very fine-grained, well-sorted, medium gray-color, moderately silty sandstone
Bioturbation intensity	Completely bioturbated (BI=6 – 100 %)
Ichnotaxa/Ichnodiversity	*Palaeophycus tubularis* =70 %, 1.0-1.5 cm (diameter), 6.0-8.0 cm (length) *Schaubcylindrichnus coronus* = 30 %, 3.0 mm (diameter)
First to last-event **Percentage of area**	1. Diffuse bioturbated texture (chaotic bioturbated-sand) = 70 % 2. *Palaeophycus tubularis* (Pal) = 21% 3. *Schaubcylindrichnus coronus* (Sch) = 9 %
Palaeoenvironment	Lower shoreface

Table 3.6: *Ichnofabric analysis of a Palaeophycus – Ichnofabric.*

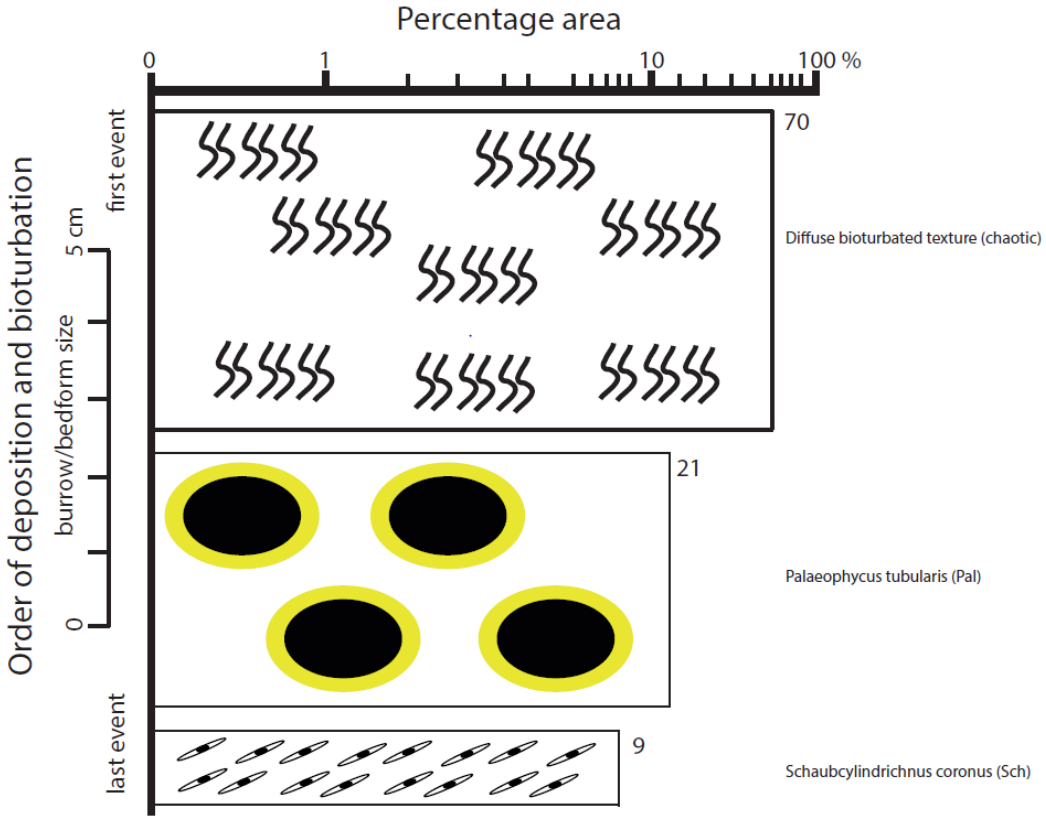

***Figure 3.25**: An ichnofabric constituent diagram based on* (Table 3.6).

Schaubcylindrichnus – Ichnofabric

Schaubcylindrichnus – Ichnofabric (Figure 3.26) occurs in Lithofacies F.2-F.4 (Chapter 4.1), and is best represented in Lithofacies F.3. Here it accounts for 13.3 % of the total amount of ichnofabrics present (Figure 3.28). A detailed description of the ichnofabric is given in (Table 3.7), and based on this description an ichnofabric constituent diagram is illustrated in (Figure 3.27).

Sample/Interval	Well BH-9-2006. Sample 5. Depth: 314.89-315.00 (11 cm)
Lithology	Silt/very fine-grained, very well-sorted, dark-color, sandy siltstone
Bioturbation intensity	Completely bioturbated (BI=6 – 100 %)
Ichnotaxa/Ichnodiversity	*Schaubcylindrichnus coronus* = 45 %, 2.0-3.0 mm (diameter) *Nereites* = 35 %, 0.2-0.5 mm (diameter), 1.0-2.0 mm (length) *Virgaichnus undulatus* = 20 %, 0.5 mm (diameter), 1.0 cm (length)
First to last-event Percentage of area	1. Diffuse bioturbated texture (chaotic bioturbated-silty substrate) = 60 % 2. *Nereites* (Ne) = 14 % 3. *Virgaichnus undulatus* (Virga) = 8 % 4. *Schaubcylindrichnus coronus* (Sch) = 18 %
Palaeoenvironment	Offshore

***Table 3.7:** Ichnofabric analysis of a Schaubcylindrichnus – Ichnofabric.*

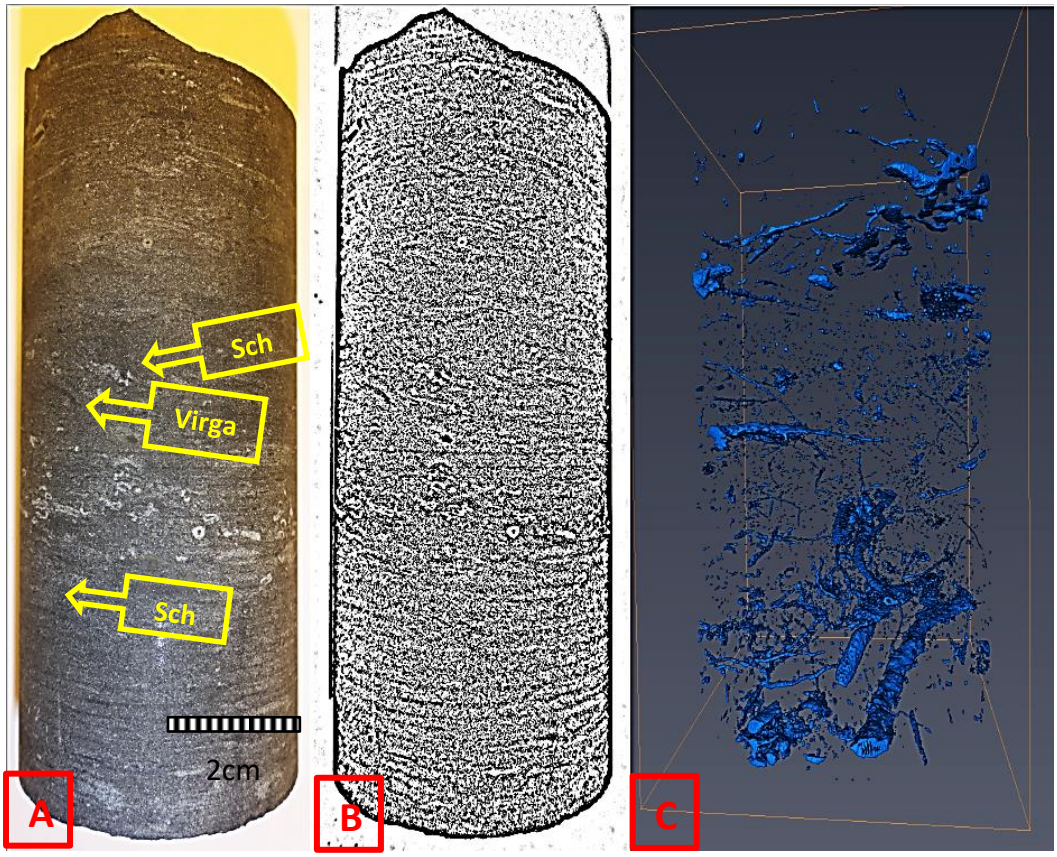

Figure 3.26: *(A) Vertical-section with Schaubcylindrichnus – Ichnofabric in well BH-9-2006, sample 5, depth: 314.89-315.00 m. (B) Black&white filter applied to the original in order to better visualize Schaubcylindrichnus as a tube with a characteristic white ring appearing isolated or in closely packed groupings. (C) 3D-result of the sample from the micro-CT scan. Nereites and Virgaichnus are also well represented in the sample.*

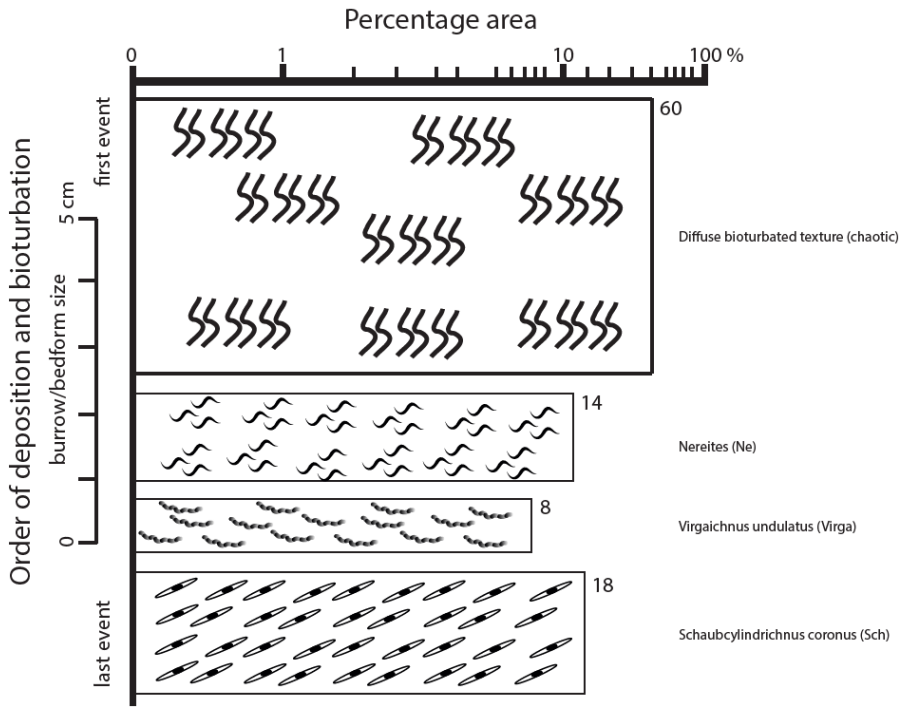

Figure 3.27: *An ichnofabric constituent diagram based on* (Table 3.7).

3.2.1 Ichnofabric distribution within the Grumantbyen Formation

In the three logs made from the study of both wells and the outcrop, a column describing the ichnofabric present is available, see Appendix 11, Appendix 12 and Appendix 13. Based on the ichnofabrics present in the different wells and the outcrop studied (Locality 1, Bolterdalen), a graphical visualization of their appearance is presented (Figure 3.28). The figure is based on a calculated mean percentage of the ichnofabrics present within the two wells and the outcrop studied (Locality 1, Bolterdalen) (Appendix 1).The chart illustrates the percentage of different ichnofabrics within four of the defined lithofacies in the Grumantbyen Formation, introduced in Chapter 4.1. The percentage is based on the number of appearances of the different ichnofabrics within each lithofacies. On the horizontal axis the lithofacies are arranged from distal to proximal affiliation.

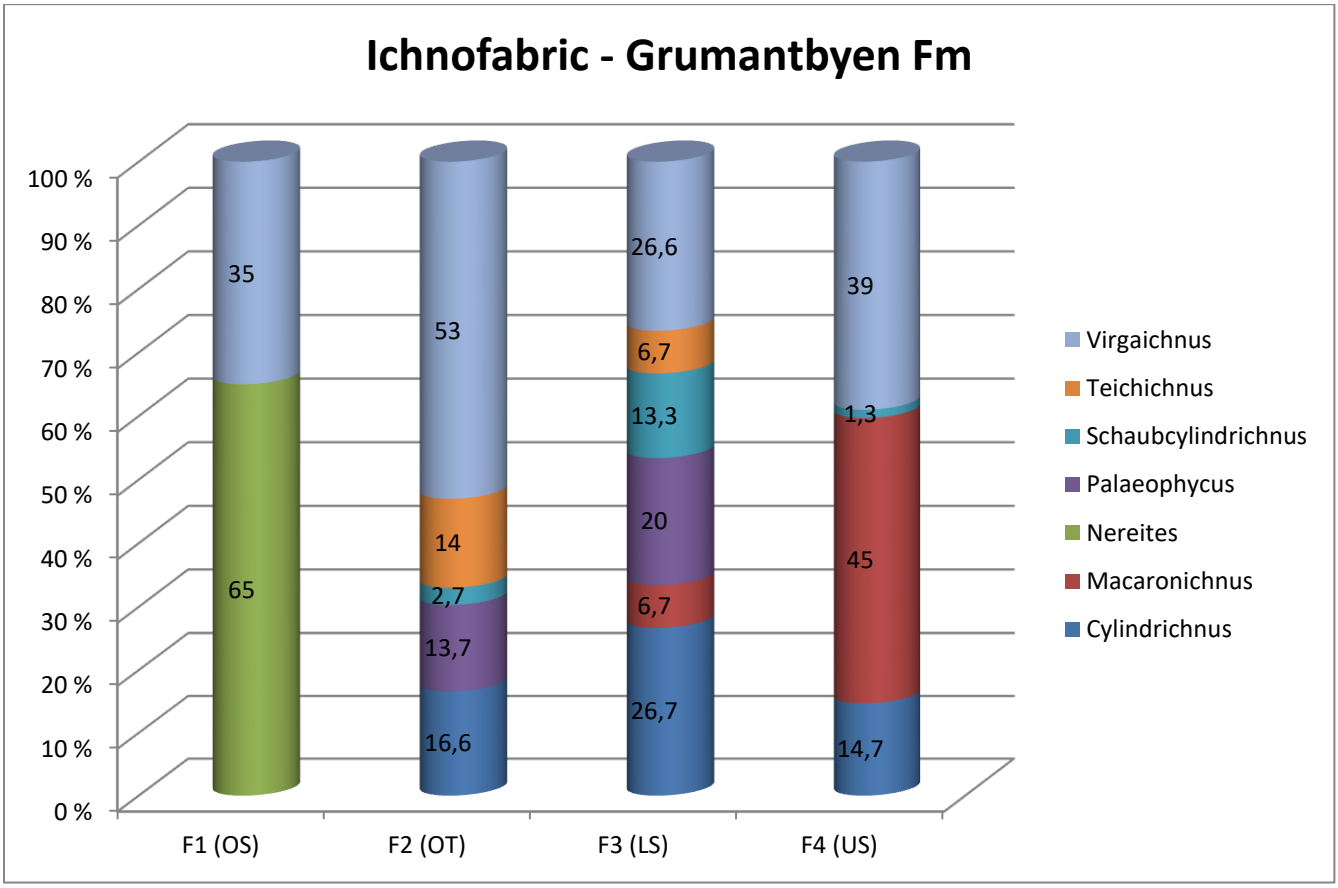

***Figure 3.28**: A graphical visualization of the different ichnofabrics present within four defined lithofacies (F1-F4) in the Grumantbyen Formation. On the horizontal axis the lithofacies are arranged from distal to proximal affiliation. OS= offshore, OT=Offshore transition, LS= Lower shoreface and US= Upper shoreface. The different ichnofabrics are arranged vertically in alphabetical order from bottom to top.*

4 Lithology

The sedimentary rocks within the Grumantbyen Formation have been organized into separate lithofacies. The descriptions of the different lithofacies are based on sedimentary textures and structures, trace fossil diversity and ichnofabrics, bioturbation intensity and color. A total of five lithofacies have been interpreted from the different wells and the outcrop studied. A summary of the different lithofacies are presented in Table 4.1, and they are each briefly described later in the chapter. The different lithofacies are arranged from distal to proximal affiliation. An interpretation of the associated palaeoenvironment of the different lithofacies is given, and a summary of these interpretations are listed in Table 4.1. Because the Grumantbyen Formation is characterized as being intensely bioturbated throughout the whole succession, a study of its ichnology (Chapter 3) has been most valuable in terms of defining a possible depositional environment for the different lithofacies, when physical sedimentary structures are nearly absent.

4.1 Lithofacies

Table 4.1: *A quick summary of the description of the different lithofacies observed (F1-F4). The ichnofabric marked in bold is the most abundant one within the specific lithofacies* (Figure 3.28). An interpretation of the palaeoenvironment of the individual lithofacies is presented.

Lithofacies	Characterization	Grain Size	Silt/Sand (%)	Ichnofabrics	Sedimentary structures	Color Code	Bioturbation (%)	Thick-ness (m)	Palaeo-environment
F1	Sandy Siltstone	Clay/ Silt – Vf Sand	≥80/≤ 20	**Nereites** Virgaichnus	Little PPL	N2	90 – 100	0.40 – 15 m	Offshore
F2	Silty Sandstone	Silt – Vf Sand	≥50/≤ 50	Cylindrichnus Palaeophycus Schaubcylindrichnus Teichichnus **Virgaichnus**	Little WRCL	N4	80 – 100	1 – 38.25 m	Offshore-transition
F3	Moderately Silty Sandstone	Vf Sand – Vf/F Sand	≥30/≤ 70	**Cylindrichnus** Macaronichnus Palaeophycus Schaubcylindrichnus Teichichnus Virgaichnus	Moderate WRCL HCS	N5	80 – 100	0.25 – 34.5 m	Lower-shoreface
F4	Light Silty Sandstone	Vf/F Sand – M/Crs Sand	≥0/≤100	Cylindrichnus **Macaronichnus** Schaubcylindrichnus Teichichnus Virgaichnus	Abundant WRCL TCS	5Y 8/1, 10G 6/2, 5G 6/1	0 – 100	0.40 – 77.60 m	Upper-shoreface
F5	Gravel	VCrs Sand - Granule	0/100	Macaronichnus Schaubcylindrichnus	Little WRCL	N2, N5, 5G 6/1	0 – 50	0.15 – 0.25 m	Trangsgressive lag

Facies F.1 – *Sandy Siltstone*

Description

A dark sandy siltstone occurs at the bottom and top of the Grumantbyen Formation (Figure 4.1). The lithofacies is especially well developed and up to 15 m thick in the lower part of well BH-10-2008 (Appendix 11), but it also occurs in thinner intervals in well BH-9-2006 (Appendix 13). The same lithofacies was not observed in the outcrop section studied (Locality 1, Bolterdalen). The thinnest intervals measured are around 25 cm in well BH-10-2008. In the upper part of both wells the lithofacies is also resting sharply on top of Lithofacies F.4, where it measures a thickness greater than 2 meters in both wells studied (Figure 4.6-A). The grain-size is a mix between clay/silt and very fine sand, with a sand percentage up to 20% in an otherwise dark siltstone. A few planar-parallel-laminations (PPL) are the only physical sedimentary structures seen in the lithofacies which is dominated by nearly complete bioturbation (90 – 100 %). *Nereites*, *Schaubcylindrichnus* and *Virgaichnus* are all very common trace fossils in the lithofacies. Other trace fossils such as *Teichichnus* occur in minor quantities in well BH-9-2006.

Well rounded and coarse-grained pebbly rock fragments of chert and quartzite were observed in scattered intervals in the wells studied within Lithofacies F.1. These rock fragments are noted as intra clasts in the logs. Microfaults and mud clasts were also observed in minor proportions in the wells. An abundance of pyrite is also typical for this lithofacies and occurs frequently throughout the succession. Intervals with siderite – nodules are sporadically seen in both wells.

Interpretation

Lithofacies F.1 in the lower part of the wells are interpreted to be a transitional lithofacies from the underlying dark shale of the Basilika Formation., while the same lithofacies in the upper part of the wells are interpreted to mark the start of the superimposed Eocene Frysjaodden Formation (Figure 2.2). The lithofacies is dominated by fine-grained material resulting from suspension of fines leid down from the water column under quiet conditions, with occasional input of sandy material. *Nereites* burrows have been proven to occur largely in highly soft muds just above the redox boundary (Wetzel, 2002). According to Wetzel (2002, p. 513) ‘the depth of the redox boundary in sediment is influenced by many factors, including the sedimentation rate and accumulation rate of organic matter, the depth of the *Nereites* level potentially could provide a proxy for one or both of these factors’. Based on the abundance of *Nereites* burrows, the lithofacies seems to be associated with offshore settings. Slow, but still continuous sedimentation rates from suspension are commonly associated with *Nereites* Ichnofacies (Hubbard et al., 2012). Ichnofabric analysis of the lithofacies section reveals that it is dominated by *Nereites* and *Virgaichnus*-Ichnofabric (Figure 3.28). Recent studies indicate that *Virgaichnus* burrows appear in a wide range of deposits from continental to deep marine settings

(Knaust, 2009). *Schaubcylindrichnus* is known to be a good indicator of shallow-marine environments (Frey and Pemberton, 1991), but modern studies also reveals a more offshore appearance (Nara, 2006).

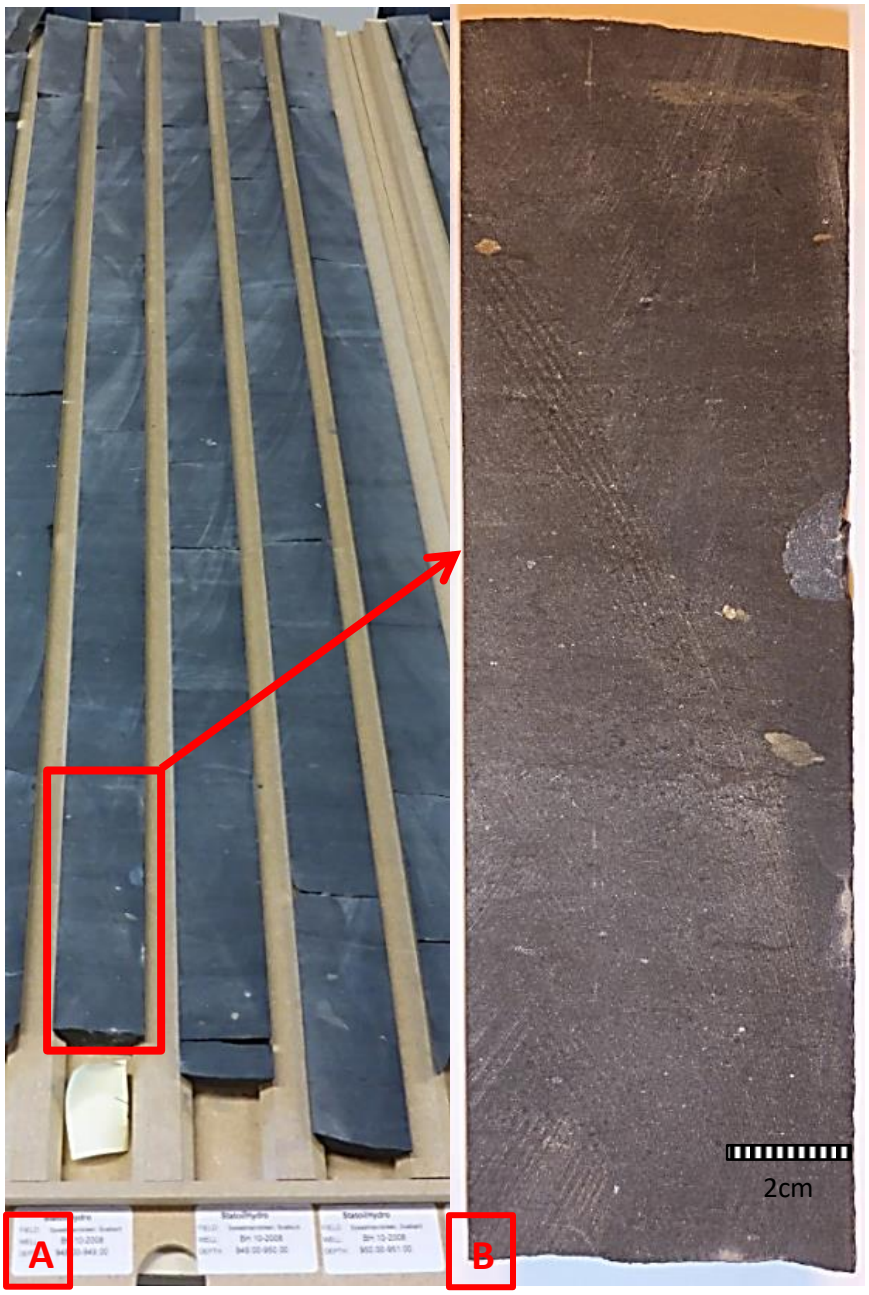

Figure 4.1: *(A) Core photo of Lithofacies F.1 in well BH-10-2008, depth: 947.00-952.00. (B) Core sample of Lithofacies F.1, depth: 948.90-949.00.*

The chert clasts discovered in the wells originated from the Permian Kapp Starostin Formation, which is known to be highly dominated by biogenic silicate (Grundvåg, pers. comm. 2015). The rock fragments seen in the succession has most likely been transported from the beach zone by seasonal winter ice and transported across the shelf, were they have been dropped to the bottom as a result of the gradual melting of the ice (Dalland, 1977). The succession also has a high abundance of pyrite, which is formed in reduced conditions (Fisher and Hudson, 1987) under the redox boundary (Raiswell

and Berner, 1986). Marine environments with sulphate – rich waters are required, but not necessarily restricted to anoxic conditions (Curtis, 1980). These are also favorable conditions for high concentrations of microbial biomass which *Nereites* producers feed on (Wetzel, 2002). The high degree of bioturbation (90 – 100 %), might be an indication that lithofacies F.1 is deposited in quiet conditions under the storm-wave base. Also the grain-size of the lithofacies supports this, indicating short lived events of sandy input with the sand possibly being transported to the distal shelf as a result of major storm events. An offshore environment is suggested based on the fine-grained character of the lithofacies, trace fossils observed and sedimentary structures (Table 4.1). These are also environments were *Nereites* Ichnofacies are considered diagnostic (Seilacher, 1967).

Facies F.2 – *Silty Sandstone*

Description

Lithofacies F.2 is a dark gray silty sandstone (Figure 4.2) seen in both wells and also in the outcrop section studied (Locality 1, Bolterdalen). The lithofacies is especially well developed in well BH-9-2006 where it measures a total thickness of 38.25 meters in the thickest interval (Appendix 13). It is also prominent in well BH-10-2008 were it is measures 10 meters at its maximum and 1 meter at the thinnest interval (Appendix 11). The grain-size alternates between silt and very fine sand, with a silt percentage ranging from 50 % to less than 80 %. A few obscure appearances of wave-ripple-cross laminations (WRCL) are the only physical sedimentary structures seen in the lithofacies which is otherwise dominated by intense to complete bioturbation (80 – 100%).

Virgaichnus, *Teichichnus* and *Cylindrichnus* are abundant in the lithofacies. Other trace fossils such as *Schaubcylindrichnus*, *Palaeophycus*, *Macaronichnus* and *Nereites* are also present in various intervals. *Nereites* is only observed in the deepest intervals in the two wells studied. *Virgaichnus* is particularly prominent in this lithofacies. There is also a clear variation in the trace fossils observed between wells and the outcrop sections studied. *Palaeophycus* is well developed in the outcrop section (Appendix 12) together with *Virgaichnus*, but almost absent in both wells albeit thick intervals of the same lithofacies.

Two intervals composed of green very fine-grained clay sized sediments occur within the lithofacies in well BH-9-2006 (Appendix 13), the intervals measure 10 and 30 cm respectively. These intervals show no indication of bioturbation. Angular to well-rounded and coarse-grained pebbly rock fragments of quartzite were also observed at various intervals in well BH-9-2006 and also at the outcrop section in Locality 1 (Bolterdalen). A relative abundance of pyrite and siderite – nodules is also prominent throughout the lithofacies, especially in well BH-9-2006. Intervals with mud clasts and microfaults are also sporadically seen in both wells.

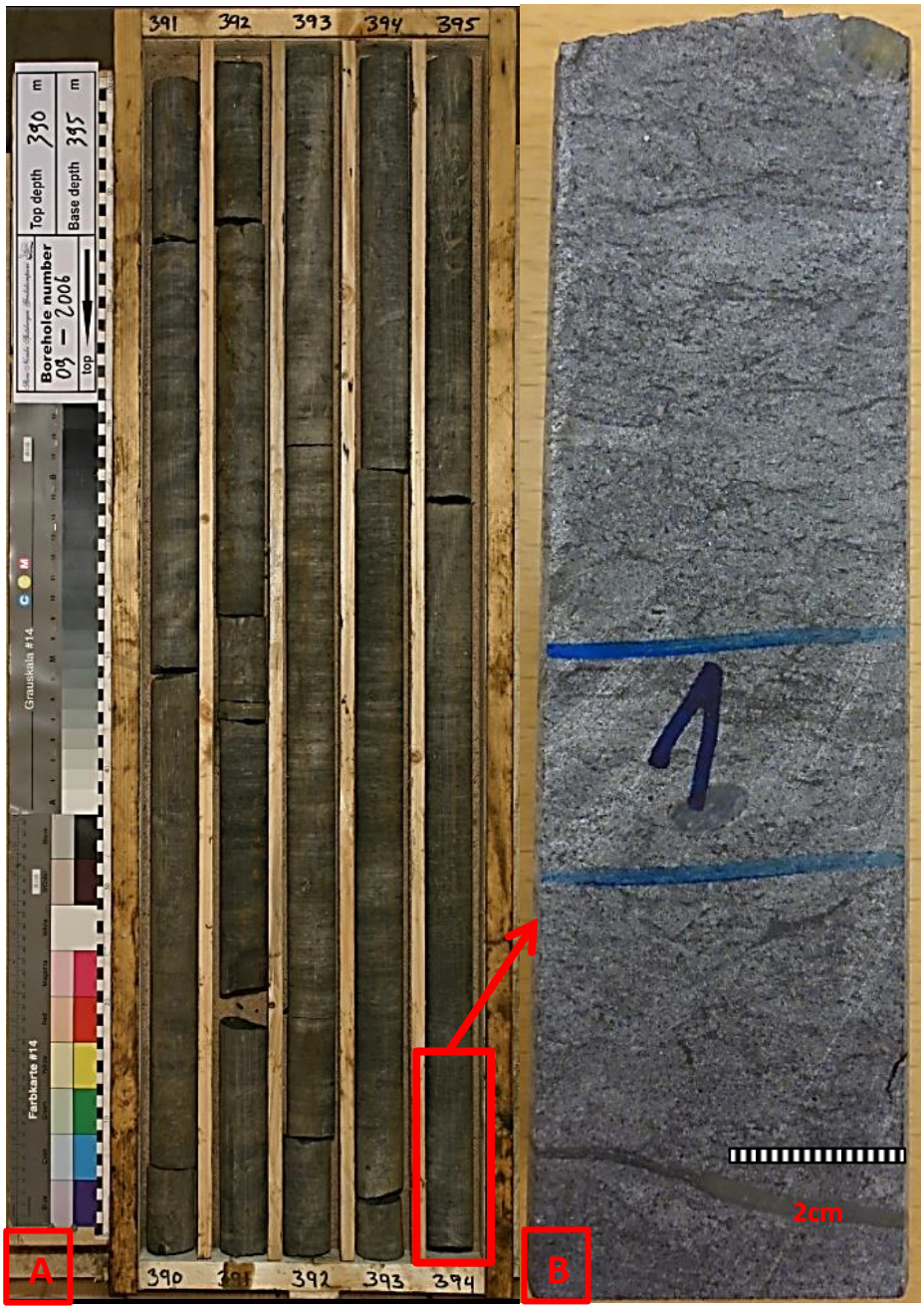

Figure 4.2: *(A) Core photo of Lithofacies F.2 in well BH-9-2006, depth: 390.00-395.00. (B) Lithofacies F.2 in core sample 1, depth: 394.00-394.14.*

Interpretation

Lithofacies F.2 is interpreted to have a more proximal offshore depositional location than the underlying Lithofacies F.1. The input of silty material in otherwise very fine-grained sandstone is a result of suspension of fines from the water column during quiet conditions. Storms waves are able to create enough turbulence to bring silt and very fine-grained sand into suspension, which can further be transported by relatively weak currents across the shelf (Steel, 1977). The silt has most likely been mixed together with the sand as a consequence of bioturbation during colonization of the sediments. The different grain-sizes have been deposited in thin separate layers, and then later activity of different organisms has reorganized these sediments. This might be an indication of a slow sedimentation rate at

the time of deposition. The few wave-ripple-cross-laminations described might indicate that the environment of deposition was close to the storm-wave base. These sedimentary structures are made by storm waves creating oscillatory currents in shelf settings were the waves are big and convey lots of energy. The fact that only a few sets of wave-ripple-cross-laminations have been observed and with the sediments otherwise being almost completely bioturbated, still points to fairly quiet conditions.

The differences in appearance of trace fossils in the two wells and in the outcrop sections studied is probably related to proximal and distal position in the basin. The occurrence of *Nereites* in well BH-10-2008, which is drilled on Nathorst Land (Figure 2.3), points to a more distal origin as this trace fossil is associated with offshore settings (Seilacher, 1967). Well BH-9-2006 is drilled close to Locality 1 (Bolterdalen) at Nordenskiöld Land (Figure 2.3) and both the well and outcrop section shows a domination of trace fossils associated with more proximal settings. The difference in appearance of trace fossils in outcrop and well is most likely due to intense weathering of the outcrop, making it harder to identify certain t
race fossils compared to core-sections in the wells. Ichnofabric analysis of the lithofacies reveals that it is dominated by *Virgaichnus*, *Teichichnus* and *Cylindrichnus* – Ichnofabric (Figure 3.28). It is not uncommon to find *Teichichnus* occurring in high – diversity ichnoassemblages including *Cylindrichnus concentricus* and *Palaeophycus tubularis*. These burrows are all associated with diverse shallow-marine to offshore transition zone environments in the *Cruziana* Ichnofacies (Frey and Howard, 1990; Pemberton and MacEachern, 1992; Pemberton et al., 2001). *Virgaichnus undulatus* is known to appear in a number of different depositional environments ranging from shallow-marine to deep marine settings.

The rock fragments observed has the same mineralogical composition as in Lithofacies F.1, and they are interpreted to be deposited as a result of transport by seasonal winter ice across the shelf (Dalland, 1977). The green clay intervals are interpreted to be bentonite layers. The bentonite layers are composed of weathered and altered volcanic ash transported by the wind and deposited in the sea (Ramberg et al., 2008). A relative high abundance of pyrite points to reduced conditions in marine environments with sulphate – rich waters (Curtis, 1980; Fisher and Hudson, 1987). The very fine sandstones with considerable amount of in-mixed silt as a result of intense to complete bioturbation states that there have been good conditions for organisms to thrive. Obscure wave-ripple-cross-laminations however points to energy levels typically occurring above or close to the storm-wave base. The appearance of *Macaronichnus* could also support this, as the trace fossil in some circumstances is associated with tempestites created by storm waves (Pemberton et al., 2001). The trace fossils observed relates the environment of deposition to the *Cruziana* Ichnofacies, and based on this observation an offshore transition environment has been proposed for this lithofacies (*Table 4.1*).

Facies F.3 – *Moderately Silty Sandstone*

Description

Lithofacies F.3 is a medium gray moderately silty sandstone (Figure 4.3) seen in both wells and at Locality 1 (Bolterdalen). The lithofacies measures a total thickness of 34.5 meters in the thickest interval at Locality 1 (Appendix 12), and it is generally well developed in the outcrop section studied (Bolterdalen). In well BH-10-2008 the lithofacies is also prominent were it measures 17 meters at its maximum and 0.25 meters at the thinnest interval (Appendix 11). Although having a 15 meter interval measured in the upper half of well BH-9-2006, the lithofacies overall is not particularly abundant in this well (Appendix 13). The grain-size of the lithofacies alternates between very fine and very fine/fine – sand, with a silt percentage from 30 % to less than 50 %. A moderate number of sets of wave-ripple-cross-laminations (WRCL) and a few hummocky-cross-stratifications (HCS) have been identified in the lithofacies which is otherwise dominated by intense to complete bioturbation (80 – 100 %).

In terms of ichnodiversity, there are some minor differences between the two wells and the outcrop section studied (Locality 1, Bolterdalen). *Virgaichnus, Palaeophycus* and *Cylindrichnus* are frequently observed in the lithofacies. The outcrop studied shows a great abundance of *Palaeophycus* and *Schaubcylindrichnus*, but fewer occurrences of *Virgaichnus* and *Cylindrichnus* in the lithofacies compared to the wells studied. *Macaronichnus* is also especially well developed in the two uppermost intervals of the lithofacies in the outcrop (Appendix 12), which differs from the wells studied. Well BH-9-2006 shows a great variety of trace fossils, with *Teichichnus, Cylindrichnus* and *Palaeophycus* in equal appearance, as opposed to *Macaronichnus* which is almost absent in this interval. Well BH-10-2008 shows a great abundance of *Cylindrichnus* and *Virgaichnus*, but lacks almost any evidence of *Teichichnus* and even no evidence of *Palaeophycus*-burrows in the same lithofacies.

Angular to well-rounded pebbly rock fragments of chert and quartzite were also sporadically observed in various intervals of the lithofacies. Siderite nodules are scattered in the interval seen in well BH-9-2006. Pyrite does not appear as frequently in this lithofacies as compared to Lithofacies F.1 and F.2.

Figure 4.3: *(A) Core photo of Lithofacies F.3 in well BH-9-2006, depth: 285.00-290.00. (B) Lithofacies F.3 in core sample 6, depth: 288.74-288.94.*

Interpretation

Lithofacies F.3 is quite similar to Lithofacies F.2, but based on the grain-size, silt content, ichnodiversity and physical sedimentary structures the lithofacies seem to have a more proximal origin. The silt content is a result of suspension of fines from the water column which later have been mixed together with the sand as a result of intense to complete bioturbation. Turbulence created by storms waves has probably brought silt and very fined-grained sand in motion, which later have been deposited during quite conditions from suspension (Steel, 1977). A slow sedimentation rate is suggested based on the reorganization of the sediments by the activity of organisms. Beginning at the limit of the fair-weather (effective) wave base, the deposits of the lower shoreface is still dominated by offshore processes (Reinson, 1984). Fair weather generated wave ripples may be present in this environment, but is highly uncommon because of the intensity of bioturbation, and therefore the wave-ripple-cross-laminations observed in this lithofacies most likely reflect a storm deposition (Pemberton et al., 2012). The presence of hummocky-cross-stratification in well BH-10-2008 which is associated with storm waves also supports this, even though it was only observed in two separate intervals and not frequently present (Appendix 11). The highly bioturbated and generally homogeneous sandstone indicates low intensity and infrequent storms, which would be a suitable environment for organisms to live in. The rock fragments observed has the same mineralogical composition as Lithofacies F.1 & F.2, and have been deposited as a result of transport by seasonal winter ice across the shelf (Dalland, 1977).

The difference in appearance of trace fossils in the two wells and in the outcrop sections studied shows a high diversity of deposit and suspension – feeding organisms. Regarding the differences seen between the two wells and in the field, this probably also relates to a proximal and distal position in the basin as seen in Lithofacies F.2. The intense weathering of the outcrop, made it more difficult to identify certain trace fossils compared to the core-sections in the wells, which would explain the difference in trace fossil observed. Ichnofabric analysis of the lithofacies points to a dominance of *Virgaichnus*, *Cylindrichnus* and *Palaeophycus*–Ichnofabric (Figure 3.28). *Cylindrichnus concentricus* is known to appear together with *Teichichnus zigzag* and *Palaeophycus tubularis* in a shoreface setting (Frey and Howard, 1990). These trace fossils represent a proximal expression of the *Cruziana* Ichnofacies (MacEachern and Bann, 2008). Considering the overlying Lithofacies F.4 which is dominated by the *Skolithos* Ichnofacies, the appearance of *Macaronichnus segregatis* in lithofacies F.3 supports the effect of a fair-weather community dominated by suspension feeders. Based on the ichoassemblage being related to a proximal *Cruziana* to distal *Skolithos*-Ichnofacies, a lower shoreface environment has been proposed for this lithofacies (Table 4.1).

Facies F.4 – *Light Silty Sandstone*

Description

Lithofacies F.4 is a pale green to greenish gray light silty sandstone (Figure 4.4, A&B) seen in both wells and at Locality 1 (Bolterdalen), in the field the lithofacies occur as a yellowish gray unit in the succession as a result of weathering (Knaust, pers. comm. 2015). The lithofacies is especially well developed in well BH-9-2006 where it measures a total thickness of 77.6 meters in the thickest interval (Appendix 13). In well BH-10-2008 the lithofacies is also prominent where it measures 31 meters at its maximum (Appendix 11). The grain-size of the lithofacies alternates between very fine, fine and medium-sand, with some minor differences between the two wells and the outcrop sections studied. In well BH-9-2006 some intervals of 1-10 meters show coarsening upward units with medium/coarse-sand at the top, while in well BH-10-2008 the overall grain-size is very fine and fine-sand. An overall coarsening upward and thickening upward of the lithofacies is observed in well BH-9-2006 and at the outcrop studied (Locality 1, Bolterdalen), measuring only a few meters to more than 10 meters. The lithofacies has a higher sand percentage than the underlying lithofacies, resulting in a silt percentage ranging between 0 and 30 %. Abundant sets of wave-ripple-cross-laminations (WRCL) (Figure 4.4-C) and a few sets of trough-cross-stratification (TCS) have been identified in the lithofacies. Bioturabation intensity is alternating between moderate to complete (50 – 100 %) throughout the lithofacies, with some minor intervals showing no sign of bioturbation being related to more sedimentary structures present. Also the bioturbation intensity seems to decrease towards the top of the lithofacies, where wave-ripple-cross-laminations are more frequent.

Macaronichnus is the most prominent and indicative trace fossil occurring in Lithofacies F.4 (Figure 3.28). Other trace fossils such as *Virgaichnus and Cylindrichnus* are also abundant in the lithofacies, with their abundance being slightly different between the two wells and the outcrop section studied. In well BH-10-2008 there is a great abundance of *Cylindrichnus* and *Virgaichnus* present in the lithofacies, while *Cylindrichnus* is poorly represented in well BH-9-2006. In the outcrop sections studied, *Cylindrichnus* was however not observed, but *Macaronichnus* is very abundant in this section.

A 50 cm interval composed of green very fine-grained clay sized sediments occurs within the lithofacies in well BH-9-2006 (Figure 4.5). Angular to well-rounded coarse-grained pebbly rock fragments of chert and quartzite were also observed sporadically within the lithofacies (Figure 4.4-C). Carbonate cemented intervals and siderite nodules are also more prominent in this lithofacies, especially in the lower part of the lithofacies in well BH-9-2006 (Figure 3.4).

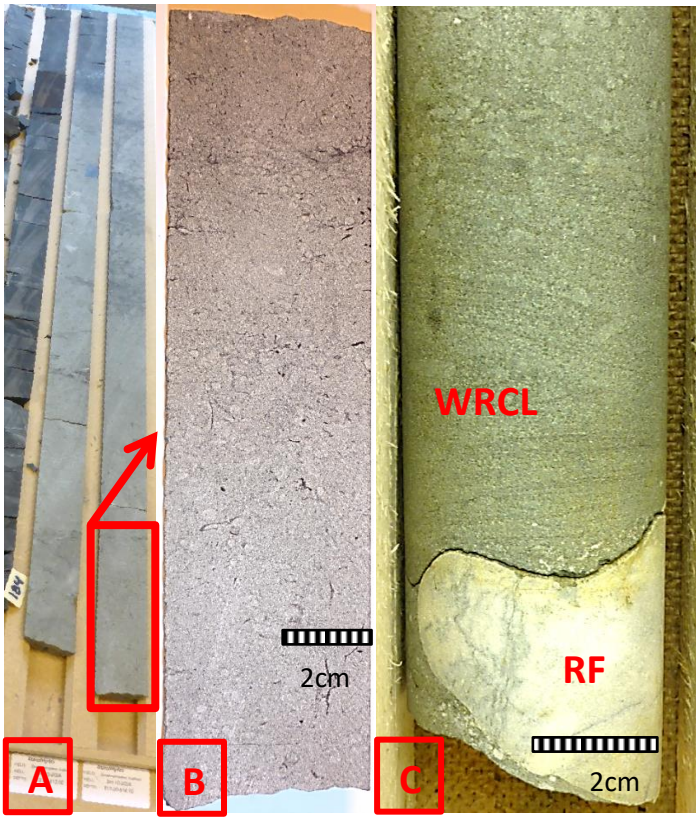

Figure 4.4: *(A) Core photo of Lithofacies F.4 in well BH-10-2008, depth: 812.00-814.00. (B) Core sample of Lithofacies F.4, depth: 813.85-814.00. (C) Wave-ripple-cross-lamination (WRCL) and a pebble size rock fragment (RF) in well BH-9-2006, depth: 198.37-198.50.*

Figure 4.5: *(A) a 50 cm bentonite layer occurs in Lithofacies F.4 in well BH-9-2006, depth: 272.50-273.00. (B) A close-up of the bentonite layer, depth: 272.56-272.68.*

Interpretation

Lithofacies F.4 is a sandstone unit that appears less silty than the underlying lithofacies and the occurrence of physical sedimentary structures is far more abundant in this interval. Since bioturbation intensity is more varying throughout the interval compared to the other lithofacies, high-energy conditions and a more proximal origin is expected. The silt content in the lithofacies is explained by the mixing between sand and silt as a consequence of bioturbation (reorganization) during colonization of the sediments, as seen in the underlying lithofacies. The silt content gradually decreases upward in the interval as a result of a general coarsening upward trend in the lithofacies. The characteristic green expression seen in the lithofacies is a result of a high glauconitic content (Steel et al., 1981). A slow sedimentation rate is suggested based on the abundant glauconite, relative homogeneous sandstone succession and the high bioturbation intensity (Odin and Matter, 1981). Slow sedimentation rates creates suitable conditions for organisms to live and thrive in, leading to high bioturbation intensity still being in a high-energy environment. The green clay interval in BH-9-2006 is similar to the once seen in Lithofacies F.2, and is therefore interpreted to be a bentonite layer. The pebble size rock fragments are deposited by seasonal winter ice across the shelf (Dalland, 1977). They share the same mineralogical composition as the other lithofacies already described, and therefore they most likely originate from the Permian Kapp Starostin Formation.

Sets of wave-ripple-cross-lamination and trough-cross-stratification indicate a shallow-marine environment dominated by wave processes. The middle shoreface is characterized as a zone of shoaling and breaking of waves being strongly influenced by storms, were wave energy is high enough to erode the sea bed and storm-induced scouring takes place (Pemberton et al., 2012). Well sorted, fine to medium-grained sandstones beds are typically found in the middle shoreface. The upper shoreface is characterized as the surf zone in front of the breaking zone, were wave-and storm-driven currents causes the sediment to be transported by multidirectional flow (Pemberton et al., 2012). Well sorted, medium to coarse-grained sandstone beds with multidirectional trough-cross-stratification are common in the upper shoreface. Lithofacies F.4 shows a general coarsening upward trend in the succession were silt content decreases and the number of physical sedimentary structures increases. This could possibly indicate a gradual vertical (lateral) shift from the middle to upper-shoreface. A high abundance of suspension-feeding organisms, especially *Macaronichnus segregatis* which is a characteristic shallow-marine trace fossil occurring in foreshore and upper/middle-shoreface environments, supports this interpretation (Clifton and Thompson, 1978; Seike, 2007; Bromley et al., 2009; Pemberton et al., 2012). As seen in the other lithofacies, also in Lithofacies F.4 the intensity of bioturbation overtakes the number of physical sedimentary structures, making it difficult to accurately position the environment of deposition. The most accurate statement would however be to suggest an upper shoreface environment in the *Skolithos* Ichnofacies based on sedimentary texture, structures and the ichnodiversity present in Lithofacies F.4 (Table 4.1).

Facies F.5 – *Gravel*

Description

A gravel layer measuring a thickness from 15-25 cm occurs in the lower part of Lithofacies F.1 at the top of each well, marking a transition with an erosive boundary to the underlying Lithofacies F.4 (Figure 4.6, B&C). Similar layers also occur in the very top of Lithofacies F.4 in well BH-9-2006 (Appendix 13). A single layer also occurs at the bottom of an over-scattered section at Locality 1, Bolterdalen (Appendix 12). The gravel layers are dominated by very coarse sand and granules with some scattered pebbles. The gravel is poorly sorted without imbrication or grading. The grains constituting the gravel layer are angular to well-rounded, and measure a size from 2mm to 3-4 cm in diameter. The layer shows none to moderately degrees of bioturbation (0 – 50 %).

Interpretation

The gravel layers occurring in the wells and at the outcrop studied are interpreted to be a locally derived lag associated with marine erosion during transgression. This can also be referred to as a wave ravinement surface created by wave processes during marine flooding (Knaust, pers. comm. 2016). The transgressive lag marks the start of the major flooding on top of the shallow-marine environment of the Grumantbyen Formation and deposition of the superimposed Frysjaodden Formation. High-energy conditions enable the movement of the grain-sizes found in the lag creating the erosive boundaries to the underlying Lithofacies F.4.

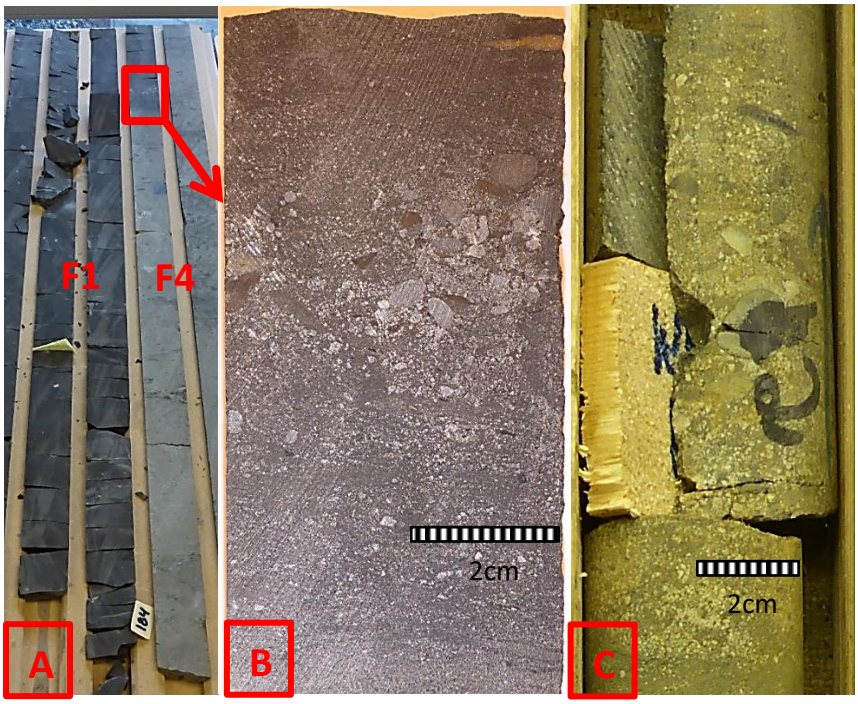

Figure 4.6: *(A) Core photo of Lithofacies F.1 in the upper part of well BH-10-2008, depth: 810.00-813.00. (B) Between 812.20-812.25 a transgressive lag separates the underlying Lithofacies F.4 from the superimposed Frysjaodden Formation. (C) A similar transgressive lag can be seen in the top of well BH-9-2006, depth: 127.80-127.90.*

5 Petrography

Ten samples from outcrop Locality 1 (Bolterdalen) and 11 samples from well BH-9-2006 were selected for thin-section analysis. They were selected with the aim of displaying the different lithological and ichnological variations at pore scale. The samples are each briefly described and can be found in Appendix 3 and Appendix 4. In total, 21 samples were analyzed by the use of optical microscope, 5 which were also analyzed by scanning electron microscope (SEM) and X-ray diffraction (XRD). This was done in order to describe the composition of the samples. The composition of the samples is sub-divided into the following categories: texture, framework and authigenic-constituents, matrix, cement and porosity. A modal analysis was done in order to classify the samples and to get a more detailed description of the different constituents, matrix and pore-space distributions within 12 selected thin-sections from the well and outcrop. Chapter 5.3 presents a description of the relationship between authigenic minerals and diagenesis, and at the very end of Chapter 5 a description on how compaction and cementation has had an impact on the porosity distribution in the analyzed samples is presented. The result presented in this chapter is well related to and supportive to the result from Chapter 4; therefore multiple references to the defined lithofacies (Chapter 4.1) will be given throughout the petrography chapter. Since there were no samples taken from Lithofacies F.5 (Chapter 4.1), this lithofacies has been disregarded within this chapter.

5.1 Composition

5.1.1 Texture

The resulting textures of the samples are presented in Appendix 5 and Appendix 6. The grain-size value is calculated based on counting points with a 10X10 magnification in the optical microscope, assisted by length measurement of grains through the NIS – Elements BR software (Chapter 1.2). The calculated grain-size value is a mean value based on all the grains measured in the sample, and the value given is defined by the Udden-Wentworth scale. Other properties determined, such as sorting, roundness, shape and fabric, are defined by Pettijohn et al. (1972).

Referring to the lithofacies descriptions in Chapter 4.1, the analysis shows that samples taken from the same defined lithofacies display similar textural properties. Hence the textures described from the samples might indicate characteristics of certain depositional environments. The samples from the most distal interpreted lithofacies show a matrix-supported fabric, while the other lithofacies are dominated by grain-supported fabric. The analysis shows that the grain-size is ranging between coarse

silt to fine-grained sand, and that the majority of the samples are dominated by very fine grain-sizes. Figure 5.1 illustrates the grain-size distribution, indicating that the interpreted distal deeper-water deposits have a finer grain-size than the most proximal shallow-water deposits, which supports the visual grain-size determination in Chapter 4.1. The grain-sizes might also explain why the majority of the analyzed samples have an angular/sub-angular roundness (Figure 5.2), because larger grains are more easily rounded than smaller grains. The sorting of the samples is dominantly well and very well-sorting, with a notably better sorting of the most proximal and most distal lithofacies (Figure 5.3). The shape of the grains in the samples displays a higher sphericity (Figure 5.4) towards the more proximal lithofacies (F3 and F4), in which the energy levels were presumably higher due to more storm and wave action.

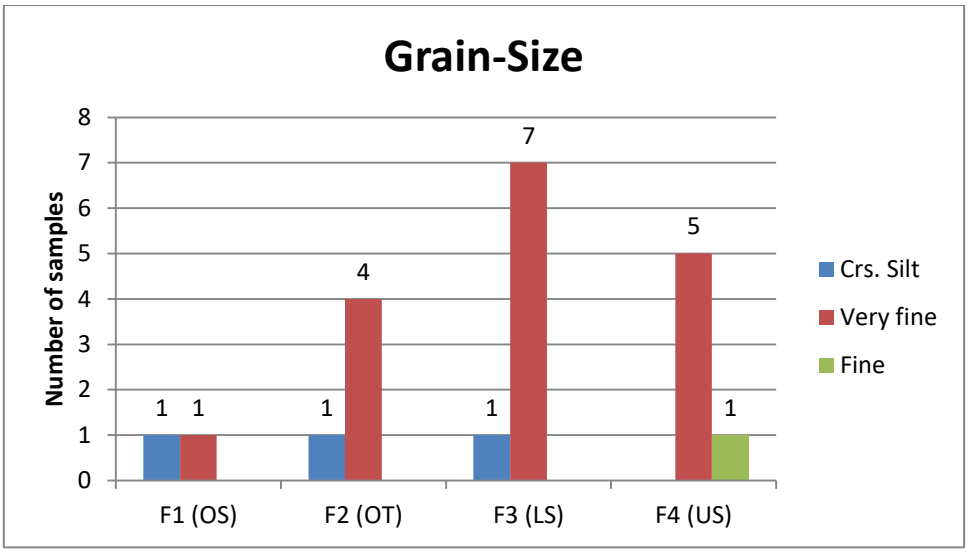

Figure 5.1: *Grain-size distribution of the different analyzed samples, organized as lithofacies (F1-F4) (Chapter 4.1). OS=Offshore, OT=Offshore transition, LS=Lower shoreface and US=Upper shoreface.*

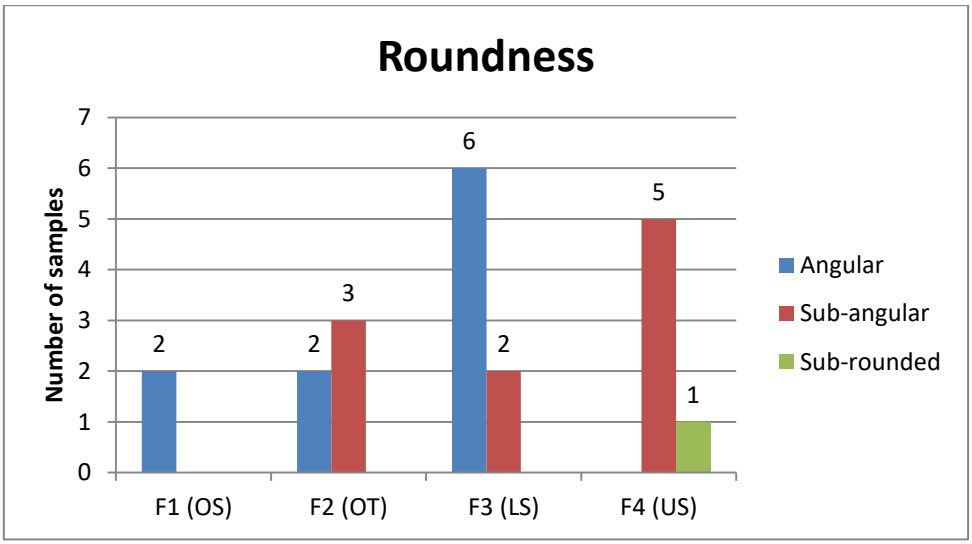

Figure 5.2: *Degree of roundness of the different analyzed samples, organized as lithofacies (F1-F4) (Chapter 4.1). OS=Offshore, OT=Offshore transition, LS=Lower shoreface and US=Upper shoreface.*

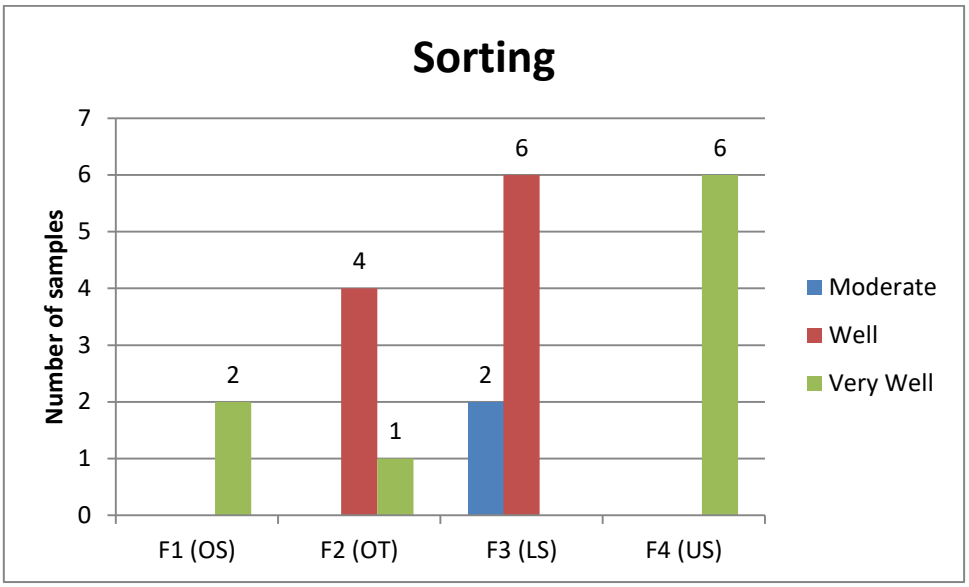

Figure 5.3: *Degree of sorting of the different analyzed samples, organized as lithofacies (F1-F4) (Chapter 4.1). OS=Offshore, OT=Offshore transition, LS=Lower shoreface and US=Upper shoreface.*

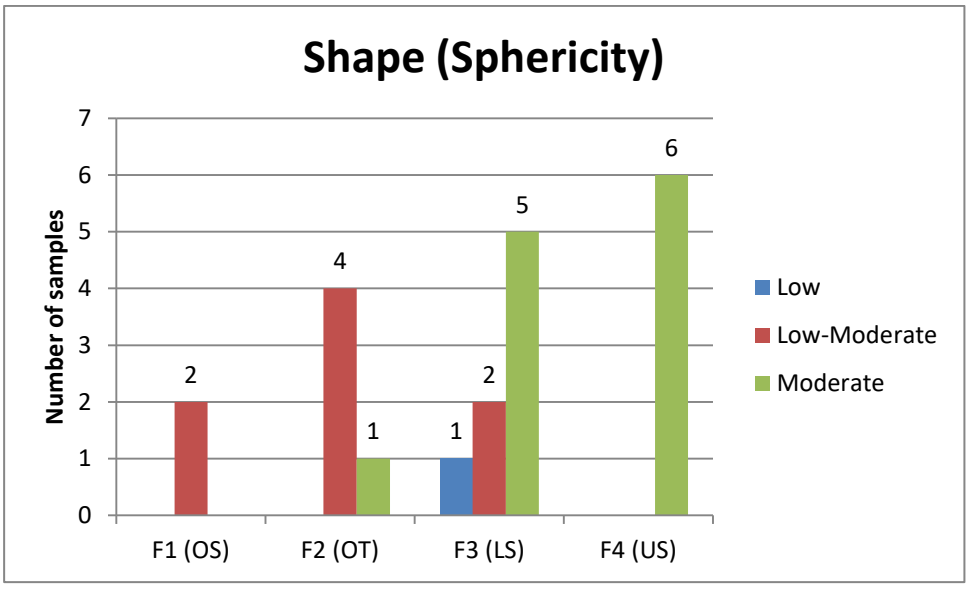

Figure 5.4: *Shape of the different analyzed samples, organized as lithofacies (F1-F4) (Chapter 4.1). OS=Offshore, OT=Offshore transition, LS=Lower shoreface and US=Upper shoreface.*

5.1.2 Modal analysis

The modal analysis is presented in Table 5.1 and shows the occurrence and distribution of framework and authigenic minerals, matrix and porosity, where the given values are based on the mean values of all the samples analyzed from well BH-9-2006 (7) and outcrop (5) within the same defined lithofacies described in Chapter 4.1. The values are presented as percentage of the total composition of the different lithofacies. The table shows that Lithofacies F.2 & F.3 have quite similar composition. From Lithofacies F.1 to F.4 there is a gradual increase in quartz content, while the matrix content is gradually decreasing. Also the amount of chlorite, which is a clay mineral under the definition of authigenic minerals (Chapter 5.1.4), is gradually increasing from Lithofacies F.1 to F.3 with an abrupt increase in Lithofacies F.4. Glauconite, which is described as a diagnostic clay mineral in the Grumantbyen Formation, is most abundant in Lithofacies F.2 & F.4. Calcite and siderite is more abundant in Lithofacies F.4 than in all the other defined lithofacies.

The number of samples within each lithofacies is not equal, which gives some uncertainty to the values presented (Figure 5.5). The values originate from samples of both, well and outcrop data, which may have an impact on the results in terms of weathering and erosion of the exposed outcrop. Appendix 7 and Appendix 8, presents the modal analysis of the individual samples from Locality 1 (Bolterdalen) and well BH-9-2006.

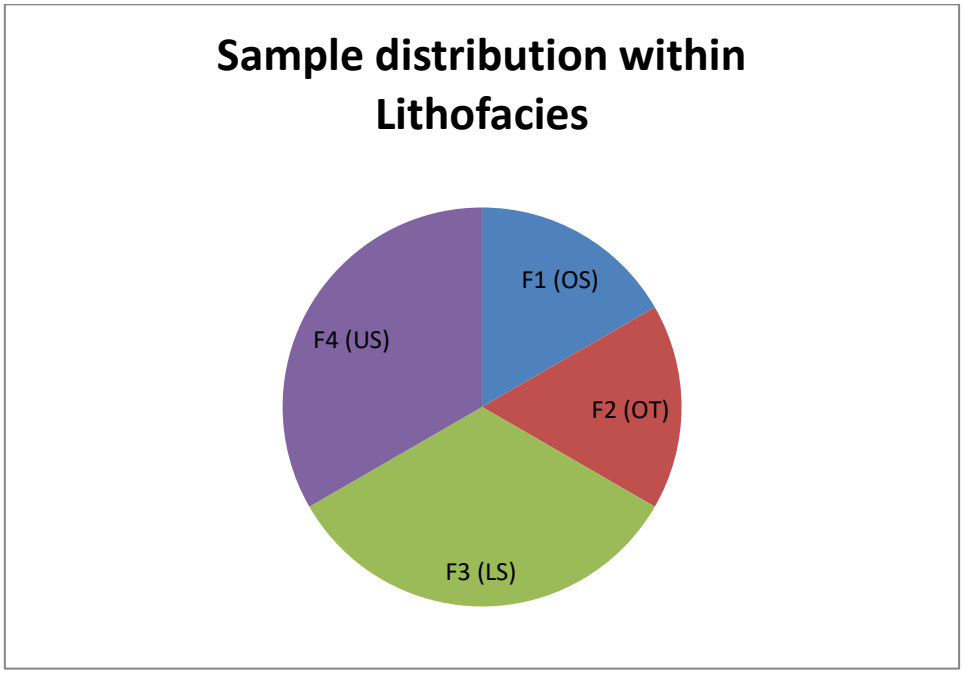

Figure 5.5: *Sample distribution within the different defined lithofacies (F.1-F.4) (Chapter 4.1), based on the 12 samples that were modally analyzed. OS= Offshore, OT=Offshore transition, LS= Lower shoreface and US= Upper shoreface.*

Table 5.1: *Modal composition of interpreted lithofacies (F1-F4) (Chapter 4.1). The values in the analysis are mean values from* Appendix 7 *and* Appendix 8*, presented as percentage of the total composition of the different lithofacies. The analysis is based on point-counting of 300 points within each thin-section through an optical microscope with a 20X10 magnification. X = not observed within sample.*

	Framework constituents							Matrix	Authigenic minerals							Porosity	
Lithofacies (number of samples)	Quartz	Feldspar		Mica	Rock fragm	Heavy minerals	Organics		Silica	Calcite	Siderite	Glauconite	Chlorite	Pyrite	Sericite	Primary	Secondary
		K-feldspar	Plagioclase														
F.1 (2)	34.0	1.0	8.2	0.3	2.2	0.1	x	42.1	1.5	0.3	1.2	0.5	0.5	0.2	2.0	5.6	0.3
F.2 (2)	33.0	1.9	15.0	x	1.8	x	x	31.0	0.9	x	0.2	2.8	0.6	x	5.1	6.3	1.4
F.3 (4)	37.5	2.3	18.8	0.1	1.5	0.1	0.1	25.6	1.7	0.1	0.2	1.3	2.6	x	3.1	3.8	1.2
F.4 (4)	49.6	1.5	12.9	0.3	1.1	0.3	x	6.0	0.8	6.3	3.0	2.1	9.7	x	1.3	2.4	2.7

5.1.3 Framework constituents

Framework constituents that are dominating in the Grumantbyen Formation are quartz, feldspar (K-feldspar and plagioclase), rock fragments (chert and quartzite), mica, whereas heavy minerals and organics are subordinate.

Quartz is the most prominent framework mineral in the formation, and it appear both as individual grains and intergranular within other rock fragments. Minor alteration has been noticed, such as irregular grain boundaries and slight deformation. Some of the quartz grains show distinct to conchoidal fracture/cleavage in plane-polarized-light (PPL, from now on), although this feature is less common. No twinning and undulatory extinction angle was identified in cross-polarized-light (XPL, from now on). Most of the quartz grains are monocrystalline (Figure 5.6-A) with point contacts to the surrounding grains, although some also have sutured contacts. Some of the samples contain polycrystalline quartz (Figure 5.6-B), but in minor quantities compared to the monocrystalline counterpart. The quartz grains are angular and sub-angular and the majority of the grains have a moderate sphericity.

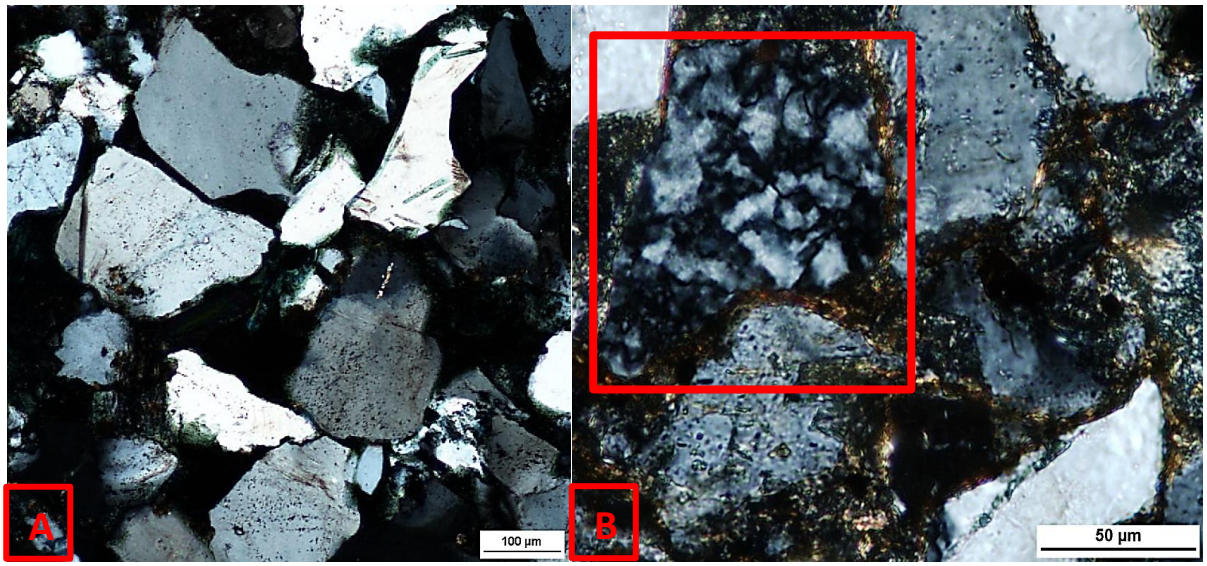

Figure 5.6: *(A) Monocrystalline quartz grains in sample 9, well BH-9-2006. (B) Polycrystalline quartz in sample 1.1, Locality 1 (Bolterdalen). Both pictures are in XPL with scale in microns, 100 microns = 0.1 mm, 50 microns = 0.05 mm.*

Feldspar is the second most abundant framework mineral in the formation, especially plagioclase which is well represented in all the lithofacies based on the modal analysis (Chapter 5.1.2). Feldspars are most abundant in Lithofacies F.3 (Chapter 4.1) based on the analyzed samples. Both K-feldspars and plagioclase appear colorless in PPL and with an inclined extinction angle in XPL, so they are best distinguished by studying their twinning in XPL. K-feldspars, both orthoclase and microcline, show tartan twinning in XPL (Figure 5.7-A), while plagioclase, both albite and anorthite, show polysynthetic twinning (Figure 5.7-B). Based on Bowen's reaction series (Bowen, 1922), feldspars are

known to easier dissolve than quartz during diagenesis, especially plagioclase which often show signs of alteration. Sericitization is an alteration process of sodium-bearing plagioclase such as albite ($NaAlSi_3O_8$), which gets replaced by very fine-grained muscovite (sericite) appearing as lamellas in the plagioclase (Shelley, 1992). Saussuritization is also an alteration process attacking calcium-bearing plagioclase such as anorthite ($CaAl_2Si_2O_8$), which gets replaced by saussurite (Shelley, 1992). These alteration processes are most likely a result of hydrothermal alteration (Shelley, 1992). If the feldspars have a very small grain-size or if the twinning is not well developed, it can be difficult to distinguish the feldspars from the quartz in the samples just by the use of an optical microscope. The Scanning Electron Microscope-analysis (SEM) therefore proved helpful in terms of identifying K-feldspars and plagioclase on a small scale (Figure 5.8).

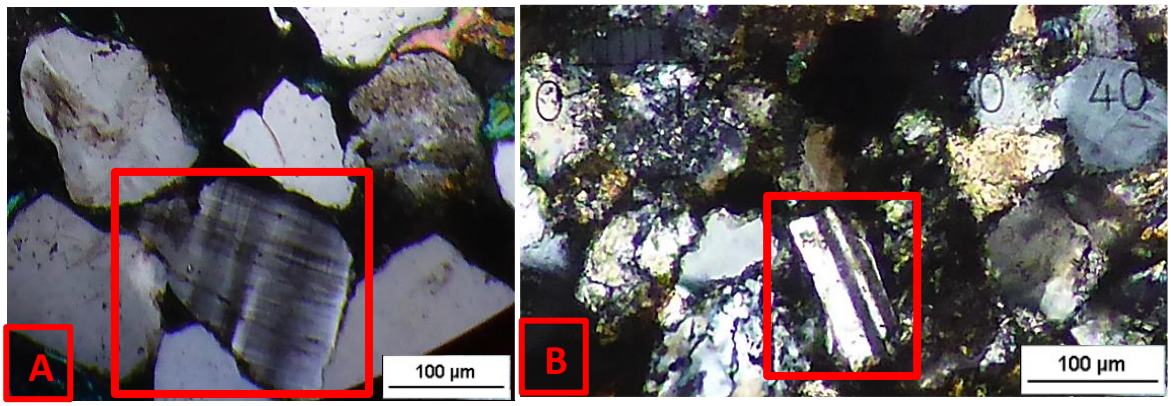

Figure 5.7: *(A) K-feldspar showing tartan twinning in sample 9, well BH-9-2006. (B) Plagioclase showing polysynthetic twinning in sample 1.9, Locality 1 (Bolterdalen). Both pictures are in XPL with scale in microns, 100 microns = 0.1 mm.*

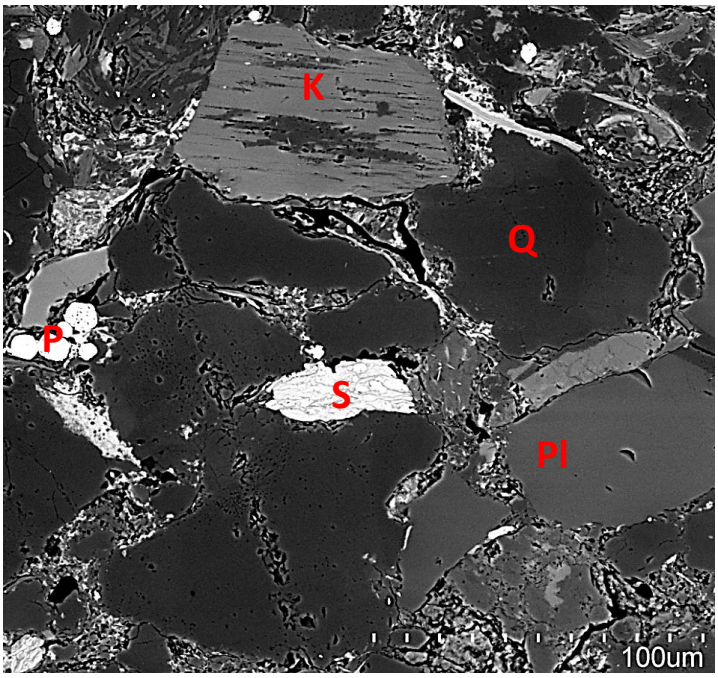

Figure 5.8: *SEM-analysis of sample 2, well BH-9-2006. The minerals are identified based on their chemical composition. The K-feldspar shows signs of alteration with Na-bearing plagioclase as the dark phase horizontally distributed in the grain. Q=quartz, K=K-feldspar, Pl=plagioclase, P=Pyrite & S=Siderite. Scale in microns, 100 microns = 0.1 mm*

Rock fragments in the samples primarily constitute chert and quartzite. They appear frequently in the logged sections described in the lithology chapter (Chapter 4), but not as frequent in the thin-section samples. The chert grains identified in the thin-sections originated from the Permian Kapp Starostin Formation, which is known to be highly dominated by biogenic silicate (Grundvåg, pers. comm. 2015). The chert grains appear quite diagnostic in XPL, with clear and cloudy zones of radial-fibrous quartz (Figure 5.9). The black and white zones express a sort of "zebra" pattern, which makes it easy to identify. Quartzite is a metamorphic rock fragment, described as a recrystallized clean sandstone protolith implying a metamorphic origin. The rock fragments seen in the Grumantbyen Formation are suggested to be deposited as a result of a cross-shelf transport by seasonal winter ice (Dalland, 1977).

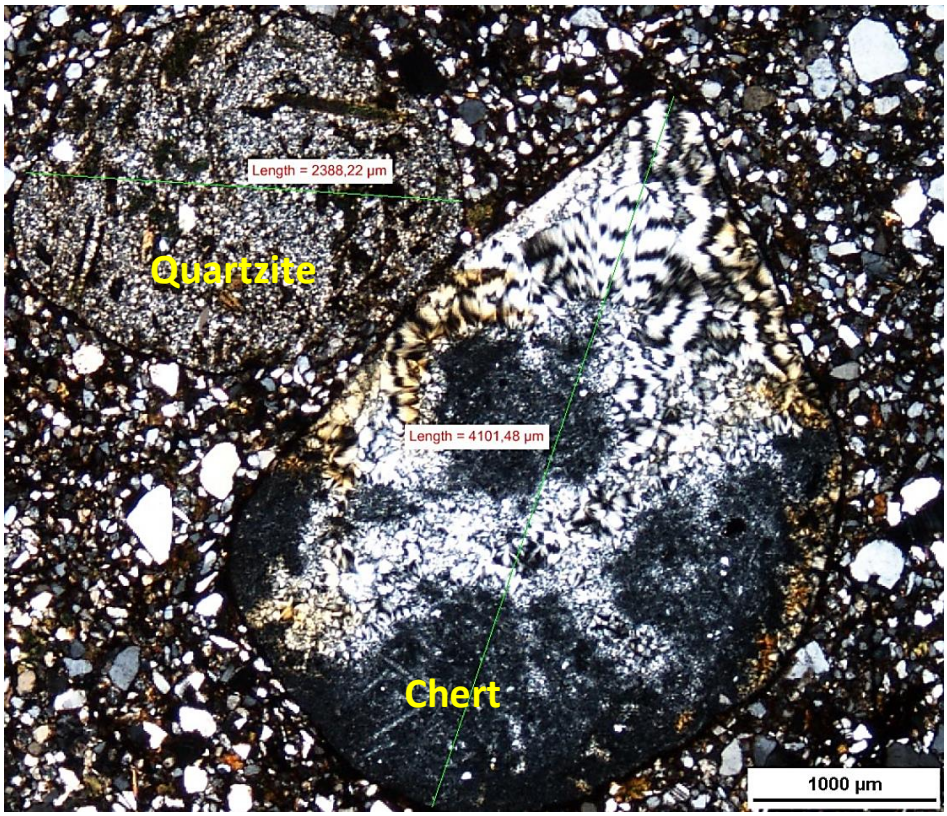

Figure 5.9: *A pebble sized (4.1 mm) chert fragment and a granule sized (2.4 mm) quartzite fragment in sample 1.4, Locality 1 (Bolterdalen). Picture is taken in XPL with scale in microns, 1000 microns = 1.0 mm.*

A few examples of muscovite (mica) are also present in the samples (Figure 5.10). The mineral tends to show evidence of alteration and foliation. It has a clear/colorless appearance in PPL and a parallel extinction angle with a "birds' eye" appearance in XPL. Also very fine-grained muscovite appears as intergranular minerals in sodium-bearing plagioclase in the samples. These mica fractions are made as a result of alteration of plagioclase (called sericitization), creating an alteration product termed sericite (Shelley, 1992), which is here characterized as an authigenic mineral described in Chapter 5.1.4.

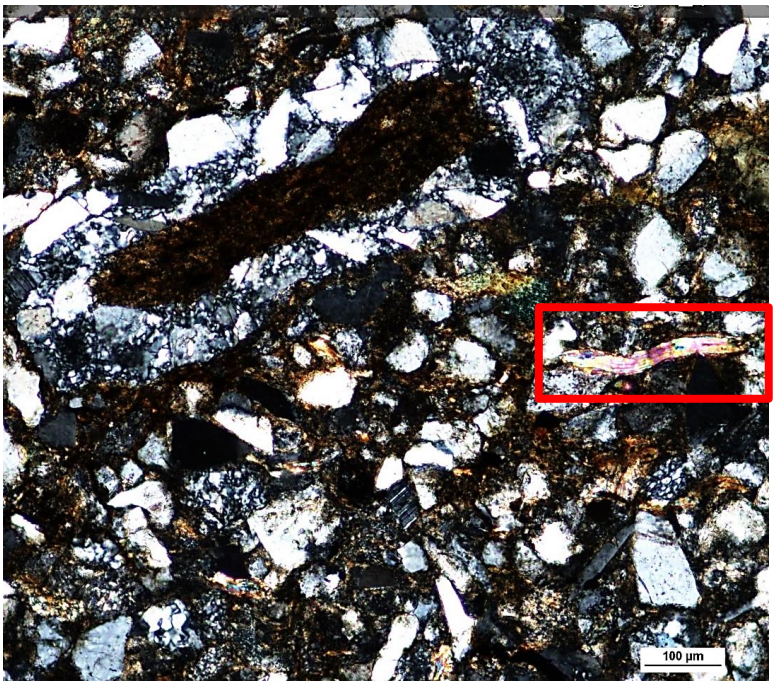

Figure 5.10: *A foliated muscovite mineral due to compaction in sample 1.5, Locality 1 (Bolterdalen). The sample also shows a white ring of sorted quartz and feldspar grains which is characteristic of* Schaubcylindrichnus coronus *(Chapter 3.1). The burrow has been partly flattened, which supports the proposed compaction. Picture is taken in XPL with scale in microns, 100 microns = 0.1 mm.*

Other framework minerals occurring in the samples are small detrial coal fragments and heavy minerals. The coal fragments are fairly small in size and are not particularly abundant throughout the formation, probably because most of the fragments have been altered into siderite which stands as an authigenic minerals described below (Chapter 5.1.4). The heavy minerals appear opaque (black) in PPL due to absorption of light (Figure 5.11), and they are very small in grain-size. This makes them hard to identify, still one can assume them to be iron oxides or sulfides.

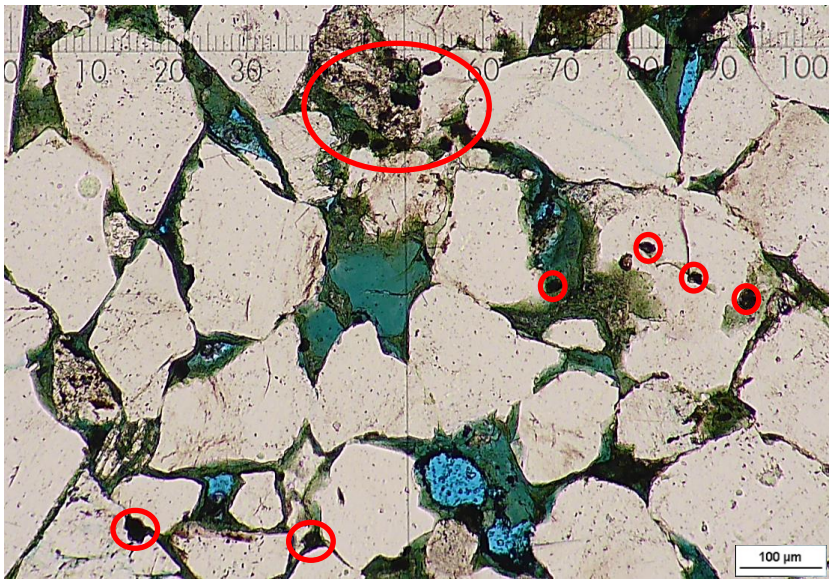

Figure 5.11: *Opaque (black) minerals in PPL, sample 9, well BH-9-2006. Thin-section is colored blue in order to highlight available pore-space in the sample. Green phase surrounding the framework minerals is chlorite, which appear as both pore-filling and coating in the sample. Scale is in microns, 100 microns = 0.1 mm.*

5.1.4 Authigenic minerals

These are minerals that have been formed after deposition of the framework minerals, also sometimes referred to as diagenetic minerals. Authigenic minerals, which are dominating in the Grumantbyen Formation, include silica, calcite, siderite, glauconite, chlorite, pyrite and sericite.

Silica occurs either as chalcedony or microcrystalline and in relative small quantities. It fills the pore-space in between the framework minerals. Chert or chalcedony has typically clear and cloudy zones of radial-fibrous quartz in XPL. However, most of the chert and chalcedony in the formation does appear as individual rock fragments. Quartz cement is almost absent, which might be due to the matrix and clay coating of the feldspar and quartz grains, described further in Chapters 5.1.4 and 5.3.

Calcite cement is quite abundant in samples from Lithofacies F.4 (Table 5.1). In PPL, calcite appears colorless, but in XPL, a high birefringence gives the mineral a characteristic rainbow color (Figure 5.12). The mineral occurs as pore-filling and often in association with siderite cement. It is most abundant in sample 1.10 from Locality 1, Bolterdalen (Appendix 7), where the calcite cement accounts for 20 % of the total bulk volume. Calcite cement reduces the porosity significantly in the samples (further described in Chapter 5.3.1). The mineral is also observed to occur as prismatic sparry cement, which is an indication of low matrix content and deposition in agitated water (Bjørlykke et al., 1989), which fits well with the matrix content of Lithofacies F.4 (Figure 5.20).

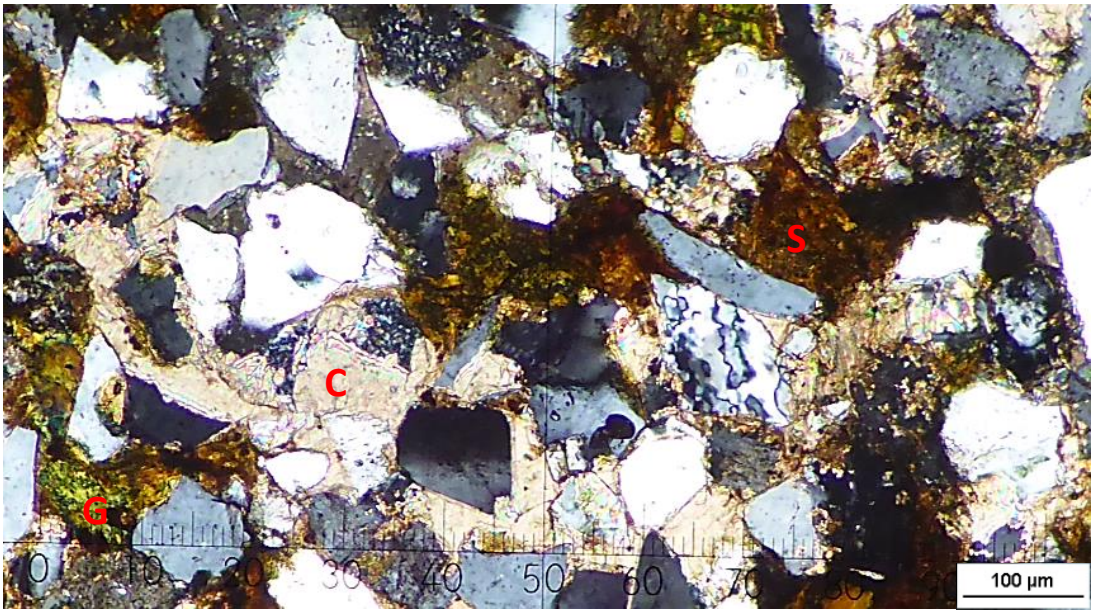

Figure 5.12: *Calcite cement in sample 1.10, Locality 1 (Bolterdalen). The calcite cement (C) has a characteristic high birefringence between the framework minerals. Siderite cement (S) is also present as the brown phase, while glauconite (G) in the sample portrays a green-brownish color. Picture is taken in XPL with scale in microns, 100 microns = 0.1 mm.*

Siderite appears in all samples, but is most apparent in the most distal and most proximal lithofacies (Table 5.1). In the most proximal Lithofacies F.4 (Chapter 4.1) its appearance with calcite cement is common. Siderite appears both as intergranular grains with a rhombic grain shape and as pore-filling cement. It is expected that the siderite occurrence is due to replacement of calcite, biotite or coal fragments. In PPL siderite emerges as a light brown mineral, while in XPL it changes into a darker brown colored mineral. In sample 1.10 it is possible to see the boundary between calcite and siderite-cementation both in hand specimen and in optical microscope (Figure 5.13).

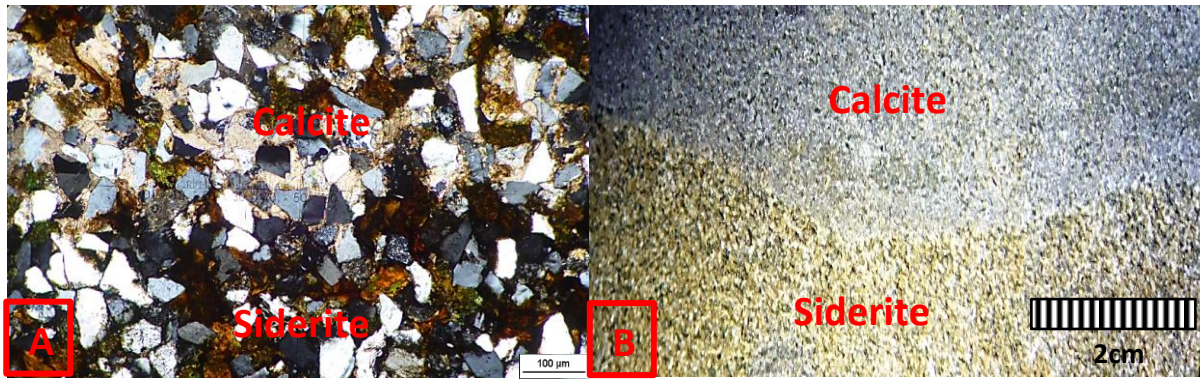

Figure 5.13: *(A) A boundary between calcite and siderite-cement in sample 1.10, Locality 1 (Bolterdalen) seen through optical microscope. Scale in microns, 100 microns = 0.1 mm. (B) Same boundary seen in hand specimen, scale in cm.*

The presence of glauconite and the accompanying green color is the reason why the formation was previously named “the green sandstone series” (Nathorst, 1910). The mineral appears in nearly all the samples, and is most abundant in Lithofacies F.2 & F.4 (Table 5.1). Glauconite is easily identified in PPL by its green or brownish-green color (Figure 5.14). The mineral has a moderate birefringence in cross-polarized-light, which make it appear in its natural colors. Glauconite is a hydrous potassium iron alumino-silicate mineral which exclusively forms in shallow-marine waters (Odin and Matter, 1981). In the samples studied the mineral is observed to be both pore-filling and coating, implying precipitation after deposition of the framework minerals. The process behind its occurrence is further described in Chapter 5.3.

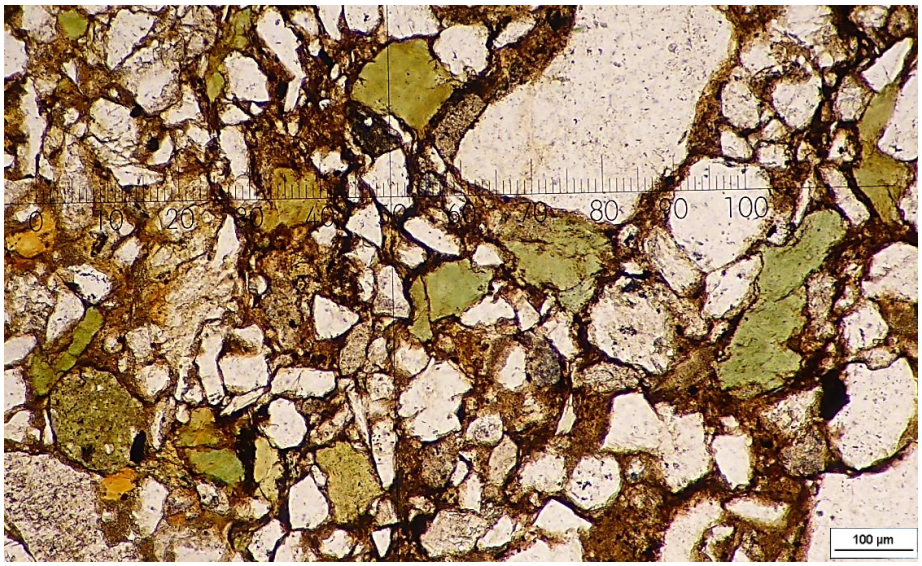

Figure 5.14: *Brownish-green glauconite acting pore-filling amongst quartz and feldspar grains in sample 1.4, Locality 1 (Bolterdalen). Picture is in PPL with scale in microns, 100 microns = 0.1mm.*

Chlorite is a clay mineral which gradually increases from the most distal Lithofacies F.1 towards the most proximal Lithofacies F.4 (Table 5.1), where the mineral has proven to be most abundant. It can sometimes be hard to distinguish chlorite from glauconite due to its green color in PPL, but the clay minerals are best differentiated based on the birefringence in XPL. In plane-polarized-light chlorite appears colorless to pale green, while in cross-polarized light the clay mineral appears with an inclined extinction angle and a weak birefringence. In the samples the clay mineral appears as both pore-filling and coating. Both in optical microscope and SEM analysis, sample 9 clearly displays how the clay mineral is coating quartz and feldspar grains, while also being pore-filling (Figure 5.11, Figure 5.15). The SEM-results display the fibrous characteristic of the clay mineral, being composed of small needles of chlorite (Figure 5.16). Chlorite coating of quartz grains is known to prevent quartz from overgrowth, which can lead to preservation of primary porosity in a state of deep burial and compaction (Ehrenberg, 1993), this is further described in Chapter 5.3.1.

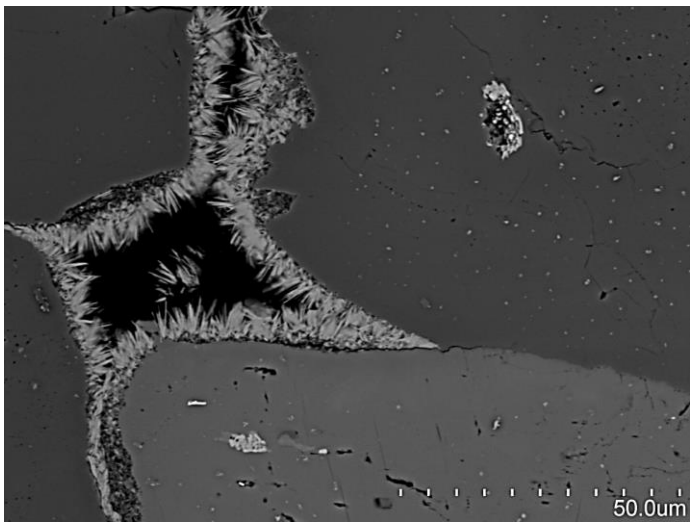

Figure 5.15: *SEM-result of sample 9, well BH-9-2006. Fibrous chlorite is coating the framework grains and filling the pore-space. Scale in microns, 50 microns = 0.05 mm.*

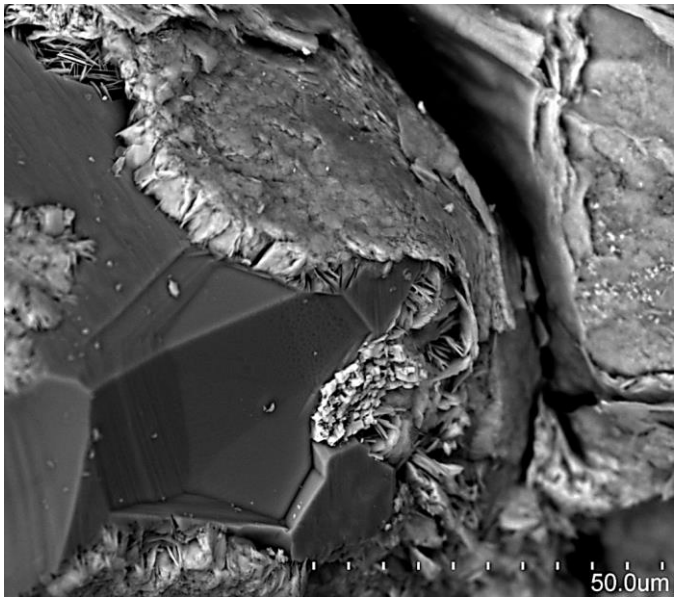

Figure 5.16: *SEM-result of sample 9, well BH-9-2006. Fibrous chlorite composed of multiple small needles is coating a quartz grain. Scale in microns, 50 microns = 0.05 mm.*

Pyrite is an iron sulfide mineral (FeS_2) that appears as opaque (black) in PPL due to absorption of light, and the mineral is small in grain-size, which makes them hard to identify in the optical microscope. Based on the modal analysis (Table 5.1), pyrite is only observed to occur in Lithofacies F.1. The SEM-analysis does however show minor quantities of the mineral in samples associated with other lithofacies in the formation as well. Associating pyrite with the most distal Lithofacies F.1 is not unexpected, as pyrite is common in an eogenetic marine environment in shales and silts, with sulphate (SO_4^{2-}) present (Raiswell and Berner, 1986). The SEM-analysis result of samples 2 and 5 shows pyrite as small white circular pellets (framboids), being either isolated or in close clusters (Figure 5.17). The pellets appear both randomly distributed in the samples matrix and also well aligned along the margins of the matrix in between the framework minerals (Figure 5.18).

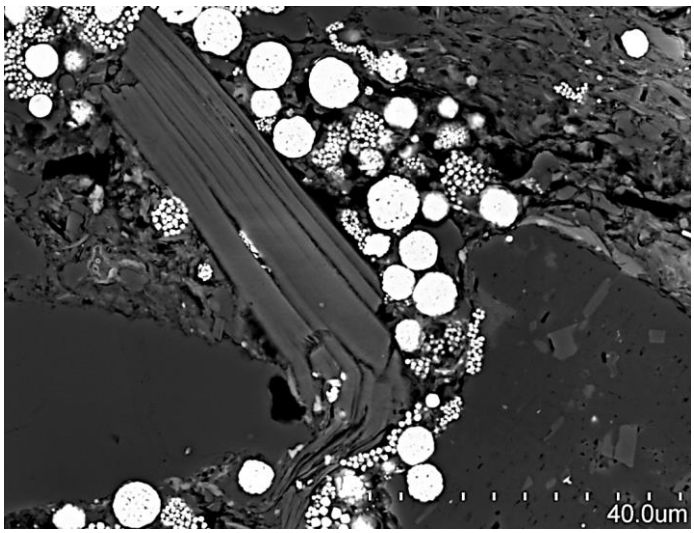

Figure 5.17: *SEM-result of sample 2, well BH-9-2006. Small white circular pellets of pyrite are surrounding the margins of a foliated muscovite mineral. Scale in microns, 40 microns = 0.04 mm.*

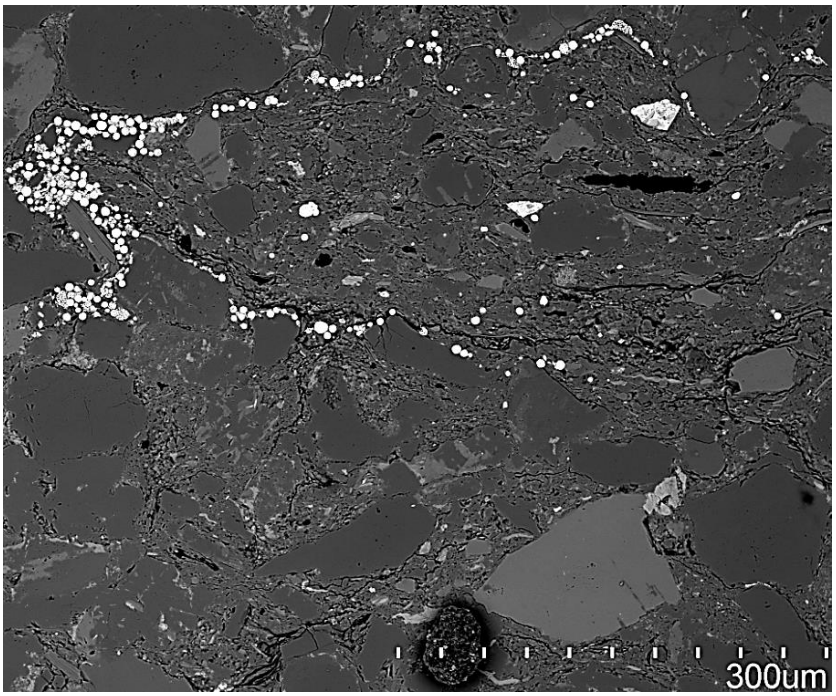

Figure 5.18: *SEM-result of sample 2, well BH-9-2006. White pellets of pyrite are distributed within and along the margins of the matrix in between the framework minerals. Scale in microns, 300 microns = 0.3 mm.*

Sericite appears in all of the defined lithofacies, but is most abundant in Lithofacies F.2 & F.3 (Table 5.1). Sericite is a product of an alteration process (sercitization) of sodium-bearing plagioclase such as albite ($NaAlSi_3O_8$), which gets replaced by this very fine-grained muscovite appearing as intergranular lamellas in the plagioclase (Figure 5.19) (Shelley, 1992). Though often small in size, the lamellas tend to build perpendicular to the twinning direction of the plagioclase. Illite, which is a clay mineral, may be a component of sericite (Warren and Curtis, 1989), which will be further described in Chapter 5.1.5 and 5.3.

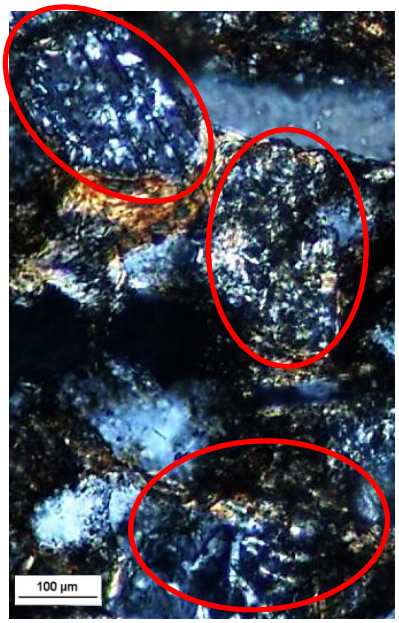

Figure 5.19: *Sample 1.5, Locality 1 (Bolterdalen) shows the alteration product of sodium-bearing plagioclase, namely sericite, which is fine-grained muscovite appearing as bright yellow spots in the altered plagioclase. Picture in XPL with scale in microns, 100 microns = 0.1 mm.*

5.1.5 Matrix

The amount of matrix in the samples was determined by the modal analysis (Table 5.1). The matrix content in the formation gradually decreases from the most distal Lithofacies F.1 towards the most proximal Lithofacies F.4 (Figure 5.20). In the modal analysis the matrix is characterized as being either depositional clay (pore-filling) or biogenic clay (burrow). Since the Grumantbyen Formation is highly bioturbated one would expect that the majority of matrix in the samples to be biogenically supplied. At pore scale through an optical microscope it can be difficult to determine if the matrix is biogenically supplied, because of the scale of investigation. Therefore the majority of the matrix observed in the samples has been categorized as depositional clay (pore-filling), except from clear biogenic supplements.

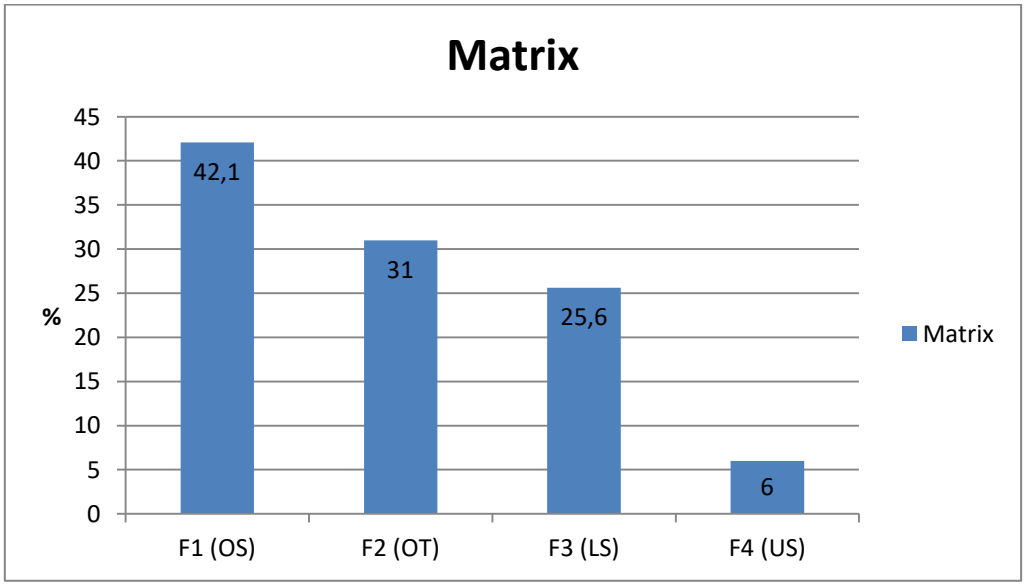

Figure 5.20: *Matrix distribution within the different defined lithofacies (Chapter 4.1), based on the modal analysis in* (Table 5.1). *Lithofacies (F1-F4) is organized from distal to proximal affiliation on the horizontal axis. OS=Offshore, OT=Offshore transition, LS=Lower shoreface and US=Upper shoreface.*

The clays and other constituents of the matrix are hard to identify through the optical microscope because of their very small grain-size, therefore an X – ray Diffraction-analysis (XRD) was done in order to get a better understanding of the chemical composition of the matrix. From the authigenic minerals in the samples it is shown that both glauconite and chlorite are clay minerals that act as pore-filling and coating, whereas the XRD results reveal that illite appears frequent in the matrix composition (Figure 5.21). Illite is quite similar to muscovite in terms of chemical composition; $KAl_3Si_3O_{10}(OH)_2$, and is often an alteration product of muscovite and feldspar, through the process of sericitization due to weathering and hydrothermal alteration (Warren and Curtis, 1989; Shelley, 1992). The XRD-results reveal illite in a transition stage between illite and its iron-rich relative, glauconite; $(K,Na)(Fe^{3+},Al,Mg)_2(Si,Al)_4O_{10}(OH)_2$. Components such as chlorite, feldspar and quartz are also

present in the matrix. The components are most likely a result of diagenetic processes and alteration of framework constituents, illite has probably replaced unstable mica fragments. In terms of samples within the different defined lithofacies (Chapter 4.1), there is also a difference in the components of the matrix content. The matrix composition in sample 9 and 10 from Lithofacies F.4 (Table 5.1) shows less illite and more abundance of chlorite and siderite (Figure 5.22).

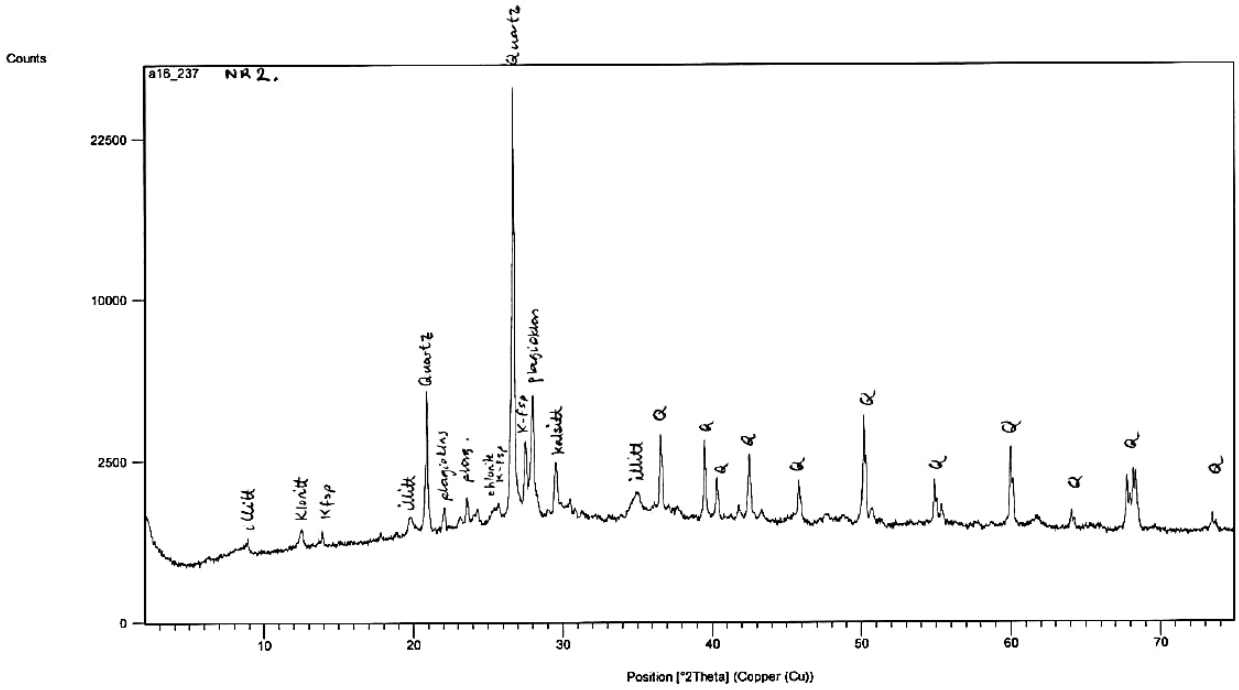

Figure 5.21: *XRD-result of sample 2, well BH-9-2006. Quartz, K-feldspar and plagioclase are the most abundant minerals, but illite also appears quite frequently. Results produced by: Ruth Elin Midtbø.*

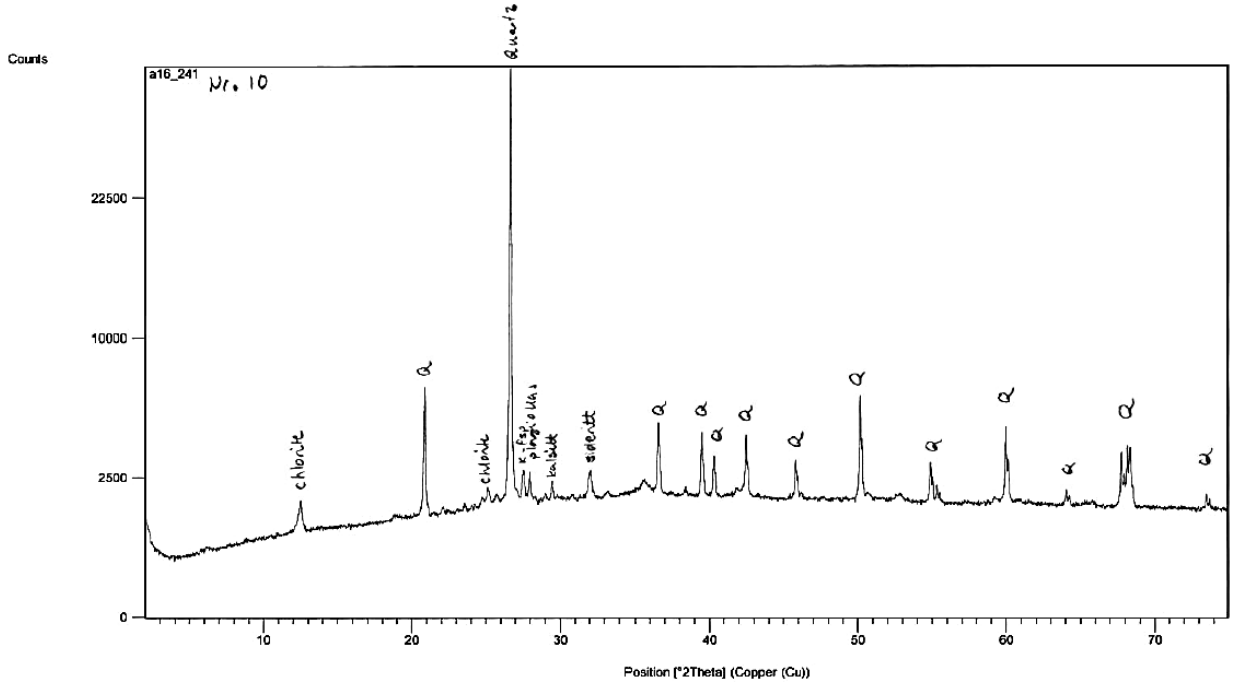

Figure 5.22: *XRD-result of sample 10, well BH-9-2006. Quartz is the most abundant mineral followed by chlorite, siderite, calcite, K-feldspar and plagioclase. Results produced by: Ruth Elin Midtbø.*

5.2 Classification

Based on the analysis of texture, modal analysis, framework and authigenic minerals and matrix in Chapter 5.1, a classification of the different lithofacies (Chapter 4.1) is presented in this chapter. Based on the results from the modal analysis, a classification is done in terms of quartz (Q), feldspars (F) and lithic fragments (L) (Dickinson, 1970). This classification displays the distribution of framework grains, and it has to be normalized from the results of the modal analysis in order to display them in the classification scheme (Q+F+L=100 %) (Dickinson, 1970). Table 5.2 displays the matrix, quartz, feldspar and lithic fragment distribution (%) within each defined lithofacies (Chapter 4.1), which is based entirely on the modal analysis results of each sample within the same defined lithofacies in both well BH-9-2006 and Locality 1, Bolterdalen (Appendix 7 and Appendix 8). Matrix content is important, more than 15 % matrix (<0.03 mm) and less than 75 % implies that the sandstone is classified as a wacke (Figure 5.23), if the matrix accounts for more than 75 % then it is classified as a mudstone (Figure 5.24) and if it is less than 15% it stands as an arenite (Figure 5.25) (Dott, 1964). The matrix content is gradually decreasing from Lithofacies F.1 towards Lithofacies F.4, the classification shows that the offshore (OS) deposited lithofacies is dominated by mudstone, the offshore transition (OT) and lower shoreface (LS) deposited lithofacies are dominated by arkosic wacke, and the most proximal upper shoreface (US) deposited lithofacies is classified as a subarkose (Table 5.2).

Lithofacies	Matrix (%)	Quartz (Q) %	Feldspar (F) %	Lithic fragments (L) %	Classification
F.1 (OS)	93.6	74.5	20.7	4.8	Mudstone
F.2 (OT)	62.3	63.8	32.7	3.5	Arkosic wacke
F.3 (LS)	43.2	62.4	35.1	2.5	Arkosic wacke
F.4 (US)	9.6	76.3	22.0	1.7	Subarkose

Table 5.2: *Matrix content and distribution of framework grains within the different lithofacies (F1-F4) (Chapter 4.1), and their resulting classification. The values are normalized from the results of the modal analysis of each sample within the same defined lithofacies* (Appendix 7 and Appendix 8). *Q+F+L=100 %* (Dickinson, 1970).

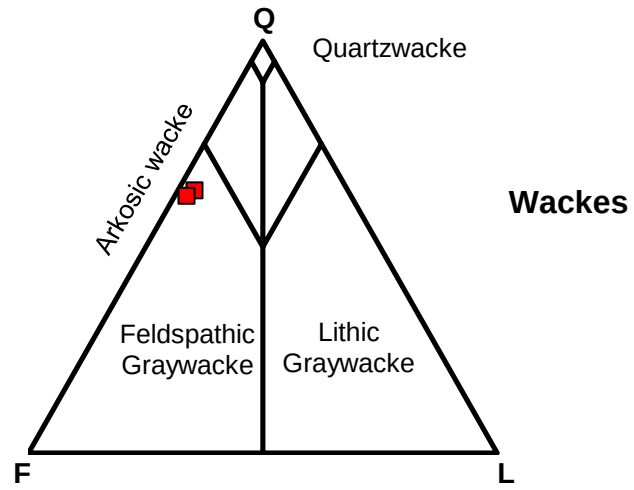

Figure 5.23: *Based on the given values in* (Table 5.2) *Lithofacies F.2 & F.3 plots as an Arkosic wacke due to over 15 % matrix and a high content of feldspars and quartz.*

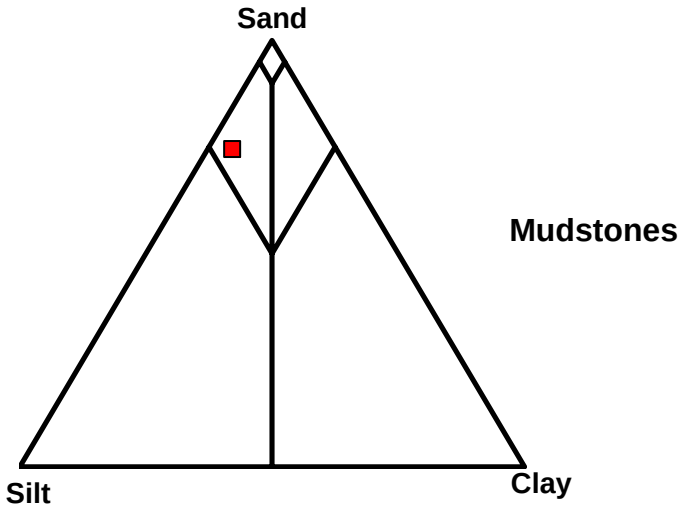

Figure 5.24: *Based on the given values in* (Table 5.2) *Lithofacies F.1 plots as a Mudstone due to over 75 % matrix.*

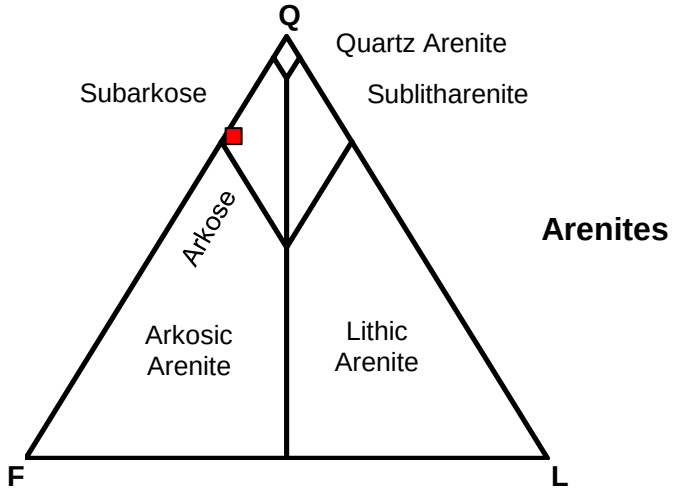

Figure 5.25: *Based on the given values in* (Table 5.2) *Lithofacies F.4 plots as a Subarkose due to less than 15 % matrix and a high content of quartz.*

5.3 Diagenesis

Diagenetic development is presented in this chapter on the basis of the results of Chapter 5.1.2, 4 and 5. Some of the most abundant authigenic minerals in the different lithofacies and their diagenetic evolution are presented in this chapter. From the lithological interpretations (Chapter 4) a general model can be used (Figure 5.26) to summarize the diagenetic reactions typical in a marine depositional environment, which is applicable to the Grumantbyen Formation. Catalyzing processes by bacteria are dominating in marine eogenesis, and the minerals found in this environment can form at varying temperatures depending on the setting (Worden and Burley, 2003). In Chapter 5.3.1 a description of the porosity and the influencing effect by compaction and cementation in the different lithofacies, based on the modal analysis (Chapter 5.1.2) is presented.

When referencing diagenesis, three different regimes are commonly recognized:

- Early diagenesis (eogenesis): includes all processes that occur at or near the surface of the sediments where the marine waters and its chemistry are highly controlled by the adjacent depositional environment (Berner, 1980).
- Burial diagenesis (mesogenesis): includes all processes that occur once the sediment has moved from being influenced by the depositional environment to the very first stages of low-grade metamorphism (Worden and Burley, 2003).
- Uplift-related diagenesis (telogenesis): includes all processes occurring after the rocks have been uplifted and exhumed, where they are being exposed to the influx of surface (meteoric) water (Worden and Burley, 2003).

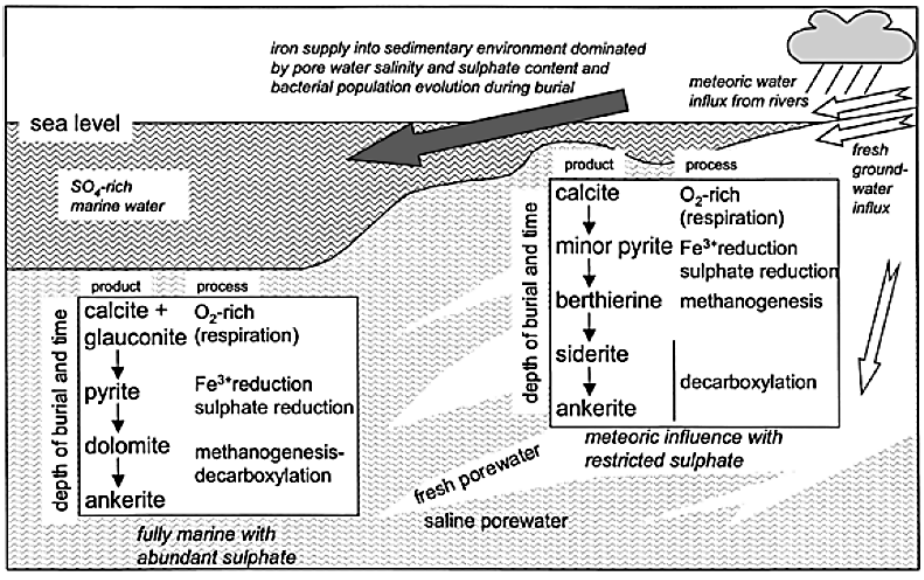

Figure 5.26: *Model summarizing the diagenetic reactions in the marine eogenetic regime after* Worden and Burley (2003). *The model can be used as an analog to the diagenetic reactions creating the authogenetic constituents seen in the Grumantbyen Formation.*

Calcite

Calcite ($CaCO_3$) is observed as an authigenic mineral (Chapter 5.1.4) and appear as a pore-filling cement amongst the framework constituents, often in association with siderite cement. Calcite cement is most abundant in Lithofacies F.4 (Table 5.1). Generally, calcite cement tend to not be evenly distributed in sandstones, their concentration is normally restricted to pore systems which can be completely filled with calcite (Bjørkum and Walderhaug, 1990). Calcite cement tends to form in alkaline waters as a result of redistribution, dissolution and re-precipitation of calcium bearing fossil shell fragments or carbonate minerals (Bjørlykke et al., 1989; Hendry et al., 1996). Calcite forms both during eogenesis as well as mesogenesis (Figure 5.26), when formed during burial diagenesis the precipitated calcite is characterized by recrystallization of pre-existing carbonate minerals (Worden and Burley, 2003). The precipitated calcite cement has a negative impact on the flow properties (permeability) and available pore space (porosity) due to pore-filling and blockage of pore throats (Worden and Burley, 2003).

Siderite

Siderite ($FeCO_3$) is an iron carbonate appearing in all the lithofacies, but is generally more apparent in Lithofacies F.1 & F.4 (Table 5.1). Siderite appears both as intergranular grains with a rhombic grain shape and also as pore-filling cement, often in association with calcite cement especially in the most proximal Lithofacies F.4 (Chapter 4.1). Siderite can develop both during eogenesis and mesogenesis (Worden and Burley, 2003). When in eogenesis, siderite is precipitated in partially reduced environments with high iron-content (Mozley, 1989). The influx of meteoric water causes Fe-ions to react with dissolved carbonate, which creates siderite. Marine conditions usually contain high amounts of sulphide (SO_4^-) due to the reduction of sulphate (SO_4^{2-}) and ferric iron, but if a meteoric influx occurs siderite might form prior to the reduction process of sulphate and iron (Love, 1967).

Dissolution of Fe-rich glauconite, although the mineral is highly resistant and well preserved in the marine environment (Harding, 2014), might be a source of iron. Dissolved biotite can also be a source of iron to the system. Since biotite was only observed in minor quantities in the SEM-analysis, a suggestion is that released iron originated from dissolved biotite. Siderite does also form when decarboxylation reactions overtake methanogenesis with further burial (Worden and Burley, 2003) (Figure 5.26). Methanogenesis takes place in the deepest part of shallow burial in organic rich shales (Curtis, 1980). During decarboxylation increased temperatures as a result of deep burial leads to loss of CO_2 from organic matter, which enables the formation of siderite (Worden and Burley, 2003).

The SEM-results show that the siderite has an impure chemical composition, with small amounts of magnesium present. This is due to the pore water chemistry in marine settings which have a higher magnesium/calcium ratio and less mangan and iron (Mozley, 1989). The observed appearance of siderite in the formation may indicate that it has been formed in a combination of different settings, including (1) influx of meteoric water to the system, (2) dissolution of biotite, (3) decarboxylation and (4) marine pore waters.

Glauconite

Glauconite ($(K,Na)(Fe^{3+},Al,Mg)_2(Si,Al)_4O_{10}(OH)_2$) is an iron clay that appears in nearly all the samples, but is most abundant in Lithofacies F.2 & F.4 (Table 5.1). The mineral is observed to be both pore-filling and pore-coating. Glauconite forms in Fe-rich, oxidized marine waters, with low sediment influx where the sediment accumulation is slow enough to allow diffusive interaction at the interface between sediment and water, such that the mineral has time to form (Odin and Matter, 1981). When formed, the mineral is highly resistant and quite well preserved in the marine environment (Harding, 2014). Favorable conditions for glauconitization is at 50-300 m water depth with temperatures ranging between 7-15^{0}C, typically in shelf-slope settings in open marine waters (Odin and Matter, 1981) (Figure 5.27). Sediment starvation typically provides suitable conditions for glauconite to precipitate. Previous work has stated a close relationship between glauconitic minerals and fecal pellets produced by burrowing organisms, where the organics associated with the feces provide a component for glauconite authigenesis (Pryor, 1975; Ekdale et al., 1984; Harding, 2014). Preservation of fecal pellets is typically found at 0-30 m depth at the seafloor, while the ideal conditions for glauconization is found at 50 m depth or more, which implies that there had to be a flooding of shallower deposits to greater depths in order to glauconitize the fecal pellets (Odin, 1988). Ideal conditions for glauconitization are 10^3 to 10^6 years with minimal sediment influx, meaning that the shallower water deposits must have been flooded for a longer period of time (Odin and Matter, 1981; Odin, 1988; Carozzi, 1993).

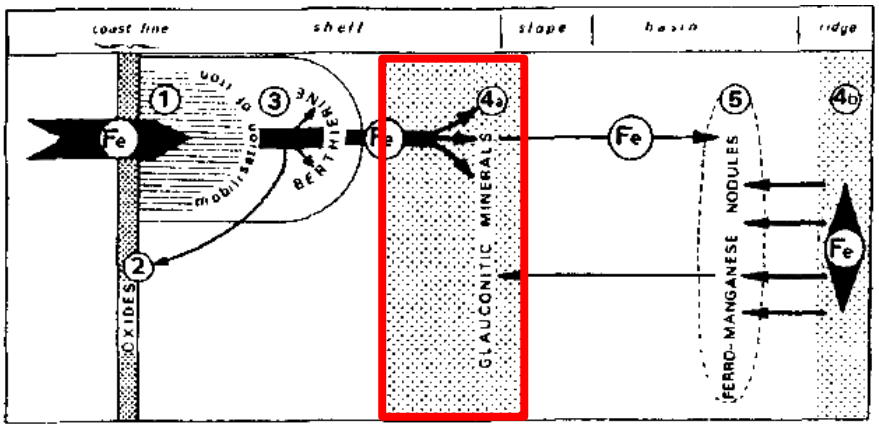

Figure 5.27: *Glauconite forms in Fe-rich oxidized marine waters, with low sediment influx, typically in shelf-slope settings in open marine waters. Model after* Odin and Matter (1981).

Chlorite

Chlorite ($[Fe\text{-}Mg]_5Al_2Si_3O_{10}(OH)_8$) is a clay mineral that gradually increases in abundance from the most distal Lithofacies F.1 towards the most proximal Lithofacies F.4 (Table 5.1). Chlorite appears as both pore-filling cement and grain-coating in the samples. It is often observed together with siderite rather than calcite cement (Worden and Burley, 2003), as seen in the XRD-results of sample 10 from well BH-9-2006 (Figure 5.22). Chlorite can form in both the eogenetic and mesogenetic regime, often in reduced marine waters (Worden and Burley, 2003). The grain-coating prevents the framework grains from further diagenetic processes, such as quartz overgrowth and possible quartz cementation. Formation of grain-coating chlorite is due to recrystallization of Fe-rich clays (glauconite) at temperatures more than 90-100^{0}C, which occurs at burial depths more than 3 km in the subsurface (Ehrenberg, 1993; Aagaard et al., 2000). Preventing quartz overgrowth at such depths could potentially lead to preservation of primary porosity in the sandstone (Ehrenberg, 1993), but the SEM-results show that the chlorite is slightly "overdeveloped" leading to pore-filling in some of the pore-space which actually has a negative impact on the porosity and permeability. This can be a result of deeper burial than ideal chlorite formation-depth, or the sandstone being buried over 3 km depth for a longer time.

Pyrite

Pyrite (FeS_2) appears most abundant in Lithofacies F.1 (Table 5.1) according to the modal analysis, but the SEM-results also reveal its appearance in other lithofacies in the formation as well. Pyrite is observed as small white circular pellets (framboid) being either isolated or in close groupings. Pyrite is formed both during eogenetic and burial diagenetic processes in fully marine conditions (Figure 5.26) (Worden and Burley, 2003). The circular pellets seen in the SEM-analysis are a result of eogenesis, where microbial reduction of ferric iron takes place in sulphate rich seawater during the earliest stage of burial (Love, 1967). Bacterial degradation takes place in the sulphate reduction zone where sulphate is reduced so that sulfur can chemically react with iron to form pyrite (Curtis, 1980). When pyrite is formed at a later stage of burial diagenesis, the mineral tends to be coarser with a subhedral shape (Worden and Burley, 2003).

Illite

Illite ($KAl_3Si_3O_{10}(OH)_2$) was only observed trough the XRD-results as a constituent in the matrix content. Illite precipitates by mesogenetic processes, meaning burial diagenesis at 70^{0}C with the presence of K-bearing pore water (Warren and Curtis, 1989). Dissolution of mica and K-feldspar is a source of potassium which can react with kaolinite. Illite then forms by replacement of kaolinite in

marine environments, when the burial temperature reaches 120-130^{0}C (Hower et al., 1976; Hoffman and Hower, 1979). Since the XRD-results revealed that illite was in a transition state between illite and glauconite, the burial depth has most likely not been deep enough in order to reach high enough temperatures for precipitation of illite in its pure form.

5.3.1 Compaction, Cementation & Porosity

In this chapter a description of the porosity and the influencing effect by compaction and cementation in the different lithofacies, based on the modal analysis (Table 5.1) is presented. There are different ways of describing porosity. The most relevant descriptions based on the modal analysis are extracted from Worden and Burley (2003):

- Primary porosity: porosity occurring between sand grains that is present at deposition
- Secondary porosity: porosity being developed as a result of diagenetic processes (dissolution)
- Micro-porosity: porosity that is only visible through an electron microscope
- Macro-porosity: porosity that can be seen with the naked eye through an optical microscope
- Inter-granular porosity: porosity developed between grains
- Intra-granular porosity: porosity within grains (micropores as result of dissolution/alteration)
- Grain-moldic: in-situ dissolution of minerals/grains, creating local pore-space (secondary)

From the modal analysis, those pores which were visible with the naked eye through the optical microscope were either distinguished as inter-granular macro-porosity or grain-moldic (dissolved framework grains). Based on the modal analysis' calculation of pore-space, the assumption that the matrix contains 10 % inter-granular micro-porosity is included. According to the modal analysis the primary porosity of the samples is dominated by micro porosity (Figure 5.28-A), while the secondary porosity is closer to a 50/50 approximation between micro and macro-porosity (Figure 5.28-B).

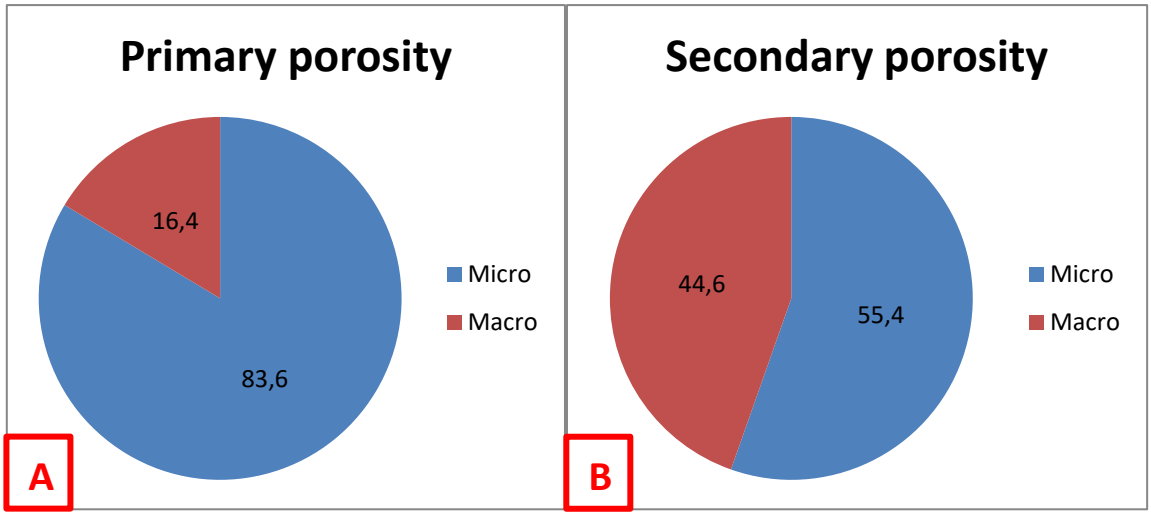

Figure 5.28: *(A) Primary porosity distributed as micro and macro-porosity. (B) Secondary porosity distributed as micro or macro-porosity. Micro and macro-porosity are presented in the figures as percentage, from the modal analysis* (Table 5.1).

From the results of the modal analysis of each sample both from well BH-9-2006 (Appendix 8) and Locality 1, Bolterdalen (Appendix 7), a mean value of the cement and porosity for all samples within the same defined lithofacies (Chapter 4.1) is presented (Figure 5.29) and (Figure 5.30). Lithofacies F.1 to F.3 have the highest measured primary porosity values, these are also the same lithofacies which have the highest matrix content (Figure 5.20) and lowest cement content. The cement content is described as all the authigenic minerals combined from the modal analysis (Table 5.1). With the assumption that the matrix contains 10 % inter-granular micro porosity, this together with the cement content could help to explain why the porosity trend shows a higher value towards the more distally deposited lithofacies. The upper shoreface deposited Lithofacies F.4 has the lowest calculated primary porosity values, while the cement content is abrubtly increasing in this lithofacies. The cement content in Lithofacies F.4 is dominated by calcite and chlorite (Table 5.1). As previously mentioned in both Chapter 5.1.4 and 5.3, calcite cement has a negative impact on the flow properties (permeability) and available pore space (porosity) due to pore-filling and blockage of pore throats (Worden and Burley, 2003). Chlorite is observed to be grain-coating quartz, which prevents quartz overgrowth and quartz cementation. Chlorite coating is known to have a positive impact on the preservation of primary porosity in sandstone during burial and diagenesis. Although the results show only a primary porosity of 2.4 %, and the SEM-results revealing that the chlorite is "overdeveloped" and actually filling the available pore-space (Figure 5.15), this actually has a negative impact on the primary porosity.

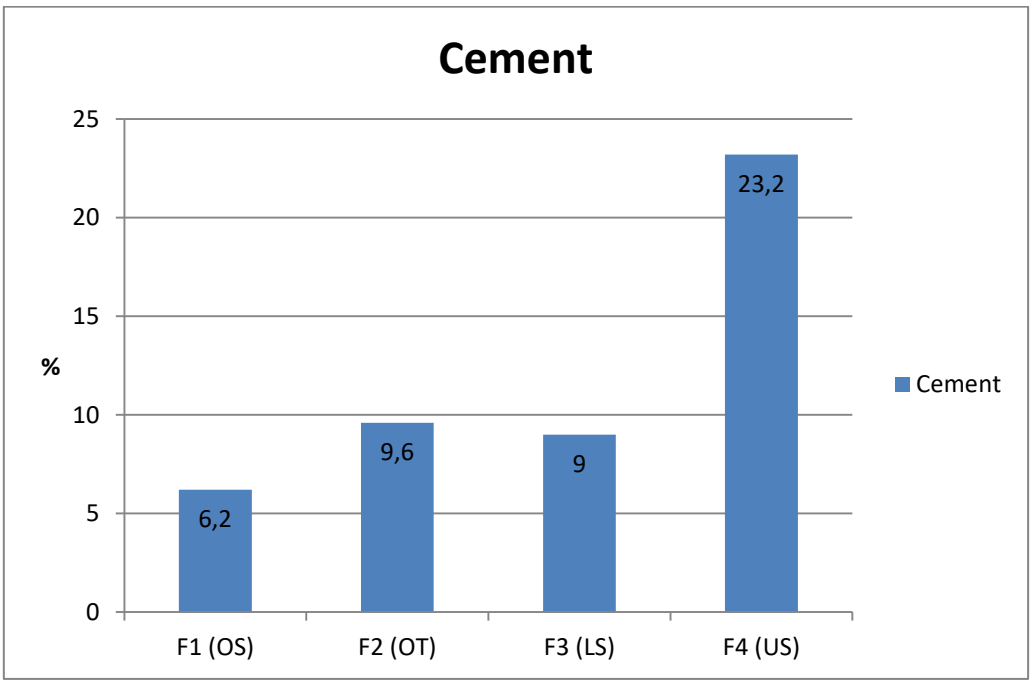

Figure 5.29: *Cement distribution within the different defined lithofacies (Chapter 4.1), based on the modal analysis in* (Table 5.1). *Lithofacies (F1-F4) is organized from distal to proximal affiliation on the horizontal axis. OS=Offshore, OT=Offshore transition, LS=Lower shoreface and US=Upper shoreface.*

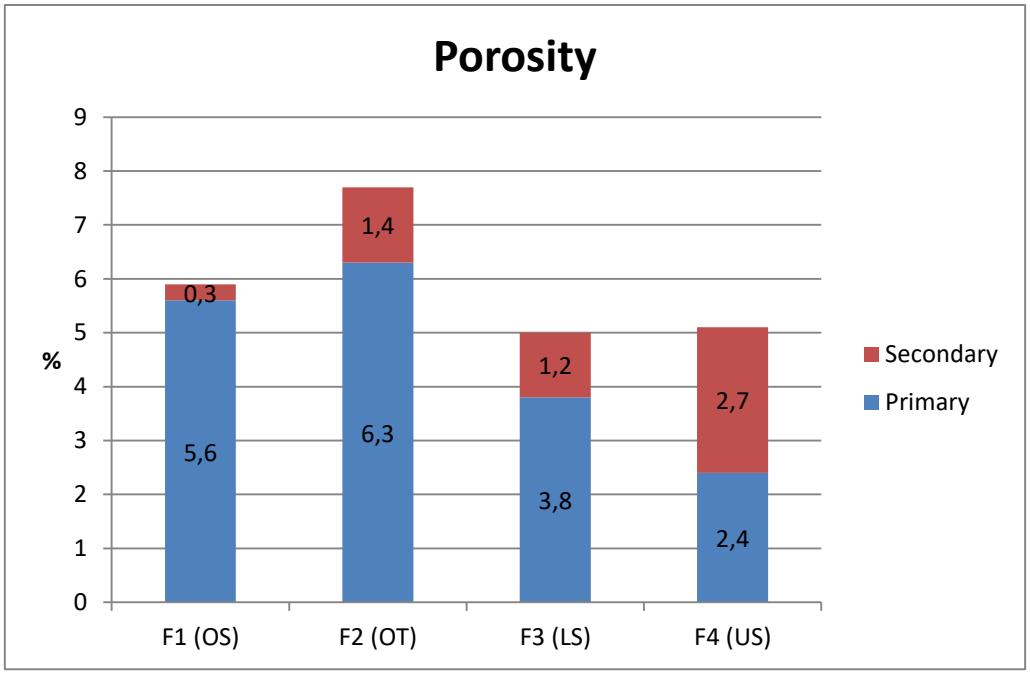

Figure 5.30: *Porosity distribution within the different defined lithofacies (Chapter 4.1), based on the modal analysis in* (Table 5.1). *Lithofacies (F1-F4) is organized from distal to proximal affiliation on the horizontal axis. OS=Offshore, OT=Offshore transition, LS=Lower shoreface and US=Upper shoreface.*

Figure 5.30 shows that the secondary porosity is higher in Lithofacies F.4 compared to the other ones. This is probably due to dissolution of cement and other unstable grains during uplift-related diagenesis (telogenesis). The influx of acidic meteoric water could possibly have dissolved calcite cement, feldspars and other clay minerals, creating both micro and macro secondary porosity (Figure 5.28-B). Figure 5.30 also displays that the primary porosity in all of the lithofacies is quite low, and this is most likely due to the effects of compaction and cementation on the rocks causing porosity-loss. Most of the inter-granular macro-pores described in the samples were randomly distributed with few signs of communication. In order to find out if the porosity-loss is compaction or cementation-dominated a classification scheme by Houseknecht (1984) is presented (Figure 5.31). With an assumed initial (depositional) porosity of about 40 % (Worden and Burley, 2003), a calculation of the intergranular volume (IGV) and the volume of cement is presented in (Table 5.3), and used to determine the dominating process of porosity-loss presented in (Figure 5.31). IGV is described as the remaining amount of primary pore-space and volume of pore-filling cement, and measures the chemical and mechanical-compaction (Houseknecht, 1984; Paxton et al., 2002). IGV does not include secondary porosity, cements replacing dissolved framework grains etc. (Worden and Burley, 2003). Porosity will decrease with increasing burial depth, being a function of lithology and fluid pressure, relative to compaction.

Lithofacies	Intergranular volume (IGV) (%)	Cement (%)
F.1 (OS)	5.6	6.2
F.2 (OT)	6.3	9.6
F.3 (LS)	3.8	9.0
F.4 (US)	2.4	23.2

***Table 5.3**: Table describing the main porosity-loss in the different defined lithofacies (F1-F4) (Chapter 4.1) based on the intergranular volume (IGV) and the volume of cement calculated from* (Table 5.1). *OS=Offshore, OT=Offshore transition, LS=Lower shoreface and US=Upper shoreface.*

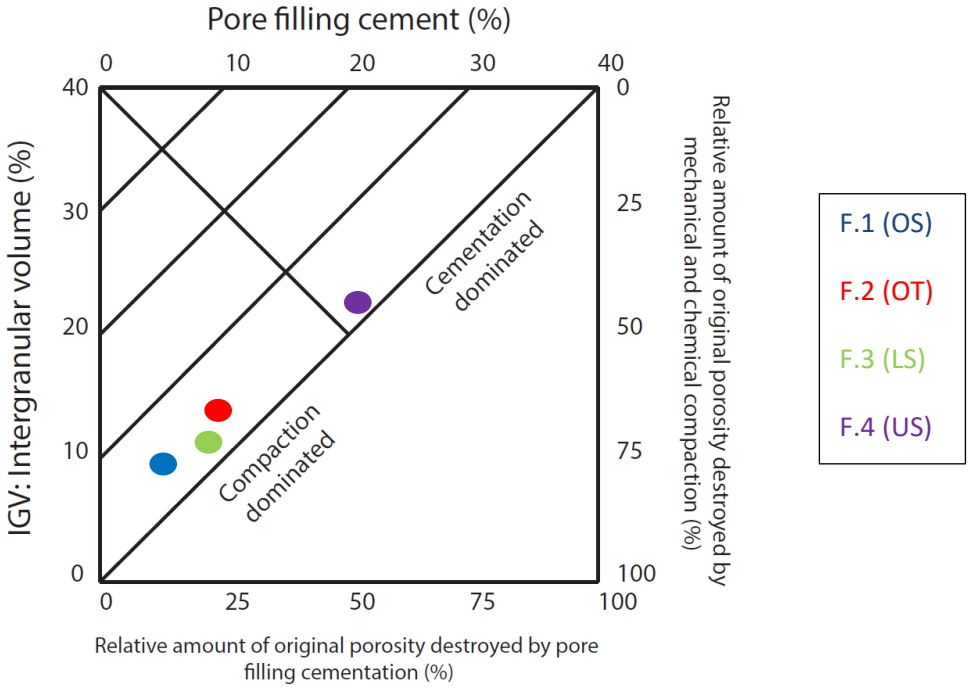

***Figure 5.31:** The classification scheme describes the dominating processes of porosity-loss in the different lithofacies described within the Grumantbyen Formation. Lithofacies F.1-F.3 has all lost porosity from compaction, while Lithofacies F.4 is dominated by cementation as the main process behind the porosity-loss. Color coding of the individual lithofacies is marked in the box on the right hand side. After* Houseknecht (1984).

The classification scheme (Figure 5.31) shows that Lithofacies F.1 to F.3 are primarily dominated by compactional porosity-loss with a little less than 25 % of the porosity-loss being affected by cementation. Lithofacies F.4 is close to a 50/50 split between compaction and cementation-dominated porosity-loss, but still falls within cementation dominated. The differences between the lithofacies are most likely connected to matrix and cement content and also the amount of framework constituents, such as quartz, feldspars and rock fragments. Quartz is a more resistant mineral both mechanically and chemically than feldspar and rock fragments. Since Lithofacies F.4 has a higher abundance of quartz than the other lithofacies (Table 5.1), this will make the sandstone more resistant to porosity-loss by compaction. The cement content in Lithofacies F.4 is also much higher than the other lithofacies (Figure 5.29), implying a strong effect on porosity-loss by cementation. The matrix and cement content in Lithofacies F.1 to F.3 could be the reason why these lithofacies are primarily dominated by compactionalporosity-loss.

6 Discussion

The Grumantbyen Formation has remained poorly understood due to its high bioturbation intensity and lack of physical sedimentary structures throughout the whole succession. The discussion in this chapter is based on the ichnological, lithological and petrographical interpretations in the previous chapters with the aim of presenting a better understanding of the sedimentological development and depositional environment of the formation, relating this to a potential reservoir quality of the sandy formation.

6.1 Depositional environment

The ichnological study shows that there are a total of seven ichnofabrics identified from the wells and the outcrop studied, and that there is a gradual transition between these ichnofabrics. The abundance and appearance of the different ichnofabrics in well BH-10-2008, BH-9-2006 and the outcrop studied (Locality 1, Bolterdalen) is slightly different. Based on the description and interpretation of the different trace fossils appearing in the succession, the behavior of their producers is strongly connected to environmental conditions by energy levels related to current activity and oxygen distributed in the sediments. Well BH-10-2008 shows a more distal placement in the system based on the strong occurrence of *Nereites* and less abundance of *Macaronichnus* (Appendix 11), compared to well BH-9-2006 showing a more proximal affiliation were *Macaronichnus* is more prominent than *Nereites* (Appendix 13). Reasons for comparing the appearance of these two trace fossils is that *Nereites* burrows are considered characteristic in offshore environments with oxygenated waters with low to moderate energy levels and slow/continuous sedimentation rates from suspension of fines (Frey and Pemberton, 1984; Hubbard et al., 2012). *Macaronichnus* is oppositely considered as being typical in more proximal shallow-marine deposits were energy levels are considerably higher and sandy substrate is more dominant, such as in an upper shoreface or foreshore environment (Clifton and Thompson, 1978; Seike, 2007; Bromley et al., 2009). Weathering of the outcrop section (Locality 1, Bolterdalen) made it harder to identify some of the trace fossils due to their size, but *Macaronichnus* did still show a great abundance in the outcrop studied (Appendix 12).

Well BH-9-2006 was drilled on Nordenskiöld Land (Figure 2.3) and the interval containing the Grumantbyen Formation is approximately 268 meters thick, while BH-10-2008 is drilled approximately 50 km further to the south on Nathorst Land (Figure 2.3) and the same interval is only approximately 140 meters thick. Seeing a thickening from the most southern well towards the northern

well, together with the abundance of ichnofabrics also implying a change from a distal to a more proximal environment, might indicate that the whole system has prograded in a southern direction during deposition. This observation fits the earlier interpretations of the system as being provided with sediments from a source in north-east and prograding in a south-western direction (Kellogg, 1975; Steel et al., 1985; Bruhn and Steel, 2003; Simonstad, 2011).

The connection between the ichnofabrics present and the different lithologies is important in terms of suggesting a potential depositional environment, since there are only a few physical sedimentary structures present in the formation. Observations of the different lithologies do however show that the appearances of sedimentary structures are increasing from Lithofacies F.1 towards F.4; despite the number of appearances are a few. A possible continuing vertical (lateral) facies shift shows that the silt content is gradually decreasing from Lithofacies F.1 towards the proximal interpreted Lithofacies F.4, most likely because the environment of deposition is moving from being under the storm-wave base to above the fair-weather wave base. This means that the energy level during deposition is getting stronger which implies better sorting of the deposits and washout of finer material. The specific appearance of different trace fossils also implies this, by having less mud-incorporating organisms and instead seeing more grain sorting behavior.

These observations and interpretations become even more reliable when we take the analyzed samples from the petrography chapter into consideration. The texture of the analyzed samples shows that roundness, sorting and shape of the grains gets better from Lithofacies F.1 towards F.4, which implies higher energy conditions. From the modal analysis, the observed matrix content (Figure 5.20) is also gradually decreasing from Lithofacies F.1 towards F.4, which supports the interpretation of a possible lateral shift in facies and that the environment of deposition is becoming shallower upward in the succession of the Grumantbyen Formation. According to the classification of the samples analyzed, which is entirely based on the modal analysis (Table 5.1), the samples taken from the most distal Lithofacies F.1 are classified as mudstones (Figure 5.24), while the samples taken from the most proximal Lithofacies F.4 are classified as subarkose (Figure 5.25). These results are based on matrix content and the distribution of framework constituents, being directly related to energy levels in the environment of deposition. Lithofacies F.2 and F.3 are classified as arkosic wackes due to their matrix, quartz and feldspar content, which could imply periodic higher energy conditions and not a continuous degree of sorting as seen in Lithofacies F.4. This fits well with the offshore transition interpretation of Lithofacies F.2 and lower shorefaces interpretation of Lithofacies F.3, which would laterally be placed in between Lithofacies F.1 and F.4.

Glauconite is one of the authigenic minerals seen in the formation, and the abundance of this clay mineral has given the formation a characteristic green color. The appearance of glauconite in

combination with the formation's high bioturbation intensity and lack of physical sedimentary structures is most likely the reason why geologists have struggled to interpret the formation's sedimentological development. Most of the previous work on the formation's sedimentological development has led to an interpretation in terms of an offshore origin (Steel, 1977; Steel et al., 1981; Simonstad, 2011; Vilberg, 2011), but a possible inner shelf setting has also been proposed (Steel et al., 1985). The observations and interpretations of this study points to a system being shoreline-attached and building out in a seaward direction. The appearance of glauconite in a highly bioturbated substrate indicates a system which has received relatively little sediment during the time of deposition. If we assume the sediment influx to be low, but still continuous, there must have been minor changes in terms of subsidence and/or relative sea level, in order to allow for glauconitization and progradation.

The sea-level during deposition of the Grumantbyen Formation is suggested to have been relatively stable (Simonstad, 2011). Although the formation is described as having an overall homogenous look, a gradual coarsening upward trend from Lithofacies F.1 to F.4 exists, implying that the low sediment influx must have been slightly greater than the available accommodation space. A suggestion is that the stacking patter is aggradational and at the same time progradational. Ideal conditions for glauconitization are 10^3 to 10^6 years with minimal sediment influx at water depths greater than 50 m (Odin, 1988). Taking that into consideration, the buildup of the Grumantbyen Formation must have been a fairly slow process. Unpublished work by Gjelberg and Steel (1997) in a journal article by Bruhn and Steel (2003), states that the Grumantbyen Formation can be divided into six small-scale sequences illustrating coastal build-out events with each of them representing approximately 500 000 years. An intermediate-scale transgressive-regressive cycle would then be the result of the stacking of these small-scale sequences (Bruhn and Steel, 2003). This interpretation would be in alignment with the conditions needed for glauconite to form, in terms of water depth (transgression) and time (low sediment-influx).

The ichnological analysis also shows that the succession is shallowing upward, based on the different ichnofabrics dominating within the individual lithofacies (Figure 3.28). A transition from the most distal *Nereites*-Ichnofacies in Lithofacies F.1 to *Cruziana*-Ichnofacies in Lithfacies F.2 and F.3 and then to the most proximal *Skolithos*-Ichnofacies in Lithofacies F.4 have been demonstrated, based on the trace fossil assemblages. This observation is also supported by the unpublished work by Gjelberg and Steel (1997) in the journal article by Bruhn and Steel (2003). The same trend is also supported by the lithological study which shows that the succession is observed to be gradually coarsening upward from a marine sandy siltstone towards a shallow-marine very fine/fine to medium-grained light silty sandstone.

Lithofacies F.5, being described as a gravel layer at the top of the formation, has in this study been interpreted to be a transgressive lag marking the start of the major flooding on top of the shallow-marine Grumantbyen Formation leading to the deposition of the superimposed Frysjaodden Formation. This gravel layer has previously caught the attention of several others who have worked with the formation. A gravel lag was first described by Kellogg (1975) as being at and near the top of the Sarkofagen Formation (=Grumantbyen Formation), as a result of regression towards west. Even more detailed work on the gravel layers were done by Steel (1977) who observed the layers to be 2-10 cm thick and excellent marker beds which could be traced for long distances, possibly deposited by seasonal winter ice. Simonstad (2011) interpreted the gravel layer to have been deposited in a shoreface environment, were higher energy conditions made it possible to deposit the larger grain-sizes as opposed to the rest of the succession which he stated had been deposited in offshore waters below storm-wave base. Simonstad (2011) concluded that the layer had been deposited as a result of a sudden drop in sea-level at the time of deposition, leading to a forced regression. Simonstad (2011) also explains the coastline-trajectory to be nearly flat, which in a case of forced regression possibly would lead to significant erosion and incision on the shelf. Such observations have not been identified in any of the wells or at the outrcrop studied in this thesis. The gravel layer is observed to be associated with only minor erosion at the top of the upper shoreface interpreted Lithofacies F.4. Lithofacies F.4 does however show intervals of coarsening upward, especially in the most proximal well BH-9-2006, and the same trend in the upper section of the formation has also been described in other previous work on the Grumantbyen Formation (Steel, 1977; Steel et al., 1981; Bruhn and Steel, 2003). The observed drop in sea-level (Simonstad, 2011) could possibly explain why these coarsening upward units are so prominent in Lithofacies F.4. The gravel layer as observed in this thesis is strongly associated with the deposition of the superimposed Frysjaodden Formation, marking a major transgressive event above the Grumantbyen Formation. A suggested transgressive lag therefore still stands as the most reliable interpretation of the observed gravel layer.

As already mentioned the abundance of glauconite, intense bioturbation, lack of physical sedimentary structures and yet high sand-content has led to a proposed offshore origin of the formation in previous works. Steel et al. (1981) first proposed the potential depositional environment to be a complex of offshore bars. According to an offshore bar model presented by Johnson and Baldwin (1996), the signatures of this type of system show striking similarities to the observations made on the Grumantbyen Formation. The issue however is related to the great extent and thickness of the Grumantbyen Formation in the Palaeogene Central Basin, where an offshore bar complex usually is recognized by thinner successions and a much smaller geographically extent. Sand bodies found in such systems are also usually enclosed by muds and silts, which results in isolated sand bodies (Johnson and Baldwin, 1996). This is however not the case in the Grumantbyen succession, since a

suggested shoreline-attachment is proposed and lateral shift between facies exists as a result of coarsening and shallowing upward based on its ichnology, lithology and petrography.

Simonstad (2011) proposed a sandy outer shelf depositional model where a delta in the north-eastern part of the system provides sandy material to the system which is further transported to the distal parts of the shelf by strong longshore currents. The observations in this study points to a shallow-marine depositional environment dominated by wave action and little sediment input. A potential delta in the north-eastern parts has probably feed the system with sediments which was affected by wave activity, as proposed by Simonstad (2011). The observations do not show any sign of lobate architectures, distributary channels or any other sign of fluvial impact. Also the low sediment influx might indicate that the depositional environment is not directly connected to the source of sediment input. The petrographical study also supports this by not seeing prominent grain-size variations in the upper shoreface analyzed samples, which would have been an indication of a possible fluvial input nearby. These observations together reject an idea of a possible wave-dominated delta system. The observations in this study do however portray evidences of a system that is closely related to a wave-dominated delta. A shoreline-attached system which broadly builds out into the basin with evidence of wave action suggests that the Grumantbyen Formation was a slightly prograding shoreface system, probably feed by one or several deltas in the north-eastern areas. A suggestion is that the shoreface slowly prograded into the system, where the conditions have been perfectly suitable for organisms to live and cause intense bioturbation. Based on the two wells studied and other previous work on the formation (Kellogg, 1975; Steel et al., 1985; Bruhn and Steel, 2003; Simonstad, 2011), there is an agreement that the formation is thinning in a south-western direction. *Figure 6.1* represents a simplified model of the proposed depositional environment of the Grumantbyen Formation in this study, illustrating the different interpreted lithofacies' placement in a possible shoreface system. In the most proximal parts of a shoreface system above the upper shoreface, one would expect to find beach deposits. A suggestion is that the major flooding of the shallow-marine Grumantbyen Formation and the resulting marine erosion could have washed away these beach deposits, since they have not been identified in this study. Remains of these beach deposits could potentially have been re-deposited as a part of the transgressive lag described earlier in the discussion.

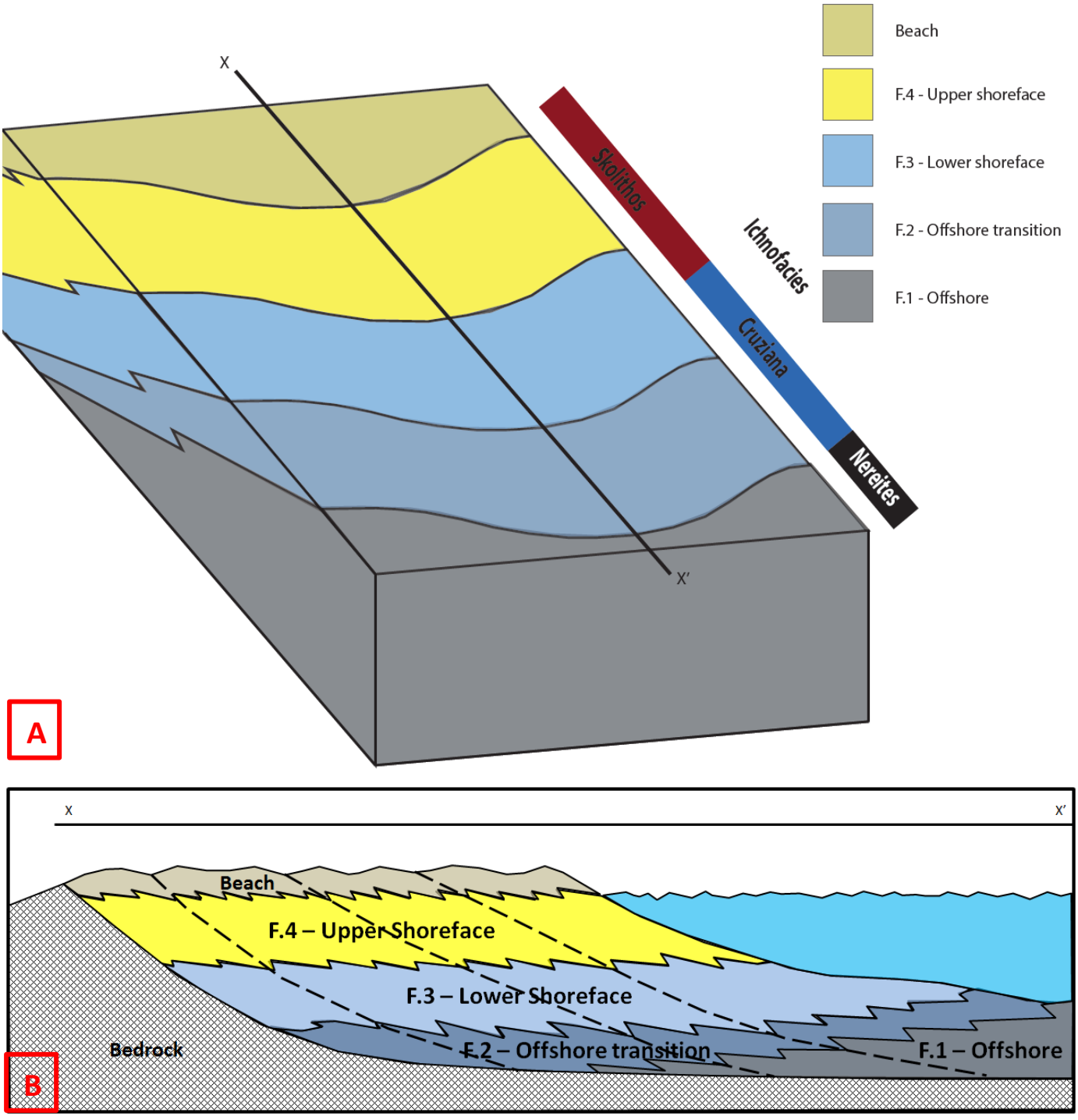

Figure 6.1: *(A) Simplified model of a slowly prograding shoreface system divided into the different defined lithofacies (F.1-F.4) in the Grumantbyen Formation. The beach facies is included in the model, but is not observed within the Grumantbyen Formation. The associated ichnofacies are noted on the side of the model, which is based on the observed trace fossil assemblages within the different lithofacies. The cross-line illustrates a transect from X to X' which is presented in figure (B), where the different defined lithofacies (F.1-F.4) are noted (modified from Nemec).*

6.2 Reservoir quality

The porosity estimation of Lithofacies F.1 to F.4 in the Grumantbyen Formation is based on the modal analysis (Table 5.1). Matrix, cementation, compaction and uplift are the most important factors which have had a significant effect on the porosity distribution. The primary porosity within the lithofacies is overall fairly low, and there is an observed trend of gradual decreasing primary porosity from the offshore interpreted Litofacies F.1 towards the upper shoreface interpreted Lithofacies F.4 (Figure 5.30). This is especially related to the matrix and cement content. Lithofacies F.1 to F.3 have the highest matrix content (Figure 5.20), where an assumed 10 % inter-granular micro-porosity is included in the primary porosity calculation. The most proximal Lithofacies F.4 has the lowest matrix values, but at the same time a higher cement content compared to the other (Figure 5.29). A further investigation on the possible porosity-loss was done by the calculation of the intergranular volume (IGV), in order to determine if the loss is dominated by either compaction or cementation. The results from the classification scheme (Figure 5.31) reveal that the primary porosity-loss within Lithofacies F.1 to F.3 were compaction-dominated, while Lithofacies F.4 was cementation-dominated. The difference between being either compaction- or cementation dominated is related to the lithofacies' matrix and cement content and also the amount of framework constituents, where the upper shoreface interpreted Lithfacies F.4 has a higher abundance of quartz which makes the sandstone more resistant to porosity-loss due to compaction. The lack of matrix in Lithofacies F.4 makes the sandstone more exposed to diagenetic reactions during burial, and that would explain the high amount of cement content within that lithofacies. The cement content within lithofacies F.4 is primarily dominated by calcite and chlorite, which is proven to have a negative impact on the porosity possibly due to a deeper burial and a resulting stronger diagenetic reaction of especially the chlorite (Chapter 5.3 & 5.3.1).

Secondary porosity also occurs within the different lithofacies, though with overall fairly low values. The secondary porosity is observed to gradually increase from Lithofacies F.1 towards F.4. The secondary porosity is most likely related to uplift-related diagenesis (telogenesis), where the exposed rocks have been influenced by meteoric water leading to dissolution of cement and other unstable grains. Dissolution of calcite cement and other authigenic clay minerals probably explains why Lithofacies F.4 has a higher calculated secondary porosity compared to its primary porosity (Figure 5.30).

An interesting question is whether or not the intense bioturbation throughout the entire succession had an impact on the porosity distribution, and how it possibly affected it in a positive or negative way. In the recent years a great focus has been turned towards biogenically enhanced reservoir quality, were discoveries actually have revealed that interconnected sand-filled burrow networks of organisms tend

to enhance the reservoir quality of the sandstones in terms of both permeability and porosity (Gordon et al., 2010; Baniak et al., 2013; La Croix et al., 2013; Knaust, 2014; Baniak et al., 2015). The Ula Formation serves as a good example of a reservoir where there is an increased recovery of fluids in the bioturbated zones (Baniak et al., 2015). Depending on the burrow character, certain burrows favoring grain sorting behavior would lead to an enhancement of the reservoir properties, while mud-filling behavior would have a negative impact (La Croix et al., 2013). In this study the ichnofabrics dominating within Lithofacies F.1 to F.4 show that due to the gradual shallowing upward and lateral shift in facies, there is also a gradual shift from distal mud-filled burrows (*Virgaichnus undulatus*) towards proximal grain-sorted burrows (*Macaronichnus segregatis*) (Figure 3.28). *Macaronichnus segregatis* appearing in the upper shoreface zone has in previous studies been proven to enhance the reservoir quality, due to grain segregation and passive sorting (Pemberton and Gingras, 2005; La Croix et al., 2013). Since the upper shoreface interpreted Lithofacies F.4 in this study is dominated by *Macaronichnus*-Ichnofabric, one could assume that the trace fossil has had a positive impact on the porosity distribution before significant burial and diagenesis took place. That being said, *Virgaichnus undulatus* is the most dominating ichnofabric throughout the entire succession and has proven to be a mud-filling burrow structure, which would oppositely have a negative impact on the reservoir quality of the sandstone. In order to get an idea of how the porosity distribution could have been before significant burial started a visualization of the primary porosity distribution, where the cement filling the pore-space has been excluded, is presented (Figure 6.2). The figure reveals a more expected realization of how the porosity was distributed within the four different lithofacies before burial and diagenetic cement affected it.

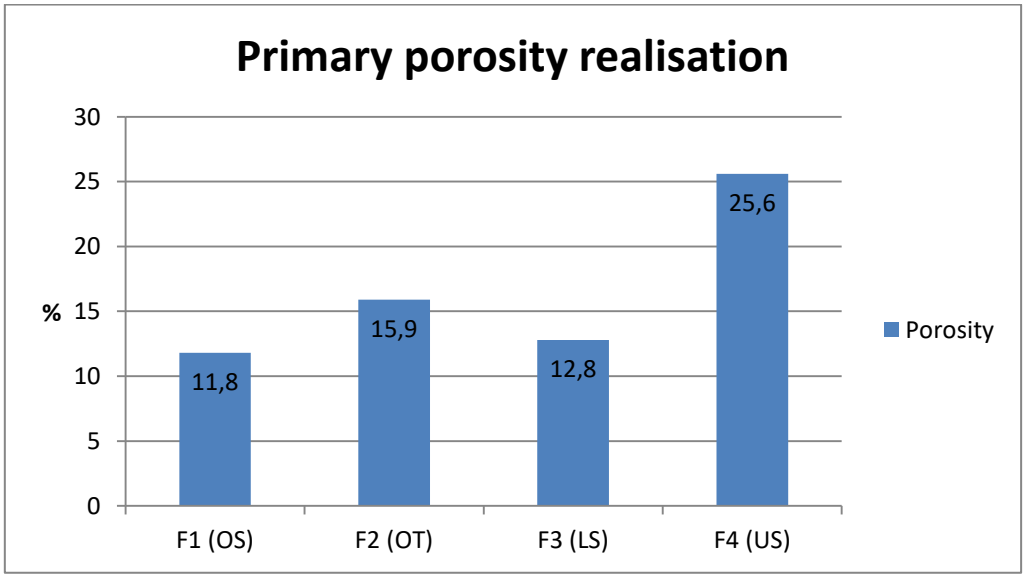

Figure 6.2: *The figure illustrates a realisation of the primary porosity distribution within Lithfacies F.1-F.4 before significant burial. The values are based on the calculated primary porosity values* (Figure 5.30) *and cement* (Figure 5.29) *within the four different lithofacies. Lithofacies (F.1-F.4) is organized from distal to proximal affiliation on the horizontal axis. OS=Offshore, OT=Offshore transition, LS=Lower shoreface and US=Upper shoreface.*

The reservoir quality of the formation is a clear result of many different processes/agents. Before significant burial, bioturbation and matrix content possibly had the greatest impact, while during burial diagenetic processes created cement, and also compaction played a role based on the matrix and framework constituents of the lithology. Later uplift caused alteration and dissolution of the different constituent, leading to secondary porosity. In this study of the Grumantbyen Formation, the amount of matrix, cement and degree of compaction has clearly had a negative impact on the reservoir quality due to substantial porosity-loss. The fact that the primary porosity is dominated by inter-granular micro-porosity as a result of the high degree of matrix is a clear negative signal (Figure 5.28-A). The inter-granular macro-porosity which was observed in the optical microscope appeared randomly distributed and almost always isolated which is a sign of poor communication in the pore-network. This would have a negative effect on the flow properties (permeability) as well. Before significant burial Lithofacies F.4 could potentially have been a good reservoir sandstone with well communication in the pore-network as a result of the burrow-network by *Macaronichnus segregatis*, but diagenetic cement has unfortunately led to a relatively poor reservoir quality.

6.3 Further research

In order to get a complete understanding of the high bioturbation intensity within the Grumantbyen Formation, more wells and outcrops need to be studied closer. Also by collecting more samples from different wells and outcrops and studying them by their petrographical means would sufficiently contribute to a better understanding of the formation's diagenetic history and depositional development. A better understanding of the biostratigraphy in the Palaeogene Central Basin would also be useful in terms of detailed correlation between the different wells and outcrops. A closer look into sea-level variations and possible source area signatures during time of deposition of the Grumantbyen Formation would contribute to a better understanding of its mineralogical constituents, sequence stratigraphic buildup and diagenetic reactions.

As mentioned in Chapter 3.1 closer study of the orientation of *Macaronichnus* traces could be used as an indicator of beach morphodynamics, palaeo-shoreline orientation, ancient sea-level and environmental conditions (Seike, 2007; Bromley et al., 2009; Seike et al., 2011; Uchman et al., 2016). An interesting angle would therefore be to study the intervals of *Macaronichnus*-Ichnofabrics within the Grumantbyen Formation in further detail. The purpose would be to investigate the indications the burrow can reveal based on orientation, and also see how the trace fossil within the formation particularly affects the reservoir quality in these zones. Permeability measurements with both gas and fluid to understand how the burrows could possibly lead to a better pore-network system and increased recovery of hydrocarbons is particularly of interest for the petroleum industry.

6.4 Sources of error

Trace fossil identification can of course be prone to a source of error since the ability to identify different trace fossils at different scales requires knowledge and experience within ichnology. Even experienced ichnologists encounter difficulties with distinguishing trace fossils which are quite similar in terms of ethology and architecture. *Palaeophycus* is in many cases often confused with *Planolites, Ophiomorpha* or *Macaronichnus* (Frey and Howard, 1985; Frey and Howard, 1990). Identifying trace fossils in core is different from outcrop, since the core section displays a 2D view while the outcrop portrays a 3D view, which can be prone to errors. During logging of the wells and at the outcrop the silt content and bioturbation intensity within the different defined lithofacies were totally based on observation, this could also be a source of error. The outcrop was also affected by intense weathering, which limited the ability to identify sedimentary structures and especially trace fossils compared to the core-sections in the wells. Since there were only two wells and one outcrop location studied, this may not be sufficient in terms of representing the sedimentological development of the whole succession. The sample collection is clearly prone to a source of error, since there is no guarantee that they will be representative for the whole succession. Appendix 2 also illustrates the distribution of the different samples within the defined lithofacies, and it shows that the distribution is uneven. The 3D scan done in the Micro-CT is usually not straight forward and requires proper knowledge of the workflow and the associated limitations. Such analysis can be prone to several sources of errors or artefacts; operator dependency, noise, imaging artefacts etc. (Cnudde and Boone, 2013). Thin-section analysis is very sensitive to heterogeneities, which would have a significant effect on the results from the modal, SEM and XRD-analysis. Point counting which is done in the modal analysis would also be prone to a source of error. The grain-sizes in the samples from this study are quite small, and with many of the samples also containing high amounts of either matrix or cement, there is of course a chance that some grains are counted wrong or even not taken into consideration. The thin-sections made from the samples taken within well BH-9-2006 were epoxy colored to highlight available pore-space. There is of course a chance that some of the pores were not filled with the contrasting blue color and was skipped during point counting.

7 Conclusion

The Grumantbyen Formation has remained poorly understood due to its high bioturbation intensity and lack of physical sedimentary structures throughout the whole succession. The two wells and the outcrop studied in this thesis shows that the formation is thinning in a southern direction, with sediments being provided from a source in north-east and prograding in a south-western direction, which is consistent with earlier interpretations of the system (Kellogg, 1975; Steel et al., 1985; Bruhn and Steel, 2003; Simonstad, 2011). The ichnological study of the different wells and outcrop has led to an interpretation of seven different ichnofabrics occurring in the formation (Figure 3.28). The trace fossils are strongly connected to certain depositional environments characterized by certain environmental conditions and oxygen distributed in the sediments. There is a gradual transition between these ichnofabrics, and they are implying a change from a distal to a more proximal environment from the bottom to the top of the succession.

The lithological study has led to an interpretation of five different lithofacies present (Table 4.1). With only few physical sedimentary structures present, the ichnological and lithological observations has had an important value in terms of suggesting a potential depositional environment. The observations of the different lithofacies has led to an interpretation that the succession is gradually coarsening and shallowing upward from an offshore deposited sandy siltstone towards an upper shoreface very fine/fine to medium-grained light silty sandstone. The environment of deposition is moving from being under the storm-wave base to above the fair-weather wave base, which is supported by a gradual increase in physical sedimentary structures present in the lithofacies as well as a decrease in silt content. Trace fossil appearance also supports a change in the environment of deposition connected to energy levels by seeing less mud-incorporating organisms and more grain sorting behavior. Lithofacies F.5 is a gravel layer appearing erosional on top of the upper shoreface interpreted Lithofacies F.4, and is strongly associated with the major flooding of the Grumantbyen Formation and deposition of the superimposed Frysjaodden Formation. The gravel layer has in this study been interpreted to be a transgressive lag.

The textural and modal analysis from the petrography chapter supports the interpretations from the lithological study by presenting results illustrating a gradual increase in grain-size, better sorting, roundness, shape of the grains and a decrease in matrix content from Lithofacies F.1 towards F.4. The results imply that the energy conditions are getting higher as a result of a gradual shallowing upward trend in the succession. The appearance of authigenic glauconite in the formation in combination with high bioturbation intensity, lack of physical sedimentary structures and sandy input have troubled the

minds of those who have previously studied the formation. The combination of these different factors has in this study been interpreted to represent a shoreline-attached system building out in a seaward direction with very little sediment input. Low, but still continuous sediment input implies that there must have been changes in subsidence and/or relative sea level, in order to have glauconization and progradation. The noticed gradual coarsening upward trend from Lithofacies F.1 to F.4 probably suggests that the low sediment influx must have been slightly greater than the available accommodation space. Glauconization is dependent on time to form in condition with minimal sediment influx, referring this to the bioturbation intensity seen in the formation, this means that the buildup and progradation of the Grumantbyen Formation must have been a slow process based on the balance between available accommodation space and sediment influx.

The observations in this study, points to a shoreline-attached shallow-marine depositional environment, possibly as a part of a slightly prograding shoreface system (Figure 6.1). The shoreface has probably been feed by one or several deltas, which brought low, but continuous sediments into the system from north-east. The shoreface possibly prograded in a south-western direction due to the thinning of the succession seen in this part of the basin. The low rates of sediment influx must have created unique conditions for organisms to thrive, causing the high degree of bioturbation seen throughout the Grumantbyen Formation.

The reservoir quality of the formation is a clear result of many different processes/agents. Matrix, cementation, compaction and uplift are the most important factors which have had a significant effect on the porosity distribution. Both primary and secondary porosity is observed in the formation. Before burial, bioturbation and matrix content probably had the greatest impact, while during burial diagenetic processes created cement, and also compaction played a role based on the matrix and framework constituents of the lithology. Later uplift caused alteration and dissolution of the different constituent leading to possible secondary porosity. The amount of matrix, cement and degree of compaction has had a negative impact on the reservoir quality leading to substantial loss of pore-space. Figure 6.2 illustrates that the reservoir quality potentially was good before significant burial, with well communication in the pore-network as a result of the grain-sorting behavior of organisms bioturbating the substrate. Unfortunately as a result of significant burial, diagenetic cementation and compaction has led to a relatively poor reservoir quality of the Grumantbyen Formation.

8 References

AAGAARD, P., JAHREN, J., HARSTAD, A. O., NILSEN, O. & RAMM, M. 2000. Formation of grain-coating chlorite in sandstones; laboratory synthesized vs. natural occurrences. *Clay Minerals,* 35**,** 261-269.

BANIAK, G. M., GINGRAS, M. K., BURNS, B. A. & PEMBERTON, S. G. 2015. Petrophysical Characterization of Bioturbated Sandstone Reservoir Facies in the Upper Jurassic Ula Formation, Norwegian North Sea, Europe. *Journal of Sedimentary Research,* 85**,** 62-81.

BANIAK, G. M., GINGRAS, M. K. & PEMBERTON, S. G. 2013. Reservoir characterization of burrow-associated dolomites in the Upper Devonian Wabamun Group, Pine Creek gas field, central Alberta, Canada. *Marine and Petroleum Geology,* 48**,** 275-292.

BELAÚSTEGUI, Z. & DE GIBERT, J. M. 2013. Bow-shaped, concentrically laminated polychaete burrows: A *Cylindrichnus concentricus* ichnofabric from the Miocene of Tarragona, NE Spain. *Palaeogeography, Palaeoclimatology, Palaeoecology,* 381**,** 119-127.

BERNER, R. A. 1980. *Early diagenesis: A Theoretical Approach,* Princeton, NJ, Princeton University Press.

BJØRKUM, P. A. & WALDERHAUG, O. 1990. Geometrical arrangement of calcite cementation within shallow marine sandstones. *Earth sandstone reviews,* 29**,** 145-161.

BJØRLYKKE, K., RAMM, M. & SAIGAL, G. C. 1989. Sandstone diagenesis and porosity modification during basin evolution. *Geologische Rundschau,* 78**,** 243-268.

BOWEN, N. L. 1922. The reaction principle in petrogenesis. *The Journal of Geology,* 30**,** 177-198.

BROMELY, R. G. 1990. Trace fossils, Biology and Taphonomy. *Unwin Hyman, London***,** (280 pp.).

BROMLEY, R. G., MILAN, J., UCHMAN, A. & HANSEN, K. S. 2009. Rheotactic *Macaronichnus*, and human and cattle trackways in Holocene beachrock, Greece: reconstruction of paleoshoreline orientation. *Ichnos,* 16**,** 103-117.

BRUHN, R. & STEEL, R. J. 2003. High-resolution sequence stratigraphy of a clastic foredeep succession (Paleocene, Spitsbergen): An example of peripheral-bulge-controlled depositional architecture. *Journal of Sedimentary Research,* 73**,** 745-755.

CAROZZI, A. V. 1993. *Sedimentary petrography,* Englewood Cliffs, NJ, PTR Prentice Hall.

CLIFTON, H. E. & THOMPSON, J. K. 1978. *Macaronichnus segregatis*: a feeding structure of shallow marine polychaetes. *Journal of Sedimentary Research,* 48.

CNUDDE, V. & BOONE, M. N. 2013. High-resolution X-ray computed tomography in geosciences: A review of the current technology and applications. *Earth-Science Reviews,* 123**,** 1-17.

CRIMES, T. P., GOLDRING, R., HOMEWOOD, P., VAN STUIJVENBERG, J. & WINKLER, W. 1981. Trace fossil assemblages of deep-sea fan deposits, Gurnigel and Schlieren flysch (Cretaceous-Eocene), Switzerland. *Eclogae Geologicae Helvetiae,* 74**,** 953-995.

CURTIS, C. D. 1980. Diagenetic alteration in black shales. *Journal of the Geological Society,* 137**,** 189-194.

DALLAND, A. 1977. Erratic clasts in the lower Tertiary deposits of Svalbard—evidence of transport by winter ice. *Norsk Polarinstitutt Årbok 1976***,** 151-165.

DALLMANN, W. K. 1999. *Lithostratigraphic lexicon of Svalbard. Upper Paleozoic to Quaternary bedrock. Review and recommendations for nomenclature use.,* Tromsø, Committee on Stratigraphy of Svalbard/Norwegian Polar Institute, Polar Environmental Centre.

DALLMANN, W. K., OHTA, Y., ELVEVOLD, S. & BLOMEIER, D. 2002. *Bedrock map of Svalbard and Jan Mayen*, 1:750,000. Tromsø: Norsk Polar Institutt.

DICKINSON, W. R. 1970. Interpreting detrital modes of graywacke and arkose. *Journal of Sedimentary Petrology,* 40**,** 695-707.

DOTT, R. H. 1964. Wacke, Graywacke and Matrix-What Approach to Immature Sandstone Classification? *Journal of sedimentary petrology,* 40**,** 625-632.

EHRENBERG, S. N. 1993. Preservation of anomalously high porosity in deeply buried sandstones by grain-coating chlorite: examples from the Norwegian continental shelf. *American Association of Petroleum Geologists Bulletin,* 77**,** 1260-1286.

EKDALE, A. A. 1992. Trace fossils and trolls: Report of the first international ichnofabric workshop in Norway. *Palaios,* 7**,** 333-334.

EKDALE, A. A., BROMLEY, R. G. & PEMBERTON, S. G. 1984. Ichnology: Trace Fossils in Sedimentology and Stratigraphy. *Society of Economical Paleontologists and Mineralogists***,** 317.

EKDALE, A. A. & HARDING, S. C. *Cylindrichnus concentricus* Toots in Howard, 1966 (trace fossil) in its type locality, Upper Cretaceous, Wyoming. Annales Societatis Geologorum Poloniae, 2015. Annales Societatis Geologorum Poloniae, 427-432.

FISHER, I. S. J. & HUDSON, J. D. 1987. Pyrite formation in Jurassic shales of contrasting biofacies. *Geological Society, London, Special Publications,* 26**,** 69-78.

FREY, R. W. & BROMLEY, R. G. 1985. Ichnology of American chalks: the Selma Group (Upper Cretaceous), western Alabama. *Canadian Journal of Earth Sciences,* 22**,** 801-828.

FREY, R. W. & HOWARD, J. D. 1981. *Conichnus* and *Schaubcylindrichnus*: redefined trace fossils from the Upper Cretaceous of the Western Interior. *Journal of Paleontology***,** 800-804.

FREY, R. W. & HOWARD, J. D. 1985. Trace fossils from the Panther Member, Star Point Formation (Upper Cretaceous), Coal Creek Canyon, Utah. *Journal of Paleontology***,** 370-404.

FREY, R. W. & HOWARD, J. D. 1990. Trace fossils and depositional sequences in a clastic shelf setting, Upper Cretaceous of Utah. *Journal of Paleontology***,** 803-820.

FREY, R. W. & PEMBERTON, S. G. 1984. Trace fossils facies models: *in* Walker, R.G., ed., Facies Models: Geoscience Canada Reprint Series, no. 1, 2nd ed.: Geological Association of Canada, Toronto. 189-207.

FREY, R. W. & PEMBERTON, S. G. 1991. The ichnogenus *Schaubcylindrichnus*: morphological, temporal, and environmental significance. *Geological Magazine,* 128**,** 595-602.

GJELBERG, J. & STEEL, R. 1997. Grumantbyen Formation - Unpublished Work.

GORDON, J. B., PEMBERTON, S. G., GINGRAS, M. K. & KONHAUSER, K. O. 2010. Biogenically enhanced permeability: A petrographic analysis of Macaronichnus segregatus in the Lower Cretaceous Bluesky Formation, Alberta, Canada. *AAPG bulletin,* 94**,** 1779-1795.

HALL, J. 1847. *Palaeontology of New York; Containing Descriptions of the Organic Remains of the Lower Division of the New-York System (Equivalent of the Lower Silurian Rocks of Europe),* Albany, N.Y., C. van Benthuysen.

HARDING, S. C. 2014. *Ichnology, mineralogy, and paleoenvironmental implications of the verdine and glaucony facies in sedimentary rocks.* The University of Utah.

HARLAND, W. B. 1969. Contribution of Spitsbergen to understanding of tectonic evolution of North Atlantic Region. *In:* KAY, M. (ed.) *North Atlantic - geology and continental drift.* American Association of Petroleum Geologists Mem.

HARLAND, W. B., ANDERSON, L. M., MANASRAH, D., BUTTERFIELD, N. J., CHALLINOR, A., DOUBLEDAY, P. A., DOWDESWELL, E. K., DOWDESWELL, J. A., GEDDES, I. & KELLY, S. R. A. 1997. The geology of Svalbard. *Geological Society, London, Memoir,* 17**,** 521.

HELLAND-HANSEN, W. 1985. Sedimentology of the Battfjellet Formation (Palaeogene) in Nordenskiöld Land, Spitsbergen. *Unpublished Candidatus Scientarium thesis.* University of Bergen, Norway.

HELLAND-HANSEN, W. 1990. Sedimentation in Paleogene Foreland Basin, Spitsbergen. *American Association of Petroleum Geologists Bulletin,* 74**,** 260-272.

HELLAND-HANSEN, W. 2010. Facies and stacking patterns of shelf-deltas within the Palaeogene Battfjellet Formation, Nordenskiöld Land, Svalbard: implications for subsurface reservoir prediction. *Sedimentology,* 57**,** 190-208.

HENDRY, J. P., TREWIN, N. H. & FALLICK, A. E. 1996. Low-Mg calcite marine cement in Cretaceous turbidites: origin, spatial distribution and relationship to sea-water chemistry. *Sedimentology,* 43**,** 877-900.

HOFFMAN, J. & HOWER, J. 1979. Clay mineral assemblages as low grade metamorphic geothermometers: application to the thrust faulted disturbed belt of Montana, U.S.A. *In:* SCHOLLE, P. A. & SCHLUGER, P. R. (eds.) *Aspects of diagenesis.* Society og Economic Paleontologists and Mineralogists, Special Publication.

HOUSEKNECHT, D. W. 1984. Influence of grain size and temperature on intergranular pressure dissolution, quartz cementation and porosity in a quartzose sandstone. *Journal of Sedimentary Petrology,* 54**,** 348-361.

HOWARD, J. D. 1966. Characteristic trace fossils in Upper Cretaceous sandstones of the Book Cliffs and Wasatch Plateau. *Utah Geological and Mineralogical Survey Bulletin***,** 35-53.

HOWER, J., ESLINGER, E. V., HOWER, M. E. & PERRY, E. A. 1976. Mechanism of burial metamorphism of argillaceous sediment, I. Mineralogical and chemical evidence. *Geological Society of America Bulletin,* 87**,** 725-737.

HUBBARD, S. M., MACEACHERN, J. A. & BANN, K. L. 2012. Chapter 20 - Slopes. *In:* KNAUST, D. & BROMLEY, R. G. (eds.) *Developments in Sedimentology.* Elsevier.

JOHANNESSEN, E. P. & STEEL, R. J. 2005. Shelf-margin clinoforms and prediction of deepwater sands. *Basin Research,* 17**,** 521-550.

JOHNSEN, S. O., MØRK, A., DYPVIK, H. & NAGY, J. Outline of the geology of Svalbard. Short geological review and guidebook. 7th ESF IMPACT Workshop, 2001. 11.

JOHNSON, H. D. & BALDWIN, C. T. 1996. I: Sedimentary Environments: Processes, Facies and Stratigraphy. *In:* READING, H. G. (ed.) *Shallow clastic seas.* Oxford: Blackwell Science.

KELLOGG, H. E. 1975. Tertiary Stratigraphy and Tectonism in Svalbard and Continental-Drift. *Aapg Bulletin-American Association of Petroleum Geologists,* 59**,** 465-485.

KIKUCHI, K., KOTAKE, N. & FURUKAWA, N. 2016. Mechanism and process of construction of tubes of the trace fossil *Schaubcylindrichnus coronus* Frey and Howard, 1981. *Palaeogeography, Palaeoclimatology, Palaeoecology,* 443**,** 1-9.

KNAUST, D. 2007. Meiobenthic trace fossils as keys to the taphonomic history of shallow-marine epicontinental carbonates. *Trace Fossils: Concepts, Problems, Prospects: Elsevier, Arcata, California***,** 502-517.

KNAUST, D. 2009. Meiobenthic trace fossils comprising a miniature ichnofabric from Late Permian carbonates of the Oman Mountains. *Palaeogeography, Palaeoclimatology, Palaeoecology,* 286**,** 81-87.

KNAUST, D. 2014. Classification of bioturbation-related reservoir quality in the Khuff Formation (Middle East): towards a genetic approach. *Permo-Triassic Sequence of the Arabian Plate. EAGE, Amsterdam***,** 247-267.

LA CROIX, A. D., GINGRAS, M. K., PEMBERTON, S. G., MENDOZA, C. A., MACEACHERN, J. A. & LEMISKI, R. T. 2013. Biogenically enhanced reservoir properties in the Medicine Hat gas field, Alberta, Canada. *Marine and Petroleum Geology,* 43**,** 464-477.

LIVSIC, J. J. 1967. Tertiary deposits in Western part of the Archipelago of Svalbard. *The British Library, Lending Division*, 1977. *In:* DALLMANN, W. K. (ed.) *1999: Lithostatigraphic Lexicon of Svalbard, Norsk Polarinstitutt, 320 p.*

LOVE, L. G. 1967. Early diagenetic iron sulphide in recent sediments of the Wash (England). *Sedimentology,* 9**,** 327-352.

LÖWEMARK, L. & NARA, M. 2010. Morphology, ethology and taxonomy of the ichnogenus *Schaubcylindrichnus*: Notes for clarification. *Palaeogeography, Palaeoclimatology, Palaeoecology,* 297**,** 184-187.

MACEACHERN, J. A. & BANN, K. L. 2008. The role of ichnology in refining shallow marine facies models. *Recent Advances in Models of siliciclastic shallow-marine stratigraphy: SEPM, Special Publication,* 90**,** 73-116.

MACEACHERN, J. A., BANN, K. L., PEMBERTON, S. G. & GINGRAS, M. K. 2007. The ichnofacies paradigm: high-resolution paleoenvironmental interpretation of the rock record. *SEPM SHORT COURSE,* 52**,** 27.

MACLEAY, W. S. 1839. Note on the Annelida *In:* MURCHISON, R. (ed.) *The Silurian System, Part. II, Organic Remains. .* J. Murray, London.

MAJOR, H. & NAGY, J. 1964. *Adventdalen: Geological map.* Norsk Polarinstitutt.

MANUM, S. B. & THRONDSEN, T. 1986. Age of Tertiary formations on Spitsbergen. *Polar Research,* 4**,** 103-131.

MOZLEY, P. S. 1989. Relation between depositional environment and the elemental composition of early diagenetic siderite. *Geology,* 17**,** 704-706.

NARA, M. 2006. Reappraisal of *Schaubcylindrichnus*: A probable dwelling/feeding structure of a solitary funnel feeder. *Palaeogeography, Palaeoclimatology, Palaeoecology,* 240**,** 439-452.

NATHORST, A. G. 1910. *Beiträge zur Geologie der Bären-Insel, Spitzbergens und des König-Karl-Landes. , Bulletin Geologiske Institionen Uppsala Universitet*.

NEMEC, W. Shorface succession resulting from shoreline progradation (normal regression). *Presentation - Sedimentology course (GEOV360).* University of Bergen, Spring 2015.

NYSÆTHER, E. 1966. Petrografisk undersøkelse av sedimentære bergarter fra tidsperioden kritt - tertiær i Nathorst land, Vest Spitsbergen, Hovedoppgave i mineralogi og petrografi. *Geologisk Institutt, Universitetet i Bergen*.

ODIN, G. S. 1988. *Green Marine Clays: Oolitic Ironstone Facies, Verdine Facies, Glaucony Facies and Celadonite-Bearing Facies-A Comparative Study,* Amsterdam, Elsevier.

ODIN, G. S. & MATTER, A. 1981. De glauconiarum origine. *Sedimentology,* 28**,** 611-641.

PAXTON, S. T., SZABO, J. O., AJDUKIEWICZ, J. M. & KLIMENTIDIS, R. E. 2002. Construction of an intergranular volume compaction curve for evaluating and predicting compaction and porosity loss in rigid-grain sandstone reservoirs. *American Association of Petroleum Geologist Bulletin,* 86**,** 2047-2067.

PEMBERTON, S. G. & FREY, R. W. 1982. Trace fossil nomenclature and the *Planolites-Palaeophycus* dilemma. *Journal of Paleontology,* 56**,** 843-881.

PEMBERTON, S. G. & GINGRAS, M. K. 2005. Classification and characterizations of biogenically enhanced permeability. *American Association of Petroleum Geologists Bulletin,* 89**,** 1493-1517.

PEMBERTON, S. G. & MACEACHERN, J. A. 1992. Trace fossil facies models: environmental and allostratigraphic significance. *Facies models: response to sea level change***,** 47-72.

PEMBERTON, S. G., MACEACHERN, J. A., DASHTGARD, S. E., BANN, K. L., GINGRAS, M. K. & ZONNEVELD, J. P. 2012. Chapter 19 - Shorefaces. *In:* KNAUST, D. & BROMLEY, R. G. (eds.) *Developments in Sedimentology.* Elsevier.

PEMBERTON, S. G., SPILA, M., PULHAM, A. J., SAUNDERS, T., MACEACHERN, J. A., ROBBINS, D. & SINCLAIR, I. K. 2001. Ichnology and sedimentology of shallow to marginal marine systems: Ben Nevis and Avalon Rerservoirs, Jeanne D'Arc Basin. *Geological Association of Canada, Short Course Notes,* 1**,** 343.

PERVESLER, P., UCHMAN, A. & HOHENEGGER, J. 2008. New methods for ichnofabric analysis and correlation with orbital cycles exemplified by the Baden-Sooss section (Middle Miocene, Vienna Basin). *Geologica Carpathica,* 59**,** 395-409.

PETTIJOHN, F. J., POTTER, P. E. & SIEVER, R. 1972. Sand and sandstone. Springer-Verlag, New York.

PRYOR, W. A. 1975. Biogenic sedimentation and alteration of argillaceous sediments in shallow marine environments. *Geological Society of America Bulletin,* 86**,** 1244-1254.

RAISWELL, R. & BERNER, R. A. 1986. Pyrite and organic matter in Phanerozoic normal marine shales. *Geochimica et Cosmochimica Acta,* 50**,** 1967-1976.

RAMBERG, I. B., BRYHNI, I., NØTTVEDT, A. & RANGNES, K. 2008. *The making of a land: Geology of Norway*, The Norwegian Geological Association, Oslo.

REINECK, H. E. 1963. Sedimentgefüge im Bereich der südlichen Nordsee.

REINSON, G. E. 1984. Barrier-island and associated strand-plain systems. *Facies models.* Geological Ass., Canada.

RICHTER, R. 1936. Marken und Spruren im Hunsrück-Schiefer. II. *Schichtung und Grund-leben. Senckenbergiana,* 18**,** 215-244.

SCHLEGEL, A., LISKER, F., DÖRR, N., JOCHMANN, M., SCHUBERT, K. & SPIEGEL, C. 2013. Petrography and geochemistry of siliciclastic rocks from the Central Tertiary Basin of Svalbard – implications for provenance, tectonic setting and climate *Zeitschrift der Deutschen Gesellschaft für Geowissenschaften,* 164**,** 173-186.

SEIKE, K. 2007. Palaeoenvironmental and palaeogeographical implications of modern *Macaronichnus segregatis*-like traces in foreshore sediments on the Pacific coast of central Japan. *Palaeogeography, Palaeoclimatology, Palaeoecology,* 252**,** 497-502.

SEIKE, K., YANAGISHIMA, S., NARA, M. & SASAKI, T. 2011. Large *Macaronichnus* in modern shoreface sediments: Identification of the producer, the mode of formation, and

paleoenvironmental implications. *Palaeogeography Palaeoclimatology Palaeoecology,* 311**,** 224-229.

SEILACHER, A. 1955. Spuren und Fazies im Unterkambrium. *In:* SCHINDERWOLF, O. H. & SEILACHER, A. (eds.) *Beiträge zur Kenntnis des Kambriums in der Salt Range (Pakistan).* Akad. Wiss. Liter. Mainz Abhandl. Math. -Nat. Kl.

SEILACHER, A. 1967. Bathymetry of trace fossils. *Marine geology,* 5**,** 413-428.

SHELLEY, D. 1992. *Igneous and Metamorphic Rocks under the Microscope*, Springer Netherlands.

SIMONSTAD, E. 2011. *Paleogeografi og avsetningsmiljø, Grumantbyenformasjonen (paleocen), Svalbard.* University of Bergen & The University Centre in Svalbard.

STEEL, R. J. 1977. Observations on some Cretaceous and Tertiary sandstone bodies in Nordenskiold Land, Svalbard. *Nor. Polarinst. Årbok 1976***,** 43-68.

STEEL, R. J., DALLAND, A., KALGRAFF, K. & LARSEN, V. 1981. The Central Tertiary Basin of Spitsbergen: sedimentary development of a sheared-margin basin.

STEEL, R. J., GJELBERG, J., HELLAND-HANSEN, W., KLEINSPEHN, K., NØTTVEDT, A. & LARSEN, M. R. 1985. The Tertiary strike-slip basins and orogenic belt of Spitsbergen. *Society of Economical Paleontologists and Mineralogists* Special publication 37**,** 339-359.

TALWANI, M. & ELDHOLM, O. 1977. Evolution of the Norwegian-Greenland sea. *Geological Association of America Bulletin,* 88**,** 969-999.

TAYLOR, A. M. & GOLDRING, R. 1993. Description and Analysis of Bioturbation and Ichnofabric. *Journal of the Geological Society,* 150**,** 141-148.

UCHMAN, A., JOHNSON, M. E., REBELO, A. C., MELO, C., CORDEIRO, R., RAMALHO, R. S. & ÁVILA, S. P. 2016. Vertically-oriented trace fossil *Macaronichnus segregatis* from Neogene of Santa Maria Island (Azores; NE Atlantic) records vertical fluctuations of the coastal groundwater mixing zone on a small oceanic island. *Geobios*.

VILBERG, A. K. 2011. *Petrography and sedimentology of Paleogene formations from Nathorstland, Spitsbergen: A diagenetic study of sedimentary facies associations.* Norges teknisk-naturvitenskapelige universitet, Fakultet for ingeniørvitenskap og teknologi, Institutt for geologi og bergteknikk.

WARREN, E. A. & CURTIS, C. D. 1989. The chemical composition of authigenetic illite within two sandstone reservoirs as analysed by ATEM. *Clay Minerals,* 24**,** 137-156.

WETZEL, A. 2002. Modern *Nereites* in the South China Sea—ecological association with redox conditions in the sediment. *Palaios,* 17**,** 507-515.

WIGHTMAN, D. M., PEMBERTON, S. G. & SINGH, C. 1987. Depositional Modelling of the Upper Mannville (Lower Cretaceous), East Central Alberta: Implications for the Recognition of Brackish Water Deposits. *The society of Economic Paleontologists and Mineralogists (SEPM)*.

WORDEN, R. H. & BURLEY, S. D. 2003. Sandstone diagenesis: the evolution of sand to stone. *In:* BURLEY, S. D. & WORDEN, R. H. (eds.) *Sandstone Diagenesis: Recent and Ancient.* International Association of Sedimentologists, Blackwell publishing.

WORSLEY, D. 2008. The post-Caledonian development of Svalbard and the western Barents Sea. *Polar Research,* 27**,** 298-317.

9 Appendix

Appendix 1: *A graphical visualization of the different ichnofabrics present within four defined lithofacies (F.1-F.4) in the outcrop (Bolterdalen) and the two wells studied. The different ichnofabrics are arranged vertically in alphabetical order from bottom to top.*

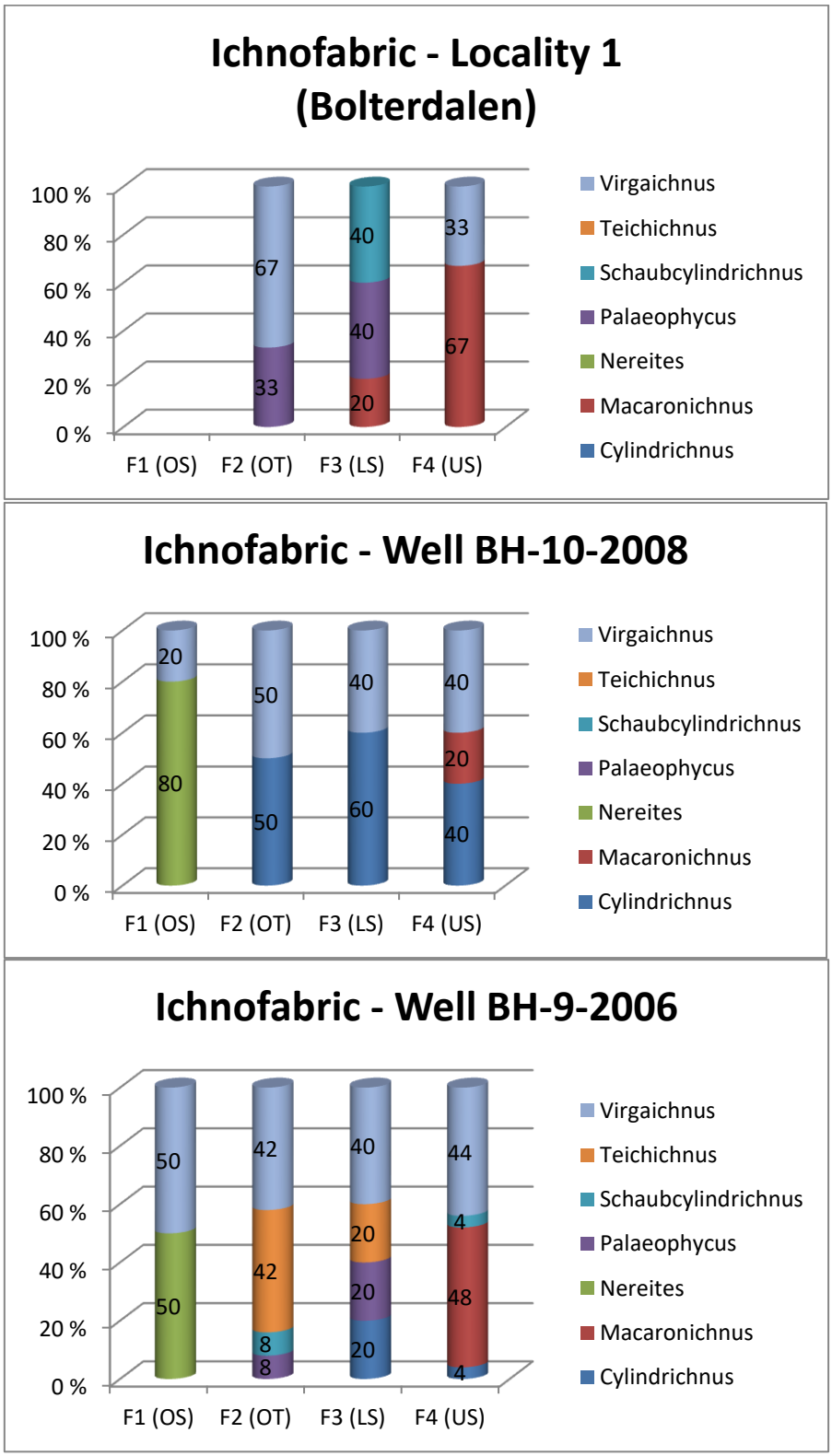

Appendix 2: *A calculated mean percentage of the 21 samples studied and their arrangement between the different associated lithofacies (F.1-F.4).*

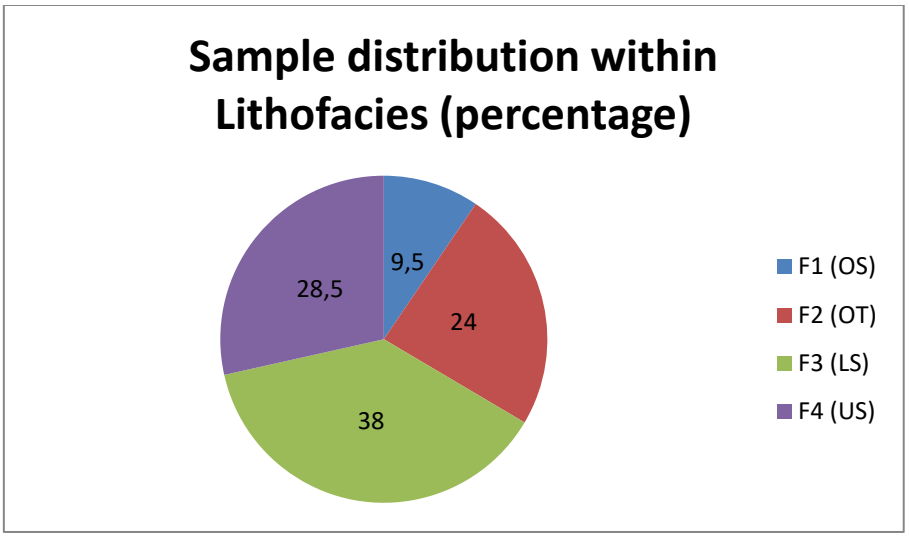

Appendix 3: *Samples from Locality 1, Bolterdalen. Samples are arranged in order from bottom to top of the logged section at the outcrop, and are based on core observations and lithofacies descriptions.*

Sample/Interval	Lithofacies	Ichnofabric	Description from log	Palaeoenvironment
1.1 (3.0 m-log)	F.3	*Palaeophycus-Schaubcylindrichnus*	Very fine-grained, medium gray-color, moderately silty sandstone. Completely bioturbated (BI=6 – 100 %).	Lower shoreface
1.2 (12.0 m-log)	F.3	*Palaeophycus-Schaubcylindrichnus*	Silt/very fine-grained, medium gray-color, moderately silty sandstone. Completely bioturbated (BI=6 – 100 %).	Lower shoreface
1.3 (19.0 m-log)	F.3	*Palaeophycus-Schaubcylindrichnus*	Very fine-grained, medium gray-color, moderately silty sandstone. Completely bioturbated (BI=6 – 100 %).	Lower shoreface
1.4 (34.0 m-log)	F.3	*Palaeophycus-Schaubcylindrichnus*	Very fine-grained, medium gray-color, moderately silty sandstone. Pebbly rock fragments of chert and quartzite are abundant in the sample. Completely bioturbated (BI=6 – 100 %).	Lower shoreface
1.5 (54.0 m-log)	F.2	*Virgaichnus*	Very fine-grained, dark gray-color, silty sandstone. Completely bioturbated (BI=6 – 100 %).	Offshore transition
1.6 (60.0 m-log)	F.3	*Palaeophycus-Schaubcylindrichnus*	Very fine-grained, medium gray-color, moderately silty sandstone. Completely bioturbated (BI=6 – 100 %).	Lower shoreface
1.7 (65.0 m-log)	F.3	*Macaronichnus-*	Very fine-grained, medium gray-	Lower shoreface

		Schaubcylindrichnus	color, moderately silty sandstone. Completely bioturbated (BI=6 – 100 %).	
1.8 (72.0 m-log)	F.2	*Palaeophycus*	Silt/very fine-grained, dark gray-color, silty sandstone. Completely bioturbated (BI=6 – 100 %).	Offshore transition
1.9 (86.0 m-log)	F.3	*Macaronichnus*	Very fine-grained, medium gray-color, moderately silty sandstone. Completely bioturbated (BI=6 – 100 %)	Lower shoreface
1.10 (95.0 m-log)	F.4	*Virgaichnus-Macaronichnus*	Very fine-grained, yellowish gray-color, light silty sandstone. The sample is split in two types of cement in between the framework, calcite and siderite – dissolution process. Completely bioturbated (BI=6 – 100 %).	Upper shoreface

Appendix 4: *Samples from well BH-9-2006. Samples are arranged in order from bottom to top depth of the core-section, and are based on core observations and lithofacies descriptions.*

Sample/Interval	Lithofacies	Ichnofabric	Description from log	Palaeoenvironment
1 - Depth 394.00-394.15 m	F.2	*Virgaichnus*	Very fine-grained, dark gray-color, silty sandstone. Pebbly rock fragments of chert and quartzite are abundant in the sample. Completely bioturbated (BI=6 – 100 %).	Offshore transition
2 – Depth 386.62-386.82 m	F.1	*Nereites-Virgaichnus*	Very fine-grained, dark-color, sandy siltstone. Pyrite and siderite is abundant in the sample. Completely bioturbated (BI=6 – 100 %).	Offshore
3 – Depth 374.80-375.00 m	F.2	*Palaeophycus-Virgaichnus*	Very fine-grained, dark gray-color, silty sandstone. Completely bioturbated (BI=6 – 100 %).	Offshore transition
4 – Depth 317.45-317.65 m	F.2	*Teichichnus*	Very fine-grained, dark gray-color, silty sandstone. Glauconite and Pebbly rock fragments of chert and quartzite are abundant in the sample. Completely bioturbated (BI=6 – 100 %).	Offshore transition
5 – Depth 314.89-315.00	F.1	*Nereites-Virgaichnus*	Silt/very fine-grained, dark-color, sandy siltstone. Pyrite and siderite is abundant in the sample. Completely bioturbated (BI=6 – 100 %).	Offshore
6 – Depth 288.74-	F.3	*Virgaichnus-*	Very fine-grained, medium gray-	Lower shoreface

288.94		*Cylindrichnus*	color, moderately silty sandstone. Completely bioturbated (BI=6 – 100 %)	
7 – Depth 273.85-274.00	F.4	*Virgaichnus*	Very fine-grained, greenish gray-color, light silty sandstone. Siderite nodules and glauconite is abundant in the sample. Intensely bioturbated (BI=5 – 95 %).	Upper shoreface
8 – Depth 260.70-260.85	F.4	*Macaronichnus-Virgaichnus*	Very fine-grained, greenish gray-color, light silty sandstone. Glauconite is abundant in the sample. Completely bioturbated (BI=6 – 100 %).	Upper shoreface
9 – Depth 227.10-227.25	F.4	*Macaronichnus*	Fine-grained, greenish gray-color, light silty sandstone. Glauconite is abundant. The sample is calcite cemented. Highly bioturbated (BI=4 – 80 %).	Upper shoreface
10 – Depth 176.00-176.20	F.4	*Macaronichnus-Virgaichnus*	Very fine-grained, greenish gray-color, light silty sandstone. Glauconite is abundant in the sample. Completely bioturbated (BI=6 – 100 %).	Upper shoreface
11 – Depth 163.60-163.75	F.4	*Virgaichnus-Macaronichnus*	Very fine-grained, greenish gray-color, light silty sandstone. Glauconite is abundant in the sample. Completely bioturbated (BI=6 – 100 %).	Upper shoreface

Appendix 5: *Textural properties pf samples from Locality 1, Bolterdalen. Samples are arranged in order from bottom to top of the logged section at the outcrop.*

Sample/Interval	Lithofacies	Grain size (mm)	Sorting	Roundness	Shape	Fabric	Palaeoenvironment
1.1 (3.0 m-log)	F.3	0.075 mm – Very fine	Well	Angular	Moderate Sphericity	Grain-supported	Lower shoreface
1.2 (12.0 m-log)	F.3	0.059 mm – Coarse Silt	Well	Angular	Low-Moderate Sphericity	Grain-supported	Lower shoreface
1.3 (19.0 m-log)	F.3	0.078 mm – Very fine	Well	Angular	Moderate Sphericity	Grain-supported	Lower shoreface
1.4 (34.0 m-log)	F.3	0.091 mm – Very fine	Moderately	Sub-angular	Low Sphericity	Grain-supported	Lower shoreface
1.5 (54.0 m-log)	F.2	0.067 mm – Very fine	Well	Angular	Low-Moderate Sphericity	Grain-supported	Offshore transition
1.6 (60.0 m-log)	F.3	0.065 mm – Very fine	Well	Angular	Moderate Sphericity	Grain-supported	Lower shoreface
1.7 (65.0 m-log)	F.3	0.074 mm – Very fine	Moderately	Sub-angular	Low-Moderate Sphericity	Grain-supported	Lower shoreface
1.8 (72.0 m-log)	F.2	0.062 mm – Coarse silt	Well	Sub-angular	Low-Moderate Sphericity	Grain-supported	Offsore transition
1.9 (86.0 m-log)	F.3	0.083 mm – Very fine	Well	Angular	Moderate Sphericity	Grain-supported	Lower shoreface
1.10 (95.0 m-log)	F.4	0.095 mm – Very fine	Very well	Sub-angular	Moderate Sphericity	Grain-supported	Upper shoreface

Appendix 6: *Textural properties of samples from well BH-9-2006. Samples are arranged in order from bottom to top of the logged section of the core.*

Sample/Interval	Lithofacies	Grain size (mm)	Sorting	Roundness	Shape	Fabric	Palaeoenvironment
1 - Depth 394.00-394.15 m	F.2	0.110 mm – Very fine	Well	Angular	Low-Moderate Sphericity	Grain-supported	Offshore transition
2 – Depth 386.62-386.82 m	F.1	0.078 mm – Very fine	Very well	Angular	Low-Moderate Sphericity	Matrix-supported	Offshore
3 – Depth 374.80-375.00 m	F.2	0.075 mm – Very fine	Well	Sub-angular	Low-Moderate Sphericity	Matrix-supported	Offshore transition
4 – Depth 317.45-317.65 m	F.2	0.096 mm – Very fine	Very well	Sub-angular	Moderate Sperhicity	Grain-supported	Offshore transition
5 – Depth 314.89-315.00	F.1	0.061 mm – Coarse silt	Very well	Angular	Low-Moderate Sphericity	Matrix-supported	Offshore
6 – Depth 288.74-288.94	F.3	0.066 mm – Very fine	Well	Angular	Moderate Sphericity	Grain-supported	Lower shoreface
7 – Depth 273.85-274.00	F.4	0.068 mm – Very fine	Very well	Sub-angular	Moderate Sphericity	Grain-supported	Upper shoreface
8 – Depth 260.70-260.85	F.4	0.077 mm – Very fine	Very well	Sub-angular	Moderate Sphericity	Grain-supported	Upper shoreface
9 – Depth 227.10-227.25	F.4	0.169 mm - Fine	Very well	Sub-rounded	Moderate Sphericity	Grain-supported	Upper shoreface
10 – Depth 176.00-176.20	F.4	0.102 mm – Very fine	Very well	Sub-angular	Moderate Sphericity	Grain-supported	Upper shoreface
11 – Depth 163.60-163.75	F.4	0.109 mm – Very fine	Very well	Sub-angular	Moderate Sphericity	Grain-supported	Upper shoreface

Appendix 7: *Modal analysis of samples from Locality 1, Bolterdalen. The analysis is based on point-counting of 300 points within each thin-section through an optical microscope with a 20X10 magnification. X = not observed within sample.*

	Framework constituents							Matrix	Authigenic minerals							Porosity	
Sample	Quartz	Feldspar		Mica	Rock fragm	Heavy minerals	Organics		Silica	Calcite	Siderite	Glauconite	Chlorite	Pyrite	Sericite	Primary	Secondary
		K-feldspar	Plagioclase														
1.1	39.3	2.0	18.3	x	x	x	0.3	28.5	x	x	0.7	2.2	x	x	3.3	4.3	1.1
1.4	37.0	1.7	15.0	0.3	1.7	0.3	x	25.5	1.3	x	x	2.8	0.7	x	5.0	5.3	3.4
1.5	25.0	2.4	19.3	x	1.7	x	x	34.5	1.0	x	0.3	1.0	1.3	x	6.7	6.3	0.5
1.9	41.7	2.7	20.0	x	2.3	x	x	22.5	3.3	x	x	0.2	3.0	x	1.7	2.6	0.1
1.10	43.0	1.4	10.3	x	1.3	0.3	x	4.5	0.3	20.0	5.0	6.3	x	x	0.7	3.7	3.2

Appendix 8: *Modal analysis of samples from well BH-9-2006. The analysis is based on point-counting of 300 points within each thin-section through an optical microscope with a 20X10 magnification. X = not observed within sample.*

	Framework constituents							Matrix	Authigenic minerals							Porosity	
Sample	Quartz	Feldspar		Mica	Rock fragm	Heavy minerals	Organics		Silica	Calcite	Siderite	Glauconite	Chlorite	Pyrite	Sericite	Primary	Secondary
		K-feldspar	Plagioclase														
2	39.3	1.0	6.0	0.3	2.3	0.3	x	40.2	1.3	0.7	0.7	0.2	1.0	0.3	1.4	4.9	0.1
4	41.7	1.3	10.0	x	2.0	x	x	27.6	0.7	x	x	4.5	x	x	3.6	6.3	2.3
5	28.7	1.0	10.3	0.3	2.0	x	x	44.1	1.7	x	1.7	0.8	x	x	2.7	6.3	0.4
6	32.0	2.7	22.0	x	2.0	x	x	26.4	2.0	0.3	x	0.2	6.7	x	2.6	3.0	0.1
8	52.7	1.7	15.0	0.7	1.0	x	x	2.7	1.0	2.7	2.3	0.5	14.3	x	2.9	1.5	1.0

9	51.0	1.3	12.0	x	x	x	x	7.2	1.7	x	4.0	1.7	15.0	x	0.7	2.3	3.1
10	51.7	1.7	14.3	0.3	2.0	1.0	x	9.6	0.3	2.3	0.7	x	9.7	x	1.0	2.1	3.3

Appendix 9: *Matrix content and distribution of framework grains within the samples from Locality 1 (Bolterdalen), and their resulting classification. The values are normalized from the results of the modal analysis.*

Sample	Matrix	Q	F	L	SUM	Classification
1.1	47,5	65,92178771	34,07821229	0	100	Arkosic wacke
1.4	46,42857143	66,86746988	30,12048193	3,012048193	100	Arkosic wacke
1.5	73,44827586	51,72413793	44,82758621	3,448275862	100	Arkosic wacke
1.9	33,75	62,5	34	3,5	100	Arkosic wacke
1.10	7,98816568	76,78571429	20,83333333	2,380952381	100	Subarkose

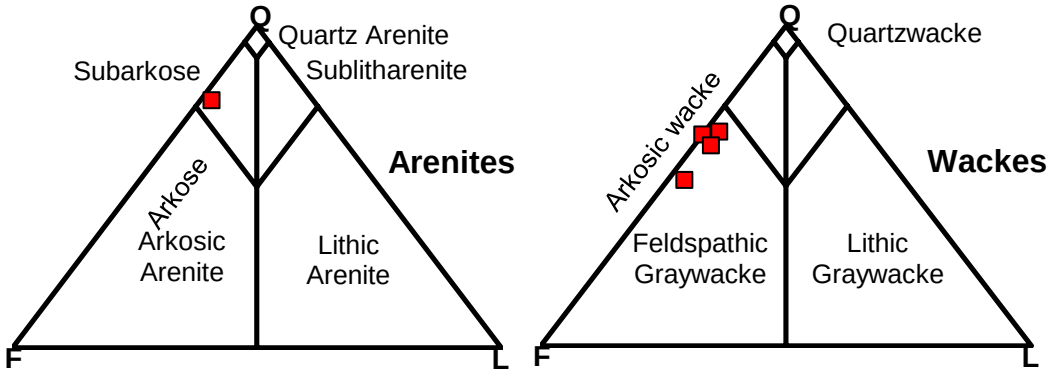

Appendix 10: *Matrix content and distribution of framework grains within the samples from well BH-9-2006, and their resulting classification. The values are normalized from the results of the modal analysis.*

Sample	Matrix	Q	F	L	SUM	Classification
2	81,8243243	80,8219178	14,3835616	4,79452055	100	mudstone
4	51,0909091	75,7575758	20,6060606	3,63636364	100	Arkosic wacke
5	105,354331	68,2539683	26,984127	4,76190476	100	mudstone
6	45	54,5454545	42,0454545	3,40909091	100	Arkosic wacke
8	4,50704225	74,8815166	23,6966825	1,42180095	100	Subarkose
9	11,7098446	79,2746114	20,7253886	0	100	Subarkose
10	14,2253521	74,1626794	22,9665072	2,8708134	100	Subarkose

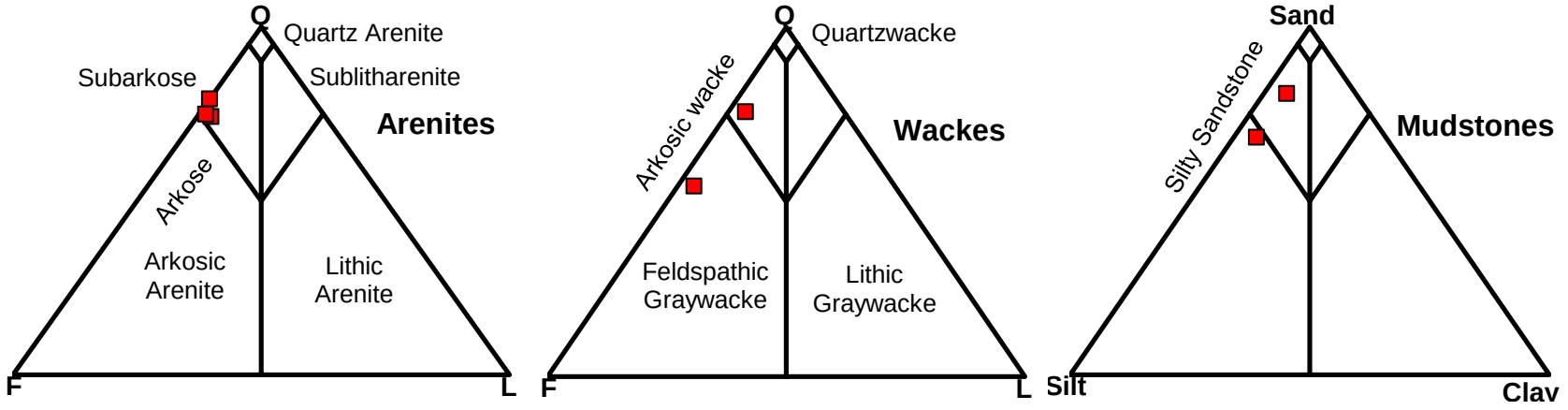

Chapter 9
Appendix

Lithologies

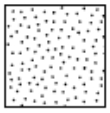
Sandstone


Matrix-supported conglomerate


Siltstone


Fine ash

Trace fossils


Cylindrichnus

Macaronichnus


Nereites


Palaeophycus


Scaubcylindrichnus

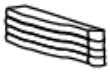
Teichichnus


Virgaichnus

Symbols


Nodules and concretions


Intraclasts


Wave ripple cross-lamination


Mudclasts


Horizontal planar lamination


Trough cross bedding


Hummocky cross stratification


Micro fault

Py Pyrite

Base Boundaries

Gradational

Sharp

Erosion

Color Code

N2 - Grayish Black

N4 - Medium Dark Gray

N5 - Medium Gray

5GY 4/1 - Dark Greenish Gray

10G 6/2 - Pale Green

5G 6/1 - Greenish Gray

5Y 8/1 - Yellowish Gray

Ichnofacies

Nereites

Cruziana

Skolithos

Chapter 9
Appendix

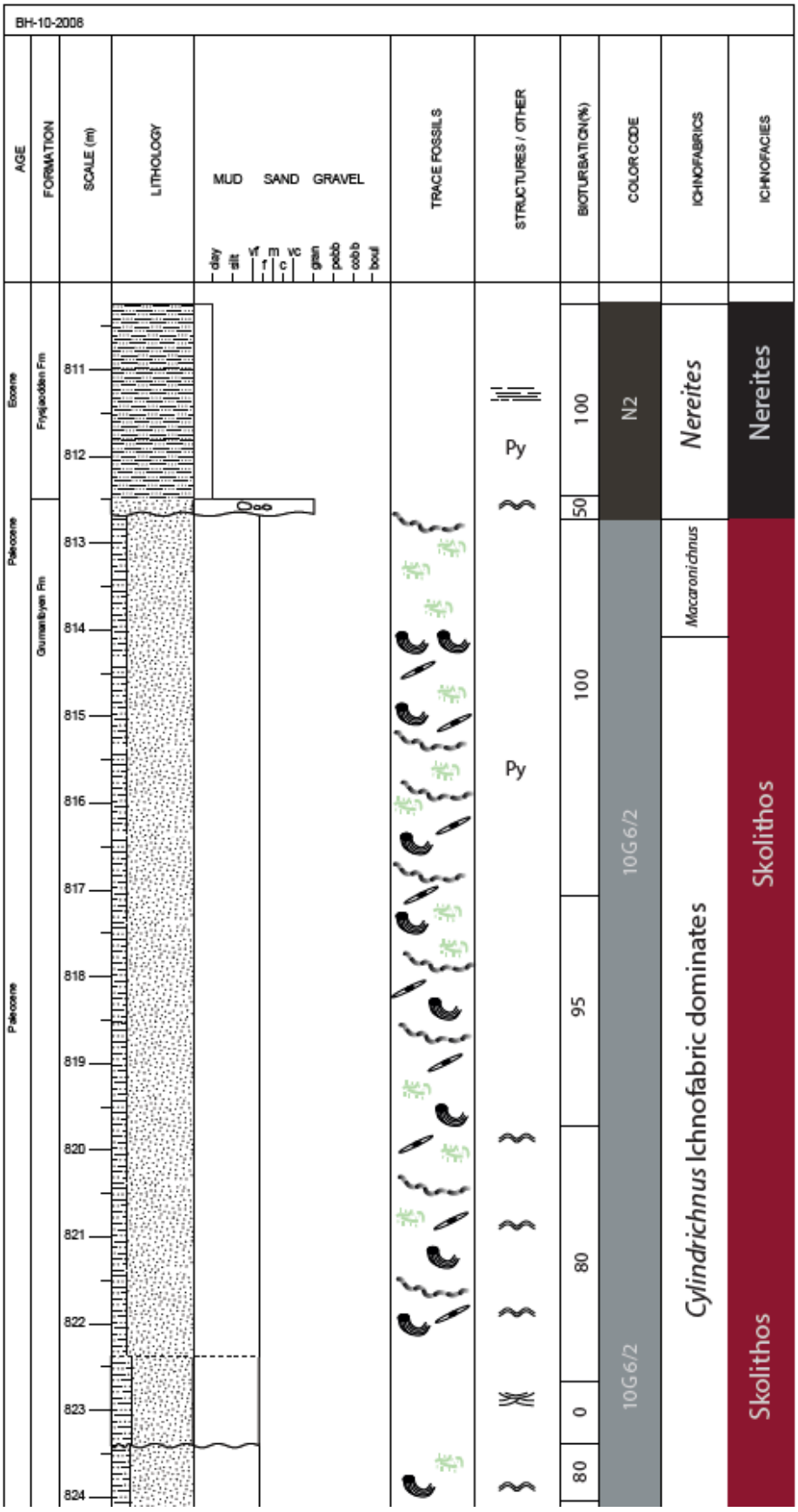

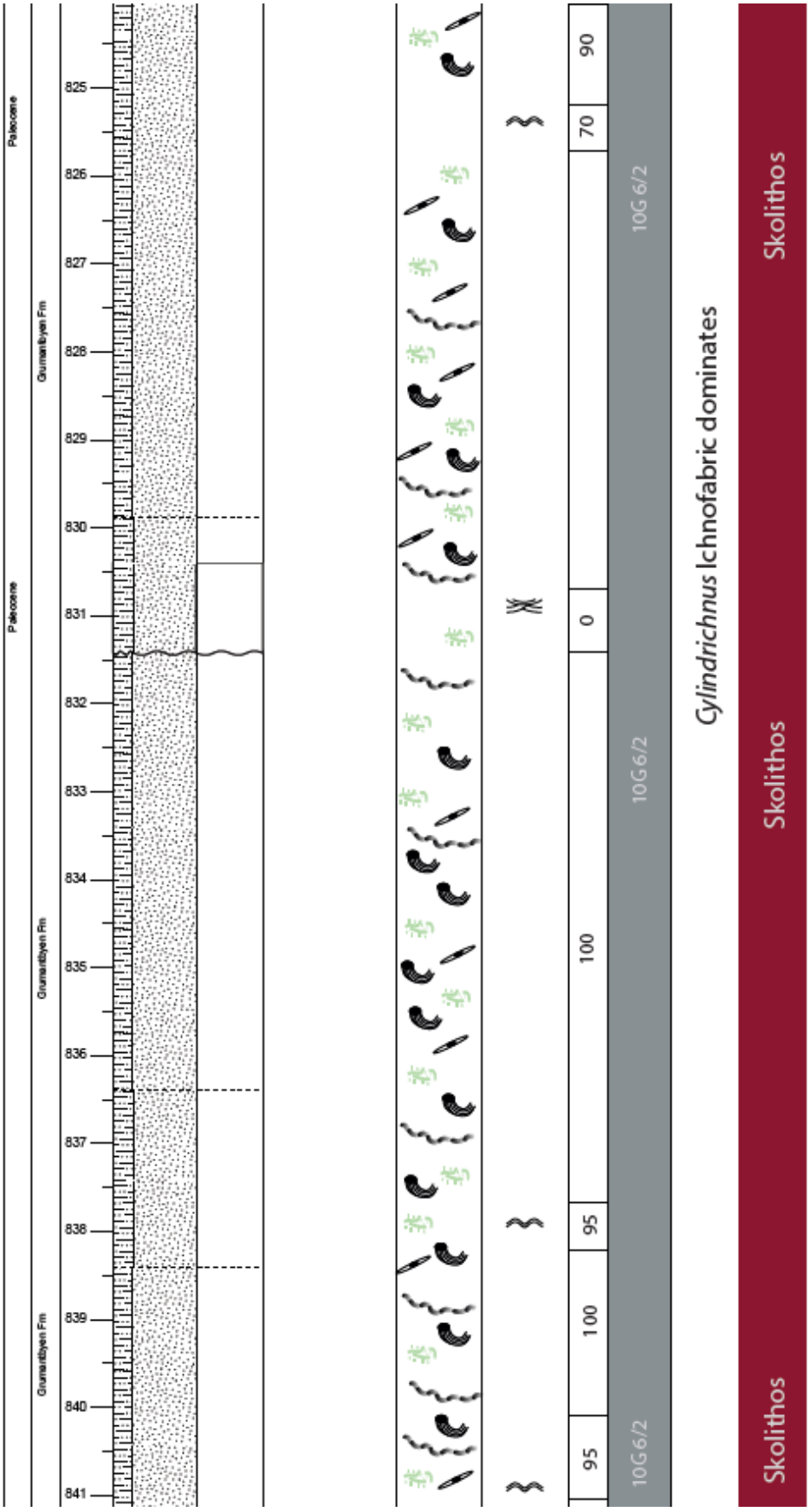
Paleocene
Grumantbyen Fm
825
826
827
828
829
830
831
832
833
834
835
836
837
838
839
840
841
95
100
95
100
0
70
90
10G 6/2
10G 6/2
10G 6/2
Cylindrichnus Ichnofabric dominates
Skolithos
Skolithos
Skolithos

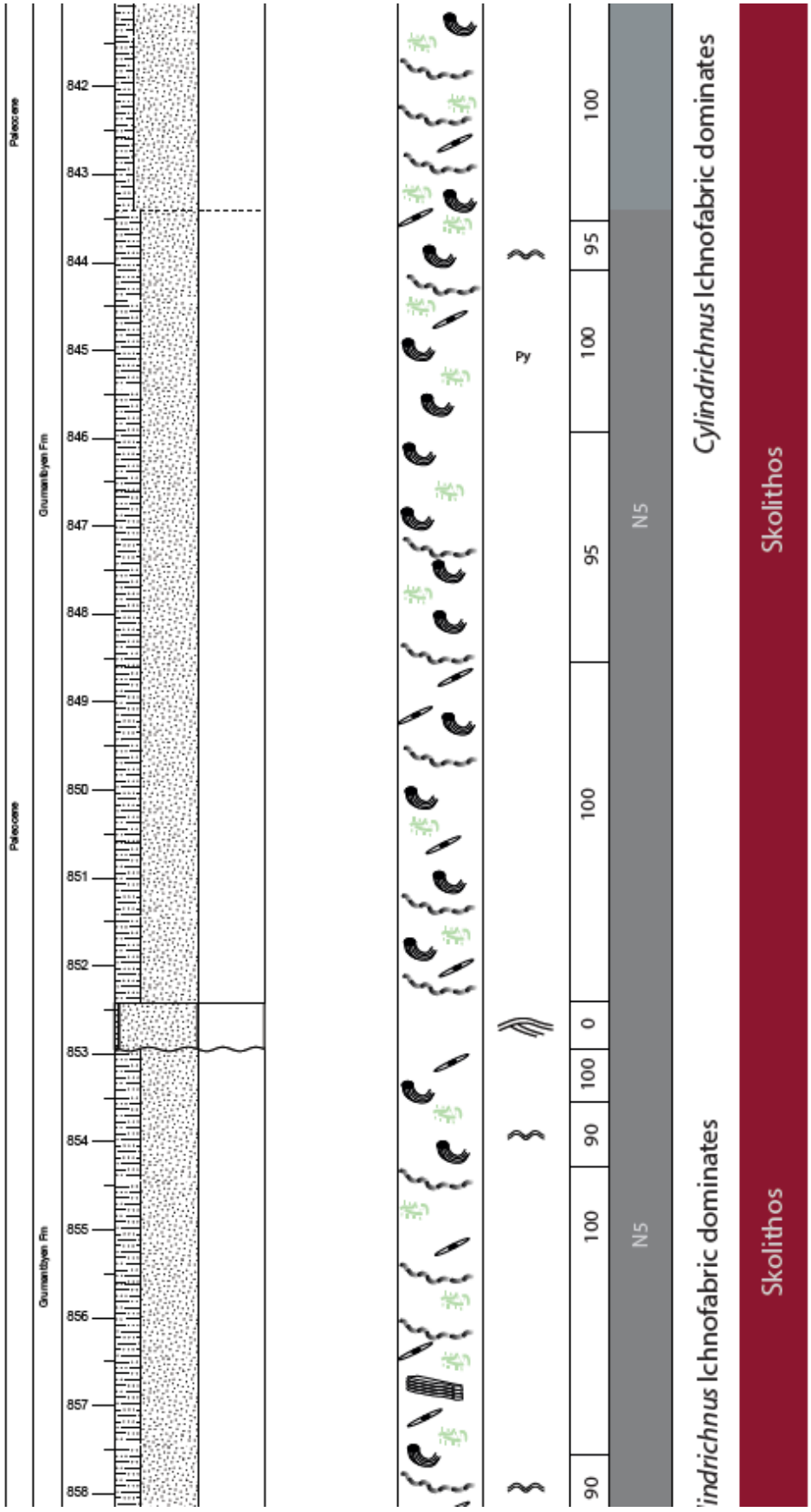
Paleocene
Grumantbyen Fm
842
843
844
845
846
847
848
849
850
851
852
853
854
855
856
857
858
Py
90
100
90
100
0
100
95
100
95
100
N5
N5
Cylindrichnus Ichnofabric dominates
Skolithos
Skolithos

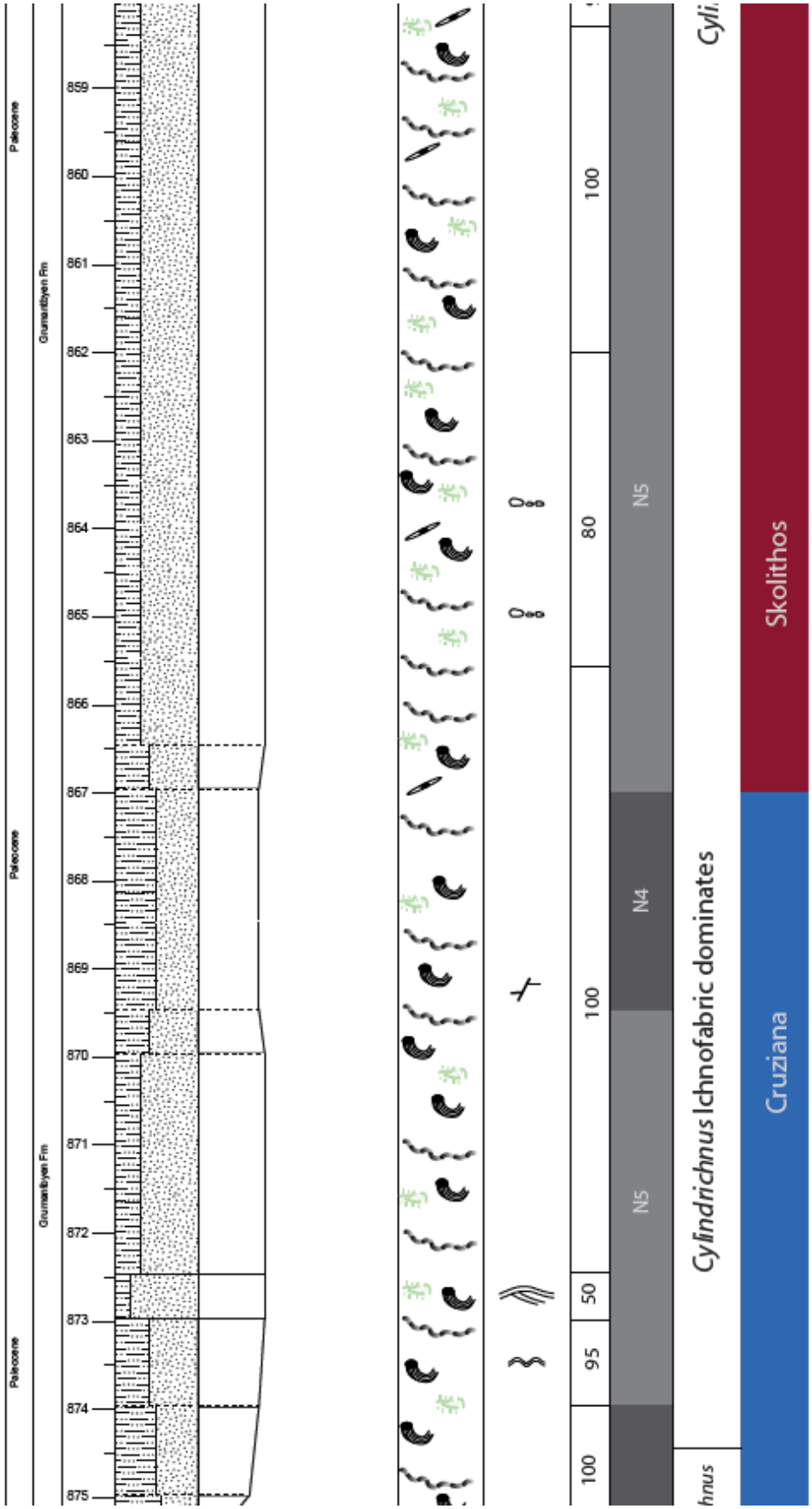
Paleocene
Paleocene
Paleocene
Grumantbyen Fm
Grumantbyen Fm
859
860
861
862
863
864
865
866
867
868
869
870
871
872
873
874
875
100
95
50
100
80
100
N5
N4
N5
Cylindrichnus Ichnofabric dominates
Cyli
Skolithos
Cruziana

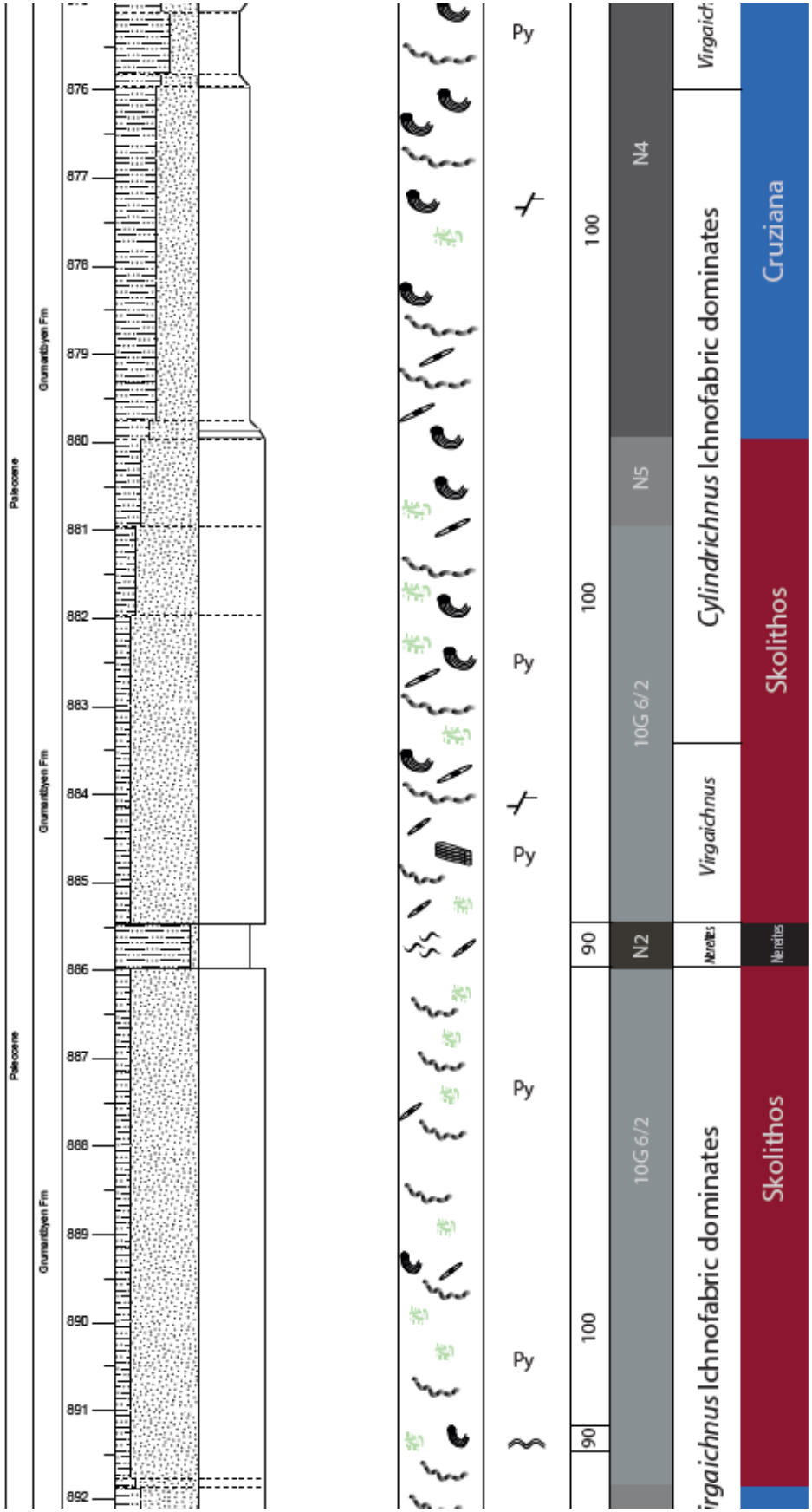
Paleocene
Grumantbyen Fm
876
877
878
879
880
881
882
883
884
885
886
887
888
889
890
891
892
Py
Py
Py
Py
90
100
100
90
100
N2
N4
N5
10G 6/2
10G 6/2
Nereites
Nereites
Virgaichnus
Cylindrichnus Ichnofabric dominates
Skolithos
Skolithos
Cruziana

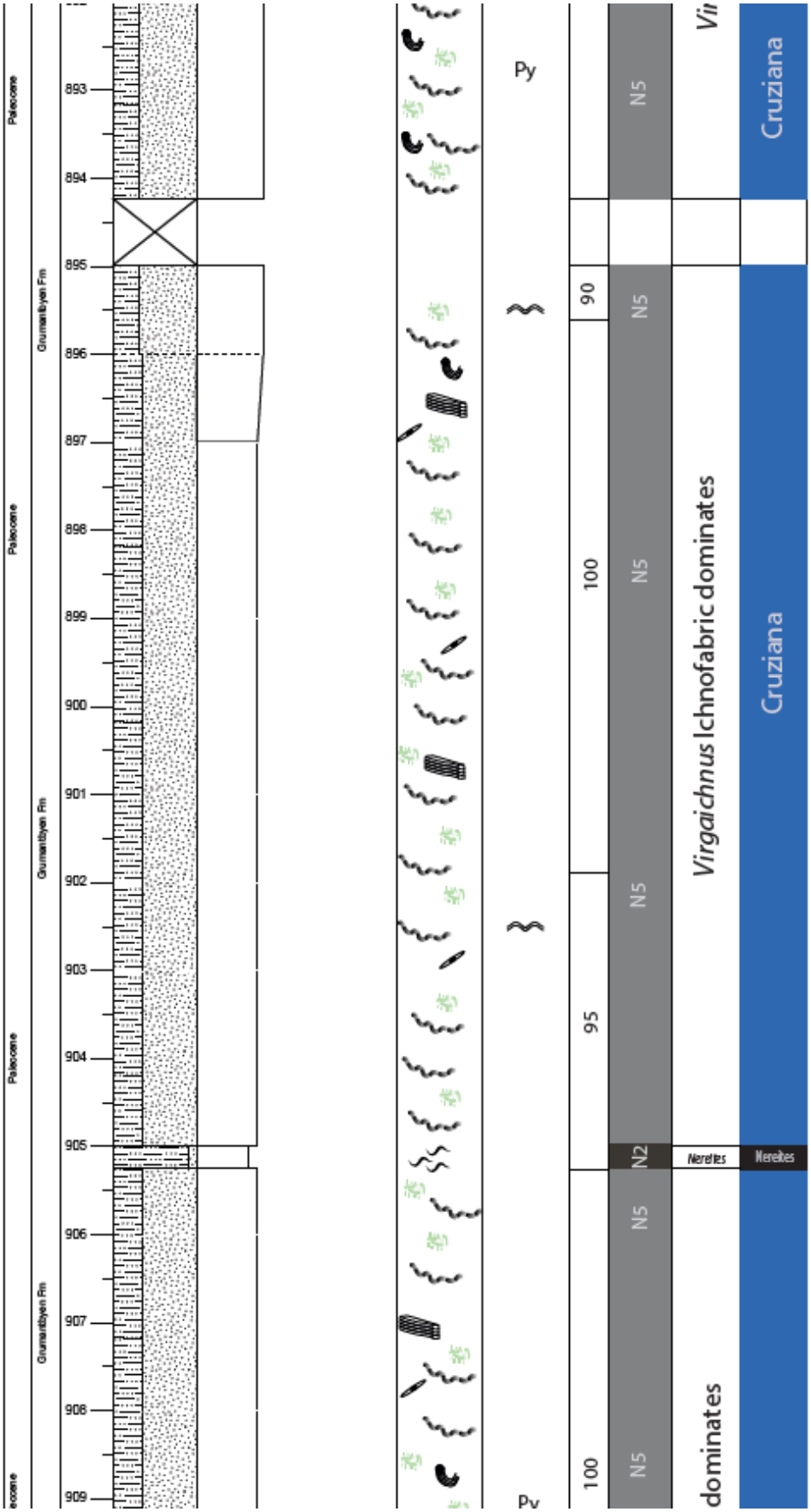
Palaeocene
Palaeocene
Palaeocene
Grumantbyen Fm
Grumantbyen Fm
Grumantbyen Fm
893
894
895
896
897
898
899
900
901
902
903
904
905
906
907
908
909
Py
Py
100
95
100
90
N5
N5
N5
N5
N5
N2
Nereites
Nereites
Virgaichnus Ichnofabric dominates
dominates
Cruziana
Cruziana

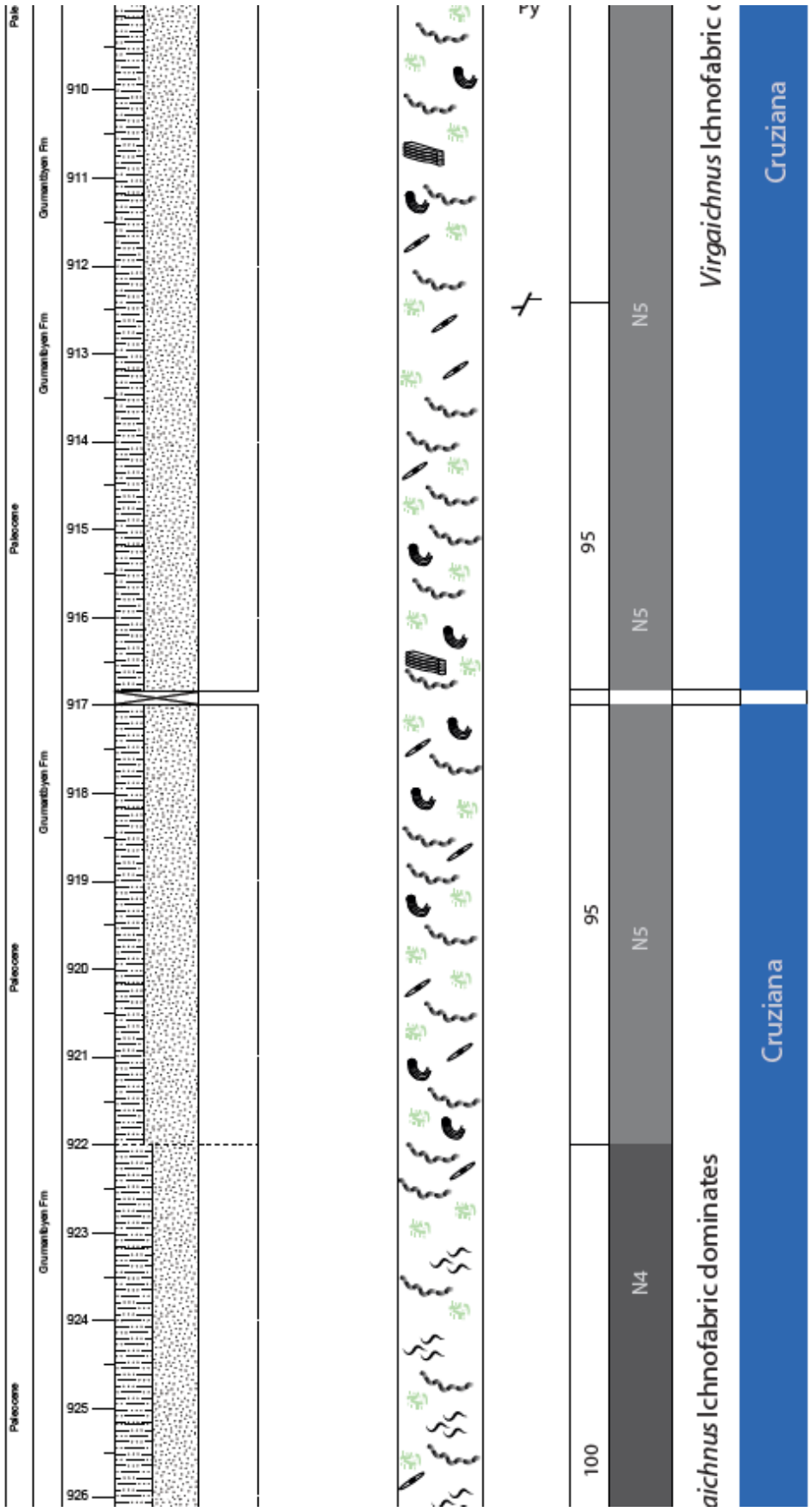
Pale
Paleocene
Grumantbyen Fm
910
911
912
913
914
915
916
917
918
919
920
921
922
923
924
925
926
Py
100
95
N4
N5
95
N5
Virgaichnus Ichnofabric
aichnus Ichnofabric dominates
Cruziana
Cruziana

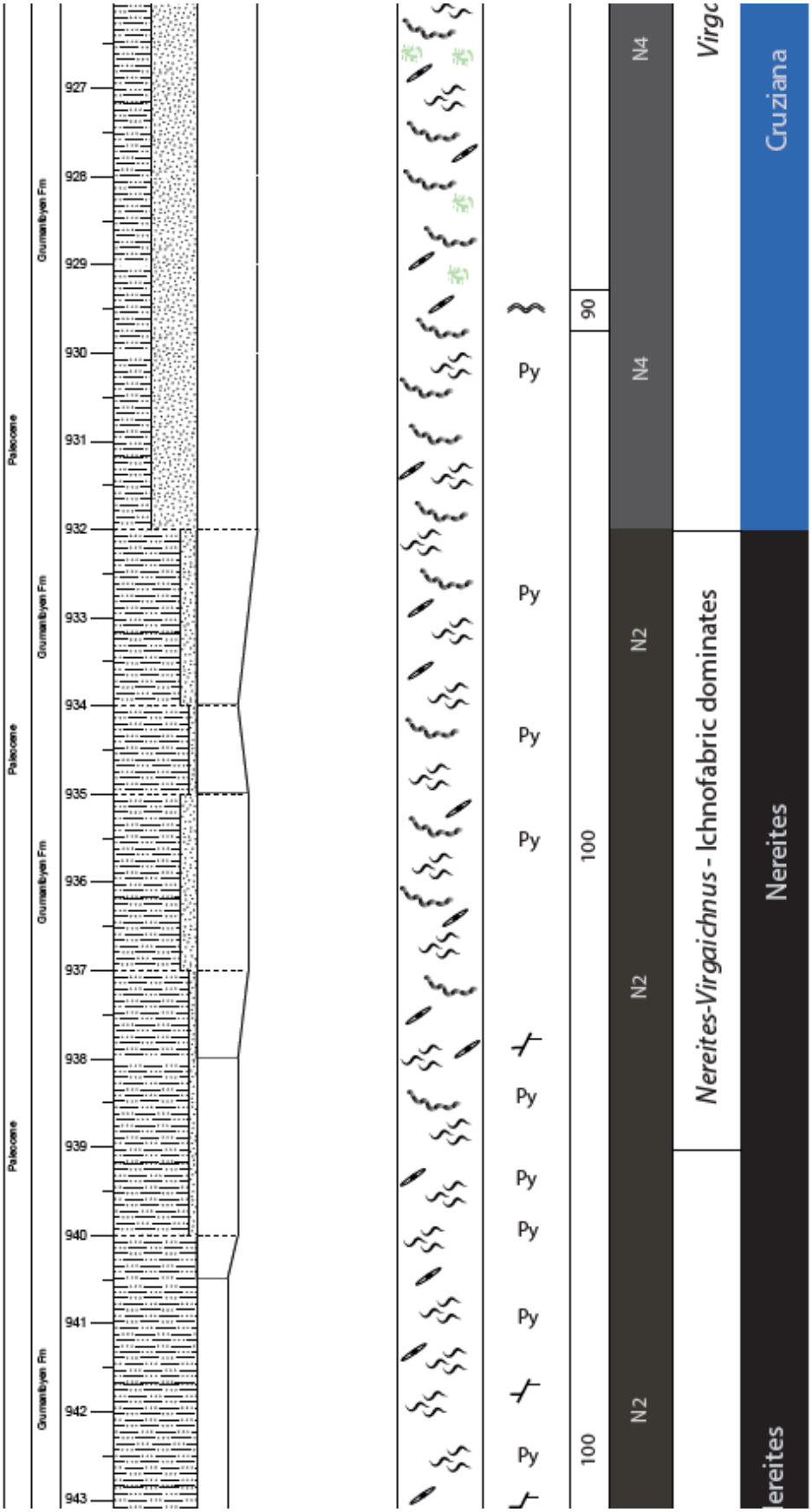
Paleocene
Paleocene
Paleocene
Grumantbyen Fm
Grumantbyen Fm
Grumantbyen Fm
Grumantbyen Fm
927
928
929
930
931
932
933
934
935
936
937
938
939
940
941
942
943
Py
Py
Py
Py
Py
Py
Py
Py
100
90
100
N2
N2
N4
N4
Nereites-Virgaichnus - Ichnofabric dominates
Nereites
Cruziana
Virg
ereites

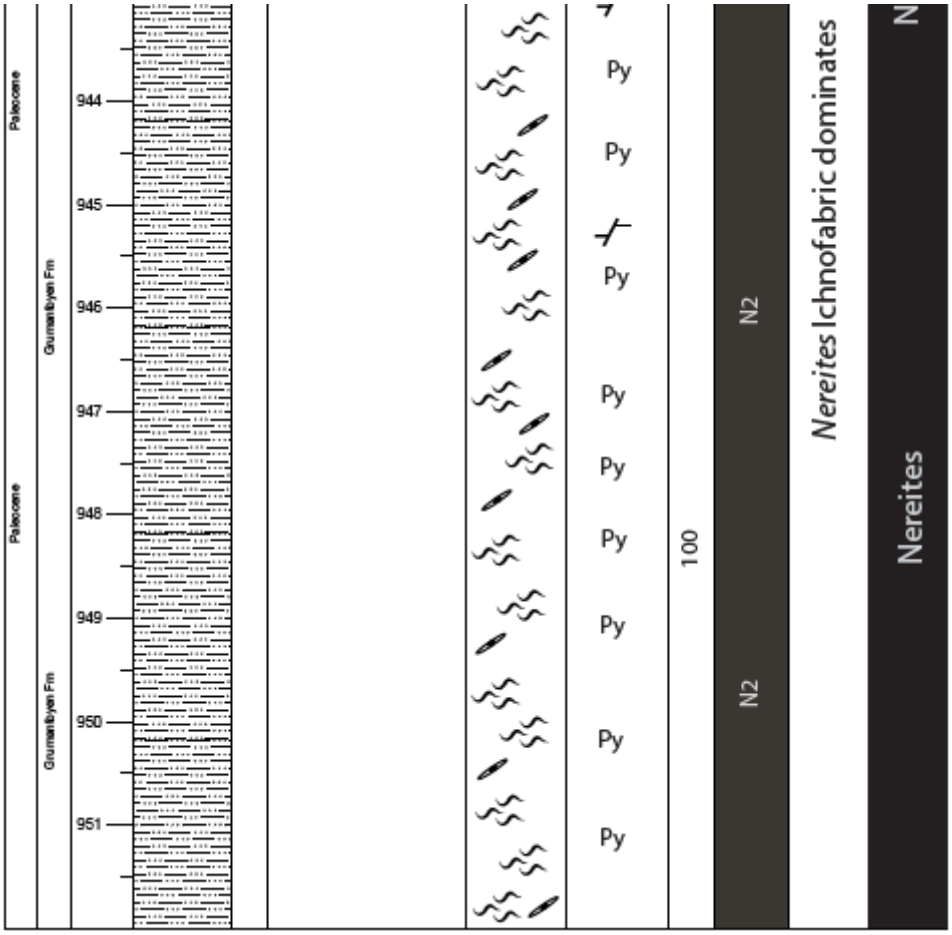

Appendix 11: *Presenting log of well BH-10-2008. The length of the core is measured in depth (meters) from the topographical point where the well has been drilled. Bottom depth of the logged interval is 952 m and top depth is 812 m. Scale 1:50.*

Chapter 9
Appendix

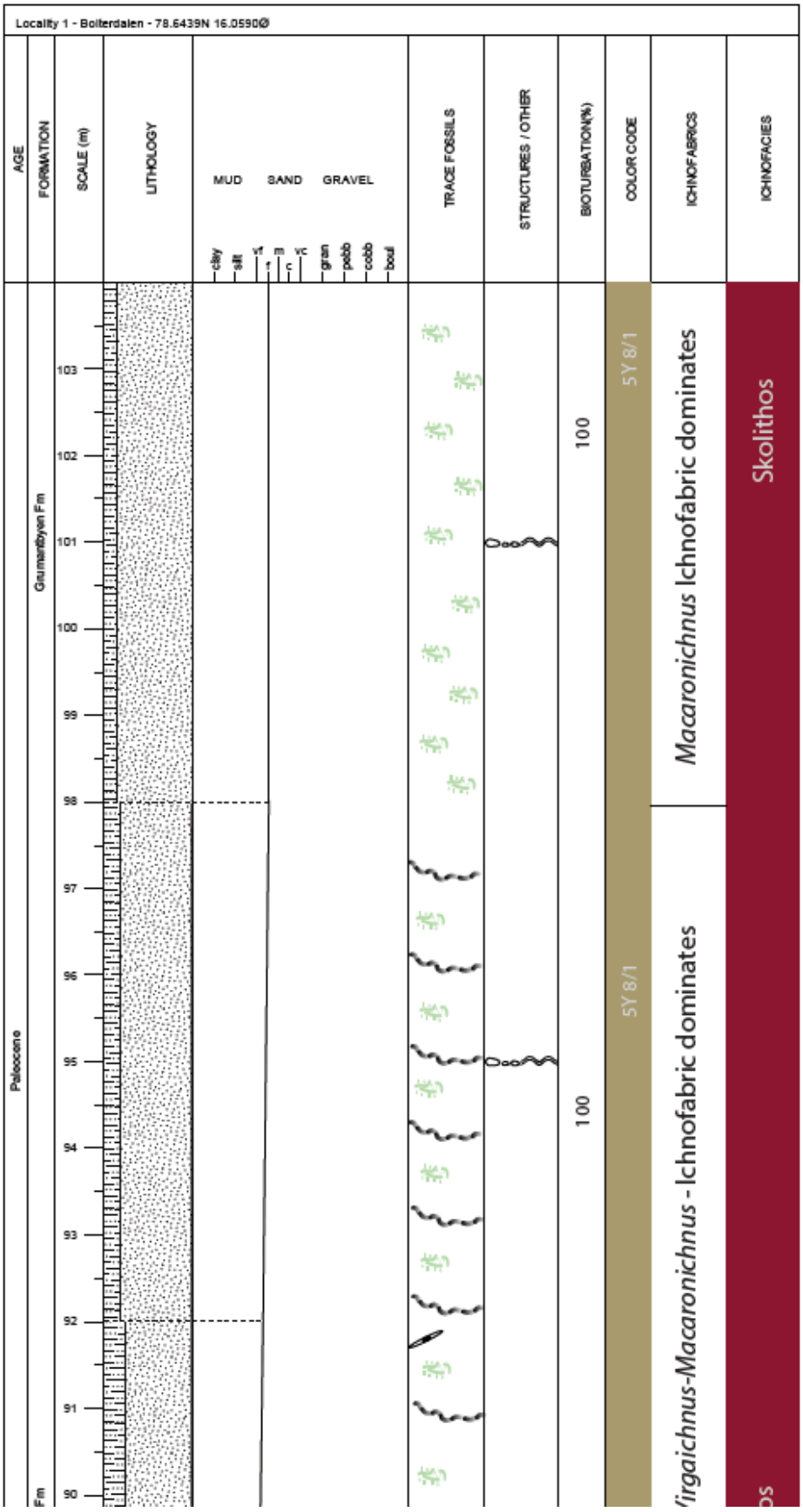

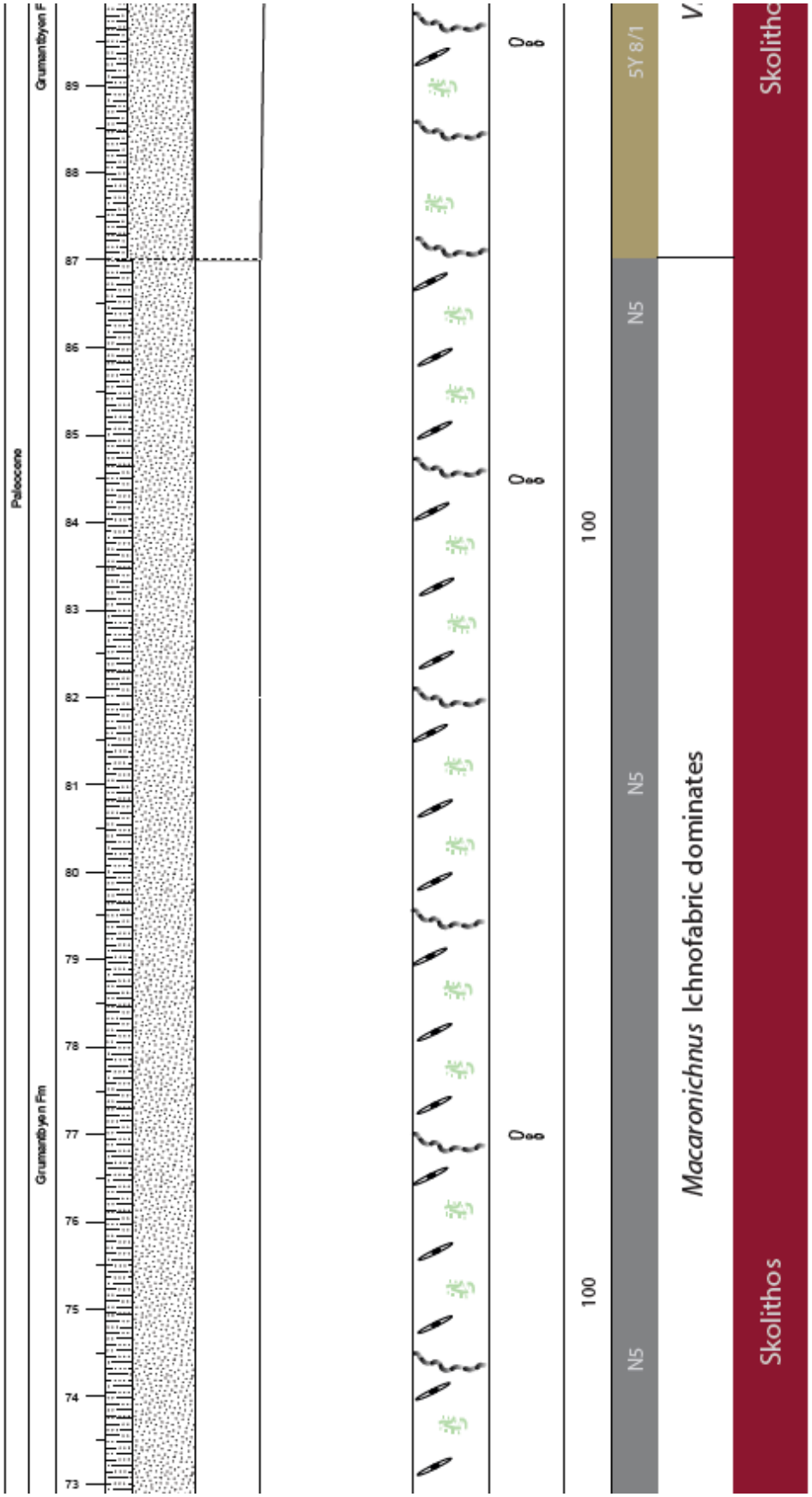
Paleocene
Grumantbyen Fm
Grumantbyen F
89
88
87
86
85
84
83
82
81
80
79
78
77
76
75
74
73
100
100
N5
N5
5Y 8/1
Macaronichnus Ichnofabric dominates
Skolithos
Skolitho

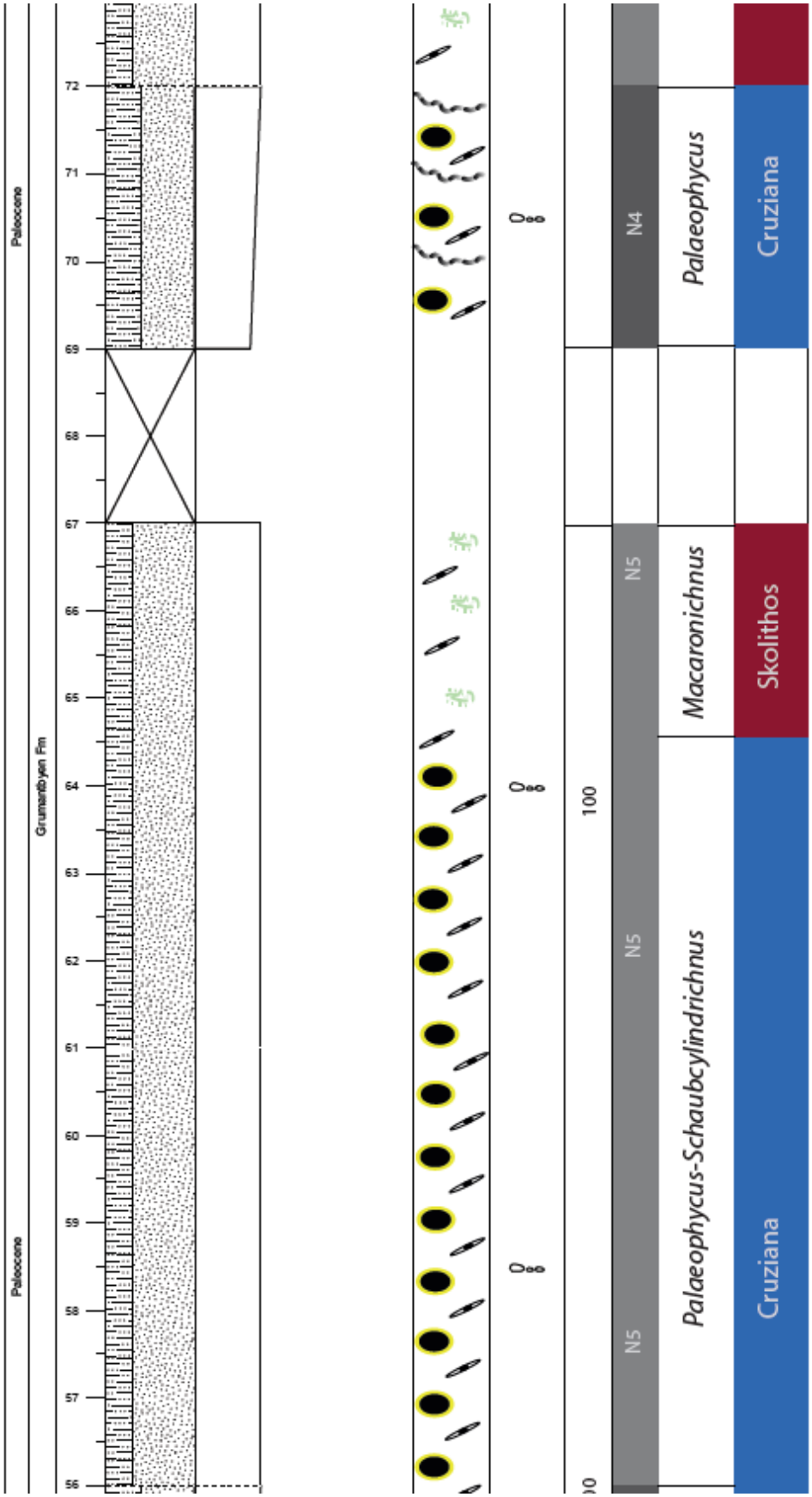
Paleocene
Grumantbyen Fm
Paleocene
72
71
70
69
68
67
66
65
64
63
62
61
60
59
58
57
56
100
N4
N5
N5
Palaeophycus
Macaronichnus
Palaeophycus-Schaubcylindrichnus
Cruziana
Skolithos
Cruziana

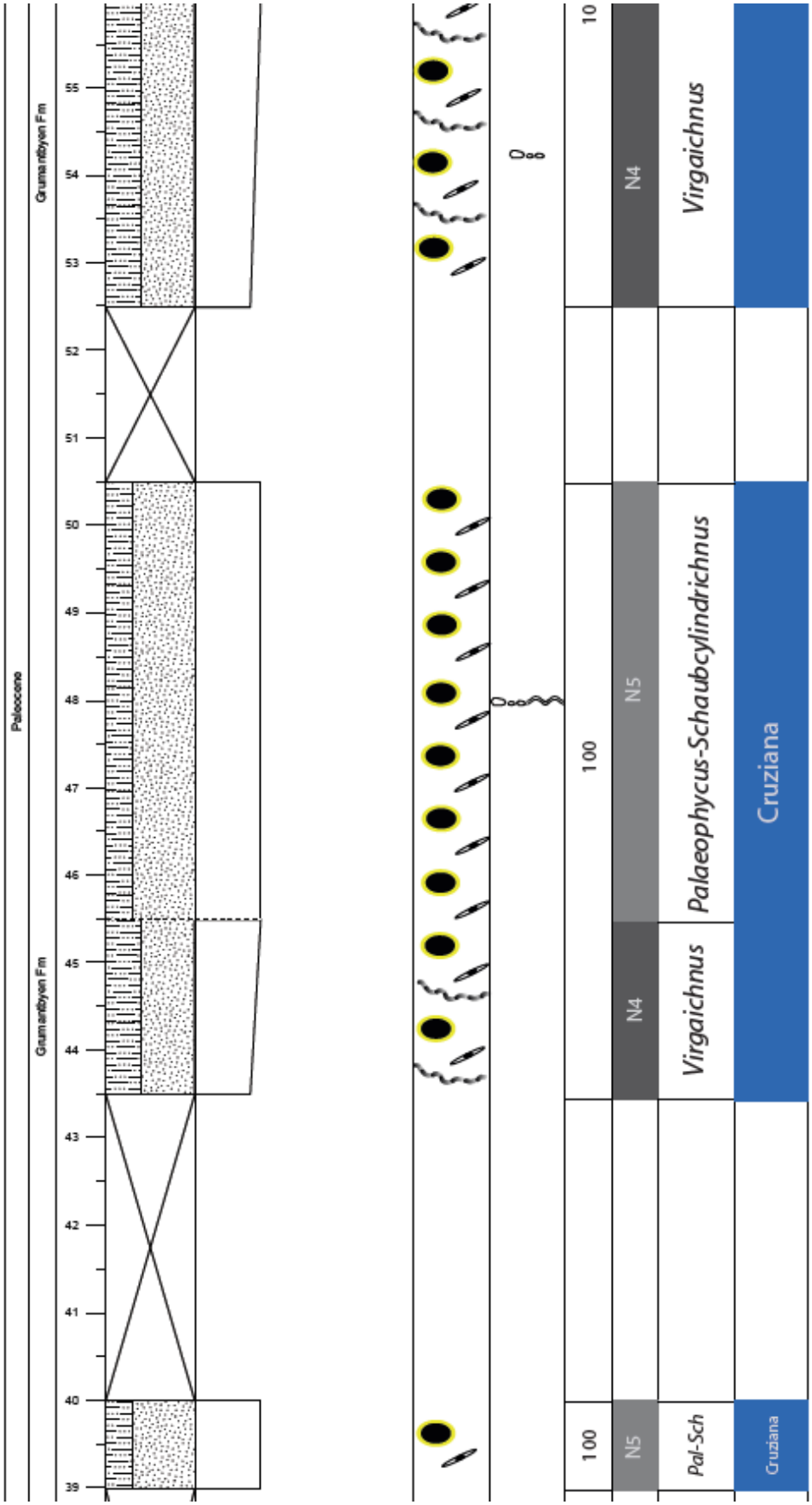
Paleocene
Grumantbyen Fm
Grumantbyen Fm
55
54
53
52
51
50
49
48
47
46
45
44
43
42
41
40
39
100
N5
Pal-Sch
Cruziana
100
N4
N5
Virgaichnus
Palaeophycus-Schaubcylindrichnus
Cruziana
10
N4
Virgaichnus

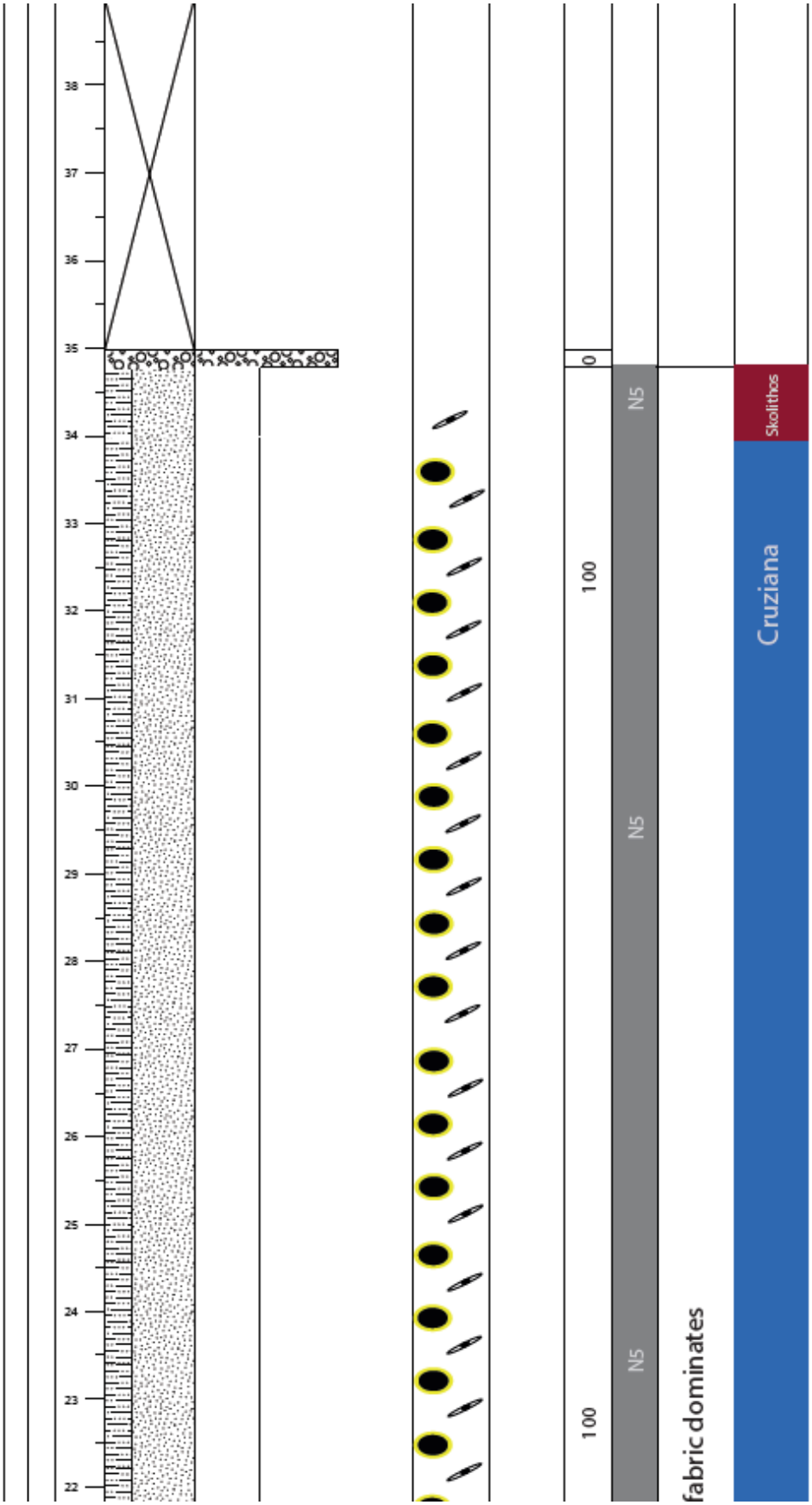
38
37
36
35
34
33
32
31
30
29
28
27
26
25
24
23
22
0
100
100
N5
N5
N5
Skolithos
Cruziana
fabric dominates

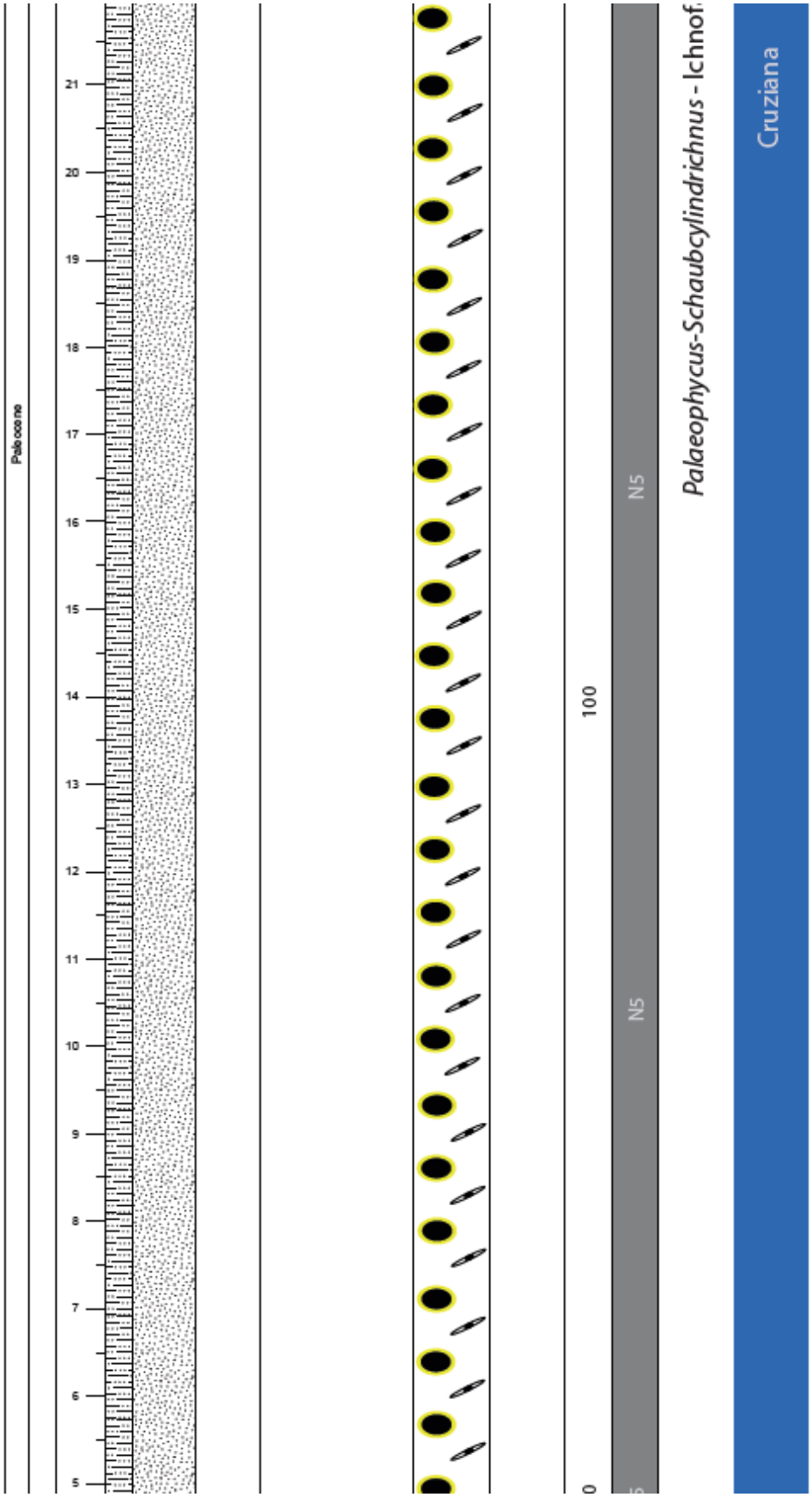
Paleoceno
21
20
19
18
17
16
15
14
13
12
11
10
9
8
7
6
5
100
0
N5
N5
Palaeophycus-Schaubcylindrichnus - Ichnof
Cruziana

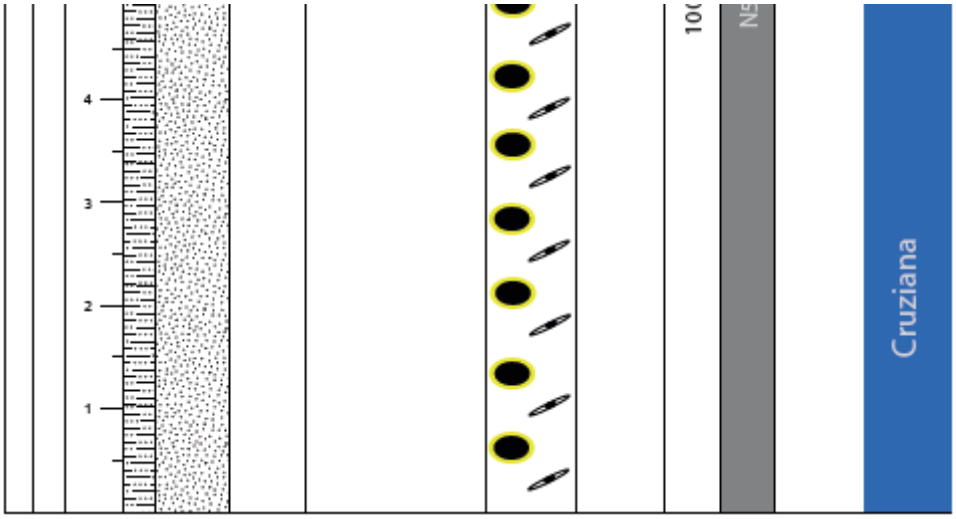

Appendix 12: *Presenting log of Locality 1, Bolterdalen. The length of the log is measured in meters from the starting point at the locality. Total length is 104 m. Scale 1:50.*

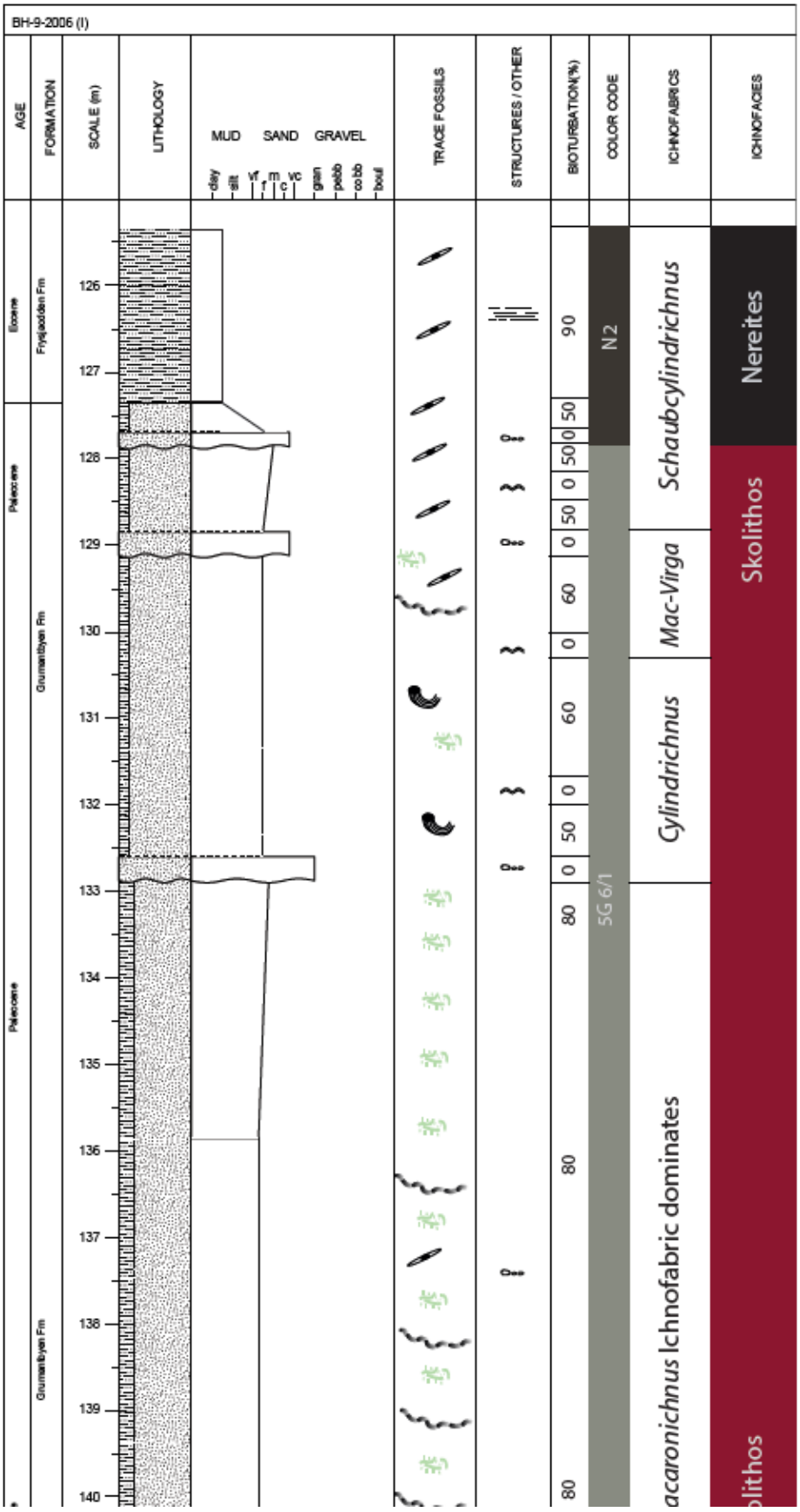
BH-9-2006 (I)
AGE
FORMATION
SCALE (m)
LITHOLOGY
MUD
SAND
GRAVEL
clay
silt
vf
f
m
c
vc
gran
pebb
cobb
boul
TRACE FOSSILS
STRUCTURES / OTHER
BIOTURBATION(%)
COLOR CODE
ICHNOFABRICS
ICHNOFACIES
Eocene
Paleocene
Paleocene
Frejlev Fm
Grumsnbyen Fm
Grumsnbyen Fm
126
127
128
129
130
131
132
133
134
135
136
137
138
139
140
80
0
50
0
60
0
50
0
50
0
50
90
80
5G 6/1
N2
Cylindrichnus
Mac-Virga
Schaubcylindrichnus
acaronichnus Ichnofabric dominates
Skolithos
Nereites
olithos

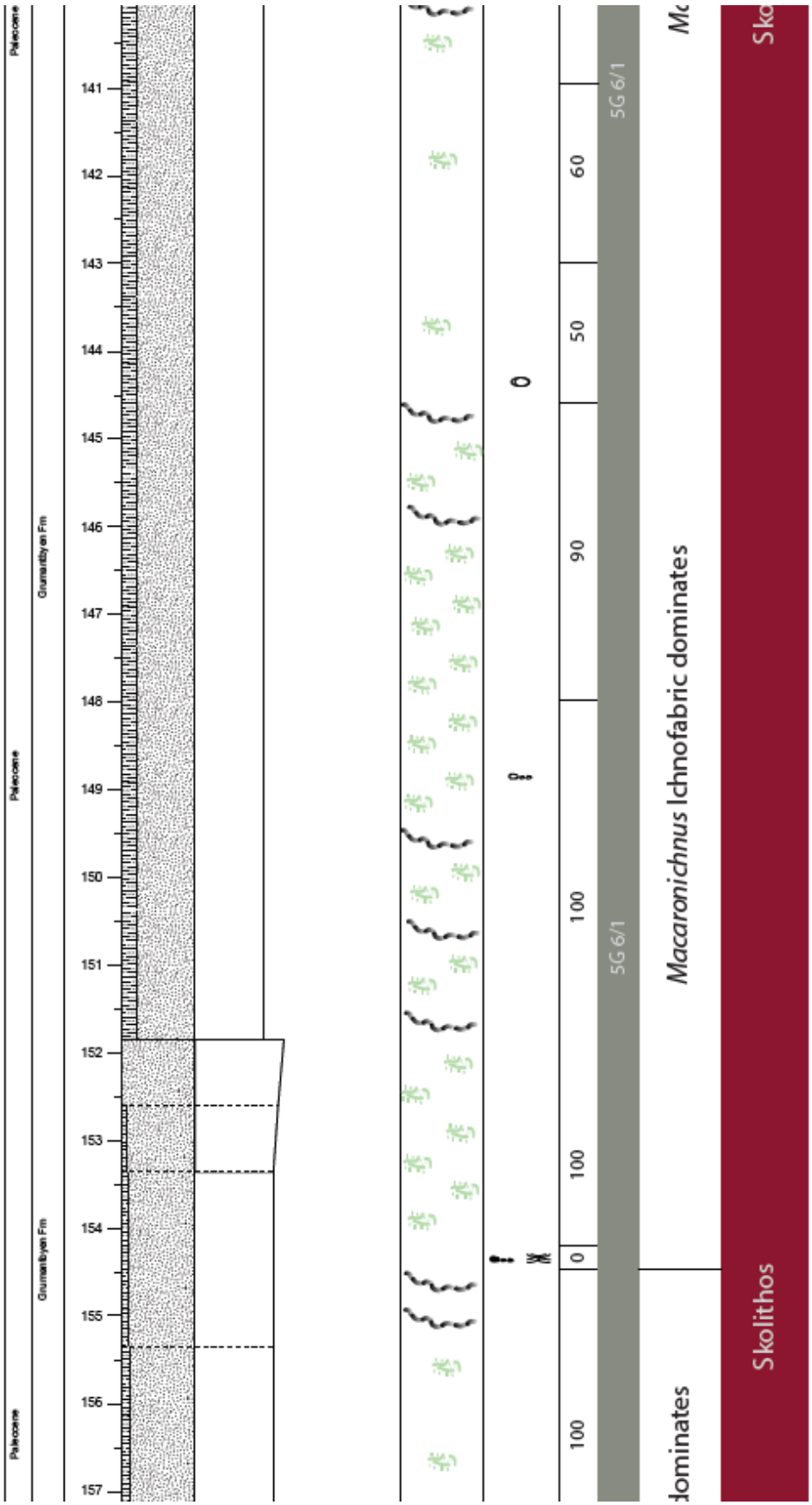
Paleocene
Paleocene
Paleocene
Grumantbyen Fm
Grumantbyen Fm
141
142
143
144
145
146
147
148
149
150
151
152
153
154
155
156
157
0
100
100
5G 6/1
5G 6/1
90
50
60
Macaronichnus Ichnofabric dominates
dominates
Skolithos

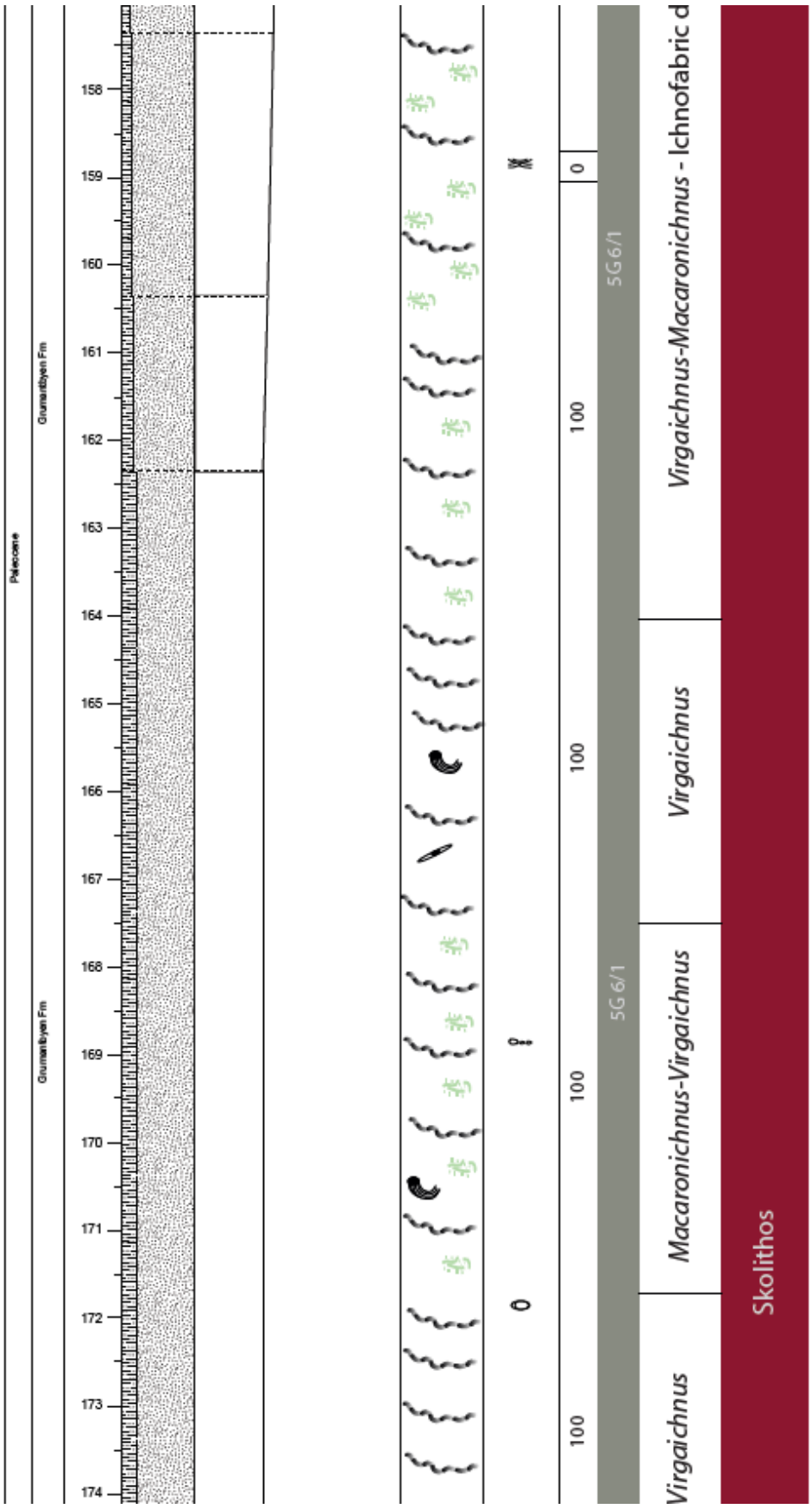
Paleocene
Grumantbyen Fm
Grumantbyen Fm
158
159
160
161
162
163
164
165
166
167
168
169
170
171
172
173
174
0
?
100
100
100
0
5G 6/1
5G 6/1
Virgaichnus
Macaronichnus-Virgaichnus
Virgaichnus
Virgaichnus-Macaronichnus - Ichnofabric d
Skolithos

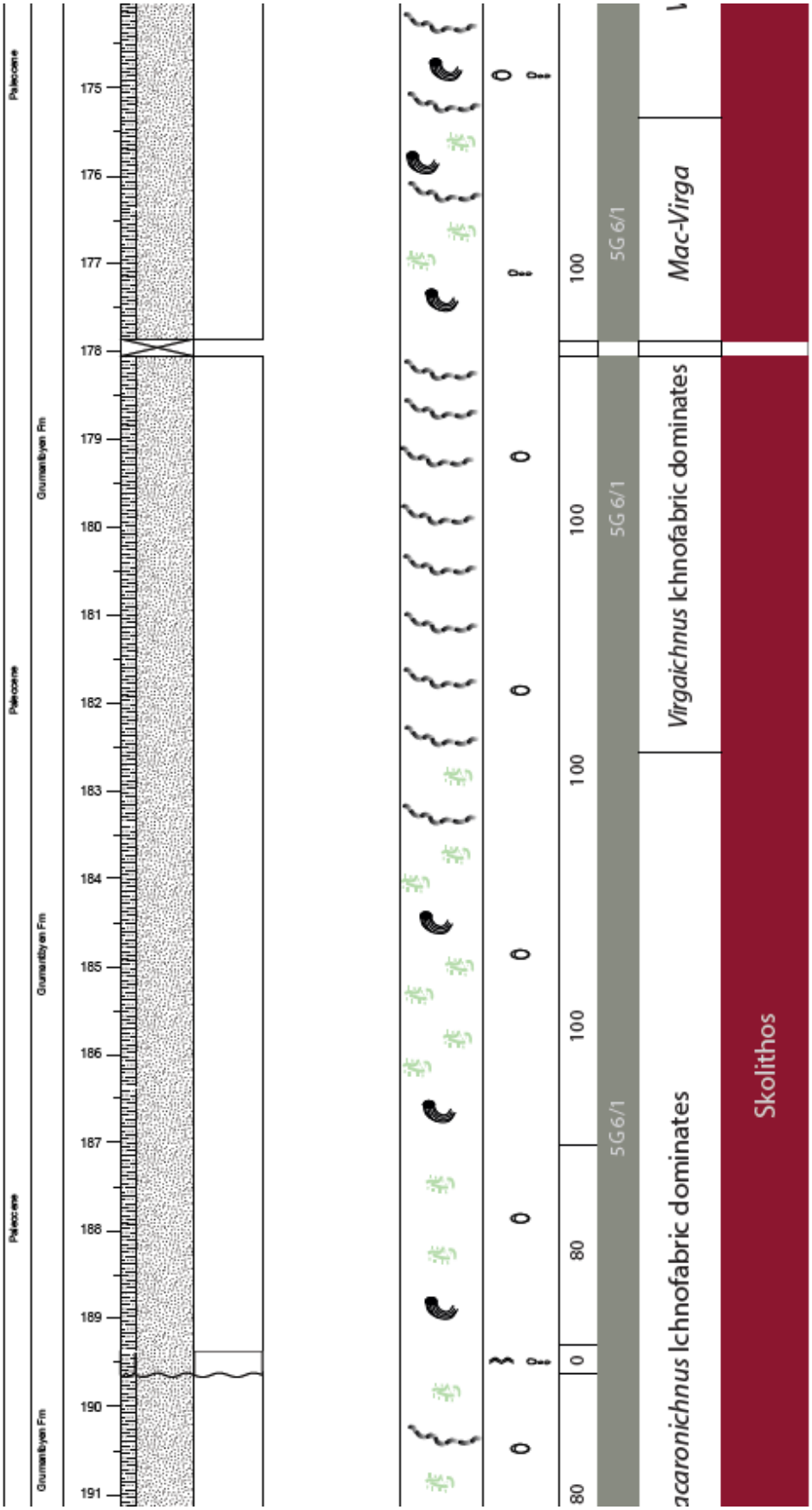
Paleocene
Grumantbyen Fm
175
176
177
178
179
180
181
182
183
184
185
186
187
188
189
190
191
0
80
100
5G 6/1
Virgaichnus Ichnofabric dominates
Mac-Virga
Skolithos

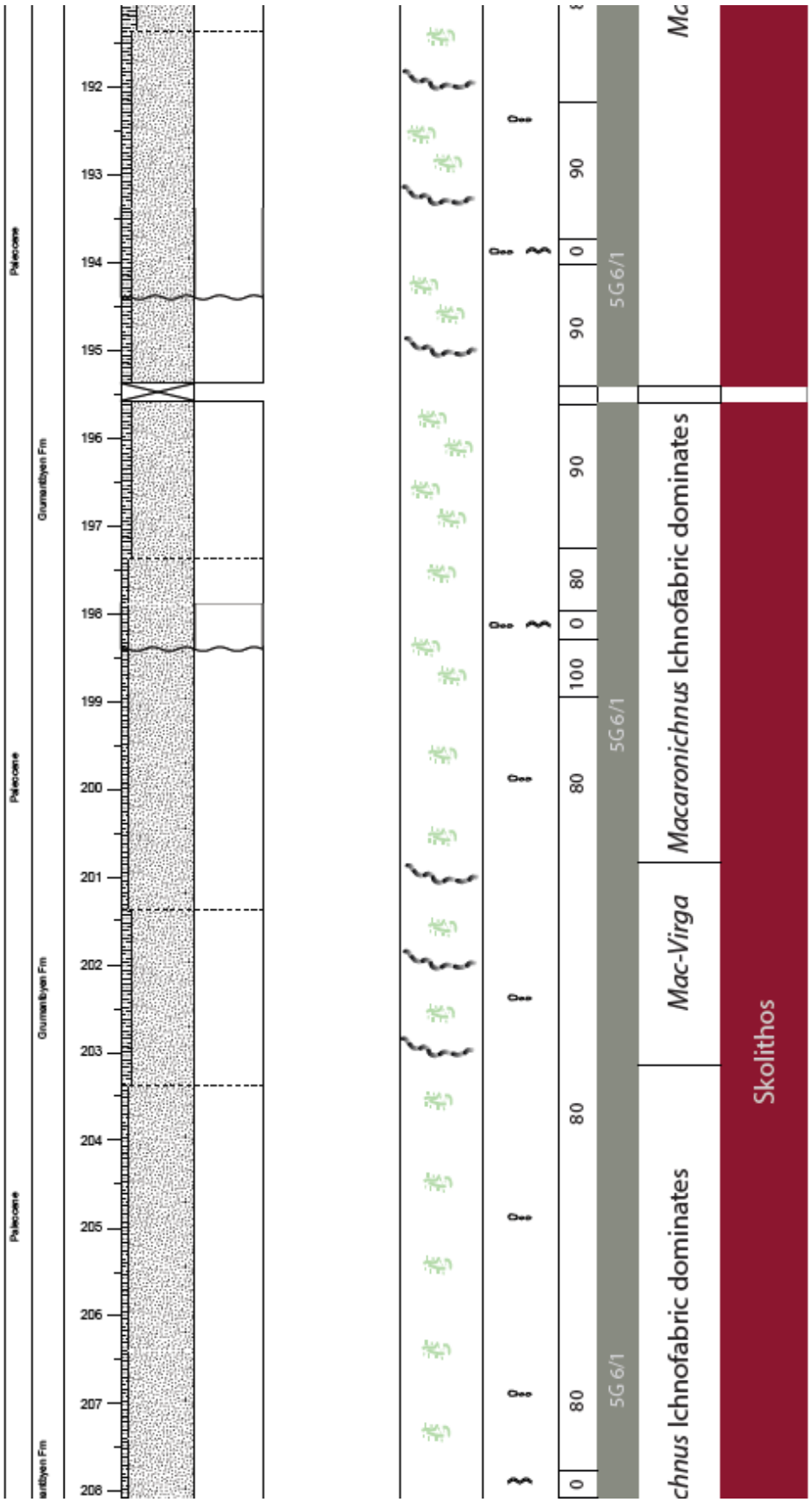
Paleocene
Paleocene
Paleocene
Grumantbyen Fm
Grumantbyen Fm
192
193
194
195
196
197
198
199
200
201
202
203
204
205
206
207
208
0
80
80
80
100
0
80
90
90
90
0
5G 6/1
5G 6/1
5G 6/1
chnus Ichnofabric dominates
Mac-Virga
Macaronichnus Ichnofabric dominates
Skolithos

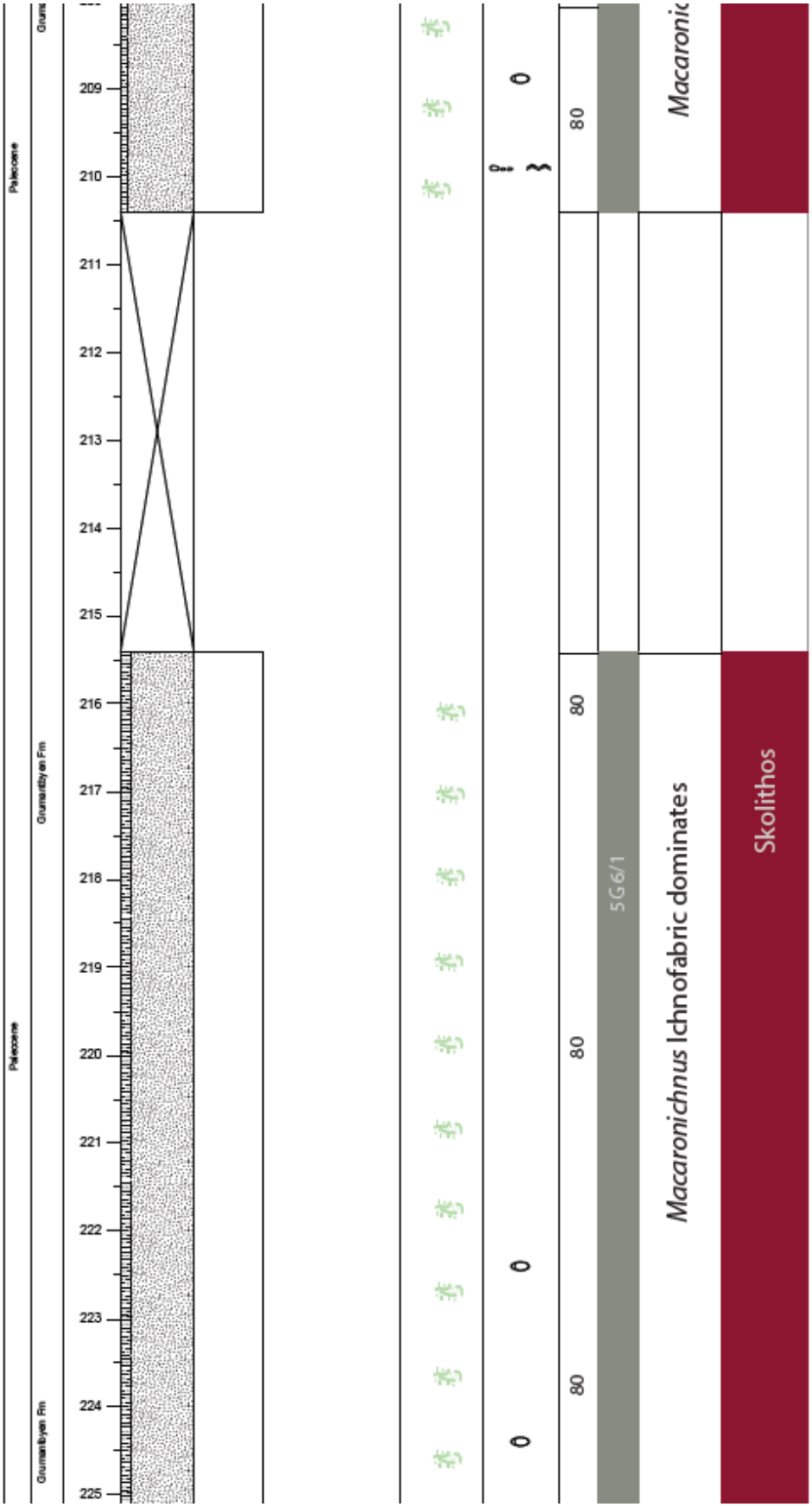
Paleocene
Grumsiltsyen Fm
209
210
211
212
213
214
215
216
217
218
219
220
221
222
223
224
225
0
0
80
80
80
SG6/1
Macaronichnus Ichnofabric dominates
Skolithos

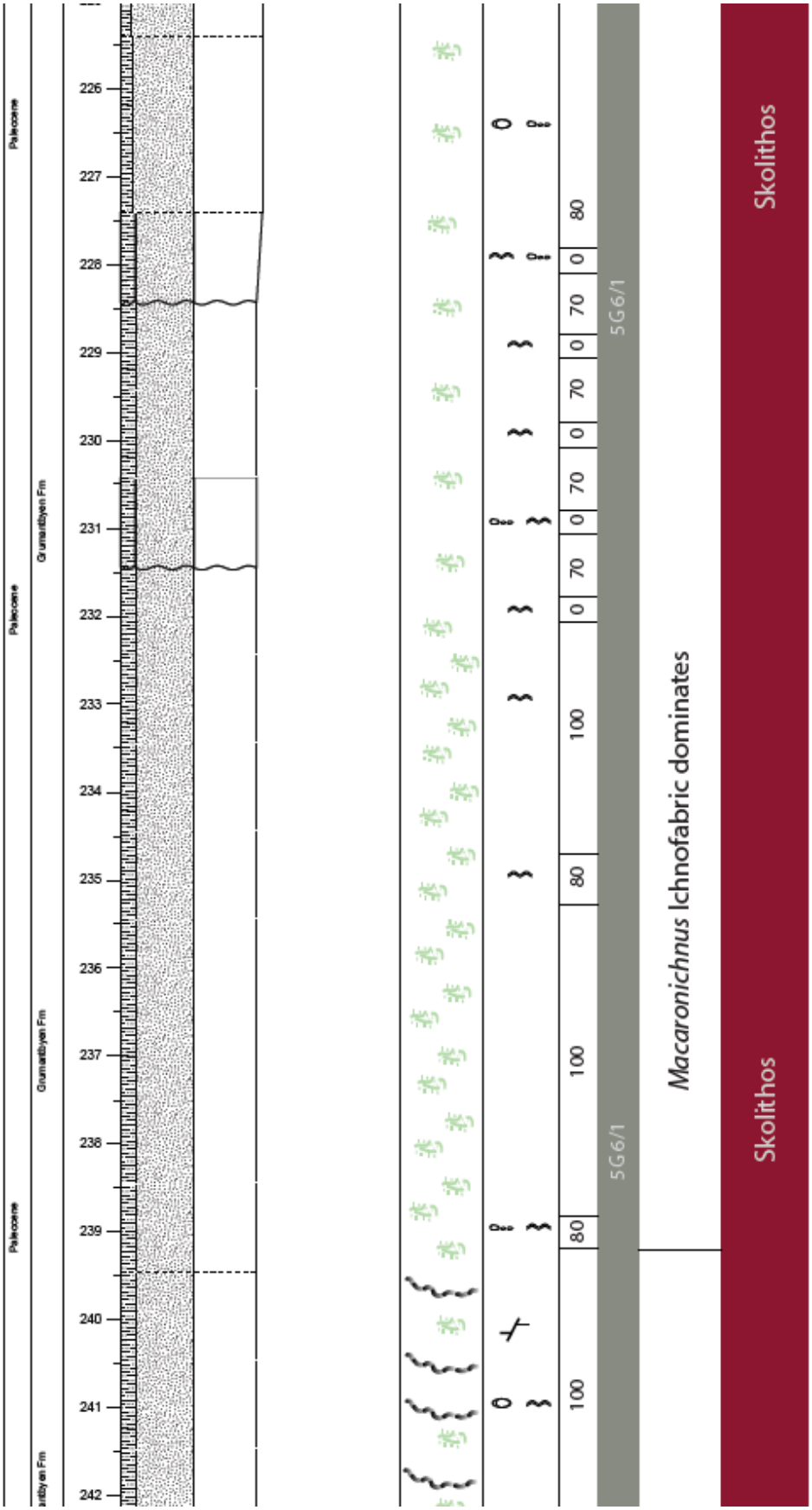
Paleocene
Grumantbyen Fm
226
227
228
229
230
231
232
233
234
235
236
237
238
239
240
241
242
100
80
100
80
100
0
70
0
70
0
70
0
70
0
80
5G6/1
5G6/1
Macaronichnus Ichnofabric dominates
Skolithos
Skolithos

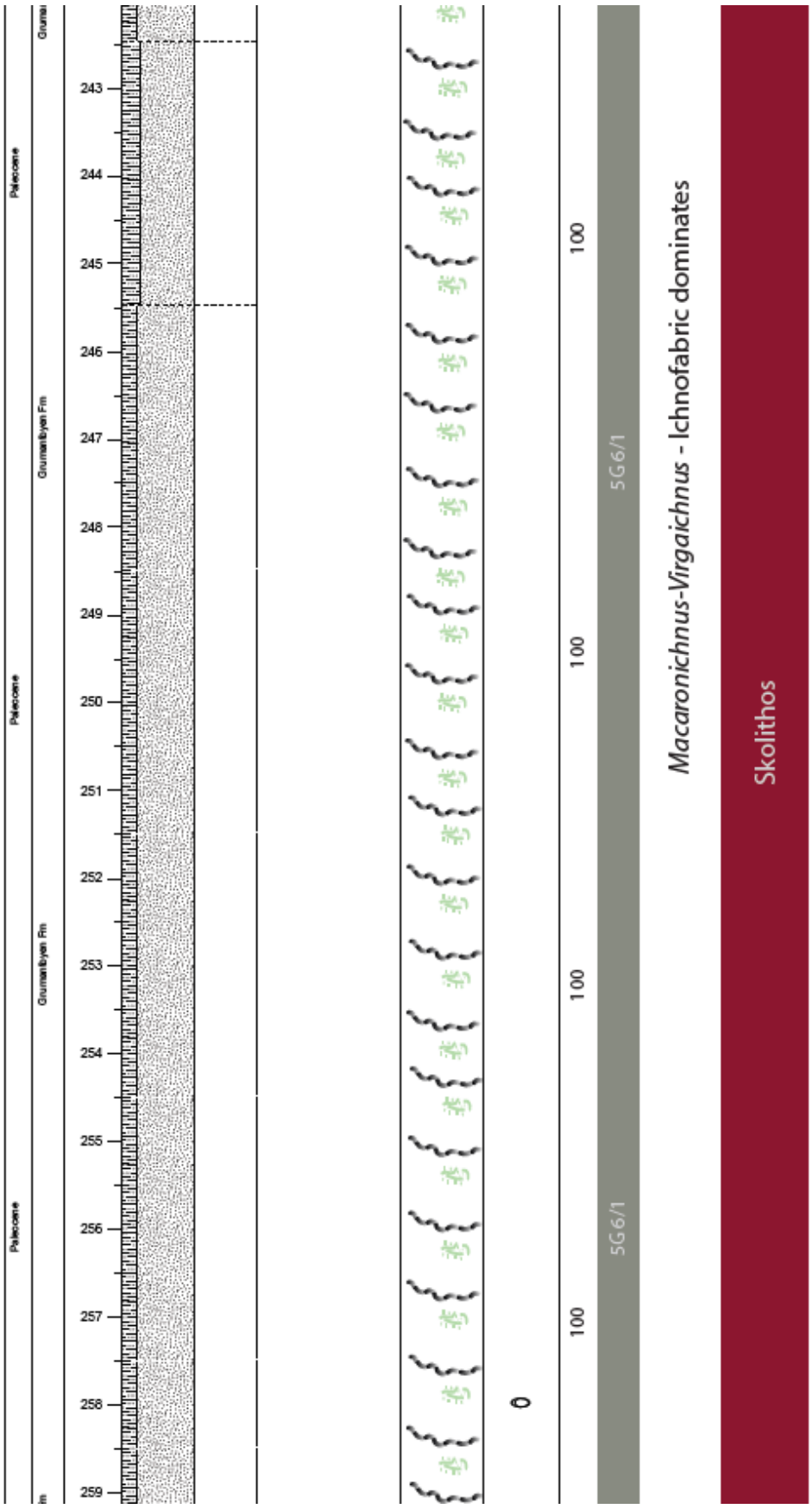
Paleocene
Paleocene
Paleocene
Grumantbyen Fm
Grumantbyen Fm
243
244
245
246
247
248
249
250
251
252
253
254
255
256
257
258
259
0
100
100
100
100
5G6/1
5G6/1
Macaronichnus-Virgaichnus - Ichnofabric dominates
Skolithos

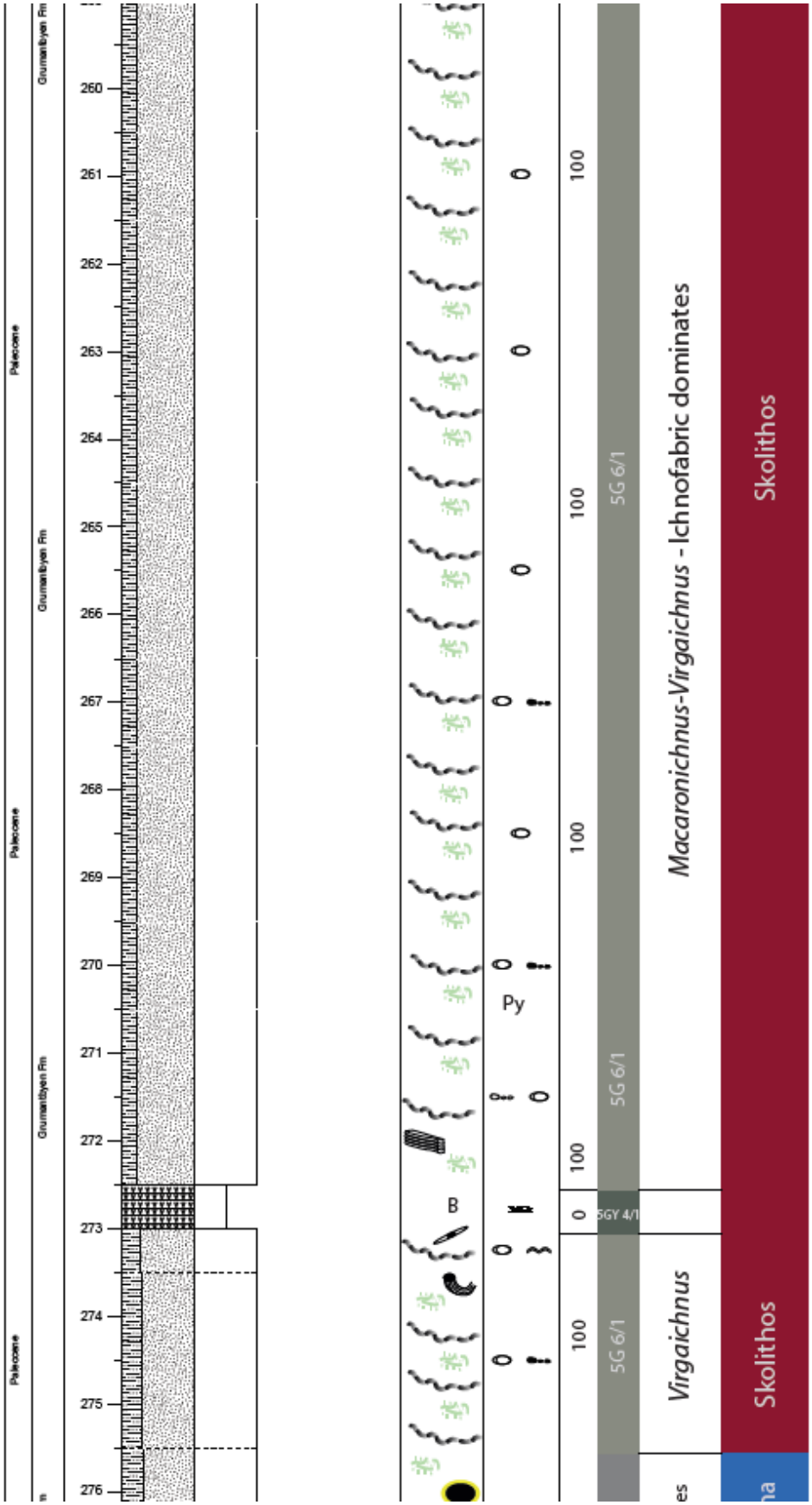
Paleocene
Paleocene
Paleocene
Grumantbyen Fm
Grumantbyen Fm
Grumantbyen Fm
260
261
262
263
264
265
266
267
268
269
270
271
272
273
274
275
276
B
Py
100
100
100
100
0
0
0
0
0
0
0
0
5G 6/1
5G 6/1
5GY 4/1
5G 6/1
Virgaichnus
Macaronichnus-Virgaichnus - Ichnofabric dominates
Skolithos
Skolithos

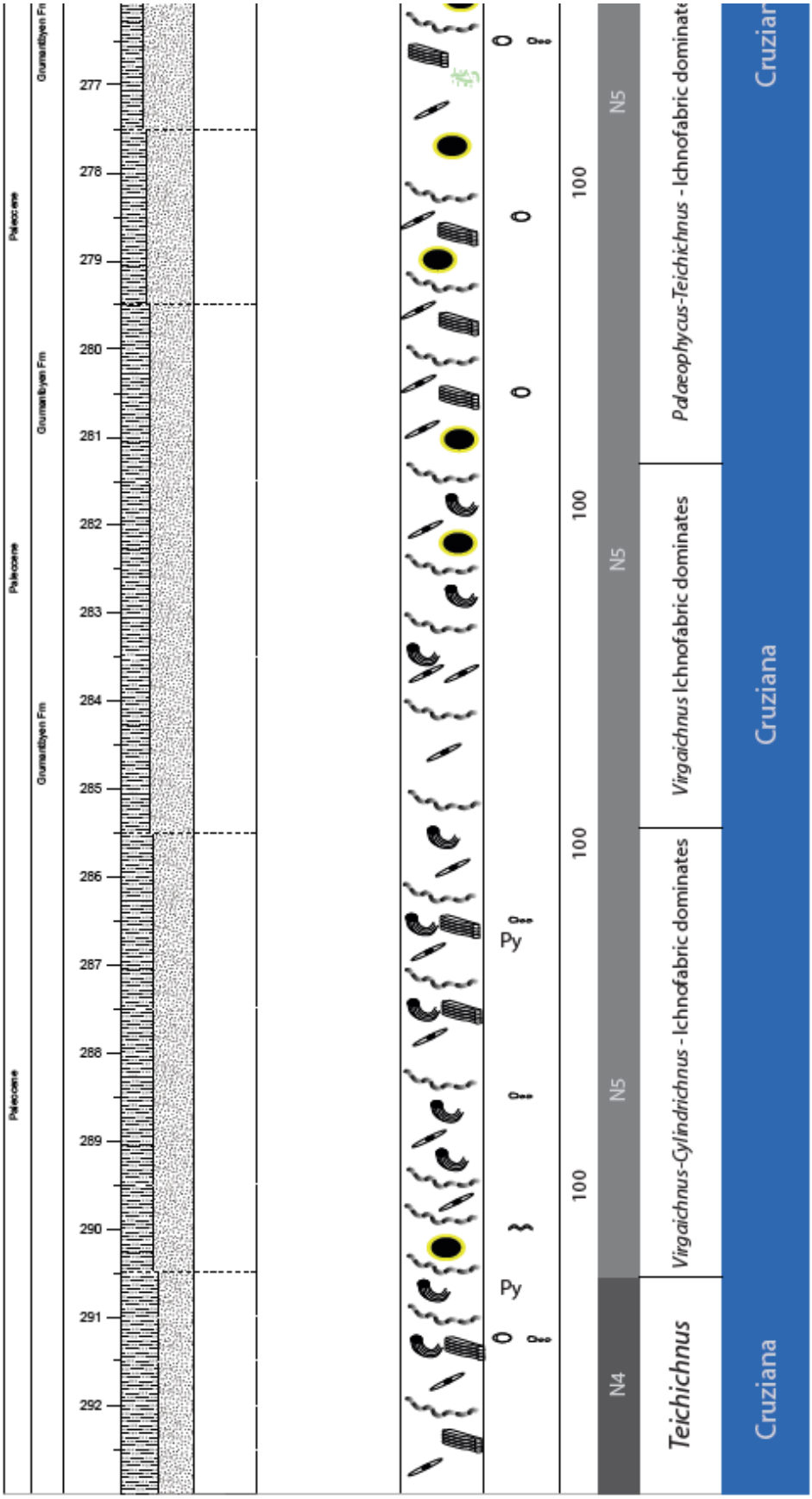
Paleocene
Paleocene
Paleocene
Grumantbyen Fm
Grumantbyen Fm
Grumantbyen Fm
277
278
279
280
281
282
283
284
285
286
287
288
289
290
291
292
Py
Py
0
0
0
0
100
100
100
N4
N5
N5
Teichichnus
Virgaichnus-Cylindrichnus - Ichnofabric dominates
Virgaichnus Ichnofabric dominates
Palaeophycus-Teichichnus - Ichnofabric dominate
Cruziana
Cruziana
Cruzian

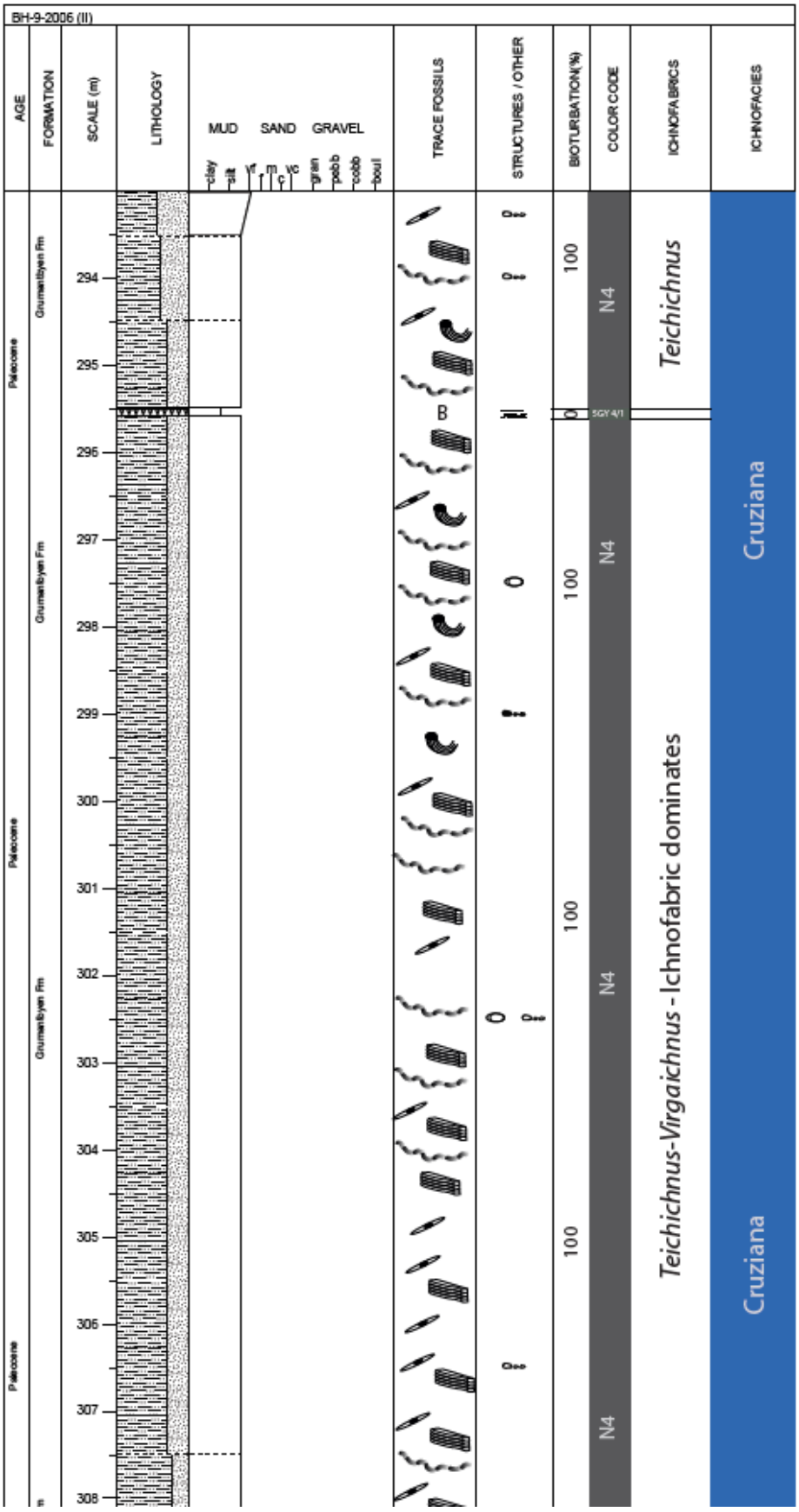
BH-9-2006 (II)
AGE
FORMATION
SCALE (m)
LITHOLOGY
MUD
SAND
GRAVEL
clay
silt
vf
f
m
c
vc
gran
pebb
cobb
boul
TRACE FOSSILS
STRUCTURES / OTHER
BIOTURBATION(%)
COLOR CODE
ICHNOFABRICS
ICHNOFACIES
Paleocene
Grumantbyen Fm
294
295
296
297
298
299
300
301
302
303
304
305
306
307
308
B
100
N4
SGY 4/1
Teichichnus
Teichichnus-Virgaichnus - Ichnofabric dominates
Cruziana

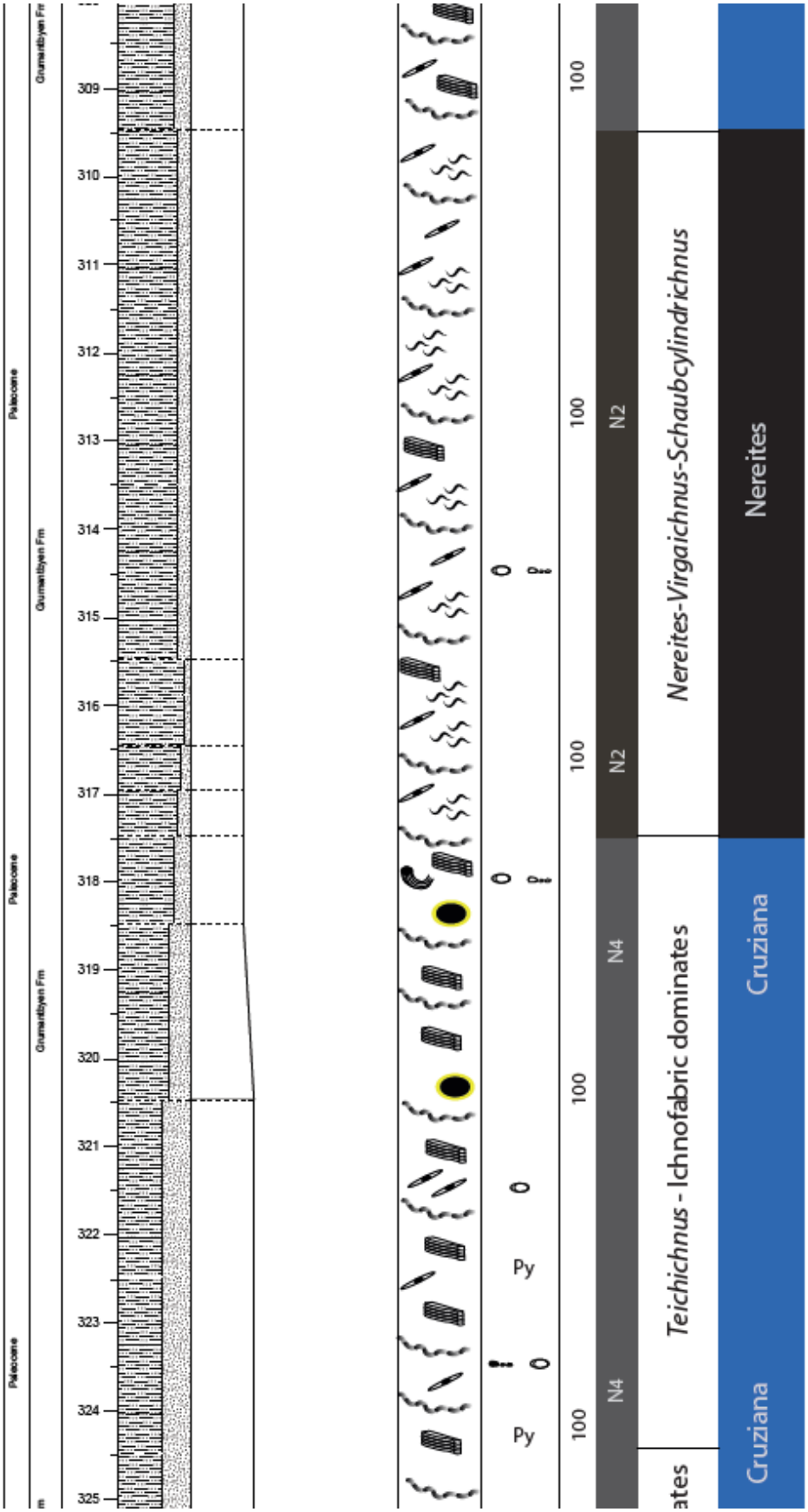
Palaeocene
Palaeocene
Palaeocene
Gruneartbyen Fm
Gruneartbyen Fm
Gruneartbyen Fm
309
310
311
312
313
314
315
316
317
318
319
320
321
322
323
324
325
Py
Py
100
100
100
100
N4
N4
N2
N2
Teichichnus - Ichnofabric dominates
Nereites-Virgaichnus-Schaubcylindrichnus
Cruziana
Cruziana
Nereites

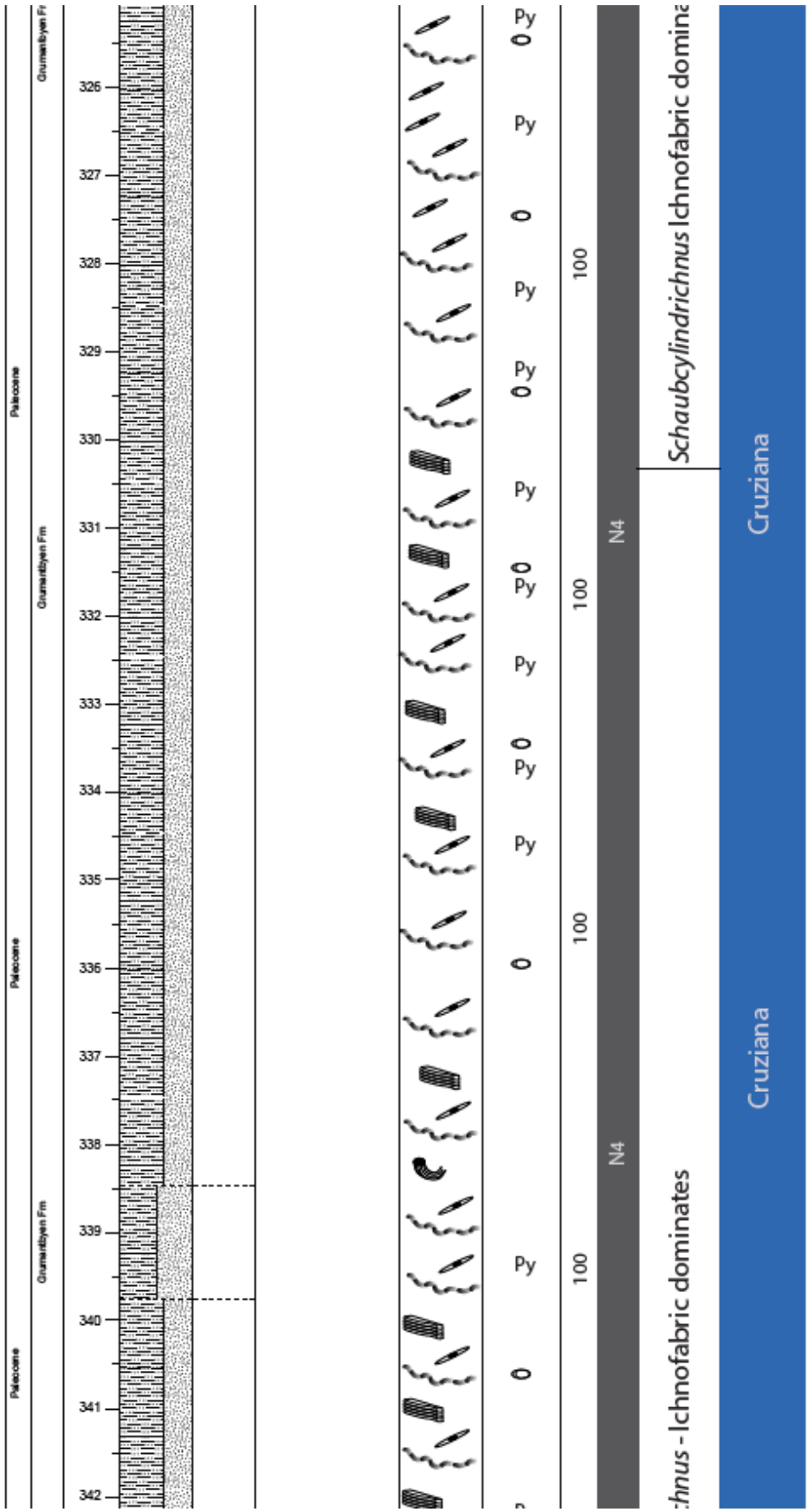
Palaeocene
Palaeocene
Palaeocene
Grumantbyen Fm
Grumantbyen Fm
Grumantbyen Fm
326
327
328
329
330
331
332
333
334
335
336
337
338
339
340
341
342
Py
0
Py
0
Py
0
Py
0
Py
0
Py
0
Py
0
Py
0
100
100
100
N4
N4
Schaubcylindrichnus Ichnofabric domina
Cruziana
Cruziana
hnus - Ichnofabric dominates

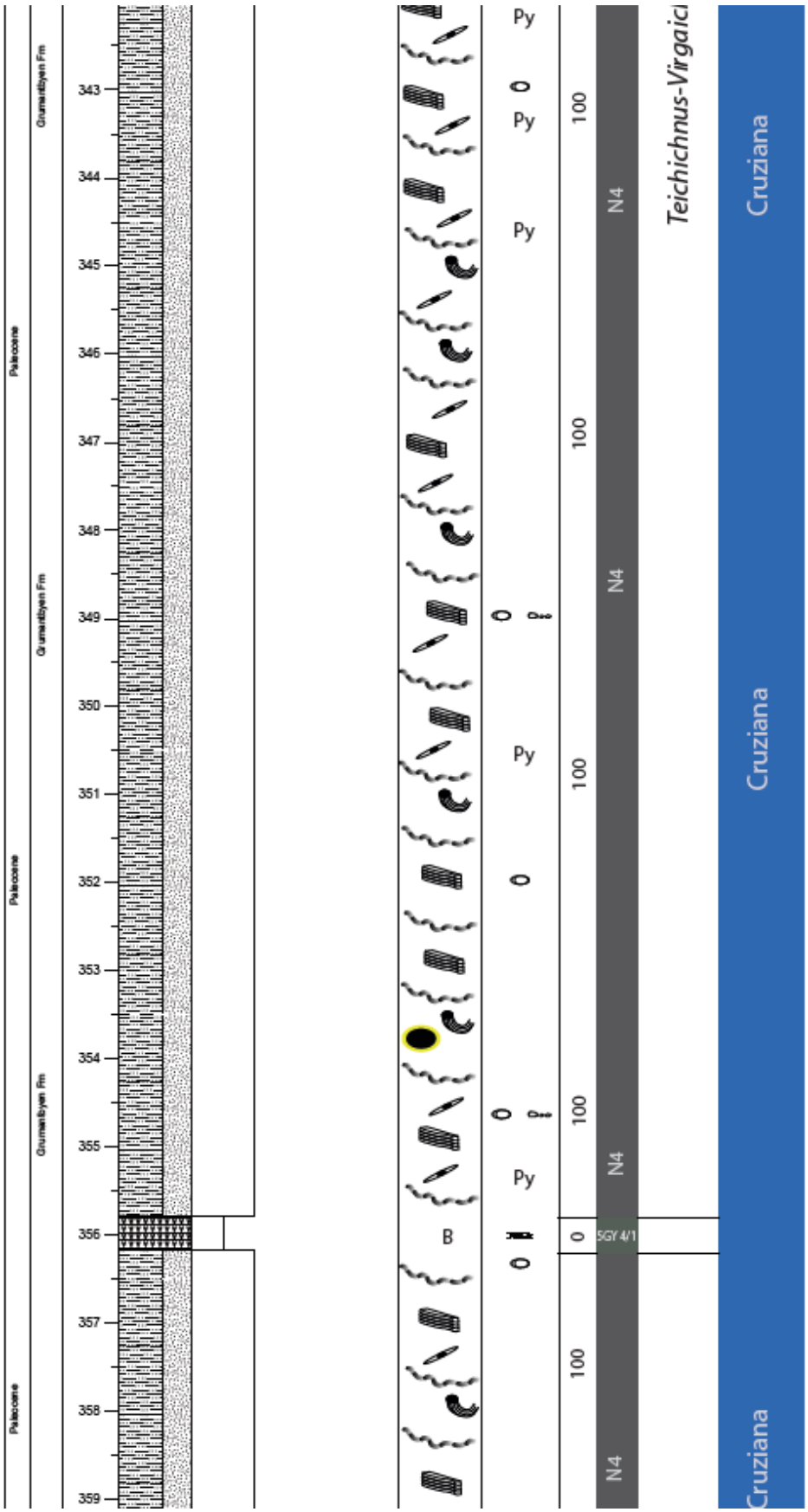
Paleocene
Paleocene
Paleocene
Grumantbyen Fm
Grumantbyen Fm
Grumantbyen Fm
343
344
345
346
347
348
349
350
351
352
353
354
355
356
357
358
359
B
Py
Py
Py
Py
0
0
0
0
0
100
100
100
100
100
N4
N4
N4
N4
SGY 4/1
Teichichnus-Virgaic
Cruziana
Cruziana
Cruziana

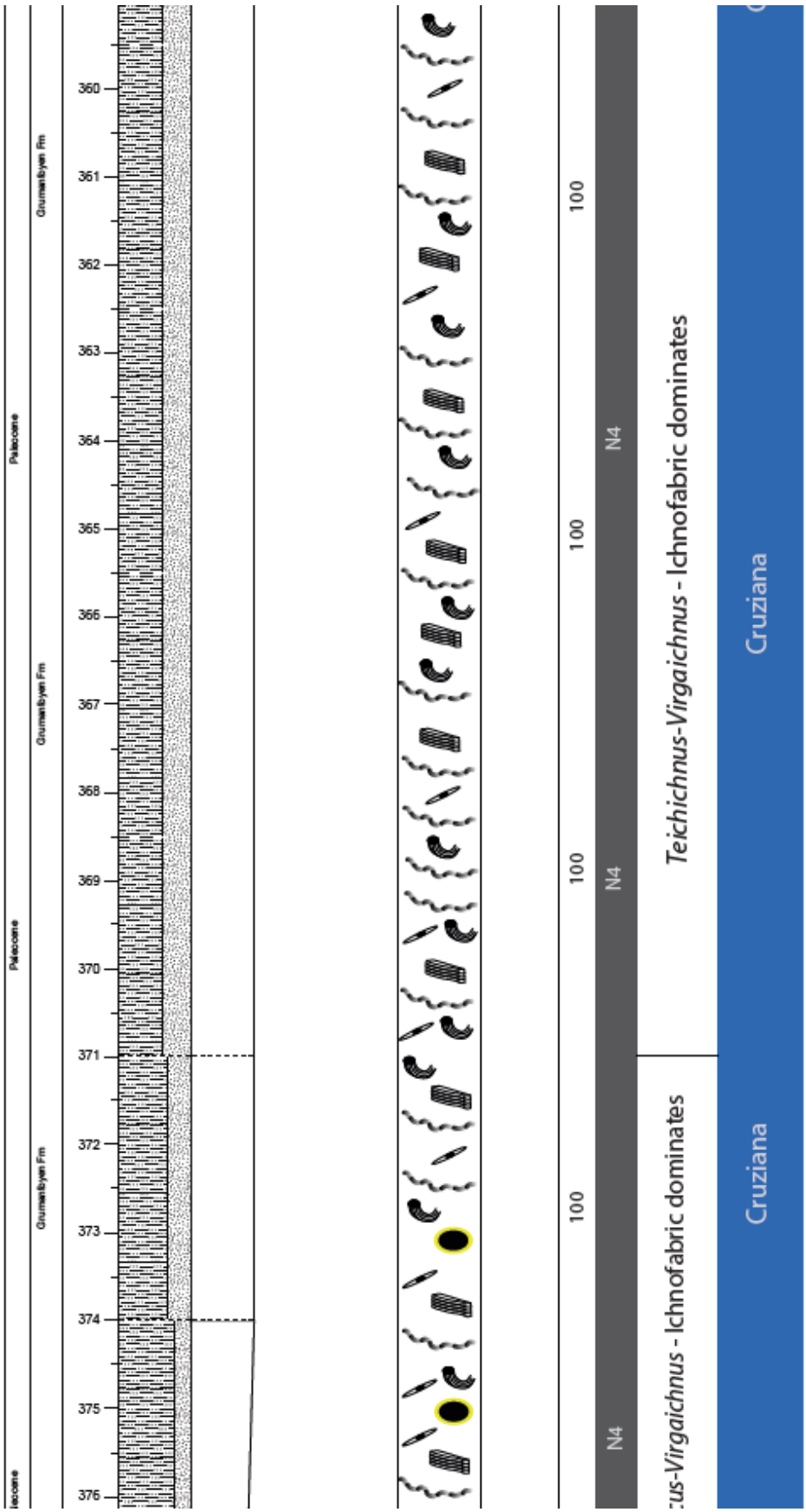
Paleocene
Paleocene
Paleocene
Gruman Byen Fm
Gruman Byen Fm
Gruman Byen Fm
360
361
362
363
364
365
366
367
368
369
370
371
372
373
374
375
376
100
100
100
N4
N4
N4
Teichichnus-Virgaichnus - Ichnofabric dominates
Cruziana
Cruziana

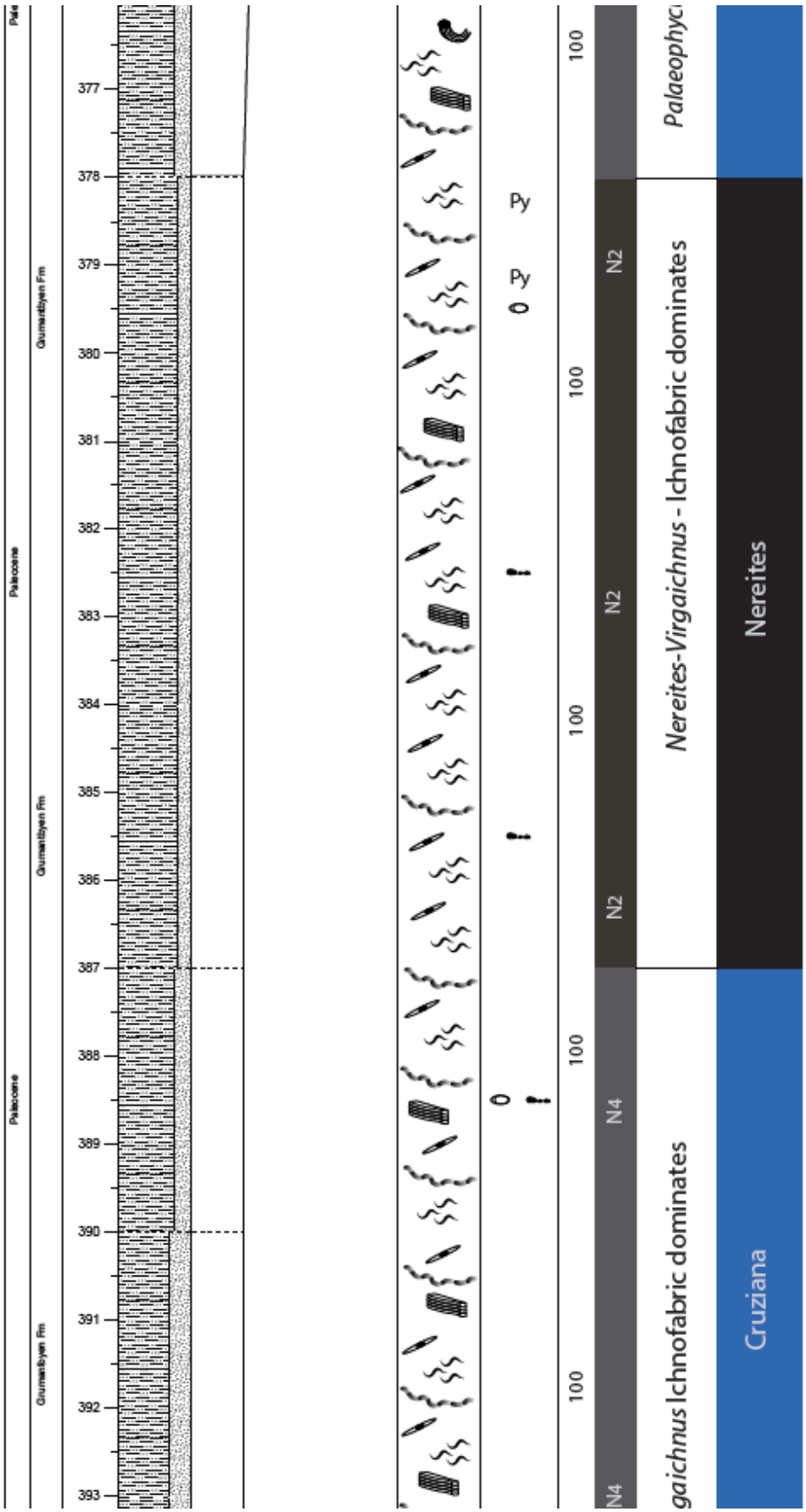
Paleocene
Grumantbyen Fm
377
378
379
380
381
382
383
384
385
386
387
388
389
390
391
392
393
Py
Py
0
100
100
100
100
N4
N2
N2
N2
N4
Cruziana
Nereites
Nereites-Virgaichnus - Ichnofabric dominates
gaichnus Ichnofabric dominates
Palaeophyc

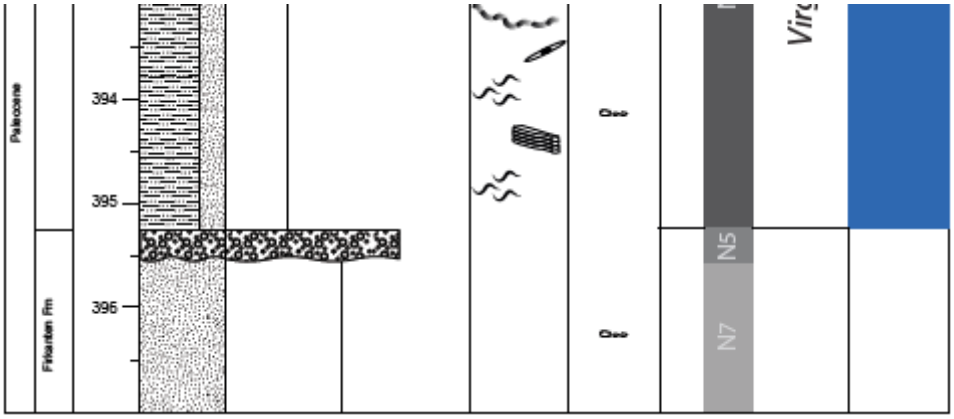

Appendix 13: *Presenting log of well BH-9-2006. The length of the core is measured in depth (meters) from the topographical point where the well has been drilled. The log has been divided into two parts at the depth of 293 m. Bottom depth of the logged interval is 397 m and top depth is 125 m. Scale 1:50.*